Poznan University of Technology
Faculty of Civil and Transport Engineering

PhD Dissertation

An Analysis of Load Bearing Capacity and Stiffness of Aluminium-Concrete Composite Elements Subjected to Bending

Dissertation by Łukasz Polus

Supervisor: Maciej Szumigała, Ph.D., Dr.Sc.

Poznań 2021

To my parents, with love.

Contents

Contents

Preface

Abstract

Aluminium-concrete composite structures are a relatively new civil engineering solution and are still being developed. They were first used in bridges, but today they could also have new applications in buildings. Most of the investigations performed on these structures to date have focused on systems in which solid slabs and non-demountable shear connectors were used. The present dissertation discusses a novel composite beam, in which a concrete slab is poured into steel sheeting and connected with an aluminium beam using demountable shear connectors. A notable benefit of using the profiled sheeting is that it acts both as a stay-in-place formwork and a structural member which may resist tension. In this research special attention was paid to the development of a demountable shear connector which makes it possible to separate the aluminium beam from the concrete slab once the design life of the structure is over. After disassembly, the materials may be reused or recycled.

The experimental work consisted of three main groups of tests: materials tests, shear connection tests and bending tests, and was followed by theoretical and numerical analyses. The slip moduli $k_{0.4}$ and $k_{0.6}$, and the load-carrying capacity of the connection were determined experimentally. Furthermore, the short-term behaviour, load carrying-capacity, mode of failure, load-deflection and load-slip response of the aluminium-concrete composite beams with profiled sheeting and demountable shear connectors were investigated. Furthermore, the author proposed a method for calculating the load-carrying capacity of such beams, based on the calculation procedure for steel-concrete composite elements. The results of the experimental tests show that it is possible to ensure composite action between an aluminium beam and a concrete slab using developed shear connectors. The clearance between the bolt and the hole made it easier to install demountable shear connectors through the holes in the aluminium beam flange. However, it had a negative impact on the stiffness of the connection. The results from the analytical estimations were compared with the results from the laboratory tests. The calculated bending plastic resistance of the aluminium-concrete composite beam with partial shear connection was 1.05 times higher than the bending resistance from the tests.

In addition, non-linear 3D finite element (FE) models of the tested composite beam and the shear connection were developed and verified against the experimental results. The comparison of the numerical and experimental results demonstrated that the adopted 3D models adequately captured the responses of the aluminium-concrete composite beams and joints.

List of publications

The present dissertation is largely based on investigations presented in the following publications:

Polus, Ł. and Szumigała, M. (2014a). *Connector for composite structures*, Patent, Exclusive right no. 232822, Application no. 406833, Application Date 13 January 2014, Patent published 31 July 2019, Warsaw: Polish Patent Office. [cited at p. 29]

Szumigała, M. and Polus, Ł. (2015). Applications of aluminium and concrete composite structures. *Procedia Engineering*, 108, pp. 544-549. [cited at p. 1, 13]

Polus, Ł. and Szumigała, M. (2016). Tests of shear connectors used in aluminium-concrete composite structures. In: M. A. Giżejowski, J. Marcinowski, A. Kozłowski and J. Ziółko, eds., *Recent Progress in Steel and Composite Structures: Proceedings of the XIII International Conference on Metal Structures (ICMS2016), Zielona Góra, Poland, 15-17 June 2016*, Boca Raton: CRC Press, pp. 113-136. [cited at p. 13, 29]

Polus, Ł. and Szumigała, M. (2017a). Badania belek zespolonych aluminiowo-betonowych. In: T. Biliński and J. Korentz, eds., *XI Konferencja Naukowa Konstrukcje zespolone, Zielona Góra, 29-30 czerwca 2017*, Zielona Góra: Oficyna Wydawnicza Uniwersytetu Zielonogórskiego, pp. 99-100. [in Polish] [cited at p. 57, 81]

Polus, Ł. and Szumigała, M. (2019a). An experimental and numerical study of aluminium-concrete joints and composite beams. *Archives of Civil and Mechanical Engineering*, 19(2), pp. 375-390, doi: 10.1016/j.acme.2018.11.007. [cited at p. 1, 31, 57, 63, 70, 72-77, 79, 81-82, 84, 102]

Polus, Ł. and Szumigała, M. (2019c). Laboratory tests vs. FE analysis of concrete cylinders subjected to compression. *AIP Conference Proceedings*, *2078*, article 020089, doi: 10.1063/1.5092092. [cited at p. 58, 60, 63-66, 81, 105-106]

In addition to the publications presented above, several publications on aluminium-concrete composite beams have been written by the author of this dissertation:

Polus, Ł. and Szumigała, M. (2014b). A numerical analysis of the resistance and stiffness of the aluminium and concrete composite beam. *Civil and Environmental Engineering Reports*, 15(4), pp. 99-112. [cited at p. 13]

Polus, Ł. and Szumigała, M. (2014c). Analiza numeryczna nośności i sztywności belki zespolonej aluminiowo-betonowej. In: T. Biliński and J. Korentz, eds., *Jubileuszowa*

List of publications

X Konferencja Naukowa Konstrukcje Zespolone, Zielona Góra, 26-27 czerwca 2014, Zielona Góra: Oficyna Wydawnicza Uniwersytetu Zielonogórskiego, pp. 393-405. [in Polish] [cited at p. 13]

Szumigała, M. and Polus, Ł. (2014a). Wpływ zespolenia na nagrzewanie się aluminiowej belki wg standardowej krzywej pożarowej ISO 834. In: L. Runkiewicz and T. Błaszczyński, eds., *Ekologia w budownictwie*, Wrocław: Dolnośląskie Wydawnictwo Edukacyjne, pp. 137-150. [in Polish] [cited at p. 11]

Szumigała, M. and Polus, Ł. (2014b). A numerical modelling of the load capacity of the shear connector of aluminium and concrete structures. In: T. Heizing and E. Urbańska-Galewska, eds., *II International Polish-Ukrainian Scientific-Technical Conference "Current Problems of Metal Structures", Gdańsk, 27-28 November 2014*, Gdansk: Foundation for the Development of Civil Engineering, pp. 221-224. [cited at p. 67]

Polus, Ł. and Szumigała, M. (2017b). Wpływ zespolenia na nośność i sztywność belki metalowej współpracującej z płytą betonową, *Inżynieria i Budownictwo*, 6, pp. 320-324. [in Polish] [cited at p. 10]

Szumigała, M. and Polus, Ł. (2017). A numerical simulation of an aluminium-concrete beam. *Procedia Engineering*, 172, pp. 1086-1092. [cited at p. 19]

Szumigała, M., Rzeszut, K. and Polus, Ł. (2017). Wybrane rodzaje konstrukcji stosowanych w budownictwie zrównoważonym. In: J. Gęsikowska and A. Mreła, eds., *Cywilizacja techniczna: nauka i technika w pierwszej dekadzie XXI wieku*, Bydgoszcz: Wydawnictwo Kujawsko-Pomorskiej Szkoły Wyższej, pp. 153-174. [in Polish] [cited at p. 1]

Chybiński, M. and Polus, Ł. (2018). Bending resistance of metal-concrete composite beams in a natural fire. *Civil and Environmental Engineering Reports*, 4(28), pp. 149-162, doi: 10.2478/ceer-2018-0058. [cited at p. 11-12, 15]

Polus, Ł., Chybiński, M. and Szumigała, M. (2018). Bending resistance of metal-concrete composite beams under standard fire conditions, *Przegląd Budowlany*, 7-8, pp. 128-132. [in Polish] [cited at p. 11]

Polus, Ł. and Szumigała, M. (2019b). Theoretical and numerical analyses of an aluminium-concrete composite beam with channel shear connectors. *Engineering Transactions*, 67(4), pp. 535-556, doi: 10.24423/EngTrans.984.20190802. [cited at p. 17, 23, 29, 31]

List of symbols and abbreviations

Symbol/Abbreviation	Description	First use
a	height of aluminium subjected to compression	page 38
a'	height of the web subjected to compression	page 39
b	part of the connector embedded in the concrete slab	page 32
b_0	width of the concrete rib	page 34
b_1	distance between one of the two loading points and the middle of the beam	page 36
b_d	initial distance between the reference points	page 66
b_{eff}	effective width of the composite slab	page 38
b_f	width of the top flange	page 38
d	diameter of the connector	page 32
d_1	distance between the neutral axis of the aluminium beam and its top	page 38
d_a	maximum aggregate size	page 62
d_c	dimension	page 36
e	Euler's number	page 36
e_e	eccentricity	page 63
e_p	height of the profiled sheeting	page 36
$\dot{e}$	strain rate	page 43
f	deflection	page 37
f_c	cylinder compressive strength of concrete	page 38
f_{ck}	characteristic cylindrical compressive strength	page 34
$f_{c,cube}$	compressive cubic strength	page 45
f_{cm}	mean value of the concrete cylinder compressive strength	page 61
f_{ct}	tensile strength of concrete	page 46
f_{b0}/f_{c0}	ratio of the concrete strength in the biaxial state to the concrete strength in the uniaxial state	page 63
f_k	characteristic resistance of a material	page 9
f_u	ultimate strength of the steel used in the shear connector	page 34
f_{uf}	ultimate strength of the aluminium in the beam flange	page 34
f_y	yield strength	page 38
h	depth of the entire section	page 36
h_a	height of the aluminium beam	page 38
h_c	thickness of the concrete slab in the section where there is no rib	page 36
h_e	height of the section of the connector embedded in the concrete slab	page 34
h_p	overall depth of the profiled steel sheeting	page 34
k	stiffness of the connector	page 31
k'	coefficient	page 59
k_t	reduction factor	page 34
$k_{t,max}$	the maximum value of the reduction factor	page 34
$k_{0.4}$	slip modulus determined for a load equal to 40% of the estimated load-carrying capacity	page 31
$k_{0.6}$	slip modulus determined for a load equal to 60% of the estimated load-carrying capacity	page 31
$k_{0.8}$	slip modulus determined for a load equal to 80% of the estimated load-carrying capacity	page 86
k_1	coefficient	page 34
l	length of the sample	page 45
l_s	length of the spreader beam	page 57
n	modular ratio	page 37
n_s	sample size	page 81
n_w	rate of weakening	page 60
n_d	number of connectors in the shear span	page 38

List of symbols and abbreviations

List of symbols and abbreviations

Symbol/Abbreviation	Description	First use
K	shear stiffness of the connector	page 36
L	span length	page 36
M	moment	page 114
M_0	mid-span moment corresponding to the first yielding of the aluminium beam	page 100
M_a	ultimate flexural capacity of the aluminium beam	page 40
M_{crack}	mid-span moment corresponding to the first cracking	page 100
M_{el}	elastic flexural capacity not taking into account the slip effect	page 38
M_{pl}	ultimate flexural capacity of the full composite beam	page 40
M_{ult}	mid-span ultimate strength of the composite section	page 39
$M_{y,Rk}$	elastic flexural capacity of the aluminium-concrete composite beam with partial shear interaction	page 38
N_{ac}	double compression force of aluminium	page 38
$N_{ac'}$	double compression force in the web	page 39
N_{at}	tensile force capacity of the entire aluminium section	page 38
P	total load	page 37
P_{min}	the lowest resistance measured per connector	page 49
$P_{Rd,AISC}$	design strength of a headed stud shear connector	page 34
$P_{Rd,Ec}$	design resistance of the demountable connector for aluminium-concrete composite structures	page 33
P_{Rk}	characteristic resistance of the connector	page 92
$P_{Rk,test}$	characteristic resistance of the connector determined from the push-out tests	page 49
P_{ult}	shear capacity of a connector accounting for the effect of the profiled sheeting and connector spacing	page 38
Q	resultant of the uniformly distributed load	page 32
R_g	reduction factor	page 34
R_p	reduction factor	page 34
R_m	ultimate tensile strength	page 81
$\dot{R}$	stress rate	page 43
S_a	first moment of area of the aluminium beam (for the top fibre of the slab)	page 103
S_c	first moment of area of the slab (for the top fibre of the slab)	page 103
W_y	section modulus of the ideal cross-section	page 103
$(EI)_e$	weighted mean stiffness of the transformed section of the composite beam	page 36
$(EI)_{eff}$	effective stiffness	page 36
$(EI)_1$	stiffness of the transformed section of cross-section 1-1	page 36
$(EI)_2$	stiffness of the transformed section of cross-section 2-2	page 36
α	coefficient	page 34
α_a	thermal expansion coefficient for aluminium	page 11
α_b	coefficient	page 34
α_c	thermal expansion coefficient for concrete	page 11
α_v	coefficient	page 34
α_1	coefficient	page 36
β	coefficient	page 34
β_1	coefficient	page 36
γ	unit weight	page 9
γ_{M2}	partial safety factor	page 34
γ_v	partial factor	page 34
δ_0	mid-span deflection corresponding to M_0	page 100
δ_{crack}	mid-span deflection corresponding to M_{crack}	page 100
δ_u	slip capacity of a specimen	page 49
δ_{ult}	mid-span deflection corresponding to M_{ult}	page 100
δ_η	deflection of a composite beam with partial shear connection	page 25
δ_s	deflection of the steel beam acting alone	page 25
δ_c	deflection of the composite beam with full shear connection	page 25
ε	strain	page 66
ε_{eng}	engineering strain	page 71

List of symbols and abbreviations

Symbol/Abbreviation	Description	First use
$\varepsilon_{ln}^{plastic}$	logarithmic plastic strain	page 71
ε_c	compressive strain	page 59
ε_{c1}	strain at average compressive strength	page 59
ε_{cr}	cracking strain	page 60
ε_c^{el}	elastic compressive strain	page 60
ε_c^{in}	inelastic compressive strain	page 60
ε_c^{pl}	plastic compressive strain	page 60
ε_t	tensile strain	page 60
ε_t^{el}	elastic tensile strain	page 61
ε_t^{cr}	cracking strain	page 61
ε_t^{pl}	plastic tensile strain	page 61
ζ	coefficient	page 38
η	degree of shear connection	page 25
η_c	coefficient	page 59
η_e	coefficient	page 36
κ	parameter used in the CDP model	page 63
λ	lightness of a material	page 9
μ	friction coefficient	page 66
μ_s	population mean	page 81
ν	Poisson's ratio	page 63
φ	sample diameter	page 45
ζ_s	parameter for the slip effect	page 36
ρ	density	page 73
σ_a	nominal upper stress	page 47
σ_b	nominal lower stress	page 47
σ_c	stress for uniaxial compression	page 59
σ_c^{eff}	effective compressive stress	page 61
σ_{eng}	engineering stress	page 71
σ_p	preload stress	page 47
σ_t	stress for uniaxial tension	page 60
σ_t^{eff}	effective tensile stress	page 61
σ_{true}	true stress	page 71
ψ	dilatation angle	page 63
Δb_d	relative vertical displacement between the reference points	page 66
ΔT	temperature change	page 79

Introduction

1.1. The motivation behind the work

Sustainable construction is a trend in modern design thanks to which new or little-known solutions are developed. Designers should focus on reducing the consumption of natural resources and on durability of buildings (Szumigała, Rzeszut and Polus 2017). What is more, structures should be designed, built and demolished in a way ensuring a sustainable use of natural sources (European Council, European Parliament 2011). The materials should be reusable or recyclable after demolition. The concept of circular economy is important for sustainable development (Ashby, Balas and Coral 2016). Moreover, buildings should generate the lowest possible costs during the entire life cycle of the structure (Bonenberg and Kapliński 2017). Both the durability of the new solutions (Błaszczyński, Ksit and Dyzman 2012) and their energy efficiency (Szczechowiak 2007) (Bromberek 2014) are essential for sustainable construction. Buildings which can be used for 50 years are more economical than buildings which require repairs (Brandt 2008). Furthermore, the life cycle of a building should be taken into account at the design stage. For these reasons, building materials engineering provides innovative solutions for the construction of buildings (Czarnecki et al. 2017). Sustainable construction is open to new solutions which can help reduce CO_2 emissions. In composite structures each component may be used efficiently. A composite element consists of two or more construction elements which are permanently joined (Jankowiak, Kąkol and Madaj 2005) (Wróblewski, Berczyński and Abramowicz 2013). Composite structures combining steel and timber (Hassanieh, Valipour and Bradford 2016a, b), timber and glass (Rodacki 2017), timber and concrete (Łukaszewska 2009), timber and timber (Bedon and Fragiacomo 2019), aluminium and timber (Chybiński and Polus 2019), and aluminium and concrete (Polus and Szumigała 2019a) are relatively new structures. In this dissertation the author presents an investigation of little-know composite structures, i.e., aluminium-concrete composite beams.

Aluminium-concrete composite elements are one of the relatively unknown solutions. They may provide an alternative to steel-concrete composite structures (Szumigała and Polus 2015). However, the question is: do they meet the requirements of sustainable construction?

Aluminium is the most common metal and the third most abundant element in the Earth's crust, making up 8.1% of the planet's mass (see Fig. 1.1) (Siwowski 2005). However, pure aluminium does not occur naturally. Aluminium atoms form compounds with other metals. For this reason, the process of aluminium production is complex and energy intensive. The production of 1 tonne of aluminium requires about 17 000 kWh of electricity (Claisse 2016). The aluminium production process consists of the Bayer and the Hall-Héroult processes. The Bayer process is used to extract the alumina (aluminium(III) oxide, Al_2O_3) from the bauxite ore at an alumina refinery.
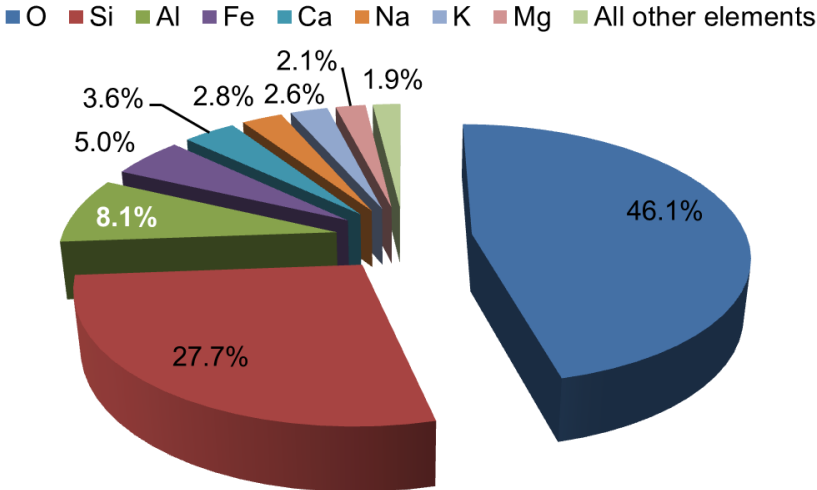
Figure 1.1. Elements in the Earth's crust

In the Hall-Héroult process, aluminium is extracted by the electrolytic reduction of the alumina dissolved in molten cryolite (Štrkaljet, Radenović and Malina 2010). The process happens at 940-980°C. Aluminium has a much higher embodied energy (the total energy used in the processes of obtaining a given material) than steel (Broniewicz 2008). What is more, the aluminium production process is detrimental both to the environment and the human health. The first aluminium smelters generated a large amount of fluorine, e.g., the fluorine emissions factor in the aluminium smelter in Skawina was 42.52 kg / Mg Al in 1980 (Włodarczyk 1987). Too high concentrations of fluorine in water cause fluorosis. It decays teeth and bones, and leads to mental disorders. The aluminium smelter in Skawina was shut down in 1981, because of the high gas and dust emissions and the storage of waste in sand pits (Rajpolt and Tomaszewska 2011). What is more, on 4 October 2010 one million cubic metres of red mud (a waste product of the Bayer process) were released after the collapse of the dam at the caustic waste reservoir in Ajka (Wikipedia 2015). It was an industrial disaster.

Despite the fact that the aluminium production process is energy intensive and may be a threat to the environment and human health, aluminium is a material which meets the criteria of suitable construction. First of all, it may be reused or recycled. The embodied energy savings may be as high as 95%, because recycled aluminium does not require electrolysis. What is more, aluminium smelters may use clean energy produced in hydroelectric power plants which do not pollute the environment. For this reason, aluminium has the potential of being an environmentally friendly "green" metal (Viami International Inc. and The Technology Strategies Group 2013). Furthermore, the aluminium smelter in Konin reduced fluorine emissions thanks to the introduced improvements (Płoszewski 1998). Nowadays, fluorides from modern smelters are almost completely recycled and reused in the electrolysis.

Furthermore, aluminium-concrete composite elements are a durable solution. Aluminium alloys are corrosion-resistant thanks to a thin surface layer of aluminium oxide. An aluminium-composite beam contains an aluminium girder, a concrete slab and steel sheeting, connectors and reinforcement. Steel sheeting and connectors should be galvanised to improve their durability. Galvanisation also limits contact corrosion between the aluminium and the steel elements. Thanks to the above-mentioned treatments, aluminium-concrete composite

structures offer high durability – one of the suitable construction criteria. Furthermore, they may also fulfil the yet another concept – that of circular economy.

New solutions should be easily deconstructed at the end of the service life of a structure, so that the building materials could be reused or recycled (Ataei et al. 2019). For this reason, it is important to use shear connectors in aluminium-concrete composite beams, which make it possible to separate the slab from the girder. Demountable shear connectors were originally developed for steel-concrete composite structures (Kozma et al. 2019). However, they have not been used for aluminium-concrete structures. For this reason, the author of the thesis proposed new demountable shear connectors which may be used in aluminium-concrete composite beams.

1.2. Literature review

1.2.1. First applications

In the first century, a Roman goldsmith presented a cup made of a shiny metal resembling silver to Tiberius, the Roman Emperor (Pliny the Elder 77–79). This metal was a lot lighter than silver and might have been aluminium. However, it was not until the 19th century that aluminium was discovered in its purest form, which does not occur naturally (see Fig. 1.2). Thanks to the developments in chemistry and the advent of electricity, aluminium began to be used both in structural and non-structural fields, e.g., to make the Sokol torpedo boat (1894), the car body (1899), the airship of David Schwarz (1893), the cladding of the dome of the San Gioacchino church in Rome (1897) (Stacey 2014) (Kwiatkowski 2012), or the hull of the Junkers J1 plane (1915).

1807	1827	1856	1886	1888
The possibility of isolating the aluminium element was predicted	The pure aluminium was produced	The the first industrial aluminium was produced	The electrolytic production method of aluminium was discovered	The Bayer Process for aluminium production was discovered
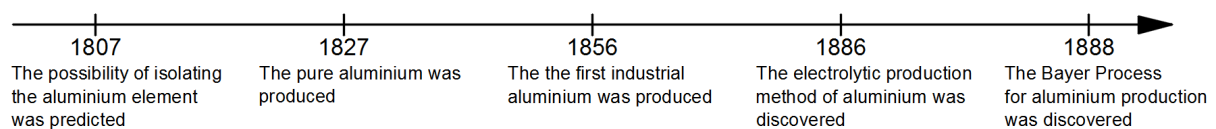
Figure 1.2. The history of the aluminium industry (Habashi 1988) (Mazzolani 2012) (Gwóźdź 2014) (web site: www.aluminiumleader.com/history/industry_history/, 05.11.2019)

Aluminium as a structural material has been used for airframes since the 1930s (Alison 1984). It was first used as a building material for bridges. The Smithfield Street Bridge in Pittsburgh was re-decked with a lightweight aluminium deck in 1933. The Grasse River Bridge was erected to span the Grasse River in 1946, to demonstrate the structural properties of aluminium for bridge-building (Kossakowski 2016). The railroad bridge has six steel spans and one aluminium span (see Fig. 1.3a), which consists of two riveted aluminium plate girders made of the 2014-T6 aluminium alloy (Siwowski 2006). In 1950 the first all-aluminium highway bridge was built in Arvida, Quebec, Canada (see Fig. 1.3b).

a)   b)
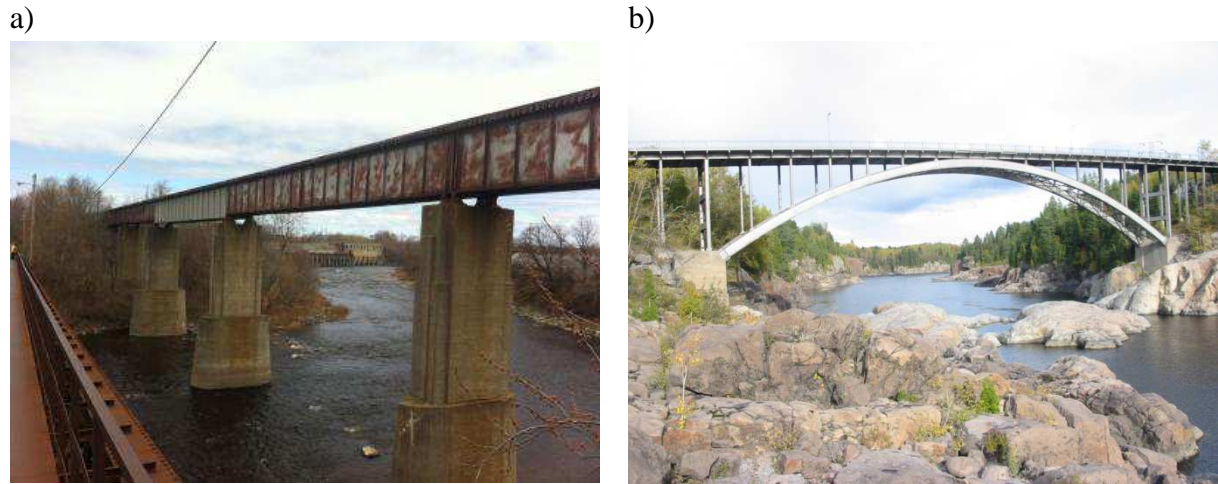
Figure 1.3. a) The Grasse River Bridge with a non-corroded aluminium span (photo taken by Michael Quiet in 2015 [1]); b) The Arvida Bridge (photo taken from Wikipedia [2])

The Clive Road Bridge was the first aluminium-concrete composite bridge (see Fig. 1.4). In the '60s of 20th century, aluminium was used as an alternative material for bridge construction. At the time, the network of roads was expanding in the USA and the amount of steel – the traditional building material – was insufficient. Aluminium became a proven construction material for which a long maintenance-free life and a light weight are required. The "Fairchild" bridge is yet another type of the aluminium-concrete composite bridge (Göner and Marx 1969). The Fairchild Engine and Airplane Corporation suggested using semimonocoque airframe aluminium structures for the construction of composite bridges. "*Monocoque refers to a metal structure, in which the skin absorbs all or most of the stresses to which the body is subjected*" (Hag-Elsafi and Alampalli 2002). It was an attempt to drastically reduce the weight (20% to 25% the weight of a steel structure) and the initial cost of the bridge (Alison 1984). Triangular box girders were made from aluminium sheets stiffened by extruded angles (see Figs. 1.5 and 1.6). Thanks to the bottom plate, which closed the span, a trapezoidal Warren truss was created (Siwowski 2006). The upper flange of the girder was made from aluminium corrugated plates, which also served as the centering of the concrete slab. "Z" shear connectors were used to ensure composite action between the aluminium structure and the concrete slab (Stonehewer 1962). Full-scale tests of this type of bridge were conducted at Lehigh University (Mindlin and Errera 1959) (Errera and Mindlin 1959). Table 1.1 presents aluminium-concrete composite bridges built in the USA.

---

[1] Web site: www.bridgehunter.com/ny/st-lawrence/mstr---grasse-river/ (30.08.2018)
[2] Web site: www.en.wikipedia.org/wiki/Arvida,_Quebec (30.08.2018)

a)

b)

c)

d)
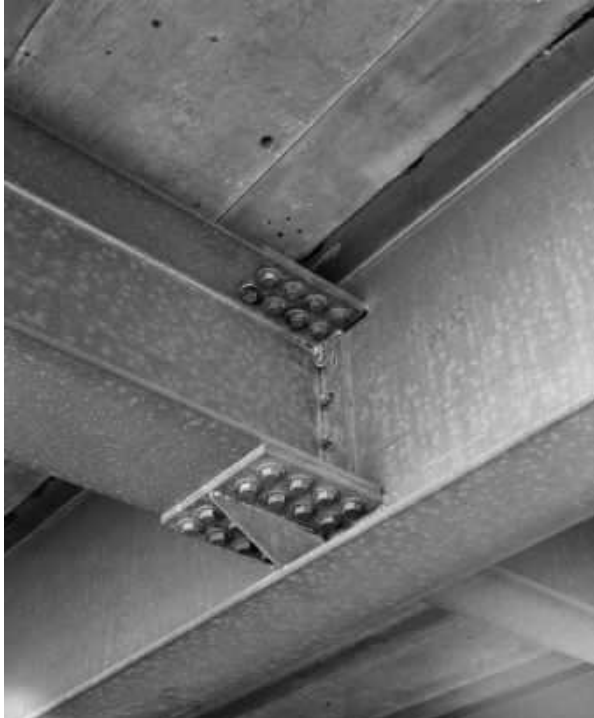
Figure 1.4. The Clive Road Bridge: a) view of the bridge; b) aluminium welded plate girders with cross-beams; c) piers of the bridge; d) high strength friction grip bolts (photos from the Historic American Engineering Record [3])

Chapter 1. INTRODUCTION

Table 1.1. Aluminium-concrete composite bridges
(Abendroth et al. 1996 & 1997) (Alison 1984) (Das and Kaufman 2007)
(Maryland Department of Transportation 2012) (Siwowski 2005 & 2006) (Stonehewer 1962)

Bridge	Erection/ Demolition Year	Dimensions	Construction
The Clive Road Bridge, over the I-80 highway Des Moines, Iowa, USA (see Fig .1.4)

Type: Welded plate girder | 1958/1993 | 4 spans: 12.5 m, 21.0 m, 21.0 m, 12.5 m

length: 67.06 m

roadway width: 9.14 m

overall width: 10.97 m | Aluminium structure: 4 aluminium welded plate girders (965-mm-high) (5083-H113 aluminium alloy) spaced 2.6 m, transversally braced with cross-beams, the aluminium surfaces which were at risk of corrosion attack from wet concrete had been painted with a zinc chromate wash primer, while the top flanges and the slab end anchorages had been additionally coated with an alkali-resistant bituminous paint; an inspection of the aluminium surfaces after the demolition of the bridge proved that this protection system was fully effective

Concrete deck: reinforced (0.2 m thick), compressive strength of 20.7 MPa

Shear connectors: angles

Reason for replacing: reconstruction and extension of the highway interchange |
| Long Island Expressway Bridges, over Jericho Turnpike, Nassau Country, USA

2 bridges

Type: Riveted plate girder | 1960/1998 | span: 23.39 m

width: 18.59 m

total width of two bridges: 33.53 m | Aluminium structure: 17 (on the westbound bridge) and 18 (on the eastbound bridge) aluminium riveted plate girders (1.37-m-high) (6061-T6 aluminium alloy), spaced 2.13 m, top flanges were painted with zinc chromate to reduce the attack of corrosion on aluminium from wet concrete, driven cold rivets (1.9 cm in diameter) (6061-T6 aluminium alloy)

Concrete deck: 17.78 cm reinforced concrete slab

Shear connectors: hot-dip galvanised steel shear connectors

Condition in 1983: no structural damage, corrosion only on steel parts adjacent to the aluminium structure, good condition of the concrete deck |

Table 1.1. Aluminium-concrete composite bridges, continued
(Abendroth et al. 1996 & 1997) (Alison 1984) (Das and Kaufman 2007)
(Maryland Department of Transportation 2012) (Siwowski 2005 & 2006) (Stonehewer 1962)

Bridge	Erection/ Demolition Year	Dimensions	Construction
Bridge over the Appomattox River on Chesterfield Avenue, Petersburg, Chesterfield County, Route 36, USA (see Fig .1.5) Type: Bolted, stiffened triangular box beam	1961/still in service	1 span: 30.58 m roadway width: 8.53 m	Aluminium structure: 5 triangular box girders (1.47-m-high) (6061-T6 aluminium alloy), AN5 and AN10 aluminium bolts, 6061-T6 aluminium rivets, there are no bottom plates Concrete deck: lightweight concrete Condition in 1983: the condition of individual aluminium components was good but with slight pitting, cadmium plated steel bolts and nuts were rusted, steel bearing plates and rocker assemblies needed painting, the longitudinal stiffeners of the upstream girder had been bent by pounding from large timbers, power poles, and other large flood debris, but no structural repair was required, no adverse reaction between the aluminium structure and the concrete deck occurred
Amityville, New York Bridges, Sunrise Highway, USA 2 bridges Type: Riveted stiffened triangular box beam	1963/2016	4 spans: 9.14 m 2 x 23.16 m, 9.14 m length: 64.62 m width: 29.26 m	Aluminium structure: Riveted triangular box stiffened sheet girders (1.83-m-high) (6061-T6 aluminium alloy) with 2.06-mm-thick side sheets, a 0.81-mm-thick corrugated top sheet, a 2.59-mm-thick bottom sheet, the sheets were riveted to specially designed longitudinal extruded sections and to lateral extruded bulb angle stiffener beams Concrete deck: concrete cast on aluminium corrugated sheets Condition in 1996: Galvanic corrosion of the aluminium superstructure at contact surfaces with the steel bearings in the presence of moisture, limited distortion or buckling of members at some of these locations, and damage to the bridge underside when struck by a vehicle taller than the available clearance were noticed, the rest of the structure appeared to be in good condition Reason for replacement: to improve the safety of motorists and pedestrians (wider span with larger shoulders and sidewalks), to reduce the possibility of striking the bridge from below (increasing vertical clearance)
Bridge over the Patapsco River, Sykesville, Maryland at Maryland Route 32, USA (see Fig .1.6) Type: Riveted stiffened triangular box beam	1963/closed to vehicular traffic in 2004	3 spans: 28.5 m, 28.7 m, 32.2 m total length: 90.22 m roadway width: 9.14 m overall width: 11.28 m	Aluminium structure: 5 riveted triangular box girders (1.7-m-high) (6061-T6 aluminium alloy) transversally braced with aluminium angles and closed with a bottom plate Concrete deck: lightweight concrete cast on aluminium corrugated plates Condition in 2004: poor, deterioration of the aluminium components due to galvanic action (the aluminium structure and the steel bearing pads were allowed to come into direct contact, contrary to specification), deterioration of the concrete bridge piers due to the leaking roadway joints (web site: www.hmdb.org/m.asp?m=115066, 31.08.2018)

a)

b)

c)

d)

e)

f)
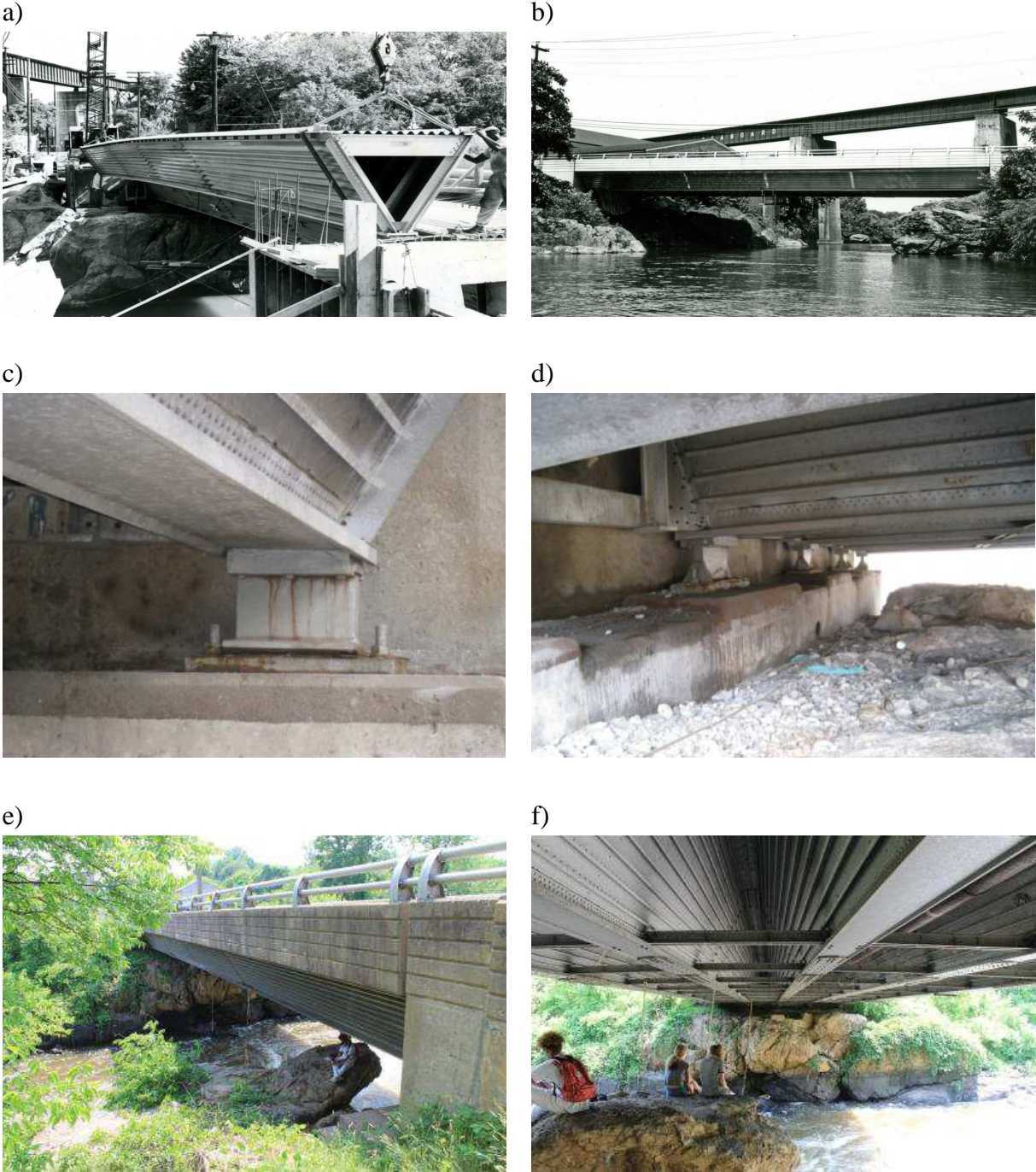
Figure 1.5. The bridge over the Appomattox River on Chesterfield Avenue: a) the bridge under construction in 1961; b) the bridge in 1963 (photos from the Virginia Department of Transportation[4]); c-d) Steel bearings (Thompson 2012); e-f) the bridge in 2017 (photos taken by Royce and Bobette Haley[4])

---

[4] Web site: www.bridgehunter.com/va/chesterfield/appomattox-river/ (30.08.2018)

a)   b)
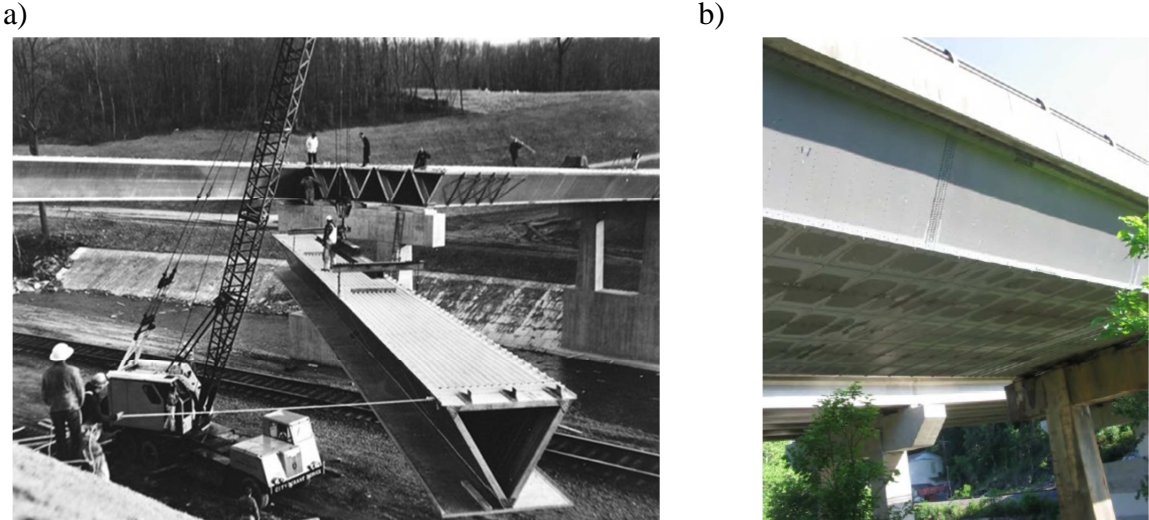
Figure 1.6. The aluminium Patapsco River Bridge: a) the bridge under construction in 1961 (photo from the Maryland Department of Transportation [5]); b) aluminium box girders with a bottom plate (Maryland Department of Transportation 2012)

"Historia vero testis temporum, lux veritatis, vita memoriae, magistra vitae" (Cicero 55 BC). The history of the first aluminium-concrete composite bridges may serve as a lesson for the future. Based on the overview of the bridges presented above, the following advantages of aluminium-concrete composite structures may be listed:

❖ Excellent corrosion resistance eliminates the need to paint the aluminium components, e.g., the Appomattox River bridge has never been painted (Thompson 2012). It reduces the costs of maintenance during the service life of a structure (Siwowski 2009a, b). Aluminium is the most corrosion-resistant when the pH of the environment ranges from 4 to 9 (Jasiczak and Hajkowski 2008).

❖ Light weight makes for convenient transport of the entire or pre-fabricated portions of the aluminium structure to the construction site and for quick erection, e.g., the aluminium structure of the Clive Road Bridge was erected in 1.5 days (Siwowski 2005). For this reason, transportation costs are low. What is more, light structures allow for the use of light supports (Mindlin and Errera 1959) and for energy saving during assembly (Mazzolani 2006). The lightness of a material is one of the most important design parameters and is calculated as follows (Gwóźdź 2007):

$$\lambda = \frac{\gamma}{f_k} \qquad\qquad\qquad (1.1)$$

where γ is the unit weight [kN/m^3] and f_k is the characteristic resistance of a material [MPa].

When comparing the lightness of basic construction materials such as concrete ($\lambda = 0.833$ for the C30/37 concrete), steel ($\lambda = 0.334$ for the S235 steel), timber

---

[5] Web site: www.preservationmaryland.org/online-exploration-of-marylands-historic-bridges/ (30.08.2018)

($\lambda = 0.262$ for the C22 timber) and aluminium ($\lambda = 0.113$ for the AW-6061 T6 aluminium alloy), aluminium alloys prove to be the lightest.

❖ A concrete slab works efficiently with an aluminium beam as a composite beam because of the relative closeness of the Young's moduli of the two materials (Alison 1984). What is more, the concrete slab increases the stability and bending resistance of I-section beams subjected to the sagging moment (Lacki, Kasza and Derlatka 2017). Polus and Szumigała (2017b) analysed the increase in the load bearing capacity and the stiffness of metal beams made of non-alloy steel, stainless steel or aluminium alloy after they had been joined with concrete slabs. The aluminium beam showed the highest increase in its load bearing capacity and stiffness.

❖ The ease of extrusion of aluminium elements makes it possible to the design an optimal cross-section (Das and Kaufman 2007).

❖ Excellent low-temperature toughness limits the possibility of brittle fracture (Formisano, De Matteis and Mazzolani 2016).

❖ Strengths comparable to steel, e.g., the yield strength of 6061-T6 aluminium alloy is 240 MPa (EN 1999-1-1) (Lacki and Derlatka 2017).

❖ If the structure is located in the open air, the contraction of the aluminium elements in winter may have a positive effect of preventing the ingress of road salt and moisture into the deck (Alison 1984).

❖ Aluminium is more resistant to impulse loads than steel due to its lower modulus of elasticity. Aluminium structures may absorb more deformation work and damped oscillations (Dokšanović, Džeba and Markulak 2017).

❖ Aluminium is fully recyclable (Gwóźdź 2007).

❖ Aluminium is non-sparking (Skejić, Boko and Torić 2015).

❖ Aluminium has an attractive appearance (Zhou and Young 2008).

❖ Aluminium is non-magnetic (Jurczak 2010).

Aluminium-concrete composite structures also have several disadvantages, which should be taken into account in design. Some of them may be minimized or even eliminated. The negative aspects of using aluminium-concrete composite structures are:

❖ Higher initial cost of aluminium structural components over comparable steel and/or concrete components, e.g., the cost a single of the Long Island Expressway Bridge was estimated to be 18 percent higher than the cost of a comparable steel structure (Alison 1984). However, the lack of the need for periodic painting of aluminium structural elements may result in a lower total cost over the entire life of a structure. What is more, the difference between the prices of aluminium and steel is gradually decreasing (Mazzolani 2003).

❖ Lack of design rules for aluminium-concrete composite structures.

❖ The modulus of elasticity of aluminium is three times lower than that of steel. Due to this fact, the deflection of aluminium beams is large compared to steel beams. However, in the case of composite beams, the transformed slab area for an aluminium-concrete composite beam is approximately three times larger than the transformed slab area for a steel-concrete composite beam. This means that the second moment of area of an ideal cross-section is larger for an aluminium-concrete composite beam than for a steel-

concrete composite beam. For this reason, the use of a composite construction decreases the impact of the low modulus of elasticity of aluminium on large deflection (Stonehewer 1962).

❖ The fatigue strength of aluminium is about three times lower than the fatigue strength of steel (Das and Kaufman 2007) (Rom and Agerskov 2014).

❖ The thermal expansion coefficient for aluminium ($\alpha_a = 24 \times 10^{-6}$ 1/°C) (Gitter 2008) is different from the one for concrete ($\alpha_c = 12 \times 10^{-6}$ 1/°C). Thermal stresses should be considered when an aluminium beam is attached to a concrete slab (Bruzzese, Cappelli and Mazzolani 1989) (Walbridge and de la Chevrotiere 2012). Bruzzese et al. showed that thermal effects are not negligible. However, they are offset by the low n ratio (the ratio of the modulus of elasticity of aluminium to the modulus of elasticity of concrete). Before the Long Island Expressway Bridges were build, the condition of the Arvida Bridge had been carefully studied in search of any cracking in the concrete deck, which could have resulted from the different displacement values for aluminium and concrete. However, only insignificant cracking discovered (Alison 1984). In the Fairchild Bridge and the Iowa Bridge, heavy cross beams at the ends of the bridge were used to anchor the slab against thermal movement (Stonehewer 1962).

❖ Aluminium expands twice as much as steel when heated. However, the increase of stress induced by limited displacement is smaller in aluminium than in steel, because aluminium has a lower modulus value (Dokšanović, Džeba and Markulak 2017).

❖ Aluminium structural elements cannot be repaired by welding or straightening in the heat treatment process because of the heat affected zones and the reduction of strength parameters (Okura 2003).

❖ The fire resistance of aluminium elements is very low, because most aluminium alloys start to lose strength when exposed to temperatures exceeding 100°C (Faggiano et al. 2004) (Szumigała and Polus 2014a) (Skejić, Ćurković and Rukavina 2015) (Polus, Chybiński and Szumigała 2018). The bending resistance of unprotected metal-concrete composite beams with girders made of non-alloy steel, stainless steel or aluminium alloy was compared in real car fires in an open car park (see Fig. 1.7) (Chybiński and Polus 2018). After 15 minutes of fire, the bending resistance of the aluminium-concrete composite beam decreased by 99.4%, while the bending resistance of the steel-concrete composite beam with the S235J2 (1.0117) steel girder decreased by 42.3%. The steel-concrete composite beam with the girder made of X6CrNiMoTi17-12-2 (1.4571) steel exhibited a slight loss of the bending resistance as the temperature increased – the bending resistance decreased by 28.9%, due to the chemical composition of said steel. However, the fire resistance of aluminium-concrete elements may be increased by concreting aluminium beams in a similar way to steel elements (ECCS 1988) (Szmigiera 2007). Partially encased composite beams may have increased fire resistance (Ahn and Lee 2017). Furthermore, aluminium is a non-toxic material, and its products burn without producing harmful gases (Kossakowski, Wciślik and Bakalarz 2017).
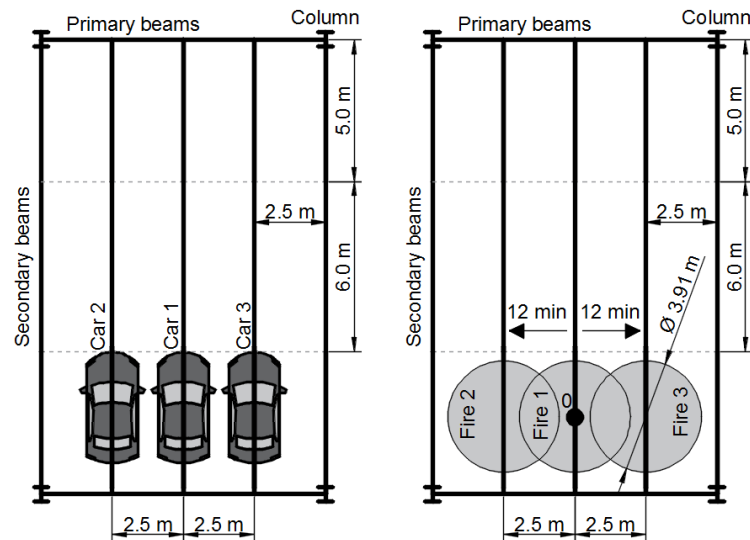
Figure 1.7. Fire scenario – three cars in a row used by (Chybiński and Polus 2018)

❖ In certain situations, aluminium may be exposed to corrosion. Aluminium alloys may corrode when they are in contact with the alkali from wet concrete (Wang et al. 2020). This type of corrosion may only occur when the concrete is setting, and for this reason the amount of corrosion may not be significant (Stonehewer 1962). Furthermore, the resulting corrosion products may form a protective film inhibiting further reaction (Pitts 1967). However, under unfavourable conditions of use, the protective film may be attacked, or may not form at all. To prevent this type of corrosion, top flanges of the aluminium beams may be painted with one coat of wash primer, one coat of zinc chromate primer, and one coat of alkali-resistant bituminous paint (Stonehewer 1962). What is more, an aluminium construction may be exposed to pitting corrosion, the most common form of corrosion found in aluminium (Aluminium Federation of South Africa 2011). However, the rate of penetration decreases with time and the pit depth is typically limited to 0.5 mm. For example, the pit depth is lower than 0.15 mm in 6061 aluminium alloy after 20 years. Although not affecting the static strength of the aluminium members, pitting corrosion affects the fatigue strength (Okura 2003). Furthermore, in composite aluminium-concrete beams there is a risk of contact (galvanic) corrosion between aluminium and steel elements (the reinforcing steel and the steel connectors in the slab). To limit contact corrosion, aluminium may be joined with galvanised steel (Thompson 2012). However, this problem may be more difficult to prevent in joints, because bolts may loss plating. Conventional aluminium and stainless bolts raise the problem of fatigue and are not used. High-strength stainless friction grip bolts may eliminate the problem of fatigue, however, they are expensive. In some situations, rivets may be used instead of bolts (Okura 2003).

1.2.2.   Aluminium in composite structures

In the previous section (1.2.1) it was demonstrated that aluminium and concrete composite structures may be used in bridges. In this section several other applications of these structures are suggested. They may be used in structures which are located in corrosive or humid

environments, e.g., in marine structures, foot bridges, swimming pools, sewage treatment plants, storage vessels and warehouses for storing fertilizers or chemicals (Szumigała and Polus 2015). What is more, they are a good solution for structures which are difficult to access, e.g., gondola lift stations in ski resorts. Aluminium beams with connectors and sheeting may be carried by a helicopter to inaccessible places and concrete may be made on the construction site. Moreover, aluminium and concrete structures may be used for structural restoration and deck repairs. For example, the Groslee bridge in France was retrofitted and the old deck structure was replaced with a new one made of aluminium truss girders and lightweight reinforced concrete (Mazzolani 2003).

Aluminium and concrete composite beams may be used as structural members of ceilings. A composite beam consisting of a solid concrete slab and an aluminium girder was discussed by (Mromliński 1975). It was characterised by lower bending stresses and shrinkage stresses than the corresponding steel-concrete composite beam. A procedure for designing this type of composite beams was presented by (Mandara and Mazzolani 1997).

An aluminium-concrete composite beam may also have profiled sheeting. The profiled sheeting acts as a stay-in-place formwork, a safe working platform and a structural member which may resist tension (Lawson, Popo-Ola and Bode 2001) (Hicks 2008) (Holomek, Bajera and Vilda 2016). It can stabilise beams during construction. Composite beams with profiled sheeting do not need centering and they contain a lower amount of concrete than composite beams with solid slabs. Therefore, the use of profiled sheeting in composite beams facilitates construction (Polus and Szumigała 2014b, c). However, concrete slabs with profiled sheeting may have different modes of failure than solid concrete slabs. Johnson and Yuan (1998) presented the results of 269 push-out tests of shear connectors used in the troughs of profiled sheeting and they showed seven modes of failure. In composite beams with profiled steel sheeting, longitudinal cracking and de-bonding between the concrete and the profiled sheeting may occur (Ranzi et al. 2009). A lot of parameters have an impact on connector resistance, e.g., the diameter of the connector, mesh position, transverse spacing, slab depth, and the number of shear connectors in the trough (Smith and Couchman 2010) (Lee, Shim and Chang 2005).

Concrete-filled aluminium alloy tubes may be used as columns. They have both high strength and high stiffness (Zhou and Young 2009). The concrete core improves both the member capacity and the fire resistance of the column (Chen, Feng and Xu 2017). The aluminium tube surrounding the concrete core reduces the construction time, because it acts as a stay-in-place formwork. The tube may have a square, rectangular or circular hollow section. It promotes the confinement effect, which increases the compressive strength of the concrete in the column core (Oliveira et al. 2010). The rectangular or square hollow sections present some loss of this effect compared to the circular hollow sections (Hu et al. 2003). What is more, the aluminium tube can split near the corner of the section and cause the failure of the columns with square or rectangular hollow sections (Zhou and Young 2008). The splitting of the circular hollow section tube is unlikely (Zhou and Young 2009). A non-linear finite element model of the concrete-filled aluminium circular hollow section column was developed and verified against experimental results by (Zhou and Young 2012). The concrete core may preclude or delay the inward and outward local buckling failure of the aluminium tubes. However, it cannot restrain the outward buckling of the concrete-filled aluminium tube

columns. Therefore, the concrete-filled aluminium alloy tubes may be reinforced at their exterior walls by the carbon fiber-reinforced polymer which has an ultra-high tensile strength, a light weight, excellent corrosion and fatigue resistances, and is easy to produce (Chen, Feng and Xu 2017). Concrete-filled aluminium alloy tubes subjected to bending were investigated by Feng, Chen and Gong (2017). The ultimate strength, flexural stiffness and ductility of the aluminium tubes increased after filling them with concrete.

Aluminium and concrete structures may be used in military bridges (Szelka and Kamyk 2013) (Kamyk and Szelka 2014). Hanus et al. (2006) presented a prototype of military bridge system which consisted of truss support components made of the 7005 T53 aluminium, a stay-in-place-form made of pultruded glass fiber reinforced polymer, reinforcement and concrete made in field conditions.

The aluminium-concrete composite structures are not the only possible composite structures containing aluminium elements. An aluminium beam can also be joined with a timber slab. Aluminium-timber composite structures are a relatively new civil engineering solution (Chybiński and Polus 2019). Saleh and Jasim suggested using aluminium-timber composite beams made of plywood slabs, hollow aluminium box beams, epoxy material and self-tapping, self-drilling screws. They analysed the structural behaviour of these beams under static and impact loads (Saleh 2014) (Saleh and Jasim 2014a, b). Aluminium-timber composite beams may also be made of laminated veneer lumber (LVL) slabs, aluminium I-beams and hexagon head wood screws (Szumigała, Chybiński and Polus 2017a, b). Laminated veneer lumber has fewer defects and is more homogeneous than solid wood. It contains 3-mm-thick bonded veneers (Chen et al. 2016). LVL X is recommended for slabs, because 80% of its veneers are glued together longitudinally and 20% are glued together crosswise to improve the lateral bending strength and the stiffness of the slab (Komorowski 2017). An aluminium beam may be used for anchoring cross-laminated timber (CLT) walls, and to increase their durability and speeding installation (Scotta et al. 2017 & 2018). Aluminium-timber structures are a very attractive solution for civil engineering due to their high corrosion resistance, small self-weight and fast assembly. Nowadays, light-weight structures are preferred to heavy-weight ones (Chybiński and Garstecki 2017). On the other hand, failure in aluminium-timber structures may occur as a result of temperature change causing different displacement values for aluminium and timber (Marcinowski 1997 & 2018).

Aluminium bars and plates have recently been used to strengthen reinforced concrete beams (Abu-Obeidah, Abdalla and Hawileh 2019) (Yu, Xing and Chang 2020) (Xu et al. 2020). Rasheed et al. (2017) proved that aluminium alloy plates can be used as an external strengthening material to enhance both the strength and ductility of reinforced concrete beams subjected to bending.

1.2.3. Aluminium vs. stainless steel

As has already been presented in the previous sections, aluminium and concrete composite structures may have several applications. Nowadays, the use of innovative materials such as aluminium alloys, stainless steels, titanium alloys and shape memory alloys, is becoming more and more popular, e.g., in rehabilitation work (Mazzolani and Mandara 2002). Composite beams usually consist of steel girders and concrete slabs. The girders made of non-

alloy (carbon) steel need anticorrosion coatings. To reduce the total cost over the entire life of a structure and to avoid periodic painting, the girders may be made of stainless steel or aluminium alloy (Chybiński and Polus 2018). It is difficult to choose between aluminium and stainless steel. The durability of stainless steel is similar to that of aluminium. However, aluminium has a lower fire resistance than stainless steel. Chybiński and Polus (2018) demonstrated that the bending resistance of a composite beam with an aluminium girder rapidly decreased to zero kN·m in fire conditions. The bending resistance of a composite beam with a girder made of X6CrNiMoTi17-12-2 (1.4571) steel decreased slightly as the temperature increased, due to the chemical composition of said steel. Moreover, the modulus of elasticity of stainless steel is three times higher than that of aluminium. The production of aluminium requires more energy than the production of stainless steel. However, the recycling of aluminium does not require electrolysis, which translates to energy savings. What is more, aluminium girders are easy to transport, because there are relatively light compared to steel girders. Furthermore, aluminium may have a lower lightness ratio (the ratio between a material density and its yield strength) than stainless steel. For example, the AW-6060 aluminium alloy has a 1.9 times lower lightness ratio than the commonly used 304 L (1.4307) austenitic steel (Chybiński and Polus 2019). The yield strength of selected aluminium alloys is similar to that of stainless steel, e.g., AW-6082 T6 has a yield strength equal to 260 MPa (European Committee for Standardization 2007). On top of that, the price of aluminium alloy is comparable to or lower than the price of stainless steel. Before making the final decision about which materials to use, the designers should take into account many aspects. One of them is the corrosive environment. Both materials are considered as corrosion resistant, however, they may corrode under certain conditions (Rzeszut, Szumigała and Polus 2015). The use of materials which are more expensive than carbon steel, such as stainless steel and aluminium alloys, may lead to low maintenance costs and a drastic reduction of the total cost of a structure during its lifetime.

1.2.4. Tests of aluminium-concrete composite elements subjected to bending in literature

Aluminium-concrete composite elements have been the subject of several studies:
- ❖ Test of a composite aluminium and concrete highway bridge at Lehigh University (Mindlin and Errera 1959),
- ❖ The study of aluminium-concrete composite beams at McGill University (Stonehewer 1962),
- ❖ The experimental investigation on aluminium-concrete composite beams at the University of Naples Federico II (Bruzzese, Cappelli and Mazzolani 1989),
- ❖ The tests of a continuous span aluminium girder concrete deck bridge at Iowa State University (Abendroth et al. 1996 & 1997).

The Fairchild Bridge was tested at the Fritz Engineering Laboratory, Lehigh University (Mindlin and Errera 1959). The 15.24-m-long and 7.32-m-wide bridge consisted of three hollow triangular beams and two bottom plates made of 6061-T6 aluminium alloy. Each beam had three stiffened plates, three longitudinal extruded elements, and stiffening frames (spaced at 1.52 m). The aluminium structure of the bridge weighed 5.2 t. Reinforced concrete with

lightweight slag aggregate was poured into 6.35-cm-deep corrugated decking which was attached to the top plates. "Thermal beams" were used near each end of the structure to protect it against the stresses caused by the difference in the thermal coefficients of concrete and aluminium. The test programme consisted of static, fatigue and dynamic tests. The results of these tests were compared with the results of the theoretical analysis. The behaviour of the bridge in static tests was similar to its theoretical behaviour. What is more, the bridge withstood the cyclic load without any damage. It was damaged in the final static test when the load was greater than the design live load.

Stonehewer (1962) analysed aluminium-concrete composite beams with channel shear connectors. He conducted bond tests on aluminium rods embedded in concrete, push-out tests of aluminium shear connectors and static bending tests of aluminium-concrete composite beams. The effects of applying paint on the aluminium-concrete interface were investigated in six bond tests: two specimens were unpainted, two were covered with bituminous paint, and two were covered with epoxy paint. The aluminium bars with the bituminous paint system showed insignificant bond resistance (the bar started to slip at a load of 2.2 kN). The bar with the epoxy paint and the unpainted bar had noticeable bond resistance. The maximum value of the bond stress was found in the unpainted bar. Stonehewer (1962) proved that the bond between aluminium and concrete varies depending on the treatment of the aluminium surface. However, the bond stress was low enough to be of no practical value in the design of aluminium-concrete composite structures. To obtain the load-slip curve for the channel shear connector Stonehewer (1962) conducted three push-out tests. The specimens were of the same dimensions (see Fig. 1.8) but differed in the pain treatment of the beam flange (unpainted, with a bituminous paint system or with an epoxy paint system). The failure mode of the two specimens with the painted beam flange was associated with the crushing of the concrete slab. Stonehewer (1962) received a similar load-slip curve for the specimens with the painted beam flange. Due to the fact, that the bond resistance of the bituminous paint was lower than that of the epoxy paint, the slip was slightly greater for the specimen with the bituminous paint than for the specimen with the epoxy paint for the same load. The test result of the specimen with the unpainted beam flange was considered to be unreliable because of the failure of the welds in one connector. The results for the aluminium shear channel connectors were compared with those obtained from the formula for the steel channel connectors presented by (Viest et al. 1952) with further modifications. Stonehewer (1962) suggested that this formula can be applied to aluminium channel connectors. To investigate the behaviour of aluminium-concrete composite beams with aluminium shear channel connectors, two T-beams of different spans were tested in three point bending tests. The top flanges of the aluminium beam were painted using the bituminous paint system and the connectors were painted using a zinc chromate wash primer. The cylinder strength of the concrete used in the long beam was 22.34 MPa after the test (30 days). The concrete cylinder strength of the concrete used in the short beam was 26.89 MPa after the test (244 days). The aluminium beam was made of a magnesium-silicon aluminium alloy with Young's modulus $E = 65.98$ GPa, yield strength $f_y = 275.79$ MPa, ultimate strength $R_m = 303.37$ MPa, and elongation equal to 13%. The failure mode of the composite beams was associated with the yielding of the aluminium beam and the cracking and crushing of the concrete slab. The longer aluminium-concrete beam was a full composite beam and the shorter was a partial composite beam.

a)

C-C

Load

I 152.4 x 76.2 x 6.4,
L = 305

Shear connectors
⊏ 38.1 x 19.1 x 4.0, L = 51

b)

A-A

c)

Shear connectors
⊏ 38.1 x 19.1 x 4.0, L = 51

Load

I 152.4 x 76.2 x 6.4, L = 3048

d)

Shear connectors
⊏ 38.1 x 19.1 x 4.0, L = 51

Load

I 152.4 x 76.2 x 6.4,
L = 1270

e)

B-B
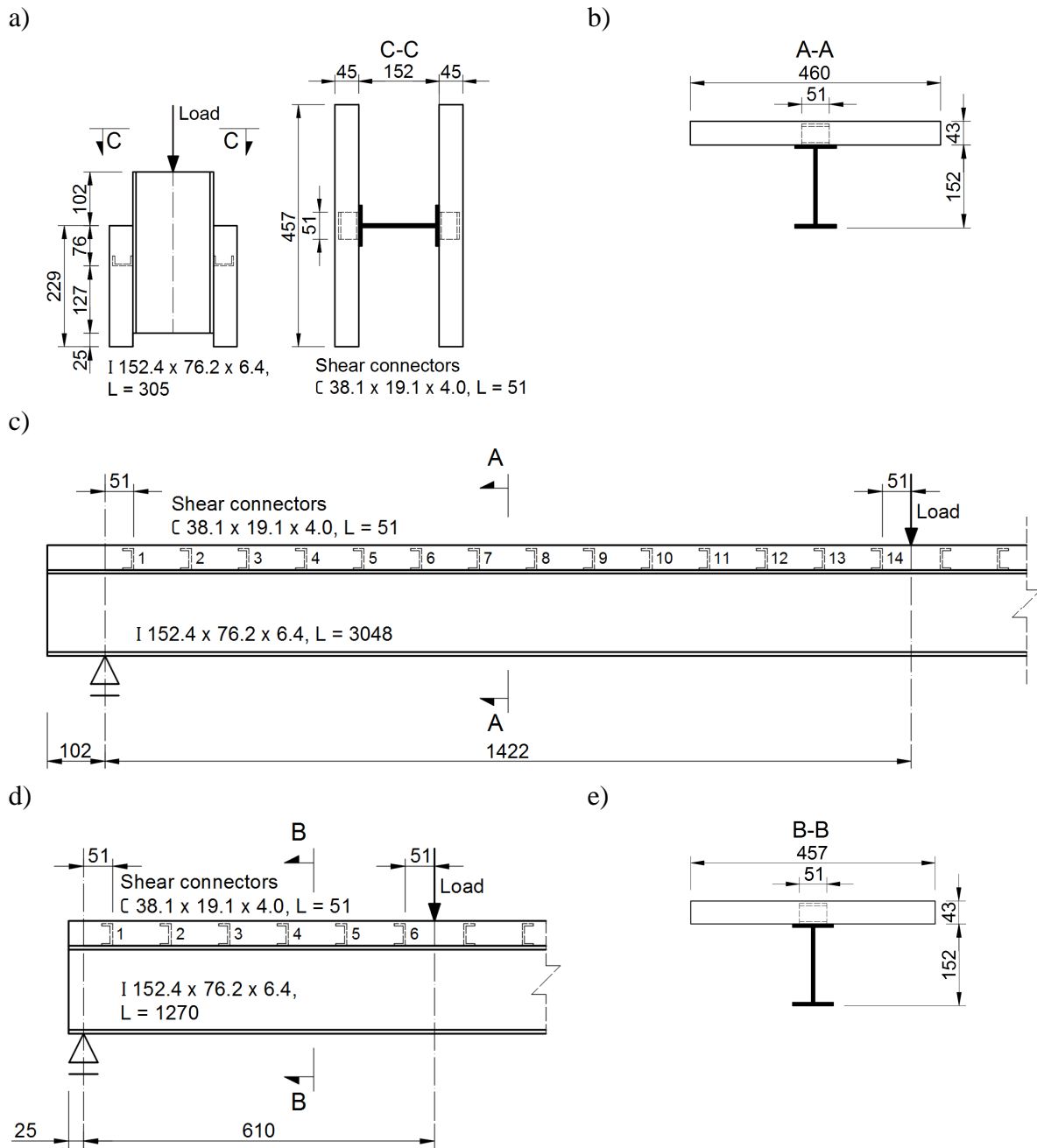
Figure 1.8. Stonehewer's specimens: a) push-out test specimen; b) cross-section of the long aluminium-concrete composite beam; c) long aluminium-concrete composite beam; d) short aluminium-concrete composite beam; e) cross-section of the short aluminium-concrete composite beam Stonehewer (1962)

Stonehewer (1962) showed that for simple beams with an almost complete interaction between the slab and the aluminium beam, the transformed section theory may be used to determine the strains in the aluminium beam and the concrete slab. He also demonstrated that the theory for incomplete interaction developed by Stussi and Newmark (Stüssi 1947) (Siess, Viest and Newmark 1952) (Viest et al. 1952) may be used for aluminium-concrete composite beams with partial shear interaction. In addition to the tests conducted by Stonehewer, Polus and Szumigała (2019b) prepared a numerical model of the aluminium-concrete composite

beam with zero-length springs. It adequately captured the elastic response of the aluminium-concrete composite beam from the laboratory test conducted by Stonehewer.

Bruzzese, Cappelli and Mazzolani (1989) tested two aluminium-concrete beams. Each beam consisted of: an aluminium beam, a concrete slab, longitudinal reinforcements, stirrups (4 mm in diameter) and bolts (see Fig. 1.9).

a)
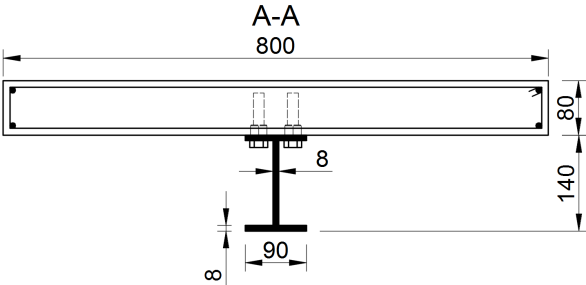
b)
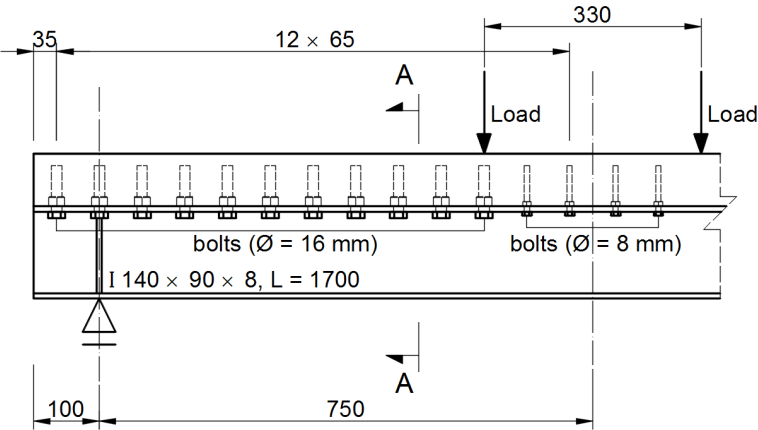
Figure 1.9. Details of the aluminium-concrete composite beams tested by Bruzzese, Cappelli and Mazzolani (1989): a) cross-section; b) longitudinal view

They had the same geometric configuration, except for the stirrup spacing (6.5 cm in the first beam and 13.0 cm in the second beam). What is more, the material parameters were different for each beam. The Young's modulus and the compressive strength of the concrete in the first beam were 31.49 GPa and 43.3 MPa, respectively. The Young's modulus and the compressive strength of the concrete in the second beam were 35.71 GPa and 55.7 MPa, respectively. The 0.2% proof strength (352.3 MPa) and the ultimate tensile strength (410.5 MPa) of the aluminium alloy in the second test were higher than in the first one (339.9 MPa and 394.9 MPa, respectively). The Young's modulus of the aluminium alloy was assumed to be equal to 70.0 GPa. The longitudinal reinforcements were used as stirrup supports. The shear connectors (8 and 16 mm bolts) had been joined to the upper flange of the aluminium beam using lock-nuts. Then, the shanks of the bolts and the lock-nuts were embedded in the concrete slab. The beams were examined in four-point bending tests. They were subjected to pure bending between the two loading points. The mid-span deflection of the beams and the strain distribution along the two sections were measured. When the load reached about 24% (beam 1) or 35% (beam 2) of the ultimate load, hairlike cracks occurred in the tensioned part of the concrete slab. When the load reached about 72% (beam 1) or 65% (beam 2) of the

ultimate load, the yield strength was achieved in the aluminium beams. In each beam, longitudinal cracks occurred when the load reached about 85% (beam 1) or 64% (beam 2) of the ultimate load. A plastic hinge occurred only in the first beam. The failure mode of this beam was associated with the damage of the compressed and tensioned edges of the concrete slab in the mid-span. The second beam had lower ductility than the first beam because of the lower number of stirrups. Due to this fact, severe, compressive and shear stresses occurred all around the connectors in the second beam. What is more, longitudinal and transverse fractures occurred in the beam under the ultimate load. In addition to the tests conducted by Bruzzese, Cappelli and Mazzolani (1989), a theoretical study was performed (Bruzzese et al. 1991). Furthermore, Szumigała and Polus (2017) prepared a numerical model of one of the aluminium-concrete composite beams from Bruzzese's tests. The results of the numerical analysis were compared with the load bearing capacity and the mid-span deflection obtained in the experimental study.

A continuous span aluminium girder concrete deck bridge (see Fig. 1.10) was investigated by the researchers from Iowa State University (Abendroth et al. 1996 & 1997). Despite the fact that the bridge performed well, it was decommissioned in 1993 (Walbridge and de la Chevrotière 2012). Before the bridge was demolished static load tests had been conducted. Abendroth, Sanders and Mahadevan (1996) presented the results of field tests, finite element analyses and load distribution studies. What is more, the aluminium girders were removed from the bridge and fatigue tests were conducted (Abendroth, Sanders and Hansz 1997). A section of the reinforced concrete deck remained attached to the girders. Four long (7.9 m) and four short specimens (4.6 m) were prepared for the constant-amplitude fatigue tests. The long girder specimens had Category E welded details [6] from the original bridge construction. They also had new cover plates welded to their bottom flange and new, short, horizontal plates welded to their web. The short girder specimens did not have any existing weld plate attachments from the original bridge structure. They had new bottom flange plates and a new short, vertical web stiffener welded to their web. The new fillet welds were Category E welded details, except for the fillet welds between the vertical web stiffener plates and the girder bottom flange plate, which were Category C welded details [6].
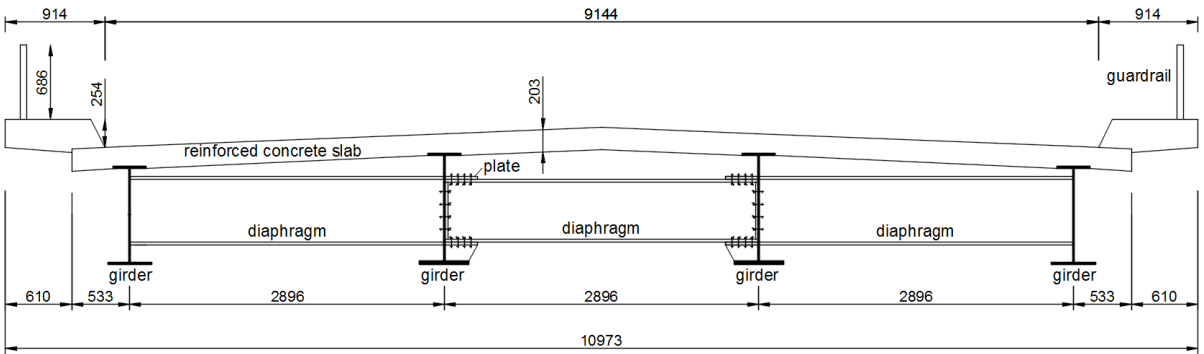
Figure 1.10. A cross-section of the continuous span aluminium girder concrete deck bridge (Abendroth et al. 1996 & 1997)

---

[6] As classified by the Specifications for Aluminum Structures (Aluminum Association 1994)

Chapter 1. INTRODUCTION

The investigation of the Clive Road Bridge provided a lot of information. Some of the conclusions are presented below. The results of the experimental tests revealed that the strength properties of aluminium are sufficient for highway bridge girders. The strains and deflections measured in the 1993 field tests were in close agreement with the analytical predictions of these values. The load distribution studies showed that the AASHTO LRFD Bridge Design Specifications criteria for load distribution (American Association of State Highway and Transportation Officials 1994) are applicable to this type of bridges. Full-size Category E aluminium weldments tend to experience fatigue fractures at a lower stress range than small-sized specimens. Fatigue fractures satisfied the requirements specified for aluminium structures in the Specifications for Aluminum Structures (Aluminum Association 1994).

1.3. The goals of the work

A review of the literature revealed that previous research on aluminium-concrete composite beams had been carried out using solid slabs and non-demountable shear connectors (channel shear connectors and bolts with nuts, threads and shanks embedded in concrete slabs). However, no research on aluminium-concrete composite beams with profiled steel sheeting and demountable shear connectors had been done prior to this study. In this dissertation, aluminium-concrete composite elements (aluminium-concrete composite beams with profiled sheeting) were subjected to bending and their load bearing capacity and stiffness were analysed. What is more, a new demountable shear connector was proposed. The shear connector makes it possible to connect parts of different materials (aluminium, steel, concrete) in a simple way and to separate the aluminium beam from the concrete slab once the design life of the structure is over. Thanks to this connector, composite action is achieved without welding, which is beneficial because welding causes the formation of heat affected zones and the reduction of strength parameters of aluminium alloys. The connector fastens the steel profiled decking to the top of the aluminium beam when concrete is poured into steel sheeting. The profiled sheeting acts as a stay-in-place formwork and a safe working platform. It can stabilise beams during construction. Aluminium-concrete composite beams with profiled sheeting do not need centering and they contain a lower amount of concrete than composite beams with solid slabs. The profiled steel sheeting and the connectors should be galvanised to limit contact corrosion between the aluminium and the steel elements.

The author examined the stiffness and the strength of the connections used to join the aluminium girder with the concrete slab. The slip moduli and the peak load capacity per one connector were determined experimentally in push-out tests. These parameters are necessary for designing aluminium-concrete composite beams because the behaviour of the beams depends on the stiffness and the strength of their connections.

Furthermore, the shear connection test and the bending test were modelled in the finite element program. Finite element analyses play a crucial role in modern civil engineering research, because they complement laboratory tests.

The purpose of this research work was to capture the short-term local and global behaviour of aluminium-concrete composite beams with profiled sheeting and new shear connectors. The author formulated the fundamental thesis of the dissertation:

Chapter 1. INTRODUCTION

Demountable shear connectors can be used to join aluminium beams with concrete slabs in aluminium-concrete composite beams. The behaviour of such connectors can be modelled using spring elements.

Research questions include the following:
- ❖ How can demountable shear connectors reduce the drawbacks of non-demountable shear connectors?
- ❖ How does the stiffness of new connectors affect the short-term performance of aluminium-concrete composite beams?
- ❖ Can the guidelines for the design of steel-concrete composite structures be applied for the ultimate limit state verifications of aluminium-concrete composite structures?
- ❖ Can zero-length springs be used in the numerical model of an aluminium-concrete composite beam to model the connection between the aluminium beam and the concrete slab?

1.4. Limitations

The study presented in the dissertation has certain limitations. In the case of the shear connectors, the effects of the hole size, the shear connector diameter, the torque moment, and the concrete rib width were not examined. What is more, the stress state in the connectors was not determined in push-out tests. In the case of the aluminium-concrete composite beams, only four beams of the same geometry were tested. Therefore, it would be reasonable to perform complementary tests to identify the optimal geometry of an aluminium-concrete composite beam. The impact of the profiled sheeting type, the spacing and the diameter of the connectors, the class of concrete, the thickness of the slab, the type of the aluminium alloy and the height of the aluminium beam on the resistance and the stiffness of the aluminium-concrete composite beam should also be investigated. What is more, no dynamic, fire or long-term tests were performed on the aluminium-concrete composite specimens. As for the numerical investigation, only a static analysis in the Abaqus/Standard module was used. It would be advisable to perform a complementary analysis in the Abaqus/Explicit module in the future. This would allow for a more detailed analysis of non-linear problems (relatively high deformations accompanying the cracking of concrete) and for studying the post-ultimate behaviour of composite beams.

1.5. Outline of the thesis

The dissertation consists of a preface, an abstract, a list of publications, a list of symbols and abbreviations, seven chapters, a bibliography and appendices.

This section ends Chapter 1, in which the motivation behind the work, the literature review and the limitations of the study are presented, and the goals of the dissertation are formulated.

In Chapter 2 shear connectors used in composite structures are discussed. This includes, in particular, demountable connectors and a new type of shear connector.

Chapter 1. INTRODUCTION

The theoretical analysis of the dowel-bolt connector and the aluminium-concrete composite beam is presented in Chapter 3. The model used to calculate the load-capacity of the new shear connector and the flexural capacity of the aluminium-concrete composite beam is presented.

In Chapter 4 materials and methods used in the dissertation are described. In particular, the programmes of materials test, shear connection tests, and bending test are presented. Furthermore, the chapter discusses the finite element models of the concrete cylinder subjected to compression, of the shear connection test and of the aluminium-concrete composite beam.

The results of the laboratory tests, and the theoretical and numerical analyses are presented and discussed in Chapter 5.

Chapter 6 presents the main conclusions of the dissertation and provides answers to the research questions presented in Chapter 1.

In Chapter 7 future research is discussed along with the limitations of the present study.

The bibliography consists of 307 citations, including 24 citations of the author's previous work.

In appendices the composition of the concrete mixture, the crack width and the cracking pattern in the analysed beams are presented.

Shear connectors

2.1. Shear connectors used in composite structures

Connections decide about the behaviour of composite elements. They play a crucial role in composite beams. Most often, in a composite beam, the slab is designed to resist compression, the beam is designed to resist tension, while shear is transferred through connectors. For this reason, the connectors which join components are referred to as "shear connectors". There are many types of connectors which differ in their stiffness.

Shear connections exhibit some slip between the upper girder flange and the bottom of the slab (Kuczma M. and Kuczma B. 2006, 2011 & 2016). They are rigid or flexible (Leskelä 2017). In the rigid connection, slipping is so low that its impact on the stiffness and the load bearing capacity of a composite beam is insignificant. In the flexible connection, slipping is not negligible and its impact on the stiffness and the load bearing capacity of a composite beam should be taken into account.

Sometimes a beam behaves like a partially composite beam because the number of shear connectors is insufficient to ensure full composite action (Nie and Cai 2003). This problem often appears in composite beams with profiled sheeting when the number of shear connectors is insufficient to prevent slipping (Nie, Cai and Wang 2005). In these beams, the connectors may be placed only in the ribs of the profiled sheeting. To take into account the effects of partial interaction, the effective value of the bending stiffness should be taken into account (Polus and Szumigała 2019b). The role of the shear connection in beams with incomplete interaction calls for more investigation. An analysis presented by Kucharczuk and Labocha (2013) showed that the partially composite beam had lower resistance and stiffness than the full composite beam.

The connection between the parts of a composite beam may consists of several connectors distributed along the composite beam or may be continuous. There are a lot of types of shear connectors used in composite structures, e.g., hat profiles, corrugated strips, welded studs, screws, bolts, block connectors, angle connectors, channel connectors, I-shape connectors, L shaped cold-formed connectors, truss connectors or welded bars (Pashan 2006) (Biegus and Lorenc 2014) (Siekierski 2014) (Nawrot 2012) (Titoum et al. 2016) (Gluhović et al. 2017) (Barbosa et al. 2019).

Headed studs welded to the top flanges of steel beams before the casting of concrete slabs are the most commonly used shear connectors, because they are economical and easy to install (Lee and Bradford 2013). However, they are not demountable or they require labour intensive processes to separate the composite beam components (Nijgh, Gîrbacea and Veljković 2018). What is more, it is difficult to use them to rehabilitate existing composite beams. Pathirana et al. (2016) suggested using blind-bolts to retrofit existing composing beams, because it is possible to attach and detach them from one side of a composite beam.

A continuous shear connection has high initial stiffness, bearing capacity and ductility (Hechler et al. 2011). Composite dowels are now the most commonly used continuous connectors (Kożuch and Lorenc 2019). Composite dowels consist of concrete and steel dowels (see Fig. 2.1).
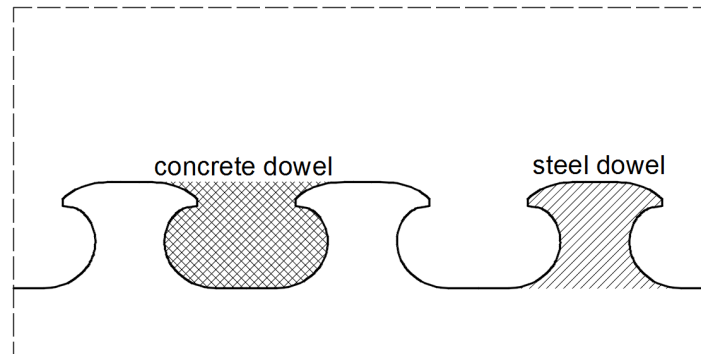
Figure 2.1. Composite dowel (Kożuch and Lorenc 2019) (Seidl et al. 2013)

They come in a variety of shapes: fin, puzzle, clothoidal, modified clothoidal (Seidl 2009) (Lorenc, Kożuch, and Rowiński 2014a) (Dudziński et al. 2011). The clothoidal shape is recommended for structures highly subjected to fatigue and the puzzle shape is recommended for structures where no fatigue occurs, e.g., building floor slabs (Seidl et al. 2013). The puzzle shape has many advantages, e.g., easy production and high bearing and fatigue capacity. An experimental study and theoretical investigations of puzzle-shaped composite dowels were performed to investigate the complex behaviour of these shear connectors (Lorenc, Kożuch, and Rowiński 2014a, b). Composite dowels are used in prefabricated steel-concrete composite beams made of steel T-elements and concrete top chords. They are not used in composite beams with profiled steel sheeting (Biegus and Lorenc 2014). The shape of the steel element allows for the transmission of shear between steel and reinforced concrete. The concrete top chord is concreted in the workshop and the residual top-layer of the concrete chord is added at the construction site. The stresses at the dowel is a sum of the stresses caused by global effects (bending moment) and the stresses caused by local effects (longitudinal shearing force) (Kożuch and Lorenc 2019).

Despite the fact that composite dowels have a lot of advantages, some of which have been listed above, they are not demountable. Similarly, shear studs welded to a steel beam flange and embedded in a concrete slab make the dismantling and deconstruction of composite beams nearly impossible. Composite beams should be easily deconstructed at the end of their service life, so that the building materials could be reused or recycled (Ataei et al. 2019). Demountable shear connectors allow for the dismantling of a composite beam at the end of its structural life. However, no design guidance for composite beams with demountable connections is currently available. For this reason, composite beams with this type of connection are the subject of many studies. Demountable bolted connections were tested in steel-concrete composite beams (Kozma et al. 2019).

Lam and Dai (2013), Dai, Lam and Saveri (2015), Lam et al. (2017) and Rehman et al. (2016 & 2018) were the ones who modified headed studs to create demountable shear connectors (see Fig 2.2a), which made it possible for steel beams to be reused without being

recycled. Lam et al. (2017) suggested using the methods available for headed studs in the Eurocode 4 (European Committee for Standardization 2004) and for bolts in the Eurocode 3 (European Committee for Standardization 2004) to predict the shear resistance of demountable shear connectors. Furthermore, the structural behaviour of a demountable composite floor system with modified headed studs was compared with the structural behaviour of a non-demountable composite floor system with conventional headed studs (Rehman et al. 2018). The composite floor systems consisted of composite slabs formed with steel profiled decking, steel beams and shear connectors. The load-bearing capacity of both composite floor systems was similar. However, the initial stiffness of the demountable composite floor system was lower than the one of the non-demountable composite floor system. The diameter of the pre-drilled holes in the steel beam flange was 1 mm larger than the diameter of the connector collar. The low initial stiffness could result from the clearance between the connector collar and the hole. Rehman et al. (2018) believe that the initial stiffness may be increased by tightening the connectors with a higher torque. After the tests, the moment capacity of the composite beam was calculated using two methods: the rectangular stress blocks method and the interpolation method. The results of the calculations were very close to the experimental results. For this reason, Rehman et al. (2018) suggested that the plastic flexural capacity of the demountable composite floor system with partial shear interaction might be calculated using simple design methods for welded headed studs and Eq. 6.1 from the Eurocode 4 (European Committee for Standardization 2004). What is more, Rehman et al. (2018) presented that the deflection of a composite beam with partial shear connection may be calculated using the formula below from the British Standard 5950-3.1 (British Standards Institution 2010):

$$\delta_\eta = \delta_c + 0.5(1 - \eta)(\delta_s - \delta_c) \tag{2.1}$$

where δ_s is the deflection of the steel beam acting alone, δ_c is the deflection of the composite beam with full shear connection and η is the degree of shear connection.

Moynihan and Allwood (2014) tested three steel-concrete composite beams with profiled steel sheeting and M20 Grade 8.8 bolts. 24 mm diameter holes were predrilled through the decking and the top flange of the steel beams. The bolts were fastened to the top flange of the steel beams using nuts and washers above and below the flange. The composite beams had a higher load bearing capacity than the one predicted using the Eurocode 4 (European Committee for Standardization 2004).

Lee and Bradford (2013), Liu et al. (2016) and Liu, Bradford and Ataei (2017) used high-strength friction-grip bolts as demountable shear connectors (see Fig. 2.2b). 24 mm diameter holes were used in the concrete slabs and in the top flanges of the steel beams. Lee and Bradford (2013) demonstrated that the load-slip curve of pre-tensioned bolted shear connectors had three regions: a region of "full interaction" (held by friction), a region of "zero interaction" (with slip equal to the clearance between the bolts and the surrounding concrete) and a region of "partial interaction" (where bolts start to bear onto the concrete). What is more, Liu, Bradford and Ataei (2017) proposed a steel-concrete composite beam consisting of

a steel beam, precast geopolymer concrete panels and high-strength friction-grip bolts. Chen et al. (2019) also presented a prefabricated steel-concrete composite beam and an advanced bolted connector, which consisted of an embedded corrugated pipe and a high-strength bolt.

Pavlović et al. (2013a, b) analysed steel-concrete composite elements with prefabricated concrete slabs. The composite action between the steel beam and the concrete slab was established by high strength bolts (see Fig. 2.2c). The construction costs of the bolts used as shear connectors were expected to be higher than those of welded studs. However, the total costs of the structure was expected to be lower due to this prefabrication of the concrete slabs and the reduction of construction time. Furthermore, Pavlović et al. (2013a, b) compared the structural behaviour of bolts in push-out tests with the structural behaviour of headed studs. The shear resistance and the stiffness of bolted shear connectors was 5% and 50% lower, respectively, than the shear resistance and the stiffness of the headed studs. What is more, the analysed bolted shear connections were classified as brittle. Hawkins (1987) also compared the shear resistance and the stiffness of bolted shear connectors and headed studs. He demonstrated that the resistance of non-preloaded anchor bolts was 20% lower than the shear resistance of headed studs and that the stiffness of non-preloaded anchor bolts was 85% lower than the stiffness of headed studs (Hawkins 1987).

Suwaed (2017) investigated two demountable shear connectors for precast steel-concrete composite structures, i.e., a locking nut shear connector and a friction based shear connector. They make it possible to replace concrete slabs in composite structures. In the steel-concrete composite bridge presented by Suwaed (2017), the precast concrete panels had several pockets to accommodate shear connectors.

In the case of locking nut shear connectors, high-strength steel bolts were fastened to a steel beam using a double nut configuration, i.e., a standard lower hexagonal nut and an upper conical nut. The upper conical nut prevented the bolt from slipping within the bolt hole. The slab pockets had the form of countersunk holes with two precast concrete plugs inside them. Each plug had a hole with a diameter that accommodated a bolt with 10 mm clearance, to improve slip capacity. A gap between the steel bolt and the concrete plug was filled with grout to ensure dowel action. The dimensions of the plug limited the risk of premature longitudinal shear failure and the risk of splitting in the concrete mass. A plate washer was used on the upper face of the concrete plug. The third nut was tightened before the grout hardened.

In the case of friction based shear connectors, friction resistance was created at the interface between the upper flange of the steel beam and the lower face of the concrete plug. High-strength steel bolts with retaining washers were positioned through the chamfered countersunk seat holes of the beam upper flange. The washers had radial gaps to ensure the penetration of grout into the clearances between the bolts and their holes in the steel beam, and to prevent sudden slip when friction resistance between the steel beam and the concrete slab was overcome. The pocket was the same as the one for the locking nut shear connectors. The concrete plug used in the friction based shear connectors did not have an enlargement in the lower part of the central hole that was created for locking nut shear connectors to accommodate a conical nut.

The locking nut shear connectors and the friction based shear connectors showed very high shear resistance and stiffness when compared to welded studs. The characteristic shear

resistance and the stiffness of the locking nut shear connector with an M16 bolt were 171 kN and 100 kN/mm, respectively, while the characteristic shear resistance and the stiffness of the friction based shear connector with an M16 bolt were 161 kN and 104 kN/mm, respectively. Furthermore, the shear connectors developed by Suwaed (2017) had large slip capacity (up to 14 mm for the locking nut shear connector and 16 mm for the friction based shear connector).

Kozma et al. (2019) presented two shear connection types: the cylinder system and the coupler system (see Fig. 2.2d). They suggested that demountable connectors should also be replaceable, because when thread damage occurs during transportation, the connectors may be replaced and the concrete slab is not lost. The cylinder system consisted of a pre-tensioned M20 Grade 8.8 bolt, and a steel cylinder welded to the L-profile and the top plate. The steel cylinder prevented the loss of pre-stress in through bolts caused by creep and shrinkage and it protected the concrete from any damage that might have occurred due to bearing. What is more, a pocket in the concrete slab ensured access to the bolt from the top of the slab. The coupler system consisted of a coupler, an embedded bolt and a removable bolt placed underneath the concrete slab. Two variants of the removable bolt were used: a pre-tensioned M20 Grade 8.8 bolt and a resin injected M20 Grade 8.8 bolt. The demountable and replaceable connectors behaved similarly to the demountable connectors tested by Lee and Bradford (2013). The initial stiffness of the connectors described by Kozma et al. (2019) was high (250–500 kN/mm for the cylinder system and 70–100 kN/mm for the coupler system) because of the pre-tensioning or the resin in the bolt holes. When the friction resistance had been overcome, the stiffness was reduced to a very small value (15 kN/mm for the cylinder system and 30 kN/mm for the coupler system). Kozma et al. (2019) observed a bearing and shear deformation and a brittle failure of the analysed systems. The demountable injected bolt-coupler system was also investigated in push-out tests by Sarri (2019).

Kwon, Engelhardt and Klingner (2010) evaluated the behaviour of 22 mm diameter post-installed shear connectors (double nut bolts, high-tension friction-grip bolts and adhesive anchors) under static and fatigue loading using the direct-shear test. The post-installed shear connectors exhibited a higher fatigue strength than welded shear studs. Kwon, Engelhardt and Klingner (2010) suggested a method for strengthening non-composite floor systems in existing bridges and buildings. According to this method, an already existing concrete slab and steel girders are joined together using bolted connectors, and act together as composite elements.

Song, Uy and Wang (2019) developed a finite element model of a stainless steel-concrete composite beam with M16 stainless steel bolts used as demountable shear connectors.

Demountable connectors, e.g., screws or high-strength bolts, have also been used in aluminium-timber composite structures, steel-timber composite structures and pultruded fibre reinforced polymer-concrete structures (Chybiński and Polus 2019) (Hassanieh, Valipour and Bradford 2016a) (Keipour 2018) (Etim et al. 2020).

a)

b)

c)

d)
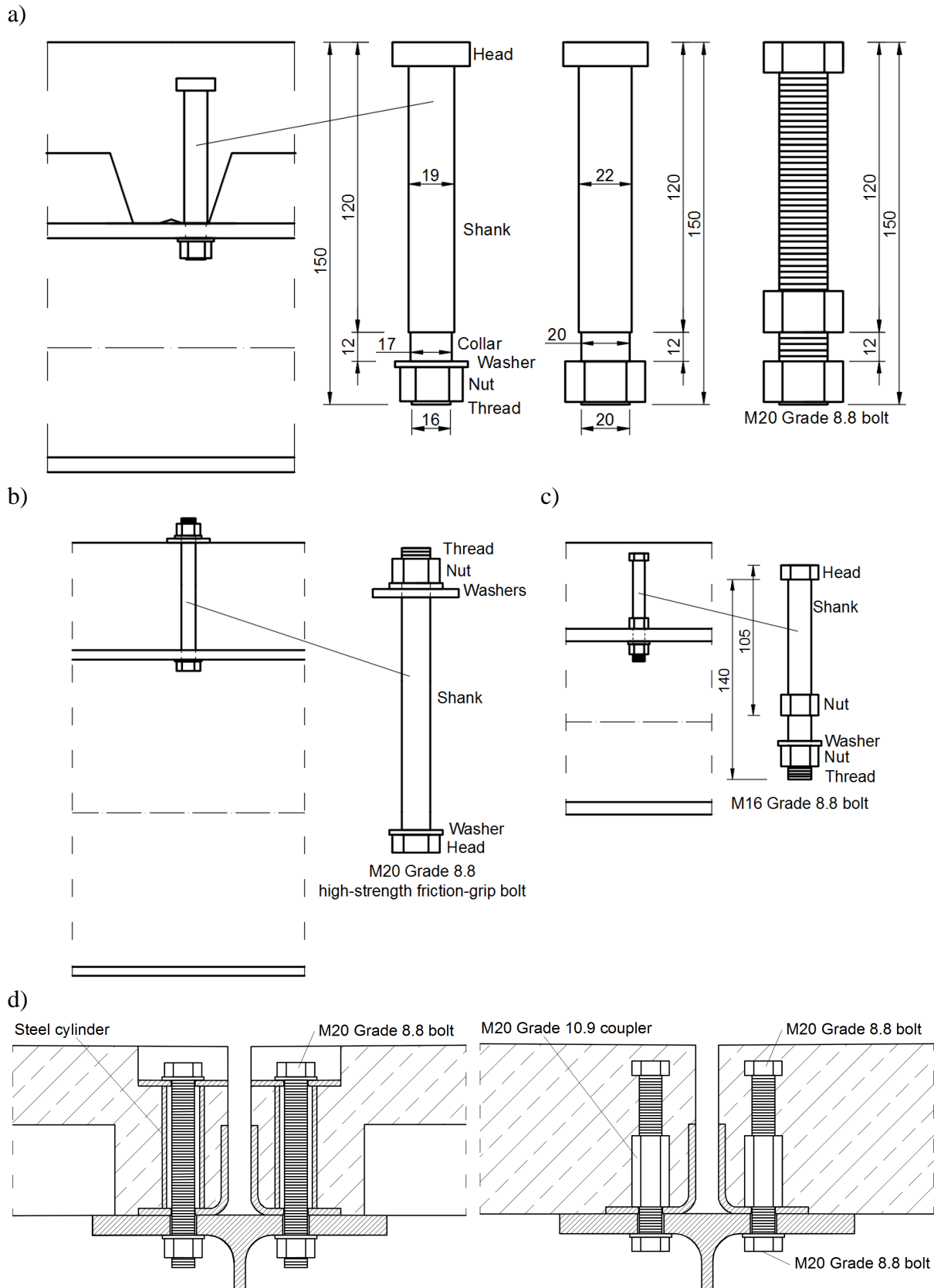
Figure 2.2. Demountable shear connectors: a) investigated by Lam et al. (2017), b) presented by Liu, Bradford and Ataei (2017), c) analysed by Pavlović et al. (2013a), d) developed by Kozma et al. (2019)

2.2. Shear connectors used in aluminium-concrete composite structures

Shear connectors ensure composite action between the aluminium beam and the concrete slab. Z-type elements and angles were used in aluminium-concrete composite bridges (Siwowski 2005) (see Fig. 2.3a). Aluminium-concrete composite beams with channel shear connectors were analysed by (Stonehewer 1962) and (Polus and Szumigała 2019b) (see Fig. 2.3b). Bolts were used in tests of aluminium-concrete composite beams conducted by (Bruzzese, Cappelli and Mazzolani 1989) (see Fig. 2.3c).
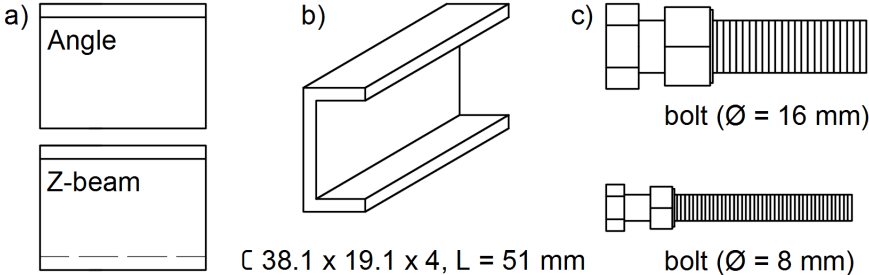
Figure 2.3. Shear connectors used in aluminium-concrete composite beams

2.3. A new shear connector for aluminium-concrete composite structures

A new type of shear connector was described in the patent specification defined with the application number 406833 and the publication number 232822 (see Fig. 2.4) (Polus and Szumigała 2014a). The inventors filed the patent application with the Polish Patent Office on 13 January 2014. After the patent prosecution, the patent was granted on 31 July 2019. The aforementioned connector consists of a head, a shank, a flange (collar) and a threaded ending (Polus and Szumigała 2016).
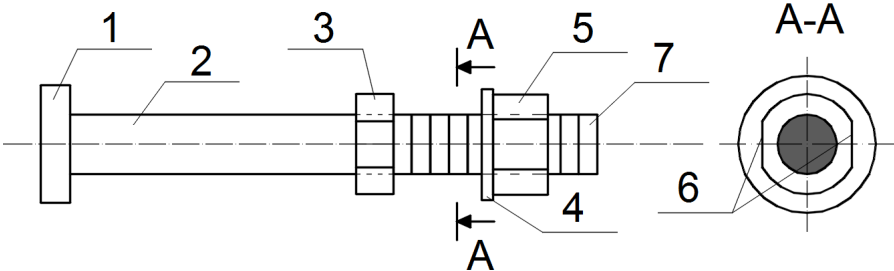
Figure 2.4. Shear connector for aluminium-concrete composite beams: 1 – head, 2 – shank, 3 – flange, 4 – washer, 5 – nut, 6 – chamfer, 7 – thread (Polus and Szumigała 2014a)

Due to the fact that it is composed of two parts – a stud and a bolt – it can be referred to as the dowel-bolt connector. One part of the connector (the head, the shank and the flange) is embedded in the concrete slab. The second part is fasten to the flange of the aluminium beam with nuts. The head facilitates the cooperation between the connector and the concrete in the slab. The shape of the flange makes it possible to use a wrench to hold the connector while the

nuts are being tightened. The connector may be used in aluminium-concrete composite beams with profiled sheeting. The steel profiled decking may be fastened to the top of the aluminium beam by the flange of the connector. The dowel-bolt connector makes it possible to separate the aluminium beam from the concrete slab once the design life of the structure is over. In accordance with the principles of sustainable development, new solutions should be easy to demount. After demounting, the materials may be reused or recycled. In addition, composite action is achieved without welding, which causes the formation of heat affected zones and the reduction of strength parameters of aluminium alloys. What is more, parts of different materials (aluminium, steel, concrete) are connected in a simple way. Demountable shear connectors can be easily installed on the construction site in the predrilled flange of the aluminium beam and the profiled steel sheeting, while the concrete can be poured into the steel sheeting. On the other hand, the concrete slab can be prefabricated off-site, with the dowel-bolt connectors cast in required locations, and then transported to the site and connected to the aluminium beam with predrilled holes. This solution is similar to that presented by Pavlović et al. (2014) and Pavlović and Veljković (2017), in which bolts are cast in prefabricated concrete slabs and connected on site to the predrilled top flange of the steel beam. Demountable dowel-bolt connectors may be used in aluminium-concrete composite beams as an environmentally-friendly alternative to channel shear connectors, or bolts with nuts, threads and shanks embedded in concrete slabs (see Fig. 2.3). They make it possible to reuse the aluminium beam after dismantling. Furthermore, the concrete from the composite beam may be recycled by crushing the concrete slabs and using the rubble as recycled aggregate in new structures (Major M. and Major I. 2015).

In order to develop the prototypes of the connectors, headed studs (Köster & Co. 2005) were modified: the screw was cut and the flange was welded to the shank (see Fig. 2.5). The flange was made of a nut.

Figure 2.5. Prototypes of the shear connectors for aluminium-concrete composite beams

The composite action of aluminium-concrete elements

3.1. The theoretical analysis of the dowel-bolt connector used in aluminium-concrete composite structures

Dowel-bolt connectors were used by the present author to join aluminium beams with concrete slabs. The information about their stiffness is important to evaluate the behaviour of aluminium-concrete composite beams. A shear force-slip curve determined in a push-out test is non-linear. Furthermore, it may be used in the finite element model of a composite beam, where connectors are modelled as zero-length springs. Despite the fact that it is a simplistic method based on discrete shear connections, it can provide reasonable accuracy (Hassanieh, Valipour, and Bradford 2016b). Non-linear discrete springs are deformable connections used to capture the shear-slip between the layers (Khorsandnia et al. 2014). For example, this method was used in the finite element models by Queiroza, Vellascob, and Nethercot (2007), Kyvelou, Gardner and Nethercot (2018), Studziński and Ciesielczyk (2019), and by Polus and Szumigała (2019d).

Sometimes, the linear response of the connector is used as a simplification, e.g., in the analytical models of aluminium-concrete or timber-concrete composite beams (Polus and Szumigała 2019b) (Łukaszewska 2009). The stiffness of connections is often described using the slip moduli $k_{0.4}$ and $k_{0.6}$. The moduli are determined for the loads equal to 40% and 60% of the estimated load-carrying capacity, respectively. When the non-linear shear force-slip relation is unknown, the stiffness of the connector is usually determined using an approximate method, in which the connector is assumed to act as a beam (Ismail et al. 2012).

The behaviour of connectors is often described using an elasto-plastic model (Van der Linden 1999). This model was also proposed for the dowel-bolt connector. The shear force-slip relation was linear elastic up to the load-bearing capacity of the connector and from that point on it was ideal plastic (see Fig. 3.1). The stiffness of the connector (k) was determined from the beam model (Polus and Szumigała 2019a). In the aluminium-concrete composite beam, one part of the connector is embedded in the concrete slab and one is fasten to the flange of the aluminium beam with nuts. The embedded part of the connector works like a cantilever beam subjected to bending (see Fig. 3.2).
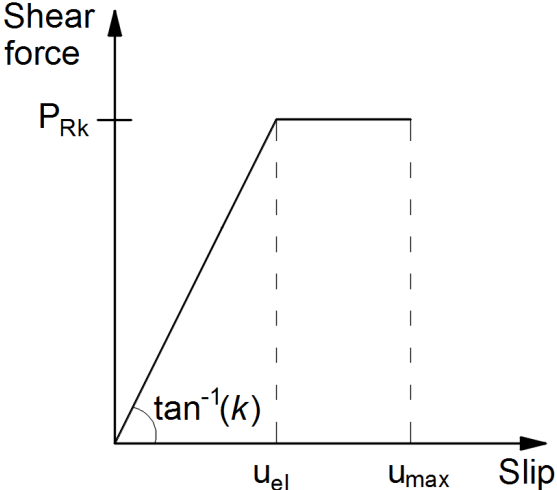
Figure 3.1. The elasto-plastic theoretical model for the dowel-bolt connector
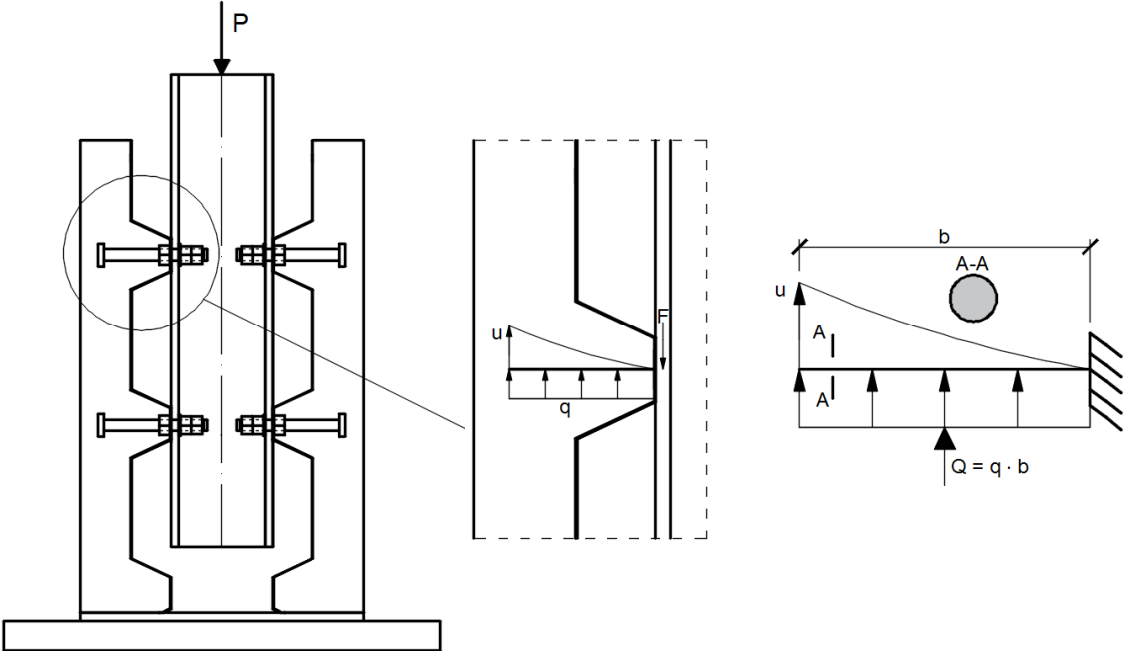
Figure 3.2. The beam model of the connector

The deflection of the beam (u) presented in Fig. 3.2. may be calculated as follows:

$$u = \frac{Qb^3}{8EI} \tag{3.1}$$

$$Q = q \cdot b \tag{3.2}$$

$$I = \frac{\pi d^4}{64} \tag{3.3}$$

where Q is the resultant of the uniformly distributed load (q), b is the part of the connector embedded in the concrete slab, d is the diameter of the connector, I is the moment of inertia of the connector cross-section and E is the Young's modulus of the material of which the connector was made.

The connector stiffness may be calculated as:

$$k = \frac{Q}{u} \tag{3.4}$$

By combining Eqs. (3.1) and (3.3) one obtains:

$$k = \frac{\pi E d^4}{8b^3} \tag{3.5}$$

Eq. (3.5) demonstrates that the stiffness of the connector depends on its diameter, the Young's modulus of the material of which it is made, and on the length of the connector embedded in the concrete slab. The beam model can be further developed, as there are other parameters which can have an impact on the stiffness of shear connections. Pavlović et al. (2013a) demonstrated that connector-to-hole clearances influence the stiffness of shear connections. Kozma et al. (2019) showed that the pre-tensioning of connectors increases their initial stiffness. Leskelä (2017) presented that the shear stiffness of the connection is smaller in composite beams with profiled steel sheeting than in composite beams with solid concrete slabs. Furthermore, Leskelä (2017) showed that the shear stiffness of connections also depends on the Young's modulus of concrete. However, Li and Cederwall (1996) proved that the strength of concrete has no impact on connector stiffness. The strength of concrete has the greatest impact on the load-carrying capacity of the connector. The push-out tests done by Li and Cederwall (1996) showed a 34% increase in the maximum shear load upon replacing normal strength concrete with high strength concrete. However, the tests also showed that the amount of slip at the maximum load was the same for specimens using both types of concrete. What is more, the shear force-slip curves for all specimens were overlapping for as long as the elastic load was applied. For this reason, the strength of concrete does not have an impact on the slip moduli of the connectors.

No design guidelines for demountable connectors are currently available. For this reason, the methods available for headed shear connectors and bolts are used to predict the shear capacity of demountable connectors.

The design resistance of the demountable connector for aluminium-concrete composite structures ($P_{Rd,Ec}$) may be calculated using the following formulas presented in the Eurocode 3 (European Committee for Standardization 2005), Eurocode 4 (European Committee for Standardization 2004) and Eurocode 9 (European Committee for Standardization 2007).

$$P_{Rd,EC} = min\left(\frac{0.8k_t f_u A_{sc}}{\gamma_v} , \frac{k_t 0.29\alpha\beta d^2 \sqrt{f_{ck} E_{cm}}}{\gamma_v} , \frac{\alpha_v f_u A}{\gamma_{M2}} , \frac{k_1 \alpha_b f_{uf} dt}{\gamma_{M2}} \right) \qquad (3.6)$$

$$k_t = \frac{0.7}{\sqrt{n_r}} \frac{b_0}{h_p} \left(\frac{h_e}{h_p} - 1 \right) \qquad (3.7)$$

where A_{sc} is the cross-sectional area of the connector, f_u is the ultimate strength of the steel used in the shear connector, h_e is the height of the section of the connector embedded in the concrete slab, d is the diameter of the connector, γ_v is the partial factor, k_t is the reduction factor (it cannot be greater than the value of $k_{t,max}$ given in the Eurocode 4), α is the coefficient and is equal to 1.0 for $h_e/d > 4$, and $0.2(h_e/d + 1)$ for $3 \leq h_e/d \leq 4$; f_{ck} and E_{cm} are the cylindrical compressive strength and the mean secant modulus of concrete, n_r is the number of connectors in one rib at the beam intersection, b_0 is the width of a concrete rib, h_p is the overall depth of the profiled steel sheeting, and β is the coefficient recommended by (Nie, Cai and Wang 2005), α_v is the coefficient from the Eurocode 3, A is the tensile stress area of the connector or the gross cross-section area of the connector, γ_{M2} is the partial safety factor, f_{uf} is the ultimate strength of the aluminium in the beam flange, and k_1, α_b are the coefficients from the Eurocode 9.

The coefficient β recommended by (Nie, Cai and Wang 2005) was added to Eq. (3.6). It should be used when the transverse spacing of the connectors (s_t) is smaller than $4d$ and is calculated using the following formula:

$$\beta = 0.95 s_t / 4d \qquad (3.8)$$

The American Institute of Steel Construction (2016) specifies the design strength of a headed stud shear connector ($P_{Rd,AISC}$) as Eq. (3.9):

$$P_{Rd,AISC} = min\left(R_g R_p f_u A_{sc}, 0.5 A_{sc} \sqrt{f_{ck} E_{cm}} \right) \qquad (3.9)$$

where R_g and R_p are reduction factors.

However, Rehman et al. (2016) demonstrated that the Specification for Structural Steel Buildings (American Institute of Steel Construction 2016) overestimated the shear resistance of demountable shear connectors. Ellobody and Young (2006) also proved that the design rules specified in the American specification overestimated the capacity of the shear connection in a composite beam with profiled steel sheeting. For this reason, the author of the dissertation used the aforementioned Eurocodes to predict the shear capacity of the analysed connector.

3.2. The theoretical analysis of the aluminium-concrete composite beam

Composite beams with profiled sheeting are often partial composite beams, because the number of shear connectors is insufficient to ensure full composite action (shear connectors may only be placed in the ribs of the profiled sheeting) (Nie, Cai and Wang 2005). The problem of slipping is inherent in partial composite beams. It has an impact on the bending stiffness (Pengzhen 2014) and the elastic and plastic flexural capacities of composite beams. Partial composite beams fail as a result of the shear connection failure (Stark 1989). The ultimate load of the partial composite beam depends on number of shear connectors and the type of shear connectors, i.e., ductile or non-ductile shear connectors.

3.2.1. The effective stiffness of the aluminium-concrete composite beam with partial shear interaction

The slip reduces the stiffness of composite beams (Nie and Cai 2003) (Nie, Cai and Wang (2005) (Jarek and Radoń 2009) (Kisała and Furtak 2016). The author of this dissertation suggests calculating the effective stiffness of the aluminium-concrete composite beam with partial shear interaction using the model for the steel-concrete composite beam with partial shear interaction presented by Nie and Cai (2003) and Nie, Cai and Wang (2005) (see Fig. 3.3). The following assumptions were made:
- ❖ the beam is simply supported,
- ❖ the shear stress at the interface is proportional to the slip,
- ❖ the aluminium girder and the concrete slab have the same curvature,
- ❖ the profiled sheeting is not taken into account when calculating stiffness.
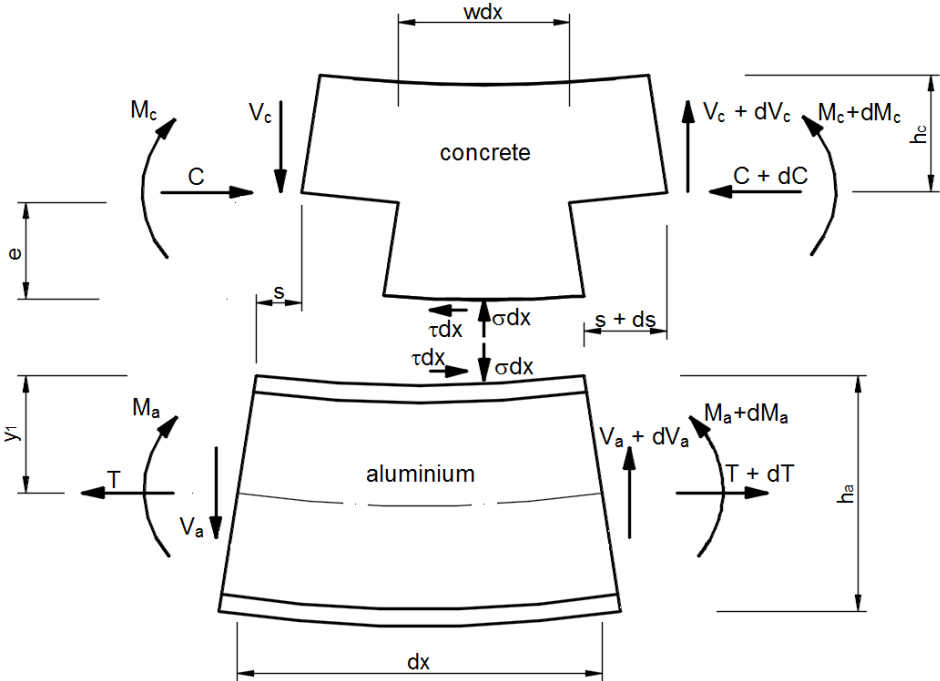
Figure 3.3. Deformation of finite length (Nie and Cai 2003) (Nie, Cai and Wang 2005)

The effective stiffness of the aluminium-concrete composite beam with partial shear interaction may be calculated using the following formulas:

$$(EI)_{eff} = \frac{(EI)_e}{(1 + \xi_s)} \tag{3.10}$$

$$(EI)_e = (EI)_1 w_{rw} + (EI)_2 (1 - w_{rw}) \tag{3.11}$$

where $(EI)_e$ is the weighted mean stiffness of the transformed section of the composite beam, ξ_s is the parameter for the slip effect, $(EI)_1$ is the stiffness of the transformed section of cross-section 1-1 (see Fig. 3.3), $(EI)_2$ is the stiffness of the transformed section of cross-section 2-2 (see Fig. 3.3), and w_{rw} is the ratio of the mean width of the rib (w_r) to the width of one wavelength of the profiled sheeting (w_w) (see Fig. 3.4).
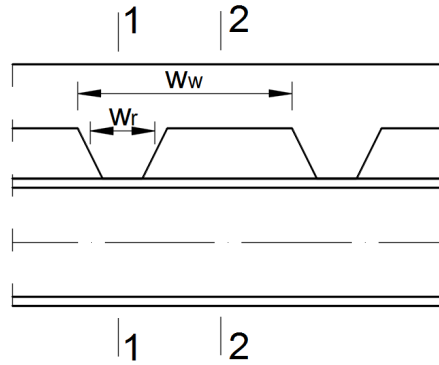
Figure 3.4. The cross-sections $(1 - 1, 2 - 2)$ of the aluminium-concrete composite beam

The parameter for the slip effect may be calculated using the following formulas, proposed by (Nie and Cai 2003) for a two-point load:

$$\xi_s = \eta_c \left[\frac{0.5 - b_1/L - e^{-\alpha_1 L(b_1/L)}/(\alpha_1 L)}{4\left(2(0.5 - b_1/L)^3 + 3(0.5 - b_1/L)(1 - b_1/L)b_1/L\right)} \right] \tag{3.12}$$

$$\eta_c = 24(EI)_e \beta_1 / (L^2 h) \tag{3.13}$$

$$d_c = (h_c + e_p) / 2 + y_1 \tag{3.14}$$

$$\alpha_1 = \sqrt{\frac{K}{E_a I_0 A_1 p}} \tag{3.15}$$

$$\beta_1 = \frac{A_1 d_c p}{K} \tag{3.16}$$

$$A_1 = \frac{A_0}{d_c\left[d_c + \frac{I_c}{2I_2}e_p(1-w_{rw})\right]A_0 + I_0} \tag{3.17}$$

$$A_0 = \frac{A_a A_c}{nA_a + A_c} \tag{3.18}$$

$$I_0 = I_a + I_c / n \tag{3.19}$$

$$I_c = \frac{I_1 I_2}{(1-w_{rw})I_1 + w_{rw}I_2} \tag{3.20}$$

$$A_c = \frac{1}{\frac{w_{rw}}{A_{c1}} + \frac{(1-w_{rw})}{A_{c2}}} \tag{3.21}$$

where L is the span length, b_1 is the distance between one of the two loading points and the middle of the beam, h is the depth of the entire section, h_c is the thickness of the concrete slab in a section where there is no rib, e_p is the height of the profiled sheeting, y_1 is the distance from the top of the aluminium girder to its neutral axis, p is the longitudinal spacing of shear connectors, n is the modular ratio ($n = E_a / E_c$), A_a is the area of aluminium section, A_c is the equivalent concrete area, A_{c1} is the area of the concrete slab section with the rib, A_{c2} is the area of the concrete slab section without the rib, I_a is the moment of inertia of aluminium, I_c is the moment of inertia of concrete, I_1 is the moment of inertia of the concrete slab section with the rib, I_2 is the moment of inertia of the concrete slab section without the rib, K is the shear stiffness of the connector.

The effective stiffness of the aluminium-concrete composite beam with partial shear interaction has an impact on deflection (Nie and Cai 2003):

$$f = \frac{P}{12(EI)_{eff}}\left[2\left(\frac{L}{2}-b_1\right)^3 + 3b_1\left(\frac{L}{2}-b_1\right)(L-b_1)\right] \tag{3.22}$$

where P is the total load.

3.2.2. The elastic flexural capacity of the aluminium-concrete composite beam with partial shear interaction

Slip reduces the elastic flexural capacity of composite beams. The elastic flexural capacity corresponds to the first yielding of the extreme fibre of the cross-section. The author of this dissertation proposes to calculate the elastic flexural capacity of the aluminium-concrete composite beam with partial shear interaction using the calculation model for the steel-

concrete composite beam with partial shear interaction presented by Nie and Cai (2003) and Nie, Cai and Wang (2005). It may be calculated as follows:

$$M_{y,Rk} = \zeta M_{el} \tag{3.20}$$

$$\zeta = 1 - \frac{h_a E_a}{6(EI)_e} \xi_s \left(2A_{ft} + A_w\right)\left(2e_p + h\right) \tag{3.21}$$

where M_{el} is the elastic flexural capacity not taking into account the slip effect, h_a is the height of the aluminium beam, E_a is the Young's modulus of aluminium, A_{ft} is the area of the top flange of the aluminium beam, A_w is the area of the web of the aluminium beam.

3.2.3. The plastic flexural capacity of the aluminium-concrete composite beam with partial shear interaction

Slip reduces the plastic flexural capacity of composite beams. Because of the slip, a composite beam has two plastic neutral axes. The author of this dissertation proposes to calculate the plastic flexural capacity of the aluminium-concrete composite beam with partial shear interaction using the calculation model for the steel-concrete composite beam with partial shear interaction presented by Nie and Cai (2003) and Nie, Cai and Wang (2005). The reinforcement, the profiled sheeting and the concrete in the ribs were not taken into account in the bending capacity calculations. The plastic flexural capacity of the aluminium-concrete composite beam with partial shear interaction depends on the location of the plastic neutral axis of the aluminium beam.

a) Case 1 (the plastic neutral axis of the aluminium beam was located in its flange)

From section equilibrium (see Fig. 3.5):

$$N_{at} = N_{ac} + F_c \tag{3.22}$$

$$M_{ult} = N_{at}(d_1 - \frac{a}{2}) + F_c(h_c - \frac{x_c}{2} + h_p + \frac{a}{2}) \tag{3.23}$$

$$N_{at} = A_a f_y \tag{3.24}$$

$$F_c = f_c b_{eff} x_c = n_d P_{ult} \tag{3.25}$$

$$N_{ac} = 2ab_f f_y \tag{3.26}$$

where d_1 is the distance between the neutral axis of the aluminium beam and its top, a is the height of aluminium subjected to compression, N_{at} is the tensile force capacity of the entire

aluminium section, N_{ac} is the double compression force of aluminium, F_c is the compression force of concrete equal to the shear force supplied by all the connectors, A_a is the cross section area of the aluminium beam, f_y is the yield strength of aluminium, b_{eff} is the effective width of the composite slab, b_f is the width of the top flange, n_d is the number of connectors in the shear span, P_{ult} is the shear capacity of a connector accounting for the effect of the profiled sheeting and connector spacing, x_c is the height of compressive concrete, f_c is the cylinder compressive strength of concrete.

From Eqs. (3.22)–(3.26),

$$M_{ult} = \frac{A_a f_y}{4b_f}(4b_f d_1 - A_a + \frac{2F_c}{f_y}) + F_c(h_c + h_p) - F_c^2(\frac{1}{2f_c b_{eff}} + \frac{1}{4f_y b_f}) \tag{3.27}$$
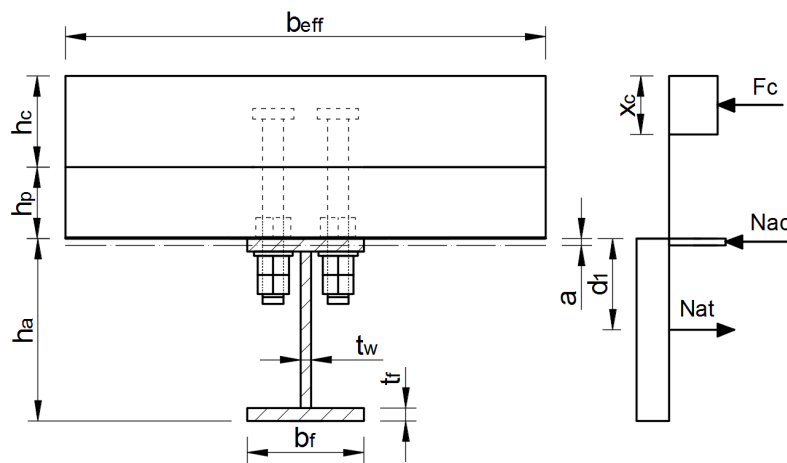
Figure 3.5. The model for calculating the plastic flexural capacity of the aluminium-concrete composite beam with partial shear interaction (the plastic neutral axis of the aluminium beam is located in its flange)

b) Case 2 (the plastic neutral axis of the aluminium beam was located in its web)

From section equilibrium (see Fig. 3.6):

$$M_{ult} = N_{ac}'\left(d_1 - t_f - \frac{a'}{2}\right) + 2f_y A_{ft}\left(d_1 - \frac{t_f}{2}\right) + F_c\left(h_c + h_p - \frac{x_c}{2} + d_1\right) \tag{3.28}$$

$$N_{ac}' = N_{at} - F_c - 2f_y A_{ft} \tag{3.29}$$

$$N_{ac}' = 2f_y t_w a' \tag{3.30}$$

where N_{ac}' is the double compression force in the web, t_f is the thickness of the aluminium flange, a' is the height of the web subjected to compression, t_w is the thickness of the aluminium web.

N_{at} and F_c are calculated using Eqs. (3.24) and (3.25).

From Eqs. (3.24), (3.25) and (3.28)–(3.30),

$$M_{ult} = M_a + (h_c + h_p + d_1)F_c - \left(\frac{1}{4f_y t_w} + \frac{1}{2f_c b_{eff}} \right) F_c^2 \tag{3.31}$$

where M_a is the ultimate flexural capacity of the aluminium beam.
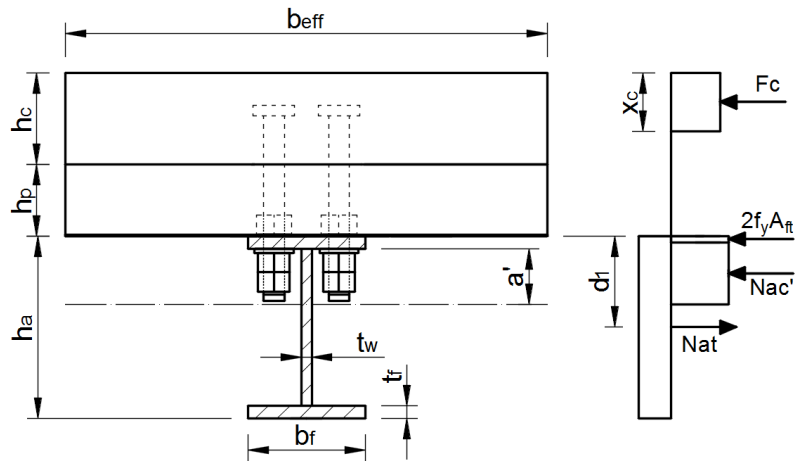
Figure 3.6. The model for calculating the plastic flexural capacity of the aluminium-concrete composite beam with partial shear interaction (the plastic neutral axis of the aluminium beam was located in its web)

For simplification, the plastic flexural capacity of the aluminium-concrete composite beam with partial shear interaction may be calculated using the following formula from the Eurocode 4 (European Committee for Standardization 2004):

$$M_{ult} = M_a + (M_{pl} - M_a)\eta \tag{3.32}$$

where M_{pl} is the ultimate flexural capacity of the full composite beam and η is the degree of composite action.

Mandara and Mazzolani (1997) pointed out that the stress block method presented in Figs. 3.5 and 3.6 may lead to overestimating the load-bearing capacity of the aluminium-concrete composite beams due to the limited ductility of both concrete and aluminium alloys. In aluminium alloys which are not ductile enough, premature collapse of the section may occur due to excessive strain. For this reason, designers should evaluate the deformation limits of the aluminium alloy which they intend to use in aluminium-concrete composite beams. Mandara and Mazzolani (1997) presented a method for designing aluminium-concrete composite beams in which the limit values of strains were applied.

David and Meyerhof (1958) developed a method for calculating stresses in metal-concrete composite beams that result from shrinkage, creep and thermal expansion or contraction. They presented expressions for calculating the stresses at the interface between the concrete slab and the metal beam. Furtak (2017) analysed the impact of concrete shrinkage on the deflection of the aluminium-concrete composite beam and pointed out that the curvature of

aluminium concrete beams depends not only on the Young's moduli but also on the geometrical characteristics of the cross-sections.

Stonehewer (1962) calculated the stresses at the slab-beam interface in the aluminium-concrete composite beam (ACC) and the steel-concrete composite (STC) beam. The composite beams were made from identical concrete slabs and from I-beams having identical cross-sections, presented in Figure 1.8. The stresses at the slab-beam interface for the composite beams mentioned above are presented in Table 3.1.

Table 3.1. Stresses at the slab-beam interface in composite beams (Stonehewer 1962)

Effect	STC beam		ACC beam	
	Stress in the beam [MPa]	Stress in the slab [MPa]	Stress in the beam [MPa]	Stress in the slab [MPa]
Thermal Contraction (100°F temperature change)	39.3	2.3	48.3	4.6
Creep	26.2	1.5	10.3	1.0
Shrinkage	13.1	0.8	4.8	0.5

The above table indicates that thermal effects are not negligible. However, they are relieved by the Young's modulus of aluminium which is three times lower than that of steel. Nevertheless, the effects of the different values of the thermal expansion coefficient, and the influence of concrete shrinkage and creep on the load-bearing capacity of the aluminium-concrete composite beam still require further analysis.

Materials and methods

The experimental work consisted of three main groups of tests:

- ❖ materials tests,
- ❖ shear connection tests,
- ❖ bending tests.

Aluminium-concrete composite elements consisted of: concrete slabs made of C50/60 concrete (beams) or C30/37 concrete (models of joints), 0.7 mm-thick T55P profiled sheeting made of S320GD steel, shear connectors made of S235J2 steel, reinforcing meshes made of 6 mm round bars (S235JRG2 steel), and aluminium beams made of AW-6060 T6 alloy. Aluminium-concrete composite elements were made of several different materials. The mechanical properties of each material were investigated in the materials tests. The behaviour of aluminium-concrete composite elements was investigated in the shear connection tests and the bending tests.

4.1. The materials test programmes

The tests of materials were conducted both on the metals and the concrete.

The tensile tests of the metals were carried out in an Instron Satec testing machine (Instron, Grove City, PA) at room temperature and according to the EN ISO 6892-1 standard (European Committee for Standardization 2009 and 2016). The maximum machine capacity was 300 kN. The uniaxial tensile tests were divided into four groups.

In the first group, the ultimate strength, the Young's modulus and the 0.2% proof strength of the AW-6060 T6 aluminium alloy were determined. The tensile tests were carried out using four flat samples and an extensometer (Epsilon, Jackson, WY, USA) with a 50 mm gauge (see Figs. 4.1a, 4.1b and 4.1d). The initial stress rate $\dot{R}$ of 2.0 MPa/s was used up to 0.2% of the nominal elongation (in the elastic range). In the plastic range, the strain rate $\dot{e} = 0.03$ mm/s was used. The samples were prepared in accordance with the rules presented in the EN ISO 6892-1 standard (European Committee for Standardization 2009 and 2016). The samples were cut out from the web of the I-beam using waterjet cutting to limit the influence of heat on the strength parameters of the aluminium alloy. In the tensile tests, the tensile direction was parallel to the direction of extrusion (0°), because in the bending tests of the composite beams the aluminium beams were subjected to tension and the tensile direction was also parallel to the direction of extrusion. The tensile strength depends on the tensile direction, i.e., the ultimate tensile strength is higher in the 0° direction than in the 45° or 90° directions (Snilsberg et al. 2010).

a)
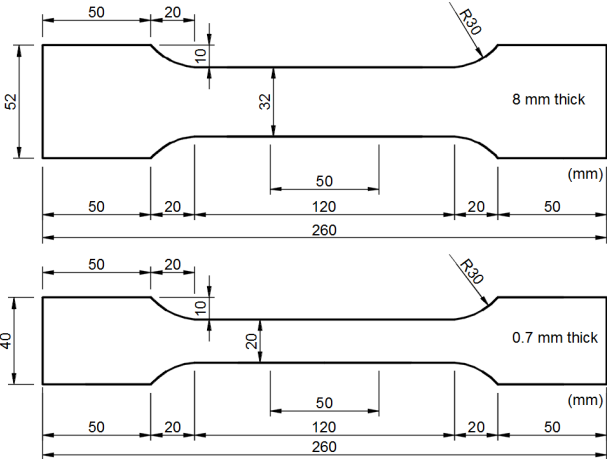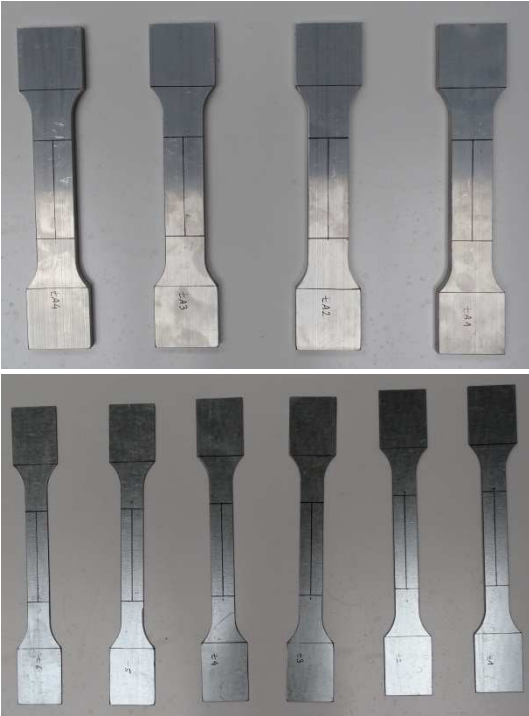
b)   c)
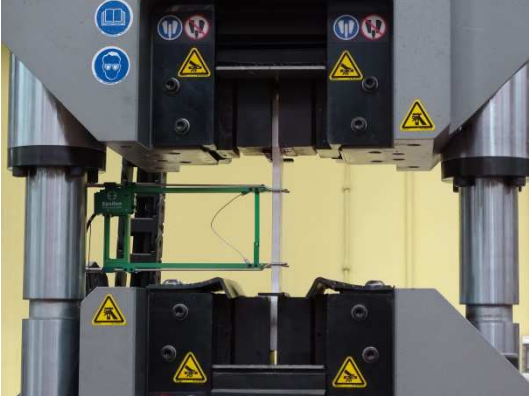
d)   e)

Figure 4.1. Metal specimens: a) the geometry of the flat samples; b) flat samples; c) round samples; d) tensile test on the flat sample; e) tensile test on the round sample

In the second group, the ultimate strength, the Young's modulus and the yield strength of the S320GD steel were determined. The tensile tests were carried out using six flat samples and an extensometer (Epsilon, Jackson, WY, USA) with a 50 mm gauge (see Figs. 4.1a and 4.1b). The initial stress rate $\dot{R}$ of 2.0 MPa/s was used up to 0.2% of the nominal elongation (in the elastic range). In the plastic range, the strain rate $\dot{e}$ = 0.35 mm/s was used. The samples were cut out from the sheet using waterjet cutting to limit the influence of heat on the strength parameters of the steel.

In the third group, the ultimate strength, the Young's modulus and the 0.2% proof strength of the S235J2 steel were determined. The tensile tests were carried out using three round samples (φ = 19 mm, l = 190 mm) and an extensometer (Instron, HighWycombe, Buckinghamshire, UK) with a 50 mm gauge (see Fig. 4.1c). The author used 19 mm headed studs (Köster & Co. 2005) made of the same steel as the 16 mm headed studs from the shear and bending tests. The 16 mm headed studs (l = 150 mm) were too short to be properly fixed in the clamps of the testing machine and there was a slip in the initial part of the stress-strain curve. For this reason, the longer samples were used. The heads of the studs were cut off to prepare round samples. The initial stress rate $\dot{R}$ of 6.0 MPa/s was used up to 0.2% of the nominal elongation (in the elastic range). In the plastic range, the strain rate $\dot{e}$ = 0.5 mm/s was used.

In the fourth group, the ultimate strength, the Young's modulus and the 0.2% proof strength of the S235JRG2 steel were determined. The tensile tests were carried out using five round samples (φ = 6 mm, l = 300 mm) and an extensometer (Instron, HighWycombe, Buckinghamshire, UK) with a 50 mm gauge (see Figs. 4.1c and 4.1e). The initial stress rate $\dot{R}$ of 6.0 MPa/s was used up to 0.2% of the nominal elongation (in the elastic range). In the plastic range, the strain rate $\dot{e}$ = 0.5 mm/s was used.

The mechanical properties of the concrete elements were obtained from the tests according to the EN 12390-3, EN 12390-6 and EN 12390-13 standards (European Committee for Standardization 2011 and 2013).

The strength parameters of the concrete used in the aluminium-concrete composite joints were obtained from the cubic (150 × 150 × 150 mm) concrete specimens (see Figs. 4.2a–c). The concrete compression machine Matest CO89-10 (Matest, Treviolo, Italy), with capacity equal to 3000 kN, was used. The stress rate was equal to 0.6 MPa/s. The concrete mixture consisted of cement (CEM I 42.5 R), fly ash, gravel (2–8 mm and 8–16 mm), sand (0–2 mm), water and plasticizer. The compressive cubic strength $f_{c,cube}$ was evaluated on the basis of 4 cubic specimens in accordance with the EN 12390-3 standard (European Committee for Standardization 2011) and 28 days after the casting of the joint samples. The compression test was repeated using 12 cubic specimens 70 days after the casting to evaluate the strength of the concrete during the shear connection tests.

The strength parameters of the concrete used in the aluminium-concrete composite beams were obtained from the cubic (150 × 150 × 150 mm) and cylindrical (φ = 150 mm, l = 300 mm) concrete specimens (see Fig. 4.2d). The concrete mixture consisted of sand (0–2 mm), gravel (2–8 mm), cement (CEM III/A 42.5N-HSR) and water. The compressive cubic strength $f_{c,cube}$ was evaluated on the basis of 4 specimens in accordance with the EN 12390-3 standard (European Committee for Standardization 2011) and 28 days after the beam casting (Zieliński 2010). The concrete compression machine Matest CO89-10 (Matest, Treviolo, Italy) was

used. The stress rate was 0.6 MPa/s. The compressive cubic strength $f_{c,cube}$ was also evaluated on the basis of 8 specimens, 196 days after the casting.

a)

b)

c)

d)
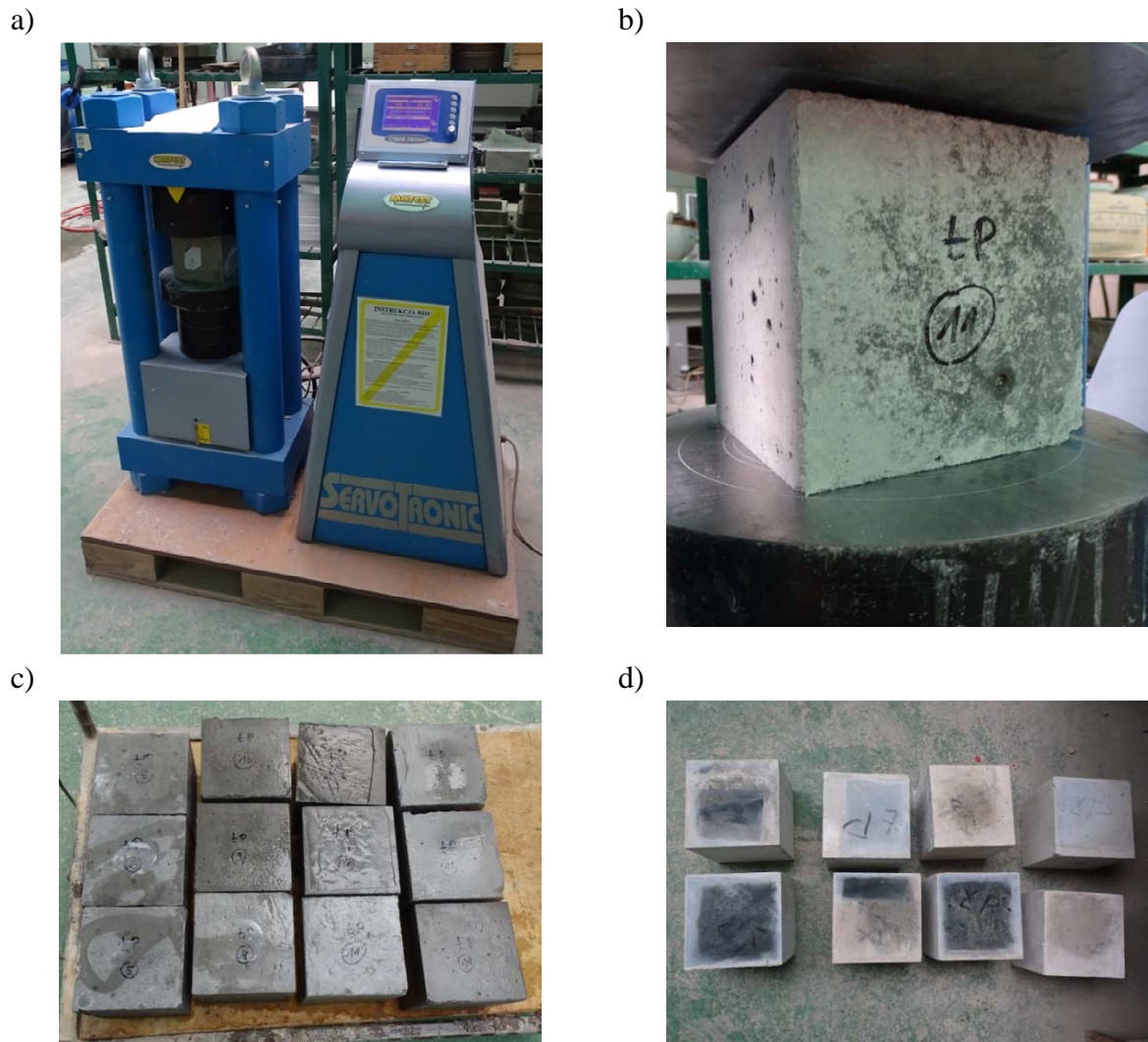
Figure 4.2. Cubic concrete specimens: a) compressive test on the cubic sample
b) cubic sample, c) C30/37 concrete samples d) C50/60 concrete samples

The tensile splitting strength f_{ct} was tested using 3 cylindrical specimens, 269 days after the casting, in accordance with the EN 12390-6 standard (European Committee for Standardization 2011) (see Figs. 4.3a and 4.3b). An Instron 8505 Plus test machine (Instron, HighWycombe, Buckinghamshire, UK) and hardboard strips were used in the test. The stress rate was equal to 0.05 MPa/s. The compressive cylinder strength f_c was evaluated on the basis of 5 specimens and in accordance with the rules presented in the EN 12390-3 standard (European Committee for Standardization 2011), 274 days after casting (see Fig. 4.3c). A stress rate of 0.6 MPa/s was used.

The initial and the stabilized secant moduli of elasticity of the concrete were tested using 4 cylindrical specimens, 314 days after the casting in accordance with method A described in the EN 12390-13 standard (European Committee for Standardization 2011 and 2013) (see Figs. 4.3d–f). The value of the compressive strength of concrete (f_c) obtained in the previous

tests was used to determine the nominal upper stress σ_a, the nominal lower stress σ_b and the preload stress σ_p.

a)

b)

c)

d)

e)

f)
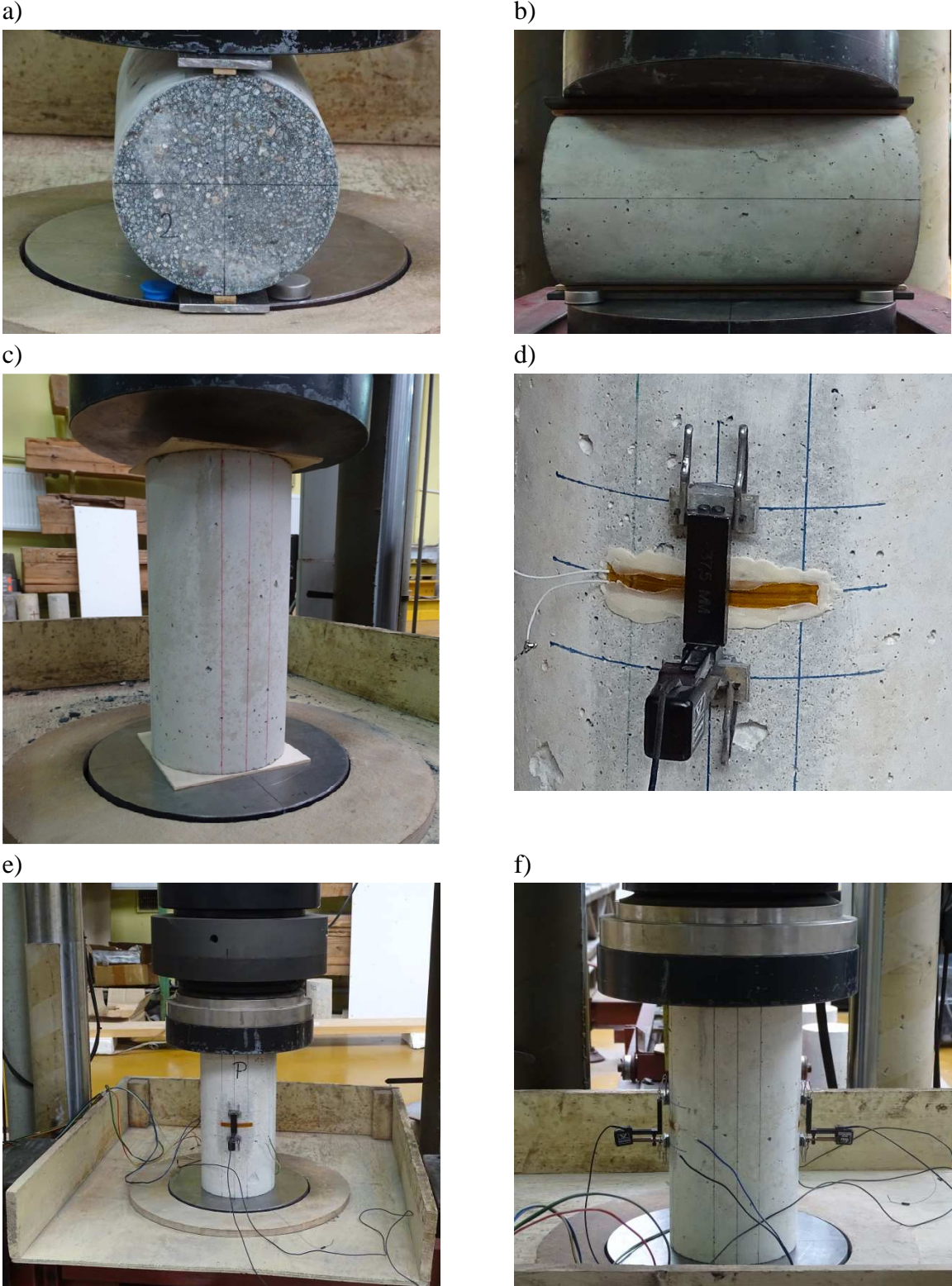
Figure 4.3. Cylindrical concrete specimens: a) splitting test of the specimen; b) a longitudinal view of the specimen in the splitting test; c) compressive strength test; d) the extensometer and the strain gauge located on the lateral surface of the specimen; e) elastic modulus testing, f) the location of extensometers

The Poisson's ratio of the concrete was also determined in these tests. Every cylindrical specimen had two strain gauges (Hottinger, Darmstadt, Germany) and two extensometers (Instron, HighWycombe, Buckinghamshire, UK) with a 50 mm gauge. The extensometers and the strain gauges were located on the lateral surface of each specimen. The extensometers were parallel to the vertical axis of the specimen, whereas the strain gauges were perpendicular to the vertical axis of the specimen. The strain gauges were used to obtain the Poisson's ratio. Each specimen was placed centrally in the testing machine. Three preloading cycles were carried out to check the wiring stability and the positioning of the specimens. Then, loading cycles were applied (see Fig. 4.4). After the loading cycles, the compressive strength of the specimens was additionally determined. During the tests, the stress was increased at a rate of 0.6 MPa/s. The average values of strain obtained from the two extensometers were used to determine the non-linear stress–strain relationships from the laboratory tests of concrete.

a)

b)

Figure 4.4. The loading cycles during the elastic modulus testing:
a) described in the EN 12390-13 standard; b) applied in the tests

48

4.2. The shear connection test programme

The shear connection test programme was used to investigate the stiffness, resistance and ductility of the new type of shear connector developed for aluminium-concrete composite structures. In addition to the investigation of the mechanical properties of the connector, the tests were conducted to capture connection modes of failure. On top of that, the load-slip model obtained from connector tests was used in the numerical analysis of aluminium-concrete composite beams. After the tests, possibility of separating the aluminium beam from the concrete slab was evaluated.

The ductility of the connection may be evaluated according to the suggestion made by (Deam et al. 2008). A connection may be defined as ductile if it withstands a relative slip of 10 mm without a reduction in strength exceeding 20% of the peak value. What is more, the connectors are deemed to be ductile if they have a characteristic slip capacity exceeding 6 mm (Johnson 2012). Shear connectors should have enough slip capacity to redistribute shear force to adjacent shear connectors after yielding (Kwon et al. 2010). The ductility of the dowel-bolt was evaluated in the push-out tests. The slip capacity of a specimen δ_u corresponded to the maximum slip measured at the characteristic load level and it was taken from the falling branch of the load-slip curve (Johnson 2012).

The characteristic resistance of the connector determined from the push-out tests may be calculated using the following formula presented by (Johnson 2012) and in the Eurocode 4 (European Committee for Standardization 2004):

$$P_{Rk,test} = 0.9 P_{min} \tag{4.1}$$

where P_{min} is the lowest resistance measured per connector.

The push-out test specimen consisted of: an aluminium beam, concrete slabs, steel profiled sheeting, shear connectors and reinforcing meshes. The aforementioned elements and the formwork for the concrete slabs were prepared in the workshop of the Institute of Structural Engineering of the Poznan University of Technology prior to the assembly of the specimens.

4.2.1. The making of the shear connectors

The prototypes of the connectors were made of headed studs (Köster & Co. 2005) and nuts in several steps (see Fig. 4.5). The making of the shear connectors was time-consuming. The total of 136 shear connectors were created for the tests: 32 for the push-out tests and 104 for the bending tests. In the future, the connectors should be produced by screw and bolt manufacturers, in an automated–, and thus less time-consuming –process.

a)

c)

b)

d)

e)

f)
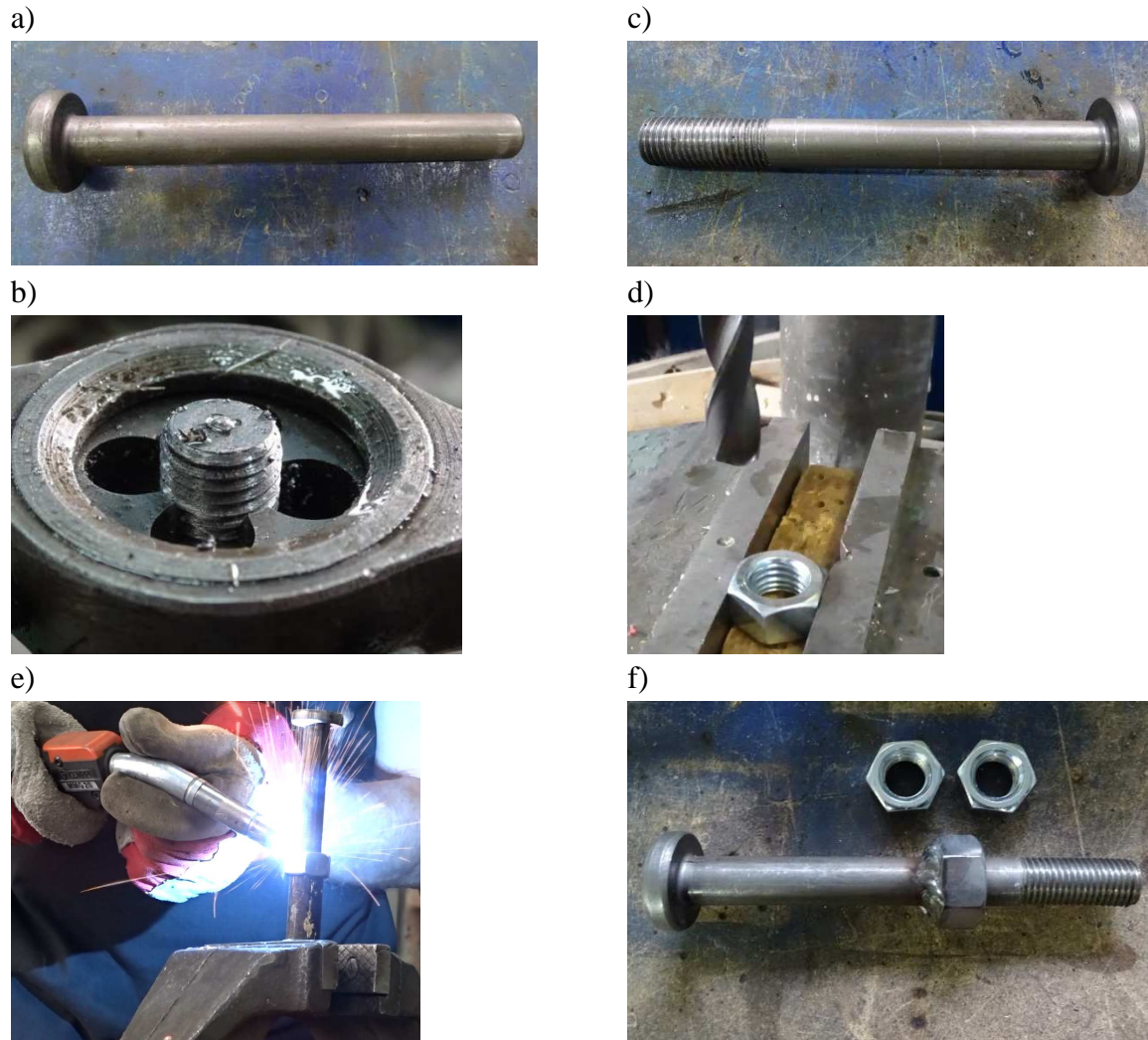
Figure 4.5. Steps of the production process: a) headed stud; b) forming threads by cutting; c) stud with threads; d) enlarging a hole in the nut by drilling; e) welding a nut to the shank; f) shear connectors after welding

4.2.2. The assembly of the specimens

Each specimen consisted of two concrete slabs made of C30/37 concrete, two steel sheets made of 0.7 mm-thick S320GD steel, eight shear connectors, two reinforcing meshes made of 6 mm S235JRG2 round steel bars, and an aluminium beam made of AW-6060 T6 alloy. 18 mm holes were drilled in the aluminium beams and in the profiled sheeting using hole saws (ProFit HM Endura and ProFit Bimetal Plus, respectively) (see Figs. 4.6a and 4.6b). The shear connectors (non-preloaded demountable dowel-bolt connectors) made of S235J2 steel were used to join the aluminium beam first with the profiled sheeting and then with the concrete slabs (see Fig. 4.6c). The reinforcing meshes were welded from 6 mm round bars made of S235JRG2 steel. The formwork for the concrete slabs was made of 12 mm-thick OSB boards (see Fig. 4.6d). The concrete slabs were simultaneously cast in the vertical position (see Figs. 4.6e and 4.6f). Due to this fact, each slab was made of the same concrete. Furthermore, 16 cubic concrete samples were prepared for testing the material compressive strength. The concrete was bought from the "Lafarge Kruszywa i Beton" company and the

precise proportion of the ingredients was a trade secret. However, it was known that the concrete was composed of cement (CEM I 42.5 R), fly ash, aggregate: gravel (2–8 mm and 8–16 mm in diameter), sand (0–2 mm in diameter), water and plasticizer. A handheld concrete vibrator was used to consolidate fresh concrete in the formwork and a vibrating table was used to consolidate fresh concrete in the cubes. The concrete was cured for 28 days. The aluminium-concrete composite joint specimens were covered with wet cloths to keep them damp during the curing process. As for the cubic concrete specimens, they were subjected to immersion curing. Four specimens were assembled. One of them had a rubber element between the aluminium beam flat and the profiled sheeting to prevent contact corrosion (see Figs. 4.6g and 4.6h). After the test, the stiffness of the connection with the rubber element was compared with the stiffness of other connections.

4.2.3. Test set-up

The tests were conducted 70 days after casting in the laboratory of the Institute of Structural Engineering of the Poznan University of Technology. The specimens were put on a 12 mm-thick OSB board placed on the base of the Instron 8505 Plus test machine (see Fig. 4.7). The load ranging between 30 kN and 70 kN was applied cyclically 25 times in accordance with the principles set out in the Eurocode 4 (European Committee for Standardization 2004), and, subsequently, failure load was applied. The longitudinal slip between the concrete slabs and the aluminium beam and the horizontal displacements were measured continuously during loading using Linear Voltage Displacement Transducers (LVDTs). The location of the LVDTs is presented in Figure 4.7. Measurements were also made when the load decreased. Displacement control was used. The vertical displacement was kept constant (constant displacement control) and the piston velocity amounted to 0.5 mm/min.

a)

b)

c)

d)

e)

f)

g)

h)
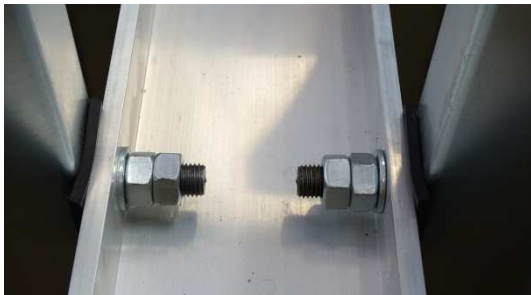
Figure 4.6. The assembly of the specimens
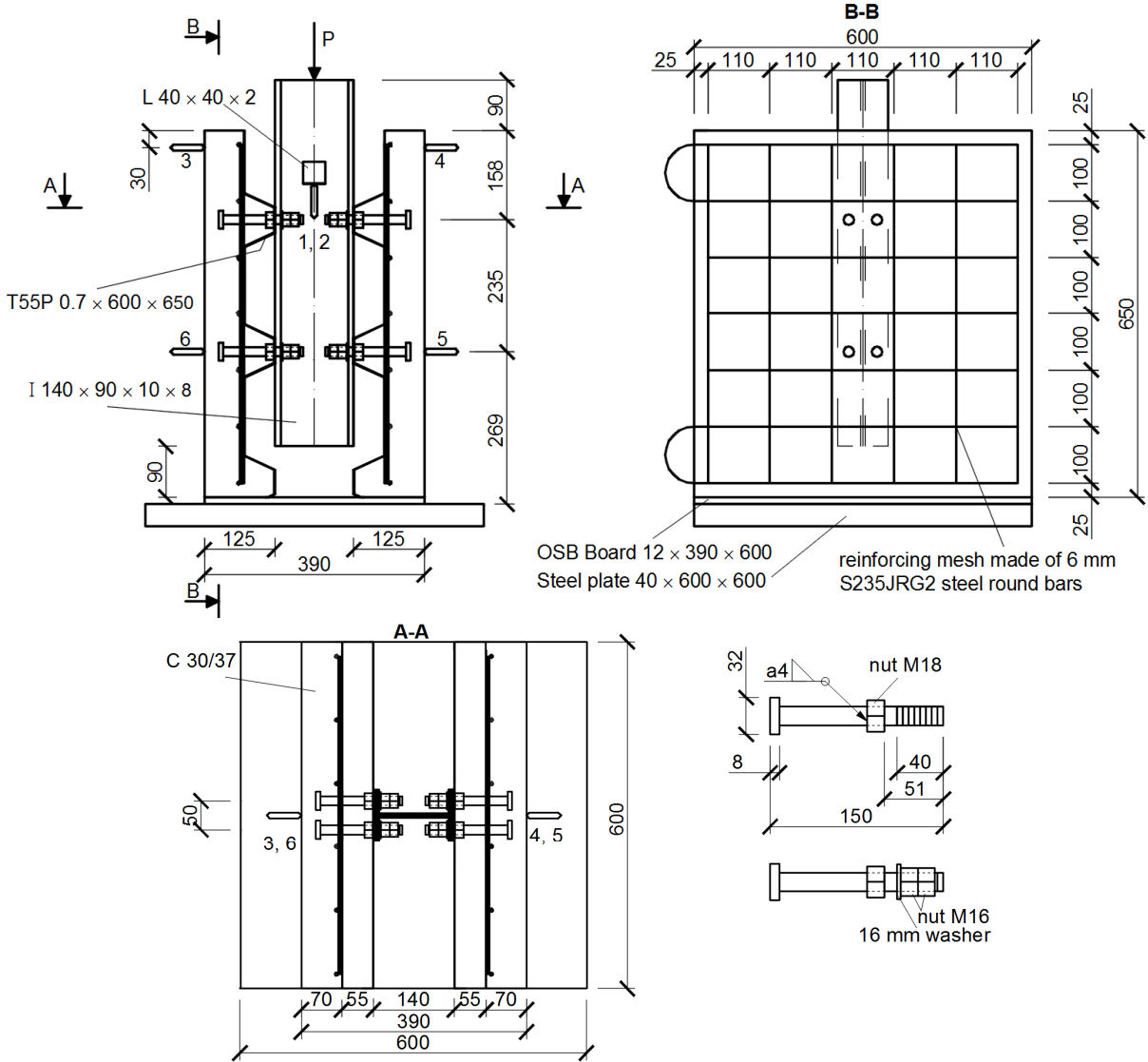
Figure 4.7. Push-out test set-up (dimensions in mm), 1–6 – LVDT

4.3. The bending test programme

The bending tests were performed in the laboratory of the Institute of Structural Engineering of the Poznan University of Technology. Four beams were tested in an attempt to capture the short-term local and global behaviour of aluminium-concrete composite beams, including the mode of failure, level of composite efficiency for the proposed type of connectors, load-deflection and load-slip response. Moreover, the structural response of the tested elements was used to validate a non-linear finite element (FE) model of the aluminium-concrete composite beam.

4.3.1. The assembly of the specimens

Each of the specimens consisted of a concrete slab made of C50/60 concrete, 0.7 mm-thick T55P profiled sheeting made of S320GD steel, 26 shear connectors, two reinforcing meshes made of 6 mm S235JRG2 round steel bars, and an aluminium beam made of AW-6060 T6

alloy. 18 mm holes were drilled in the aluminium beams and in the profiled sheeting using hole saws (ProFit HM Endura and ProFit Bimetal Plus, respectively) (see Fig. 4.8a). Metal cutting foam (ProFit) was used for a smoother cut and a longer life of the hole saw. The shear connectors (non-preloaded demountable dowel-bolt connectors) made of S235J2 steel were used to join the aluminium beam with the profiled sheeting and next with the concrete slab. The shape of the connector flange made it possible to use a wrench to hold the connector while the nuts were being tightened (see Fig. 4.8b). The degree of the shear connection was 0.79, as calculated in accordance with the principles set out in the Eurocode 4 (European Committee for Standardization 2004). The profiled sheeting was placed in an upward position and was used as a lost formwork. The sheets were joined together by overlapping and secured with self-tapping screws (see Fig. 4.8c). Self-tapping screws were also used to join the profiled sheeting and the concrete slab, and to prevent the separation of these elements (see Fig. 4.8d). Reinforcing meshes were made of 6 mm S235JRG2 round steel bars (reinforcement ratio ≈ 1.0%). The spacing between the round bars was 81.0 mm in a transverse direction and 117.5 mm in a longitudinal direction. 104 shear connectors were used in four beams (see Fig. 4.8e). The formwork for the concrete slabs was made of 12 mm-thick OSB boards (see Figs. 4.8f–h). The concrete slabs were simultaneously casted in a horizontal position (see Figs. 4.9a and 4.9b). The cubic and the cylindrical concrete specimens were made at the time of casting. The concrete was bought from "Stanbud" company and its composition is described in Appendix 1. The concrete mixture was prepared according to (EN 206-1, European Committee for Standardization 2003). The maximum aggregate size was 8 mm. A surface concrete vibrator was used to consolidate the fresh concrete in the formwork. The concrete was then cured for 28 days. The aluminium-concrete composite beams were covered with wet cloths to keep them damp during the curing process. As for the cubic and cylindrical concrete specimens, they were subjected to immersion curing (see Fig. 4.9c). The U-shape of the formwork prevented the bending of the profiled sheeting during the casting (see Fig. 4.9d). Each beam had dimensions determined before the casting (see Fig. 4.9e). The total of four aluminium-concrete composite beams were assembled (see Fig. 4.9f). In each beam, three strain gauges were glued onto the upper surface of the concrete slab and four strain gauges were glued onto the aluminium beam (see Figs. 4.9g–h). Strain distribution was measured along cross-section 3–3 (see Fig. 4.10). The cross-section was located between the two loading points and it was subjected to pure bending.

a)

b)

c)

d)

e)

f)

g)

h)

Figure 4.8. The assembly of the specimens (part 1)

a)

b)

c)

d)

e)

f)

g)

h)
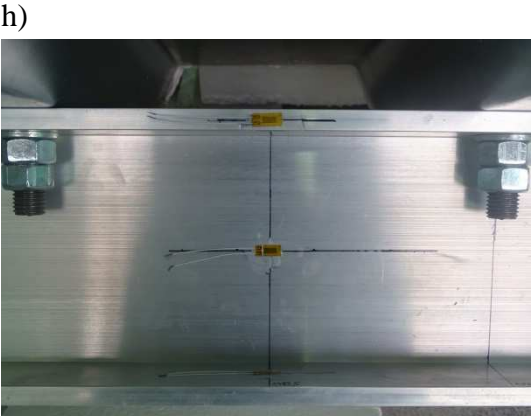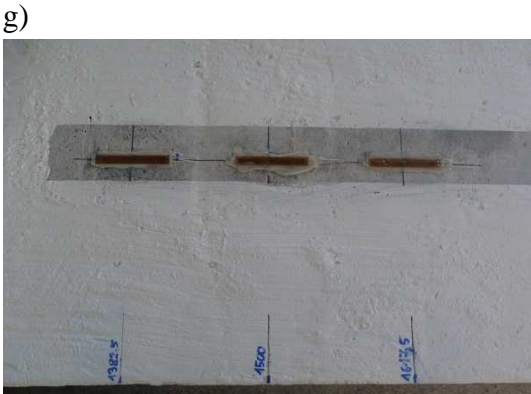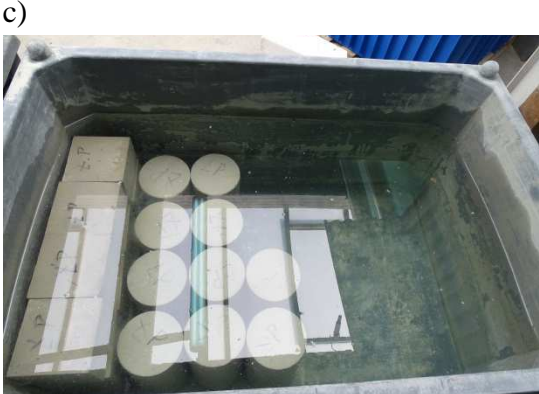
Figure 4.9. The assembly of the specimens (part 2)

4.3.2. Test set-up

Four aluminium-concrete composite elements were subjected to four-point bending tests. The geometrical configurations and the details of the beams are presented in Fig. 4.10.
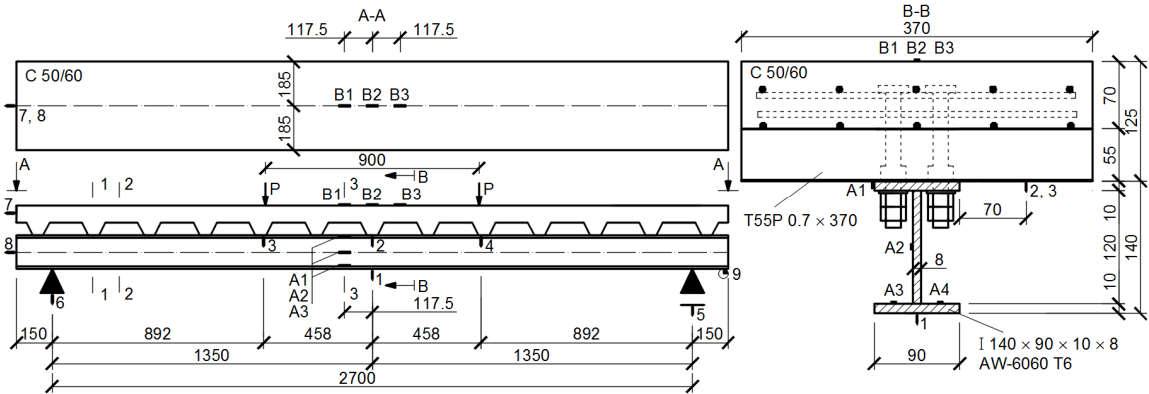
Figure 4.10. Bending test set-up (dimensions in mm): A1–3 – strain gauges on the aluminium beams, B1–3 – strain gauges on the concrete slab, 1–8 – LVDT and 9 – inclinometer (Polus and Szumigała 2017a) (Polus and Szumigała 2019a)

In each test, the mid-span deflection, the deflection under loads, the deflection of the supports, and the slip between the aluminium beam and the concrete slab were measured using LVDTs. Furthermore, the development of cracks on the surfaces of the tested elements was tracked. The specimens were located on roller supports (see Fig. 4.11). The aluminium-concrete composite elements were symmetrically loaded (in two places on each beam) using a spreader beam (l_s = 900 mm). Due to this fact, the beams between the two loading points were subjected to pure bending. The spreader beam was placed on two steel plates (8 mm × 80 mm × 210 mm) (for beams 3 and 4) to prevent the crushing of the concrete subjected to compression. The bending tests were performed 100-192 days after the casting, using the Instron 8505 Plus test machine.

Figure 4.11. The specimen with the spreader beam

LVDTs 5 and 6 were used to measure vertical displacement of the supports. LVDTs 7 and 8 were used to measure the horizontal displacement of the aluminium beam and the concrete slab (see Fig. 4.12a). The slip of the aluminium-concrete composite beam was calculated as the difference between these displacements. Strain distribution was measured along cross-section 3–3 using strain gauges glued onto the aluminium beam (see Figs. 4.12b and 4.13c) and the concrete slab (see Fig. 4.12d). Strain was measured taking into account the temperature compensation of strain gauges. One additional concrete beam and one aluminium additional beam with strain gauges were used in this process.

a)

b)

c)

d)
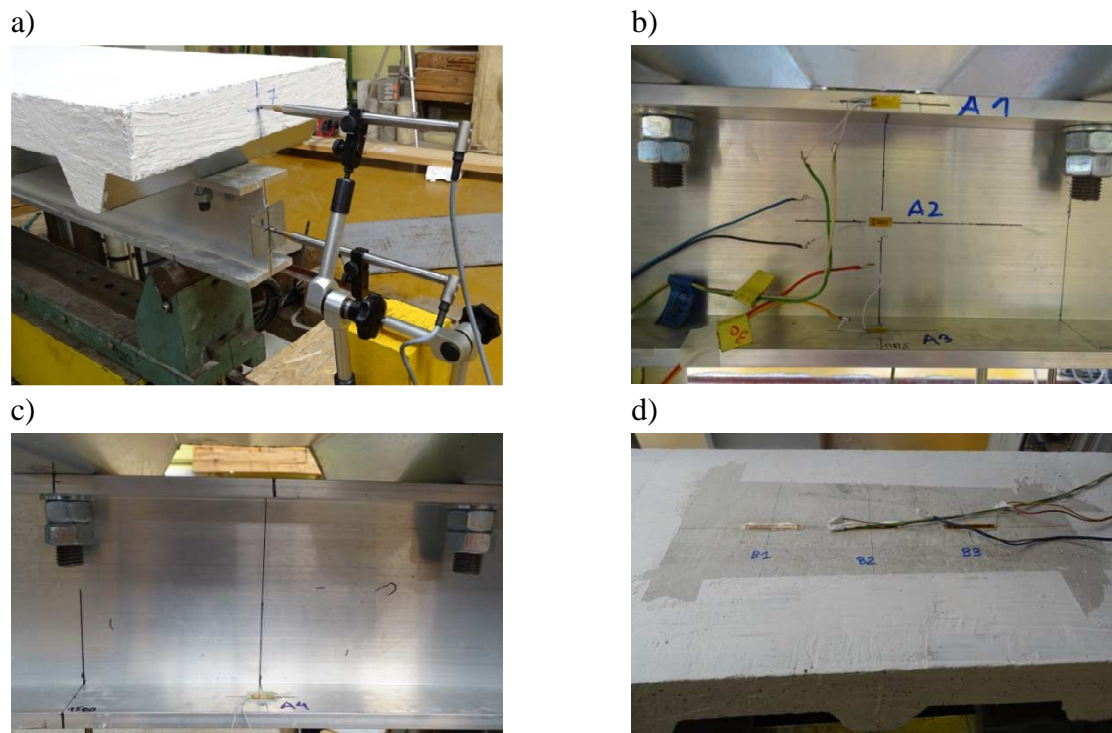
Figure 4.12. Bending test details: a) LVDTs 7 and 8; b-c) strain gauges glued onto the aluminium beam; d) strain gauges glued onto the concrete slab

4.4. The finite element modelling of the concrete cylinder subjected to compression

This section presents the main outcomes of the numerical analyses described in (Polus and Szumigała 2019c).

The behaviour of structural elements is often evaluated using numerical simulations. Concrete elements are difficult to model, because of the need to identify a number of parameters. The fracturing of concrete depends on the loading type (monotonic or cyclic), the loading velocity (quasi-static or dynamic) and the moisture level of the concrete (Marzec 2008) (Marzec and Tejchman 2013). Crushing appears in concrete subjected to compression whereas the cracking appears in concrete subjected to tension. The behaviour of concrete may be presented using two models: the concrete damaged plasticity (CDP) or gradient damage-plasticity (GDP) (Wosatko, Pamin and Polak 2015). The present author chose the CDP model to reflect the behaviour of the concrete cylinder subjected to compression. This model is available in the

Abaqus program and it reflects the cracking phenomenon, the crack closing effect and the different types of behaviour for tension and compression (Wosatko et al. 2018). The CDP may be used in conjunction with adaptive meshing to allow for the completion of the analyses even with relatively high deformation rates (Martin 2010). For example, the impacted zone of a concrete slab may be re-meshed regularly during missile impact analyses in order to avoid heavy distortion of elements. When the CDP model is used in a finite element analysis, the failure mode of a structural element must be defined by the user based on the state of damage determined in the analysis. The model was theoretically described by Lubliner et al. (1989) and Lee and Fenves (1998) and was implemented in the Abaqus program. The use of the CDP model requires the knowledge of material constants (Szczecina and Winnicki 2017). The constitutive parameters of the CDP model were discussed by Jankowiak and Łodygowski (2005 & 2010), and Kmiecik and Kamiński (2011). Many tests are required to identify the properties of concrete. For this reason, Gajewski and Garbowski (2014) developed a simple procedure for estimating concrete properties, to reduce the number of tests to one. The procedure combines a standard uniaxial test, digital image correlation measurements and an inverse analysis.

The compressive stress-strain diagram for the analysis of concrete subjected to compression was adopted from the Eurocode 2 (European Committee for Standardization 2004) (see Fig. 4.13). To present this relationship, the compressive stress was calculated using the concrete parameters obtained in the laboratory tests (f_c, E_c, ε_{c1}) and the following formulas:

$$\sigma_c = f_c \frac{k' \eta_e - \eta_e^2}{1 + (k' - 2)\eta_e} \tag{4.2}$$

$$k' = 1.05 E_c \frac{\varepsilon_{c1}}{f_c} \tag{4.3}$$

$$\eta_e = \frac{\varepsilon_c}{\varepsilon_{c1}} \tag{4.4}$$

where f_c and E_c are the compressive strength and the Young's modulus of concrete, respectively, ε_c is the compressive strain and ε_{c1} is the strain at compressive strength.
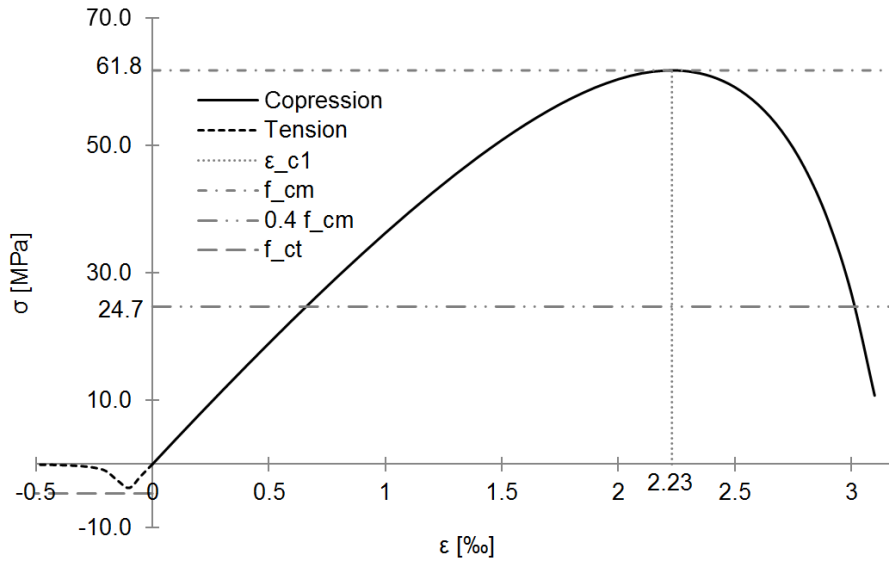
Figure 4.13. The stress-strain relationship for concrete (Polus and Szumigała 2019c)

The tensile stress-strain diagram for the analysis of concrete subjected to tension was adopted from (Kmiecik and Kamiński 2011) and (Wang and Hsu 2001). To show this relationship, the tensile stress was calculated using the concrete parameters obtained in the laboratory tests (f_{ct}, E_c) and the following formulas:

$$\left.\begin{array}{l} \sigma_t = E_c \varepsilon_t \ \textit{if} \ \varepsilon_t \le \varepsilon_{cr} \\[2mm] \sigma_t = f_{ct} \left(\dfrac{\varepsilon_{cr}}{\varepsilon_t} \right)^{n_w} \ \textit{if} \ \varepsilon_t > \varepsilon_{cr} \end{array}\right\} \qquad (4.5)$$

where n_w is the rate of weakening, ε_{cr} is the cracking strain assumed as f_{ct} / E_c, f_{ct} is the tensile strength of concrete and ε_t is the tensile strain.

The inelastic compressive strain (ε_c^{in}) was calculated using the following formulas (Kmiecik and Kamiński 2011):

$$\varepsilon_c^{in} = \varepsilon_c - \varepsilon_c^{el} \qquad (4.6)$$

$$\varepsilon_c^{el} = \frac{\sigma_c}{E_0} \qquad (4.7)$$

where ε_c is the total compressive strain, ε_c^{el} is the elastic compressive strain, σ_c is the stress for uniaxial compression and E_0 is the initial Young's modulus for undamaged concrete.

The plastic compressive strain (ε_c^{pl}) was calculated as follows (Kmiecik and Kamiński 2011):

$$\varepsilon_c^{pl} = \varepsilon_c^{in} - \frac{D_c}{(1 - D_c)} \frac{\sigma_c}{E_0} \qquad (4.8)$$

where D_c is the concrete compression damage parameter.

The stress for uniaxial compression (σ_c) and the effective compressive stress (σ_c^{eff}) were calculated using the following formulas (Kmiecik and Kamiński 2011):

$$\sigma_c = (1 - D_c)E_0(\varepsilon_c - \varepsilon_c^{pl}) \qquad (4.9)$$

$$\sigma_c^{eff} = \frac{\sigma_c}{(1 - D_c)} = E_0(\varepsilon_c - \varepsilon_c^{pl}) \qquad (4.10)$$

In the case of compression, the material was defined as linear elastic to the point where the stress reached $0.4\,f_{cm}$ (mean value of the concrete cylinder compressive strength) according to the Eurocode 2 (European Committee for Standardization 2004). After this point, the material was defined as non-linear elastic. The value of the concrete compression damage parameter D_c was assumed as 0.0 for the strain lower than ε_{c1}. The value of this parameter started to increase after the point where the compressive strength of concrete was reached (see Fig. 4.14).

In the case of tension, it was assumed that the cracking appeared when the stress was equal to f_{ct}. The cracking strain (ε_t^{cr}) was calculated as follows (Kmiecik and Kamiński 2011):

$$\varepsilon_t^{cr} = \varepsilon_t - \varepsilon_t^{el} \qquad (4.11)$$

$$\varepsilon_t^{el} = \frac{\sigma_t}{E_0} \qquad (4.12)$$

where ε_t is the total tensile strain, ε_t^{el} is the elastic tensile strain, and σ_t is the stress for uniaxial tension.

The plastic tensile strain (ε_t^{pl}) was calculated using the following formula (Kmiecik and Kamiński 2011):

$$\varepsilon_t^{pl} = \varepsilon_t^{cr} - \frac{D_t}{(1 - D_t)} \frac{\sigma_t}{E_0} \qquad (4.13)$$

where D_t is the concrete tension damage parameter.

The stress for uniaxial tension (σ_t) and the effective tensile stress (σ_t^{eff}) were calculated as follows (Kmiecik and Kamiński 2011):

$$\sigma_t = (1 - D_t)E_0(\varepsilon_t - \varepsilon_t^{pl}) \tag{4.14}$$

$$\sigma_t^{eff} = \frac{\sigma_t}{(1 - D_t)} = E_0(\varepsilon_t - \varepsilon_t^{pl}) \tag{4.15}$$

The concrete tension damage parameter D_t was increasing in proportion to the increase in the width of the crack w (see Fig. 4.14), which was calculated as follows, using the formula presented by Hordijk (1991), Wittmann et al. (1988), Jankowiak (2012), and Jankowiak and Madaj (2014):

$$w = 5.14 G_F / f_{ct} \tag{4.16}$$

where G_F is the fracture energy.

Fracture energy is the energy released in the process of crack formation (Jankowiak 2018). It depends on the maximum aggregate size and the class of concrete (Jankowiak and Madaj 2015). The crack propagates when the stress at the crack tip reaches the tensile strength of the concrete (Hillerborg, Modéer and Petersson 1976). When the crack opens, the stress decreases, and the crack width increases. The tensile stress-crack width relationship (σ_t–w) is presented in Fig 4.14. The value of the fracture energy (G_F) was calculated using the following formula proposed by Bazant and Becq-Giraudon (2002) and Comite Euro-International du Beton (1991):

$$G_F = \left(0.0469d_a^2 - 0.5d_a + 26\right) \cdot \left(\frac{f_c}{10}\right)^{0.7} \tag{4.17}$$

where d_a is the maximum aggregate size [mm].

The influence of the maximum aggregate size on the fracture parameters of concrete was investigated by Golewski (2007). In his research, he calculated the value of the fracture energy to be 78.03 N/m.

The data containing inelastic (crushing) strain values calculated from Eq. (4.6) and the cracking strain values calculated from Eq. (4.11) were entered into the Abaqus program. The crushing and cracking strain values were then automatically converted into the plastic strain values using the relationship from Eqs. (4.8) and (4.13) (Dassault Systèmes 2013). The parameters of the concrete used in the numerical analyses are presented in Tables 4.1–4.3.

Table 4.1. Concrete parameters used in the finite element modelling of the concrete cylinder subjected to compression and the aluminium-concrete composite beam (Polus and Szumigała 2019a) (Polus and Szumigała 2019c)

Parameter	Value
Young's modulus E_c [MPa]	37 300[a]
Poisson's ratio v [-]	0.19[a]
Compressive strength f_c [MPa]	61.8[a]
Tensile strength f_{ct} [MPa]	4.61[a]
Largest nominal maximum aggregate size d_a [mm]	8.0[a]
Fracture energy G_F [N/m]	89.5[b]
Rate of weakening n_w [-]	0.7[c]
Dilatation angle ψ [°]	40.0[c]
Eccentricity e_e [-]	0.1[c]
Ratio[d] f_{b0}/f_{c0} [-]	1.16[c]
Parameter κ [-]	0.667[c]
Viscosity parameter w_p [-]	0.0001[e, f], 0.00001[f]

[a] based on own laboratory tests; [b] calculated; [c] based on (Kmiecik and Kamiński 2011); [d] a ratio of the concrete strength in the biaxial state (f_{b0}) to the concrete strength in the uniaxial state (f_{c0}); [e] used in the finite element modelling of the concrete cylinder; [f] used in the finite element modelling of the aluminium-concrete composite beam
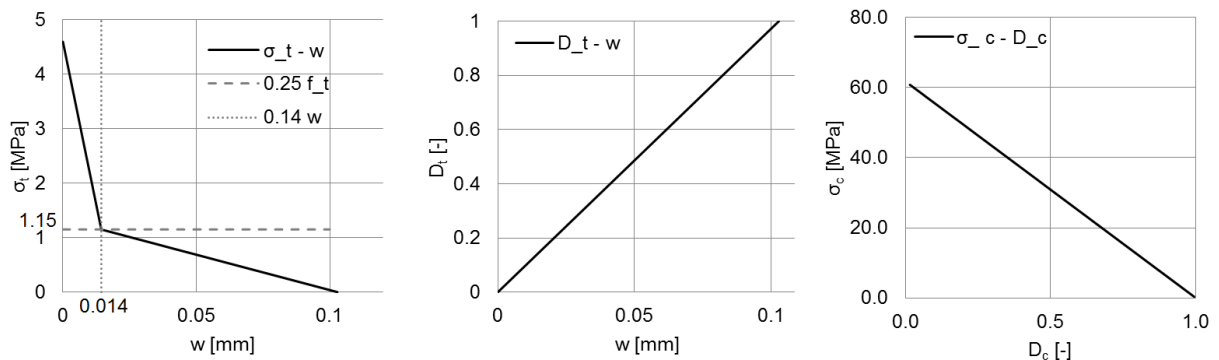
Figure 4.14. Parameters of concrete: a) tensile stress–crack width relationship (σ_t–w); b) concrete tension damage parameter–crack width relationship (D_t–w); c) compressive stress–concrete compression damage parameter relationship (σ_c–D_c) (Polus and Szumigała 2019c)

Table 4.2. Material parameters used in the CDP model for concrete subjected to compression in the finite element modelling of the concrete cylinder (Polus and Szumigała 2019c)

Concrete compression hardening		Concrete compression damage	
Stress [MPa]	Crushing (inelastic) strain [-]	D_c [-]	Crushing (inelastic) strain [-]
26.14	0.0	0.0	0.0
48.25	0.00010655	0.0	0.00010655
50.86	0.00013648	0.0	0.00013648
53.28	0.00017155	0.0	0.00017155
55.48	0.00021250	0.0	0.00021250
57.43	0.00026020	0.0	0.00026020
59.09	0.00031572	0.0	0.00031572
60.41	0.00038037	0.0	0.00038037
61.33	0.00045575	0.0	0.00045575
61.79	0.00059349	0.0	0.00059349
61.65	0.00064730	0.002	0.00064730
60.83	0.00076929	0.016	0.00076929
59.15	0.00091414	0.043	0.00091414
56.41	0.00108756	0.087	0.00108756
52.32	0.00129733	0.153	0.00129733
46.46	0.00155435	0.248	0.00155435
38.26	0.00187438	0.381	0.00187438
33.01	0.00206496	0.466	0.00206496
26.82	0.00228101	0.566	0.00228101
19.48	0.00252762	0.685	0.00252762
10.77	0.00281133	0.826	0.00281133
0.35	0.00314071	0.994	0.00314071

The concrete cylinder was placed between two steel round plates. The steel used in the round plates was model as an elastic material. The Young's modulus of steel E_s and the Poisson's ratio v were equal to 210 GPa and 0.3, respectively.

The discrete model of the concrete cylinder subjected to compression was built in the Abaqus 6.13 environment (Dassault Systèmes 2013) and then examined using the Abaqus/Standard finite element code. The Newton-Raphson method was used as a numerical technique for solving the non-linear equilibrium equations. This method uses a tangent stiffness matrix and solves the non-linear equation incrementally and iteratively (Tan 2010).

The steel plates were modelled using 4-noded shell elements with reduced integration (S4R), whereas the concrete cylinder was modelled in several variants which used different finite elements (see Table 4.4 and Fig. 4.15). C3D8R elements with hourglass control are often used to prepare concrete models. However, they should be used with reasonably fine meshes to prevent uncontrolled distortion of the mesh (hourglassing) (Dassault Systèmes 2013). In the case of a concrete slab subjected to bending, no less than four C3D8R elements should be used through its thickness (Szewczyk 2016 & 2019). What is more, C3D8I

elements may be used instead of C3D8R elements, because they are enhanced by incompatible modes to improve their bending behaviour.

Table 4.3. Material parameters used in the CDP model for concrete subjected to tension in the finite element modelling of the concrete cylinder (Polus and Szumigała 2019c)

Concrete tension stiffening		Concrete tension damage	
Stress [MPa]	Cracking strain [-]	D_t [-]	Cracking strain [-]
4.6	0	0	0
3.279224	0.0001121	0.05360	0.0001121
2.805008	0.0001748	0.07284	0.0001748
2.468921	0.0002338	0.08648	0.0002338
2.216381	0.0002906	0.09673	0.0002906
2.018599	0.0003459	0.10475	0.0003459
1.144254	0.0008693	0.14430	0.0008693
1.101756	0.0009205	0.17608	0.0009205
1.062899	0.0009715	0.20514	0.0009715
0.935546	0.0011749	0.30037	0.0011749
0.800255	0.0014785	0.40155	0.0014785
0.704371	0.0017811	0.47325	0.0017811
0.60251	0.0022338	0.54943	0.0022338
0.504445	0.0028865	0.62276	0.0028865
0.301483	0.0060419	0.77454	0.0060419
0.205641	0.0104445	0.84622	0.0104445
0.107348	0.0264471	0.91972	0.0264471
0.052517	0.0734486	0.96073	0.0734486

Table 4.4. Finite elements used in the finite element modelling of the concrete cylinder subjected to compression (Polus and Szumigała 2019c) (Zienkiewicz, Taylor and Zhu 2005)

No.	FE	Description	Size [mm]	No. of FEs
1			5	51 840
2	C3D8R	8-node linear brick elements with reduced	10	7200
3		integration and hourglass control	20	900
4			40	160
5	C3D8	8-node linear brick elements	10	7200
6	C3D8I	Incompatible mode 8-node linear brick elements	10	7200

The upper steel plate was used to compress the concrete cylinder. During the analysis the vertical displacement (downward movement) was increasing. The boundary conditions for the support and the contact between the concrete cylinder and the steel plates are illustrated in Fig. 4.16.
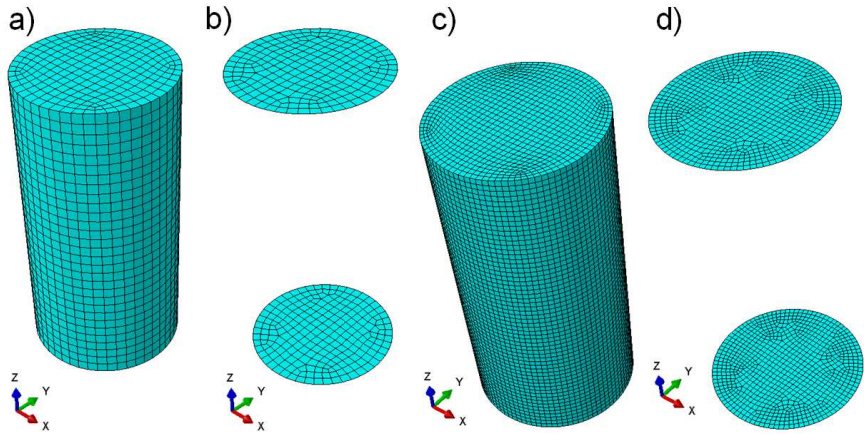
Figure 4.15. The mesh used in the numerical calculations: a) concrete cylinder (10 mm mesh), b) steel plates (10 mm mesh), c) concrete cylinder (5 mm mesh), d) steel plates (5 mm mesh)
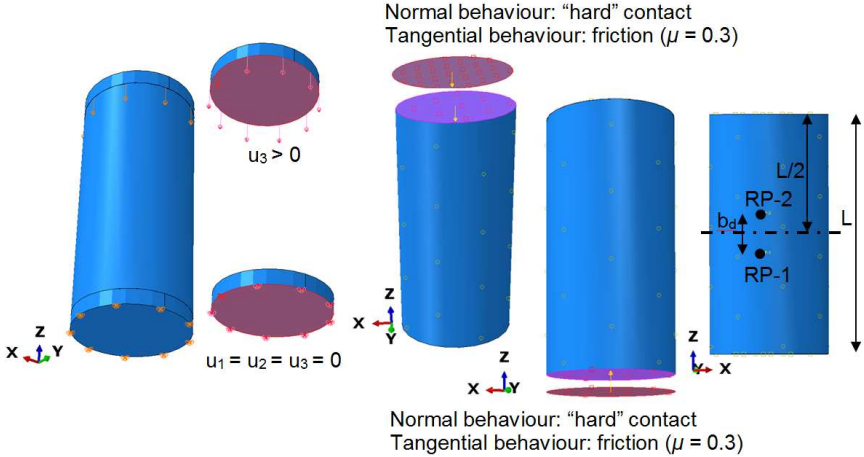
Figure 4.16. Boundary conditions for the support and the contact between the concrete cylinder and the steel plates (Polus and Szumigała 2019c)

Friction and surface-to-surface "hard" contact were defined between the steel plates and the upper and lower surfaces of the concrete cylinder. The friction coefficient μ was equal to 0.3. The same value of the friction coefficient between a steel element and a concrete element was used by Guezouli and Lachal (2012).

Two reference points (RPs) were located on the lateral surface of the concrete cylinder to record displacement (see Fig. 4.16). What is more, the initial distance between the RPs ($b_d = 50$ mm) was the same as the measuring base of the strain gauge in the laboratory tests of the concrete cylinders. After the numerical analyses, the strain was calculated from the equation:

$$\varepsilon = \frac{\Delta b_d}{b_d} \tag{4.18}$$

where Δb_d is the relative vertical displacement between the RPs and b_d is the initial distance between the RPs.

Chapter 4. MATERIALS AND METHODS

The non-linear stress-strain relationship for concrete from the laboratory tests (the elastic modulus testing) was used to validate the numerical model of the concrete cylinder subjected to compression.

4.5. The finite element modelling of the shear connection test

The discrete model of the specimen from the push-out test was built in the Abaqus 6.13 environment (Dassault Systèmes 2013) and then examined using the Abaqus/Standard finite element code. The Newton-Raphson method was used as a numerical technique for solving the non-linear equilibrium equations. The specimen had two axes of symmetry. For this reason, only ¼ of the specimen was prepared in the program and the finite element (FE) model consisted of ¼ of the aluminium I-beam, ¼ of the steel plate, ½ of the reinforcing steel mesh, ½ of the profiled steel sheeting and ½ of the concrete slab (see Fig. 4.17).
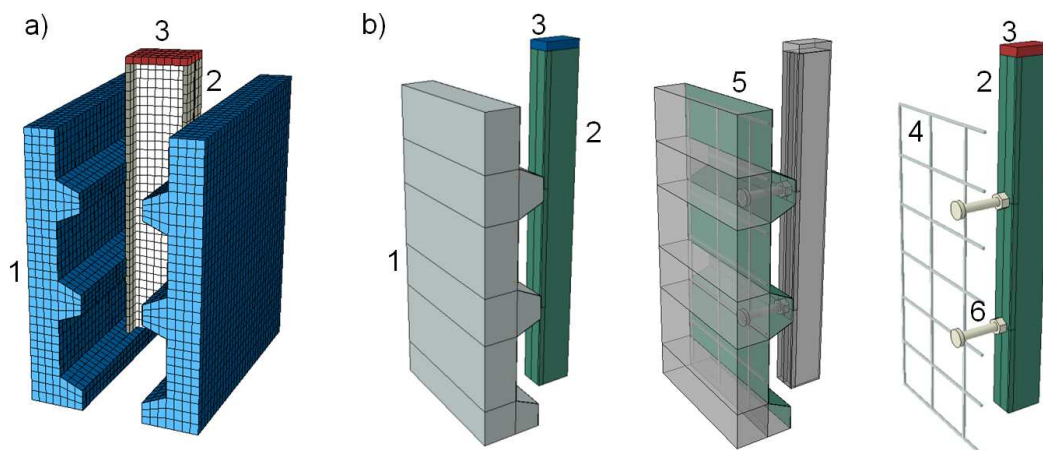
Figure 4.17. The discrete model of the specimen from the push-out test: a) complete model; b) ¼ of the model; 1 – concrete slab, 2 – aluminium beam, 3 – steel plate, 4 – steel mesh, 5 – profiled steel sheeting, 6 – connector

The validation process of a FE model should consist of many aspects (Pełka-Sawenko, Wróblewski and Szumigała 2016). The most challenging aspects in the finite element modelling of the shear connection test included: the modelling of the behaviour of the concrete and the modelling of the connection between the aluminium beam and the concrete slab. Many parameters, e.g., the damage parameters, are critical for the accurate definition of the concrete model (Genikomsou and Polak 2015). For this reason, some parameters were taken from the literature and some of them were obtained from material tests. The rule presented by Kwaśniewski, Szmigiera and Siennicki (2011), according to which one should begin with the simplest model and then build a more complex one, was used. The author of this dissertation analysed a number of FE models, some of which are presented in Table 4.5. The model of the connection between an aluminium beam and a concrete slab has an impact on the behaviour of aluminium-concrete composite beams. When the shear connectors are modelled as beams and are tied to an aluminium beam, it is impossible to take into account the slip resulting from the clearance between the shear connectors and the holes in the aluminium beam (Szumigała and Polus 2014b). Wróblewski et al. (2013) compared two connection modelling techniques. In the first model, the authors used beam elements, while in

the second model they used spring elements. A comparison of the two models revealed that the model with spring elements better reflected the behaviour of the real structure. Ding et al. (2016) used spring elements or beam elements to model connections in steel-concrete composite beams. They observed that the end slip of a beam obtained by using beam elements was lower than that obtained by using spring elements. Furthermore, spring elements provide faster computational speed than beam elements. Due to these facts, the implicit modelling of connectors was used to take slip into account in the FE model. The shear connectors were modelled by zero-length springs. Two points on the concrete slab were connected with two points on the aluminium beam using zero-length wires. These connections were axial and the orientation of the connectors was specified using the local coordinate system in which x direction was parallel to the length of the beam. The connectors enabled the slip between the concrete slab and the aluminium beam in x direction. Four models of the shear connector were used (see Figs. 4.18 and 5.10). In the first model (F–s 1), the response of the connector was non-linear to reflect the average shear force-slip curve for the three specimens from the push-out tests. In the second (F–s 2, $\gamma_v = 1.25$) and third models (F–s 3, $\gamma_v = 1.0$), the response of the connector was also non-linear to reflect the elasto-plastic theoretical model for the dowel-bolt connector presented in Section 3.1. In the last model (F–s 4, $k = 5.5$ kN/mm), the response of the connector was linear to reflect only the first branch of the shear force–slip curve for the dowel-bolt connector presented in Section 3.1. The data containing forces and displacements were used in the program. However, solid elements (shear connectors) were added (see Fig. 4.17) and embedded in the concrete slab in the FE model. It was done because these elements reinforced the concrete ribs. The author of this dissertation emphasizes the fact that they were not used to join the aluminium beam and the concrete slab, because this connection was modelled by the zero-length springs described above. The skin of the concrete slab represented the profiled steel sheeting. It was assumed that the profiled steel sheeting was perfectly bonded to the concrete slab. There was no relative slip between the profiled steel sheeting and the concrete slab (Wang 2009).
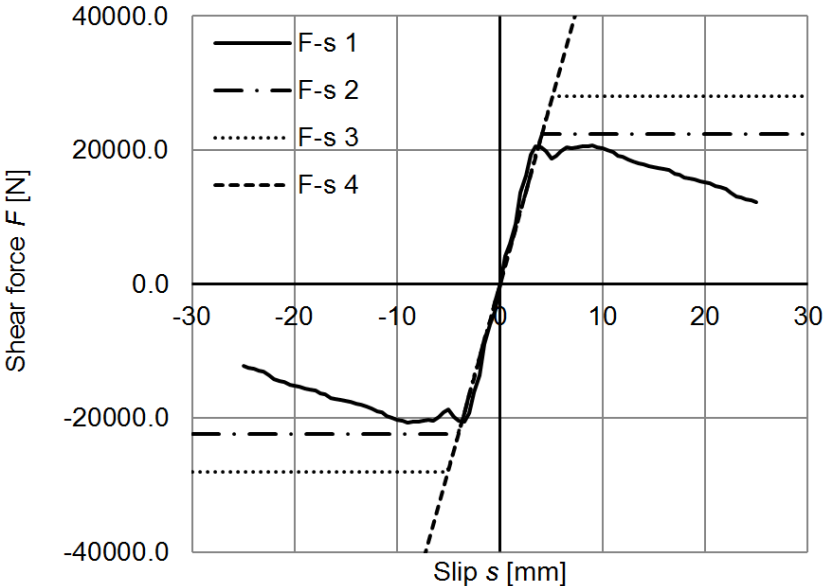
Figure 4.18. Models of shear connectors used in the FE analyses

Table 4.5. Finite element analyses of the shear connection test

FEA	FEs [a]	Mesh size [mm]	Concrete model [b]	Connection model [c]
1	1: 2355 C3D8R; 2, 3, 5: 890 S4R 4: 195 T3D2; 6: 1104 C3D10; Total: 4544	20	I	A
2	1: 2355 C3D8R; 2, 3, 5: 890 S4R 4: 195 T3D2; 6: 1104 C3D10; Total: 4544	20	II	A
3	1: 2355 C3D8R; 2, 3, 5: 890 S4R 4: 195 T3D2; 6: 1104 C3D10; Total: 4544	20	II	B
4	1: 5200 C3D8R; 2, 3, 5: 1567 S4R 4: 252 T3D2; 6: 1104 C3D10; Total: 8123	15	II	B
5	1: 2355 C3D8R; 2, 3, 5: 890 S4R 4: 195 T3D2; 6: 1104 C3D10; Total: 4544	20	II	C
6	1, 6: 2531 C3D8R, 2, 3, 5: 890 S4R 4: 195 T3D2; Total: 3616	20	II	C
7	1: 2355 C3D8R; 2, 3, 5: 890 S4R 4: 195 T3D2; 6: 1104 C3D10; Total: 4544	20	II	D
8	1: 2355 C3D8R; 2, 3, 5: 890 S4R 4: 195 T3D2; 6: 1104 C3D10; Total: 4544	20	III	D
9	1: 2355 C3D8R; 2, 3, 5: 890 S4R 4: 195 T3D2; 6: 1104 C3D10; Total: 4544	20	IV	D
10	1: 2355 C3D8R; 2, 3, 5: 890 S4R 4: 195 T3D2; 6: 1104 C3D10; Total: 4544	20	V	D
11	1: 2355 C3D8R; 2, 3, 5: 890 S4R 4: 195 T3D2; 6: 1104 C3D10; Total: 4544	20	V	E
12	1: 2355 C3D8R; 2, 3, 5: 890 S4R 4: 195 T3D2; 6: 1104 C3D10; Total: 4544	20	III	E
13	1: 600 C3D8R; 2, 3, 5: 412 S4R 4: 124 T3D2;6: 1104 C3D10; Total: 2240	30	V	E
14	1: 16 170 C3D8R; 2, 3, 5: 3497 S4R 4: 376 T3D2; 6: 1272 C3D10; Total: 21 315	10	V	E
15	1: 2355 C3D8; 2, 3, 5: 890 S4R 4: 195 T3D2; 6: 1104 C3D10; Total: 4544	20	V	E
16	1: 2355 C3D8I; 2, 3, 5: 890 S4R 4: 195 T3D2; 6: 1104 C3D10; Total: 4544	20	V	E

[a] Finite elements used to model the: 1 – concrete slab, 2 – aluminium beam, 3 – steel plate,
4 – steel mesh, 5 – profiled steel sheeting, 6 – connector
[b] Concrete model: I – elastic (E_c = 32 GPa, v = 0.2), II – CDP (rate of weakening n_w = 0.7), III – CDP (rate of weakening n_w = 1.0), IV – CDP (rate of weakening n_w = 1.2), V – CDP (rate of weakening n_w = 1.5)
[c] Connection model: A – shear force–slip curve for one connector from the laboratory tests (see F–s 1 in Fig. 4.18), B – shear force–slip curve for one connector from the theoretical analysis (γ_v = 1.25) (see F–s 3 in Fig. 4.18), C – shear force–slip curve for one connector from the theoretical analysis (γ_v = 1.0) (see F–s 2 in Fig. 4.18), D – shear force–slip curve for one connector from the theoretical analysis (k = 5.5 kN/mm) (see F–s 4 in Fig. 4.18), E – shear force–slip curve for one connector from the theoretical analysis (k = 5.5 kN/mm) (see F–s 4 in Fig. 4.18), with friction modelling (μ = 0.3)

The concrete slab was modelled with C3D8R elements (8-node linear brick elements with reduced integration and hourglass control) (FEA 1–14), C3D8 elements (8-node linear brick elements) (FEA 15), or C3D8I elements (incompatible mode 8-node linear brick elements) (FEA 16). The reinforcing mesh was modelled with T3D2 elements (2-node linear 3D truss

elements), and the aluminium beam, the steel plate and the profiled steel sheeting were modelled with S4R elements (4-node shell elements with reduced integration). The shear connectors were modelled with C3D10 elements (10-node quadratic tetrahedron elements) (FEA 1–5, 7–16) or C3D8R elements (FEA 6). For the purpose of the analyses, four mesh sizes (10 mm, 15 mm, 20 mm or 30 mm) were chosen. Surface-to-surface "hard" contact was defined between the edge of the concrete slab and the flange of the aluminium beam. The tangential behaviour between the aluminium beam and the concrete slab was taken into account in the connection model (zero-length connector). The load-slip curve from the laboratory tests took into account the impact of friction on the behaviour of the connection. However, the theoretical shear force–slip curves did not take such impact into account. For this reason, friction ($\mu = 0.3$) was defined in connection model E to investigate this impact (see Table 4.5). The same value of the friction coefficient between a steel element and a concrete element was used by Guezouli and Lachal (2012). The reinforcing mesh was embedded in the concrete slab. The displacement was applied to the steel plate to move down the aluminium beam. The boundary conditions are illustrated in Fig. 4.19.
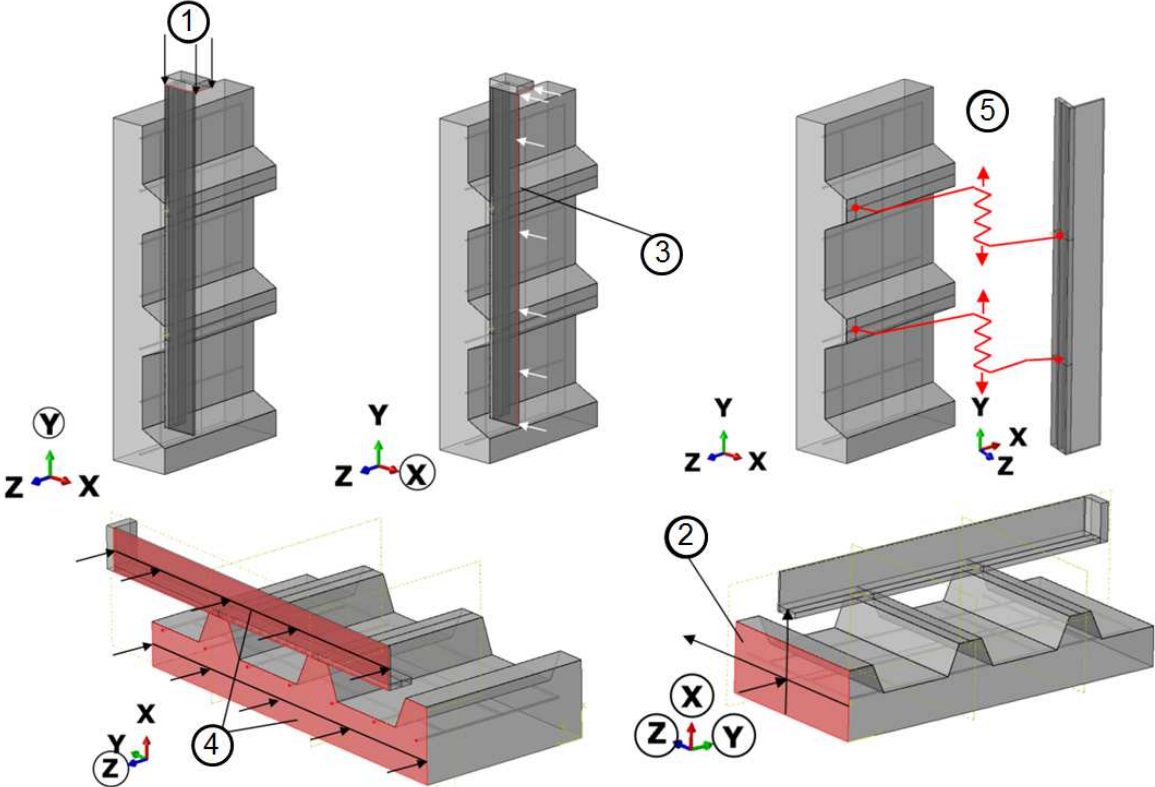
Figure 4.19. Boundary conditions: 1 – displacement, 2 – displacement in x, y, z directions (fixed), 3 – displacement in x direction (fixed), 4 – displacement in z direction (fixed), 5 – connector (zero-length spring) (Polus and Szumigała 2019a)

The results of the static tensile tests described in Section 4.1 were used to define material models in the FE analysis. The stress–strain relationships for metals are presented in Fig. 4.20. In Figure 4.20, the dotted lines represent the mean values of the engineering stress–strain curves (ESS) from the static tensile tests of the metals. The error bars reflect the distance between the mean value and the max/min test values. The non-linear curves from the

laboratory tests were then approximated using piecewise linear functions (PLF). Next, the engineering stress–strain relationship was converted to the true stress–strain relationship (TSS). The true stress (σ_{true}) and the logarithmic plastic strain $\varepsilon_{ln}^{plastic}$ (see Table 4.6) were used in the Abaqus program and they were calculated using the following formulas (Dassault Systèmes 2013):

$$\sigma_{true} = \sigma_{eng}(1+\varepsilon_{eng}) \tag{4.19}$$

$$\varepsilon_{ln}^{plastic} = \ln(1+\varepsilon_{eng}) - \frac{\sigma_{true}}{E} \tag{4.20}$$

where σ_{eng} and ε_{eng} are the engineering stress and strain, respectively.

These equations were used up to the ultimate tensile strength point. After the maximum tension stress there is the necking region where these equations cannot be used.

Table 4.6. Metals parameters used in the finite element modelling of the shear connection test and the aluminium-concrete composite beam

Metal							
AW-6060 T6		S320GD		S235JRG2		S235J2	
E [MPa]	v [-]	E [MPa]	v [-]	E [MPa]	v [-]	E [MPa]	v [-]
62 900	0.3	193 590	0.3	207 280	0.3	206 500	0.3
σ_{true} [MPa]	$\varepsilon_{ln}^{plastic}$ [-]	σ_{true} [MPa]	$\varepsilon_{ln}^{plastic}$ [-]	σ_{true} [MPa]	$\varepsilon_{ln}^{plastic}$ [-]	σ_{true} [MPa]	$\varepsilon_{ln}^{plastic}$ [-]
153.95	0.0	351.13	0.0	564.92	0.0	423.99	0.0
166.79	0.00333	381.52	0.06942	600.36	0.00309	432.22	0.00389
181.26	0.00509	388.10	0.07681	644.55	0.00486	437.57	0.00585
190.37	0.00692	394.46	0.08414	671.43	0.00671	442.49	0.00781
199.66	0.01663	400.07	0.09142	698.33	0.01447	459.57	0.01561
204.67	0.02436	405.49	0.09866	706.79	0.02226	476.18	0.02336
209.25	0.03204	410.51	0.10584	713.27	0.02999	492.04	0.03105
213.27	0.03967	415.31	0.11297			506.85	0.03869
216.69	0.04725	419.73	0.12005			521.02	0.04627
219.48	0.05478	424.09	0.12708			534.54	0.05379
221.67	0.06226	428.05	0.13407			547.3	0.06126
223.34	0.06970	431.85	0.14100			558.75	0.06868
		435.37	0.14789			570.08	0.07605
		438.66	0.15474			580.36	0.08337
		441.99	0.16153			589.96	0.09063
		445.05	0.16829			598.81	0.09785
						607.31	0.10502
						615.25	0.11213
						622.34	0.11920
						628.84	0.12623
						634.83	0.13320
						640.20	0.14013
						644.93	0.14702
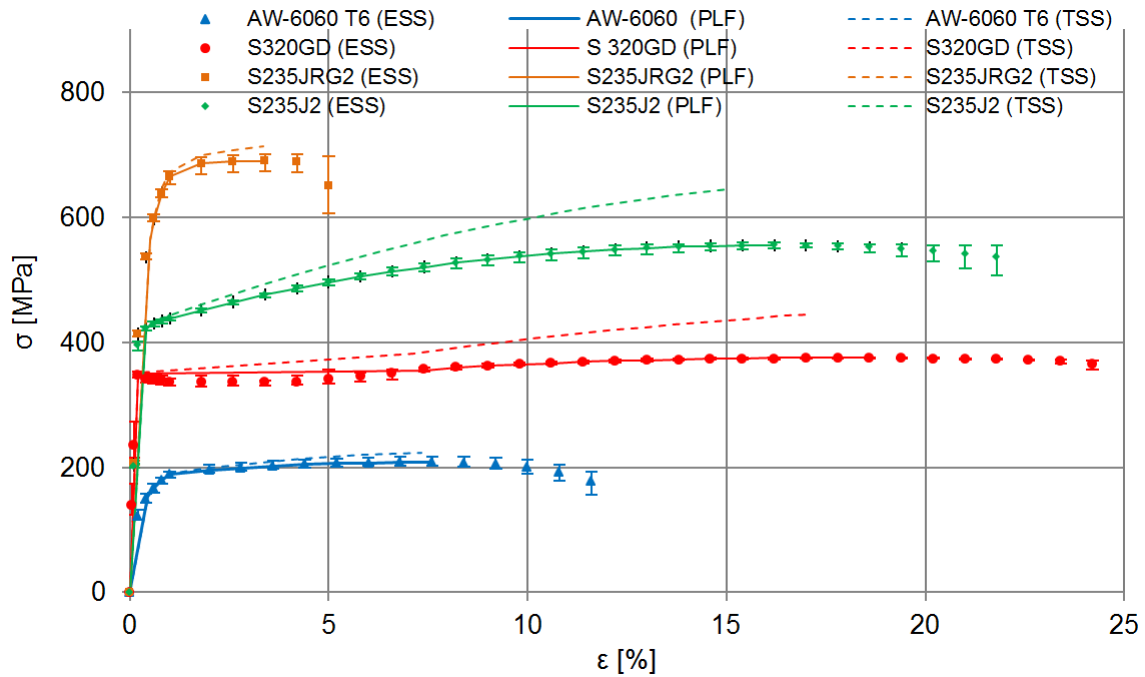
Figure 4.20. Stress–strain relationships for metals (Polus and Szumigała 2019a)

The concrete damaged plasticity (CDP) model, which is offered in the Abaqus program, was adopted to represent the behaviour of concrete. Several researchers used this model for concrete modelling, e.g., Szewczyk and Szumigała (2015, 2018).

The compressive stress–strain diagram for the analysis of the concrete subjected to compression was adopted from the Eurocode 2 (European Committee for Standardization 2004), whereas the tensile stress–strain diagram for the analysis of the concrete subjected to tension was adopted from (Kmiecik and Kamiński 2011) and (Wang and Hsu 2001) (see Fig. 4.21).
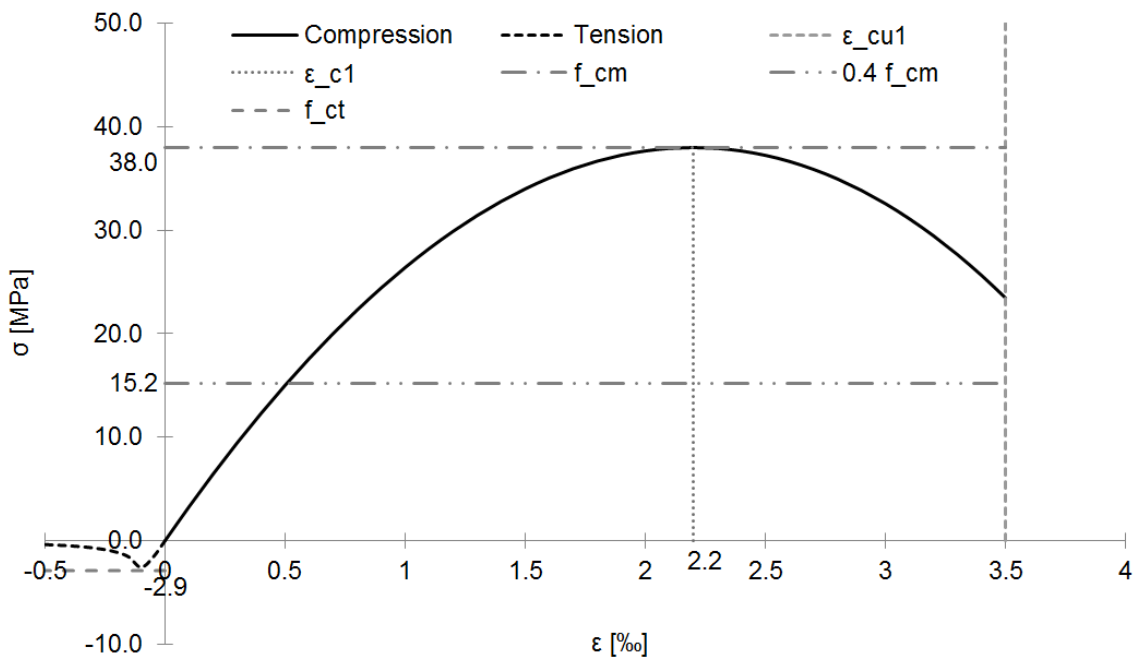
Figure 4.21. Stress–strain relationship for concrete (Polus and Szumigała 2019a)

The author evaluated only the strength of the concrete used in the push-out tests. Therefore, other strength parameters (f_{cm} = 38.0 MPa, E_c = 32.0 GPa, ε_{c1} = 2.2‰, f_{ct} = 2.9 MPa) were adopted based on the this strength and the Eurocode 2 (European Committee for Standardization 2004) (Pyrak 2012). Next, the inelastic (crushing) strain values and the cracking strain values were calculated from Eqs. (4.6) and (4.11). These data were entered into the Abaqus program. The crushing and cracking strain values were then automatically converted to plastic strain values using the relationship from Eqs. (4.8) and (4.13) (Dassault Systèmes 2013). The parameters of the concrete used in the numerical analyses are presented in Fig. 4.22 and Tables 4.7–49.
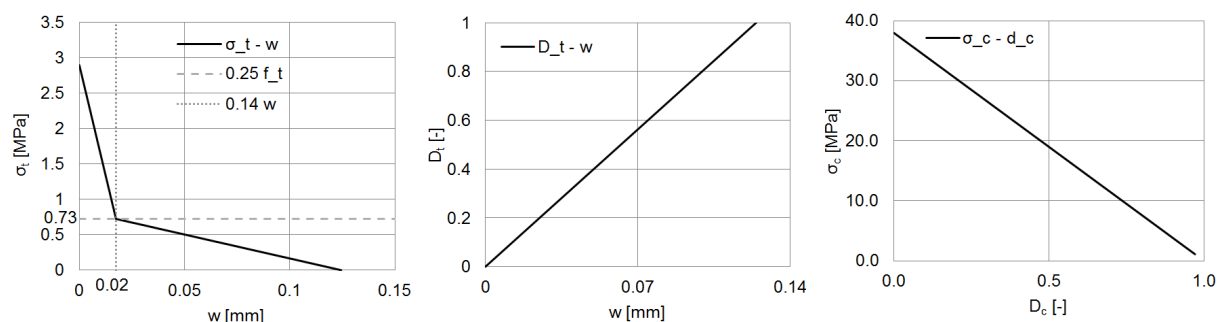
Figure 4.22. Parameters of concrete: a) tensile stress–crack width relationship (σ_t–w); b) concrete tension damage parameter–crack width relationship (D_t–w); c) compressive stress–concrete compression damage parameter relationship (σ_c–D_c) (Polus and Szumigała 2019a)

Table 4.7. Concrete parameters used in the finite element modelling of the shear connection test (Polus and Szumigała 2019a)

Parameter	Value
Young's modulus E_c [MPa]	32 000 [c]
Density [t/mm^3] ρ	2.4 · 10^{-9} [c]
Poisson's ratio v [-]	0.2 [c]
Compressive strength f_c [MPa]	38.0 [c]
Tensile strength f_{ct} [MPa]	2.9 [c]
Largest nominal maximum aggregate size d_a [mm]	16 [a]
Fracture energy G_F [N/m]	76.4 [b]
Rate of weakening n_w [-]	0.7; 1.0; 1.2; 1.5 [c]
Dilatation angle ψ [°]	40.0 [c]
Eccentricity e_e [-]	0.1 [c]
Ratio[d] f_{b0}/f_{c0} [-]	1.16 [c]
Parameter κ [-]	0.667 [c]
Viscosity parameter w_p [-]	0.00001 [c]

[a] based on own laboratory tests; [b] calculated; [c] based on literature (Kmiecik and Kamiński 2011) (European Committee for Standardization 2004) (Genikomsou and Polak 2015) (Pyrak 2012); [d] a ratio of the concrete strength in the biaxial state (f_{b0}) to the concrete strength in the uniaxial state (f_{c0})

Table 4.8. Material parameters used in the CDP model for concrete subjected to compression in the finite element modelling of the shear connection test
(Polus and Szumigała 2019a)

Concrete compression hardening		Concrete compression damage	
Stress [MPa]	Crushing (inelastic) strain [-]	D_c [-]	Crushing (inelastic) strain [-]
11.700	0.00000000	0.000	0.00000000
15.024	0.00003050	0.000	0.00003050
28.233	0.00021773	0.000	0.00021773
37.979	0.00096315	0.000	0.00096315
37.917	0.00111510	0.002	0.00111510
37.477	0.00127883	0.014	0.00127883
36.657	0.00145447	0.035	0.00145447
35.451	0.00164217	0.067	0.00164217
33.854	0.00184207	0.109	0.00184207
23.466	0.00276670	0.382	0.00276670
15.802	0.00330618	0.584	0.00330618
11.335	0.00359578	0.702	0.00359578
4.708	0.00400287	0.876	0.00400287
1.104	0.00421551	0.971	0.00421551

Table 4.9. Material parameters used in the CDP model for concrete subjected to tension in the finite element modelling of the shear connection test (Polus and Szumigała 2019a)

n_w	Concrete tension stiffening		Concrete tension damage	
	Stress [MPa]	Cracking strain [-]	D_t [-]	Cracking strain [-]
	2.9	0.000000	0.000	0.000000
	1.6663	0.000148	0.079	0.000148
	1.2545	0.000261	0.106	0.000261
	1.0257	0.000368	0.121	0.000368
	0.8774	0.000473	0.130	0.000473
	0.7723	0.000576	0.137	0.000576
	0.6933	0.000678	0.178	0.000678
	0.6314	0.000780	0.251	0.000780
0.7	0.5814	0.000882	0.310	0.000882
	0.5401	0.000983	0.359	0.000983
	0.5052	0.001084	0.401	0.001084
	0.4066	0.001487	0.518	0.001487
	0.3325	0.001990	0.606	0.001990
	0.2503	0.002992	0.703	0.002992
	0.1681	0.005295	0.801	0.005295
	0.1465	0.006445	0.826	0.006445
	2.90000	0.000000	0.00000	0.000000
	1.31406	0.000159	0.10208	0.000159
	0.87604	0.000273	0.13028	0.000273
	0.65703	0.000379	0.22063	0.000379
	0.58403	0.000432	0.30722	0.000432
1.0	0.47784	0.000535	0.43318	0.000535
	0.40433	0.000637	0.52038	0.000637
	0.32852	0.000790	0.61031	0.000790
	0.25030	0.001042	0.70310	0.001042
	0.16426	0.001595	0.80516	0.001595
	0.08343	0.003147	0.90103	0.003147
	0.04075	0.006449	0.95167	0.006449

Table 4.9. Material parameters used in the CDP model for concrete subjected to tension in
the finite element modelling of the shear connection test, continued
(Polus and Szumigała 2019a)

n_w	Concrete tension stiffening		Concrete tension damage	
	Stress	Cracking strain	D_t	Cracking strain
	[MPa]	[-]	[-]	[-]
	2.90000	0.000000	0.00000	0.000000
	1.58411	0.000100	0.08470	0.000100
	1.12166	0.000165	0.11447	0.000165
	0.68953	0.000278	0.18208	0.000278
	0.57308	0.000332	0.32021	0.000332
	0.48823	0.000385	0.42086	0.000385
1.2	0.37354	0.000488	0.55691	0.000488
	0.33317	0.000540	0.60480	0.000540
	0.24945	0.000692	0.70410	0.000692
	0.16259	0.000995	0.80713	0.000995
	0.08307	0.001747	0.90146	0.001747
	0.04183	0.003099	0.95038	0.003099
	0.01736	0.006449	0.97940	0.006449
	2.90000	0.000000	0.00000	0.000000
	1.36186	0.000107	0.09901	0.000107
	0.88456	0.000172	0.12973	0.000172
	0.63294	0.000230	0.24921	0.000230
	0.48149	0.000285	0.42885	0.000285
	0.38209	0.000338	0.54676	0.000338
1.5	0.31274	0.000390	0.62903	0.000390
	0.17023	0.000595	0.79807	0.000595
	0.07912	0.000998	0.90615	0.000998
	0.04100	0.001549	0.95137	0.001549
	0.02510	0.002149	0.97023	0.002149
	0.01644	0.002849	0.98049	0.002849

4.6. The finite element modelling of the aluminium-concrete composite beams

This section presents the main outcomes of the numerical analyses described in (Polus and Szumigała 2019a).

The discrete model of the aluminium-concrete composite beam was built in the Abaqus 6.13 environment (Dassault Systèmes 2013) and then examined using the Abaqus/Standard finite element code. The Newton-Raphson method was used as a numerical technique for solving non-linear equilibrium equations. The aluminium-concrete composite beam had two axes of symmetry. For this reason, only ¼ of the specimen was prepared in the program. The finite element (FE) model consisted of ¼ of the aluminium I-beam, ¼ of the profiled steel sheeting, ¼ of the reinforcing steel meshes, ¼ of the concrete slab, ½ of the steel plate, and 6½ shear connectors. In the place of the sheet-to-sheet connection the thickness of the profiled steel sheeting was doubled (see Fig. 4.23). The sensitivity of the model to various parameters was investigated. A number of FE models were analysed, some of which are presented in Table 4.10. The FE model of the aluminium-concrete composite beam used the same type of connection (zero-length springs) as the FE model of the aluminium-concrete composite connection presented in Section 4.5. Figure 4.24 presents the boundary conditions used in the computer model.
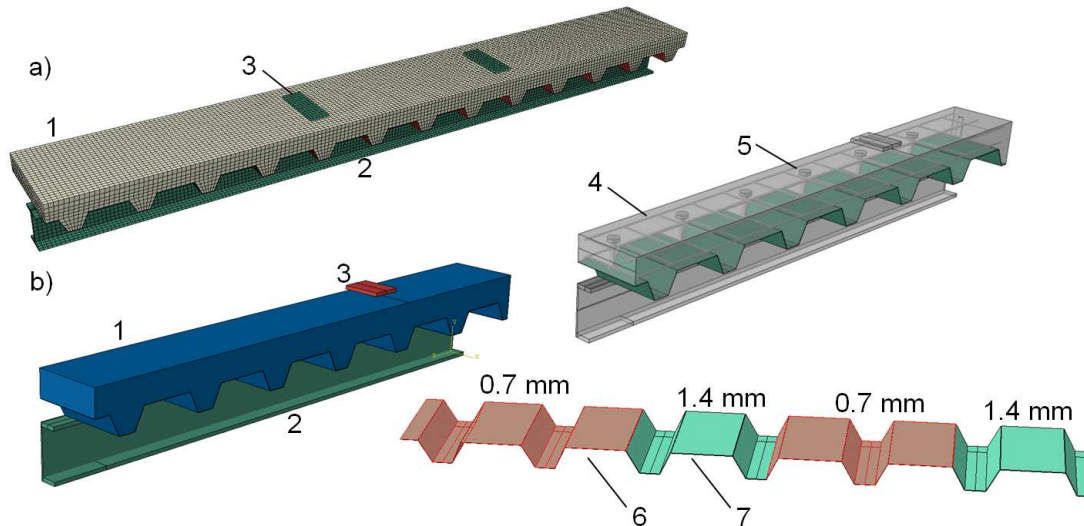
Figure 4.23. The FE model of the aluminium-concrete composite beam in the Abaqus environment: a) complete model; b) ¼ of the model; 1 – concrete slab, 2 – aluminium beam, 3 – steel plate, 4 – reinforcing steel mesh, 5 – shear connector, 6 – profiled steel sheeting (0.7 mm), 7 – profiled steel sheeting (1.4 mm) (double thickness in the place of the sheet-to-sheet connection) (Polus and Szumigała 2019a)

Seven points were selected on the aluminium beam and the same number of points was selected on the concrete slab. The locations of the points corresponded to the locations of the connectors in the beam tested in the laboratory (see Fig. 4.10). Zero-length wires were created between the points. An axial connection was selected for each wire and the position of each connector was specified using the coordinate system in which x direction was parallel to the length of the aluminium beam. The connectors enabled the slip between the concrete slab and the aluminium beam in x direction. Three models of the shear connector were used (see Fig. 4.25). In the first model (F–s 1), the response of the connector was non-linear to reflect the average shear force-slip curve for the three specimens from the push-out tests (see also Fig. 5.10). In the second (F–s 5, $k = 5.5$ kN/mm, $P_{ult} = 43.4$ kN) and third models (F–s 6, $k = 12.5$ kN/mm, $P_{ult} = 43.4$ kN), the responses of the connectors were also non-linear to reflect the elasto-plastic theoretical model of the dowel-bolt connector presented in Section 3.1 (see also Tables 5.4 and 5.6). The data containing the values of forces and displacements were used in the program. In the FE model of the aluminium-concrete beam steel solid elements (shear connectors) were added (see Fig. 4.23) and embedded in the concrete slab to increase its stiffness. It was done because the stiffness of the flexural member depends not only on the second moment of area, but also on the Young's modulus of the material. The author of this dissertation emphasizes the fact that these elements were not used to join the aluminium beam and the concrete slab. They were only used to account for the fact that the slab was made not only of concrete but also of steel (in shear connectors). When the steel elements were embedded in the concrete slab, the stiffness of the aluminium-concrete composite beam increased slightly. What is more, a tie function was analysed as a connection between the aluminium beam and the concrete slab, to investigate its impact on the behaviour of the computer model. A continuous "tie" type contact is used to model full composite action in composite beams (Aliawdin and Urbańska 2011). The behaviour of the numerical model with

discrete springs was compared with the behaviour of the numerical model with the continuous "tie" type contact between the concrete slab and the aluminium beam.
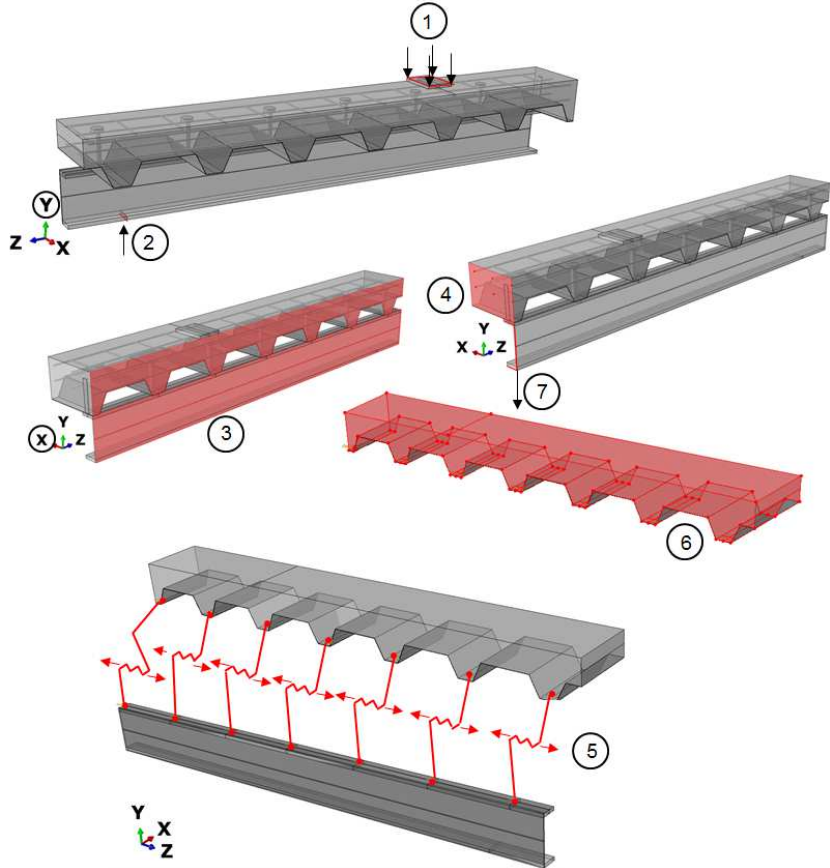
Figure 4.24. Boundary conditions: 1 – displacement, 2 – displacement in y direction (fixed), 3 – displacement in x direction (fixed) and rotation around y and z axes (fixed), 4 – displacement in z direction (fixed) and rotation around x and y axes (fixed), 5 – connector (spring), 6 – predefined field (temperature), 7 – dead load (Polus and Szumigała 2019a)
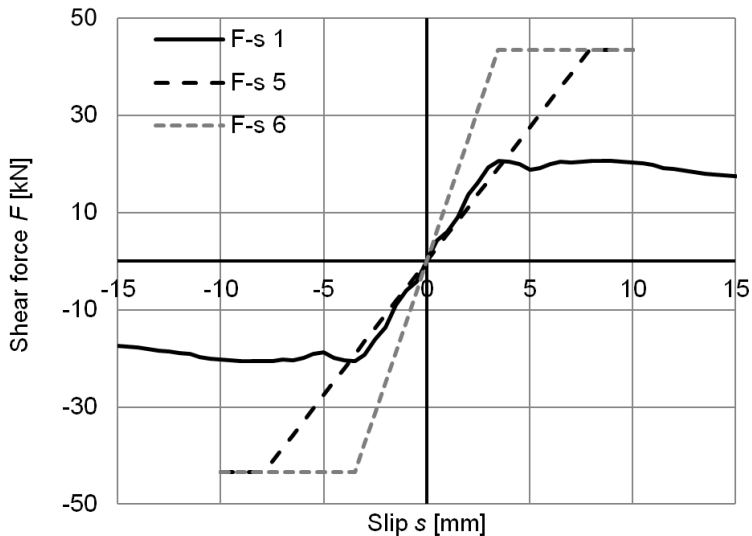
Figure 4.25. Models of shear connectors used in the FE analyses of the aluminium-concrete composite beam

Table 4.10. Finite element analyses of the aluminium-concrete composite beam

FEA	FEs [a]	Mesh size [mm]	Concrete model [b]	Connection model [c]
1	1: 3006 C3D8R; 2, 3, 5: 1794 S4R 4: 664 T3D2; 6: 3990 C3D10, 10 C3D8R Total: 9464	20	I	C
2	1: 3006 C3D8R; 2, 3, 5: 1794 S4R 4: 664 T3D2; 6: 3990 C3D10, 10 C3D8R Total: 9464	20	II	A
3	1: 3006 C3D8R; 2, 3, 5: 1794 S4R 4: 664 T3D2; 6: 3990 C3D10, 10 C3D8R Total: 9464	20	II	B
4	1: 3006 C3D8R; 2, 3, 5: 1794 S4R 4: 664 T3D2; 6: 3990 C3D10, 10 C3D8R Total: 9464	20	II	C
5	1: 3006 C3D8R; 2, 3, 5: 1794 S4R 4: 664 T3D2; 6: 3990 C3D10, 10 C3D8R Total: 9464	20	II	D
6	1: 3006 C3D8R; 2, 3, 5: 1794 S4R 4: 664 T3D2; 6: 3990 C3D10, 10 C3D8R Total: 9464	20	III	D
7	1: 852 C3D8R; 2, 3, 5: 878 S4R 4: 462 T3D2; 6: 3990 C3D10, 6 C3D8R Total: 6188	30	II	D
8	1: 7878 C3D8R; 2, 3, 5: 3520 S4R 4: 866 T3D2; 6: 3990 C3D10, 14 C3D8R Total: 16 268	15	II	D
9	1: 3006 C3D8; 2, 3, 5: 1794 S4R 4: 664 T3D2; 6: 4085 C3D10 Total: 9549	20	II	D
10	1: 3006 C3D8I; 2, 3, 5: 1794 S4R 4: 664 T3D2; 6: 4085 C3D10 Total: 9549	20	II	D

[a] Finite elements used to model the: 1 – concrete slab, 2 – aluminium beam, 3 – steel plate, 4 – steel mesh, 5 – profiled steel sheeting, 6 – connector

[b] Concrete model: I – elastic (E_c = 37.3 GPa, v = 0.2), II – CDP (viscosity w_p = 0.00001), III – CDP (viscosity w_p = 0.0001)

[c] Connection model: A – tie function, B – shear force–slip curve for one connector from the laboratory tests (see F–s 1 in Fig. 4.25), C – shear force–slip curve for one connector from the theoretical analysis (k = 5.5 kN/mm and P_{ult} = 43.4 kN) (see F–s 5 in Fig. 4.25), D – shear force–slip curve for one connector from the theoretical analysis (k = 12.5 kN/mm and P_{ult} = 43.4 kN) (see F–s 6 in Fig. 4.25)

The concrete slabs were modelled with C3D8R elements (8-node linear brick elements with reduced integration and hourglass control) (FEA 1–8), C3D8 elements (8-node linear brick elements) (FEA 9) or C3D8I elements (incompatible mode 8-node linear brick elements) (FEA 10). The shear connectors were modelled with C3D8R elements and C3D10 elements (10-node quadratic tetrahedron elements). The reinforcing mesh was modelled with T3D2 elements (2-node linear 3D truss elements). Several researchers used these elements for modelling reinforcement bars, e.g. Ciesielczyk, Szumigała and Ścigałło (2016) and Jankowiak and Madaj (2017). The aluminium beam, the steel plate and the profiled steel sheeting were

modelled with S4R elements (4-node shell elements with reduced integration). These shell elements were also used by Ciesielczyk and Studziński (2017) to model thin-walled Z-beams and steel facings of a sandwich panel.

Depending on the FEA, the size of the mesh was 15, 20, 30 mm and the total number of all elements was 6188, 9464, 9549 and 16 268 (see Fig. 4.26).
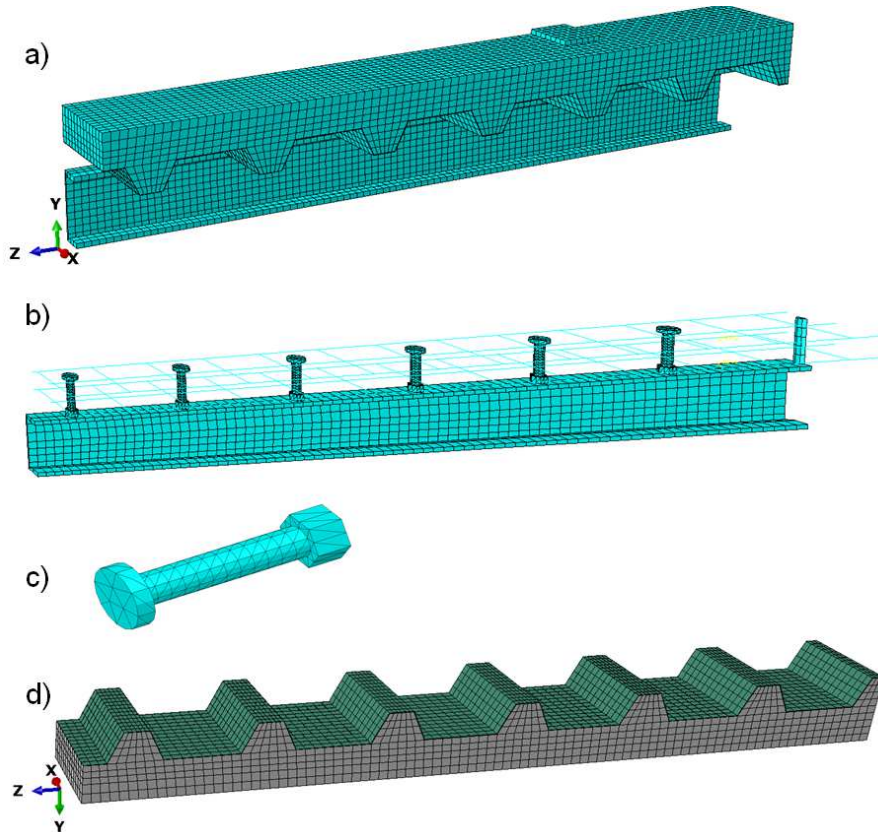
Figure 4.26. The mesh used in the numerical calculations: a) ¼ of the model,
b) aluminium beam with steel meshes and connectors, c) connector, d) profiled steel sheeting
(Polus and Szumigała 2019a)

The surface-to-surface "hard" contact and the friction ($\mu = 0.3$) were defined between the flange of the aluminium beam and the edge of the concrete slab. The same value of the friction coefficient between a steel flange and a concrete slab was used by Guezouli and Lachal (2012). The perfect bond was assumed to exist between the concrete and the reinforcement. The reinforcing steel meshes were embedded in the concrete slab.

The analysis was divided into three steps. In step one, the concrete slab was cooled down ($\Delta T = -23.4$ K) to take into account the shrinkage of concrete, which, along with the ratio of girder stiffness to concrete deck stiffness, the strength of concrete and the diameter of the shear connector, have influence on the adhesion of a concrete slab to a metal girder (Furtak 2015). Adhesion has a strong impact on the load bearing capacity of the flexible connection. What is more, shrinkage has an impact on the ultimate load capacity and serviceability limit states of structural elements (Flaga 2015). The total shrinkage strain was the sum of drying shrinkage strain (0.140‰) and autogenous shrinkage strain (0.094‰) according to (Puchalska and Kuczma 2017) and the Eurocode 2 (European Committee for Standardization 2004).

Drying shrinkage is the result of the loss of capillary water from the hardened cement mixture (Raczkiewicz 2012). Autogenous shrinkage is the result of the uniform reduction of internal moisture due to cement hydration (Jianxia 2012). The relationship between temperature, the linear coefficient of thermal expansion ($10 \cdot 10^{-6}$ 1/K) and strain was taken into account. In step two, the dead load of the aluminium-concrete composite beam was applied. In step three, the load was applied in the form of displacement.

The models of the metals used in the numerical simulation are presented in Fig. 4.20. The parameters of the metals used in the finite element modelling of the aluminium-concrete composite beam are listed in Table 4.6.

The behaviour of concrete was described using a concrete damaged plasticity model. The same concrete was used for the cylinders and the aluminium-concrete composite beams. Therefore, the parameters of the concrete used in the finite element modelling of the aluminium-concrete composite beam were the same as the parameters of the concrete used in the finite element modelling of the concrete cylinder subjected to compression (see Section 4.4).

Results and discussions

This chapter presents the main outcomes of the analyses described in (Polus and Szumigała 2017a) (Polus and Szumigała 2019a) (Polus and Szumigała 2019c).

Measurement uncertainty was calculated for each test using a statistical method called Method A (Słowik and Bartkowiak 2016) and the results were presented with a confidence interval. According to Słowik and Bartkowiak (2015), in each test the sample size n_s was very small ($n_s \leq 10$) or small ($10 < n_s \leq 30$). For this reason, the author of this dissertation assumed that the random variable in each test had the Student t-distribution with ($n_s - 1$) degrees of freedom (Ramachandran and Tsokos 2015). The arithmetic means, the standard deviations, and the 95% confidence interval for the population mean were calculated. The 95% confidence interval for the population mean μ_s was calculated as (Zieliński 1972):

$$\left[\bar{x} - \frac{t_s s_d}{\sqrt{n_s - 1}}, \bar{x} + \frac{t_s s_d}{\sqrt{n_s - 1}} \right] \tag{5.1}$$

where:
$\bar{x}$ – sample mean
s_d – standard deviation
t_s – value from t table
n_s – sample size.

5.1. Properties of the materials

The mechanical properties of the metals were obtained from the uniaxial tensile tests and are presented in Table 5.1.
Figure 5.1 demonstrates the types of fractures which were observed in the metal specimens. In the first, third and fourth groups of tests, ductile cup and cone fractures occurred, while in the second group of tests, shear fractures were observed. In the case of cup and cone fracture, the outer regions of a specimen fail in shear, while the interior regions fail in tension (Roylance 2001).

Chapter 5. RESULTS AND DISCUSSIONS

Table 5.1. Metal specimens, measured mean values (Polus and Szumigała 2019a)

No.	Material	Specimens	f_y [MPa]	R_m [MPa]	E [GPa]
1	4 specimens of AW-6060 T6 aluminium alloy		153.26 ± 9.31 6.07% [c] 5.85 [a]	207.68 ± 10.55 5.08% [c] 6.63 [a]	62.87 ± 7.14 11.36% [c] 4.49 [a]
2	6 specimens of S320GD grade steel		350.43 ± 3.44 0.98% [e] 3.28 [a]	374.42 ± 0.96 0.26% [e] 0.91 [a]	193.59 ± 12.4 6.40% [e] 11.80 [a]
3	5 specimens of S235JRG2 grade steel		562.11 ± 7.39 1.31% [d] 5.95 [a]	689.88 ± 14.95 2.17% [d] 12.04 [a]	207.28 ± 2.38 1.15% [d] 1.92 [a]
4	3 specimens of S235J2 grade steel		422.3 ± 9.40 2.23% [b] 3.79 [a]	557.2 ± 4.72 0.85% [b] 1.90 [a]	206.50 ± 19.43 9.41% [b] 7.82 [a]
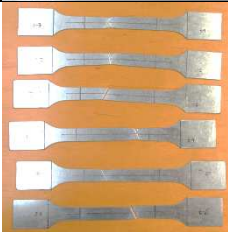
[a] Sample standard deviation
[b] Measurement errors were calculated according to Student's t-distribution using 2 degrees of freedom and a confidence level of 0.95.
[c] Measurement errors were calculated according to Student's t-distribution using 3 degrees of freedom and a confidence level of 0.95.
[d] Measurement errors were calculated according to Student's t-distribution using 4 degrees of freedom and a confidence level of 0.95.
[e] Measurement errors were calculated according to Student's t-distribution using 5 degrees of freedom and a confidence level of 0.95.

a)

b)

c)

d)
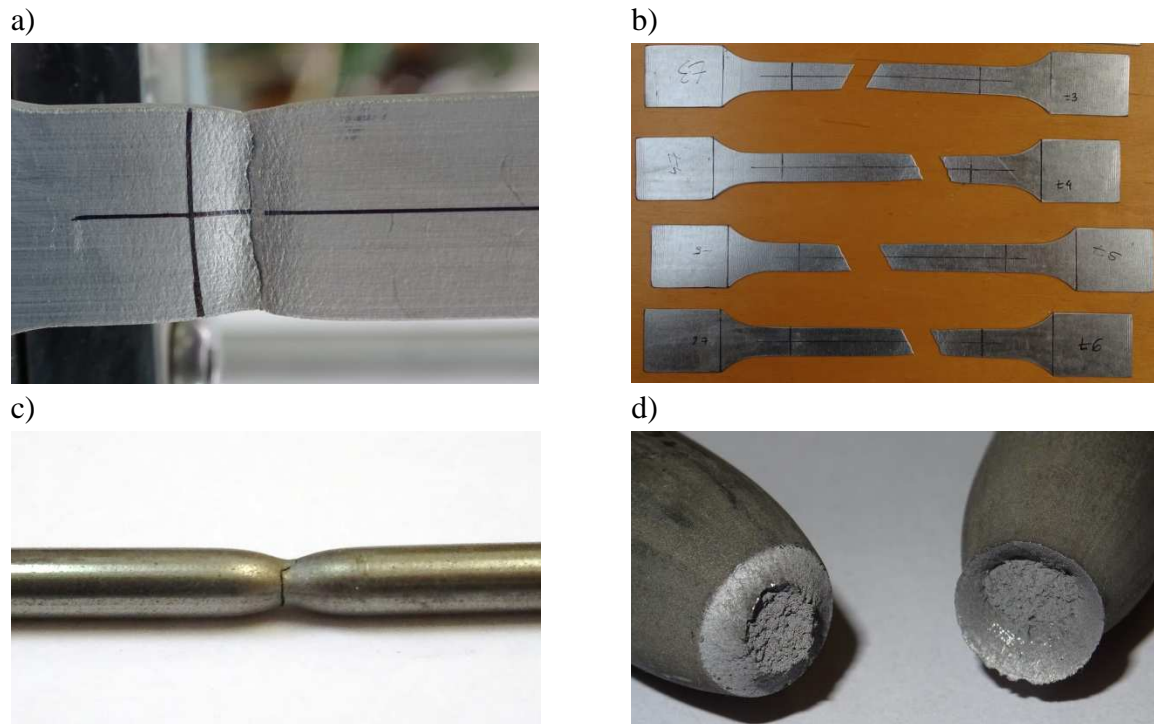
Figure 5.1. Types of fractures observed in the metal specimens: a) ductile cup and cone fracture in the AW-6060 T6 aluminium alloy specimen, b) shear fracture in the S320GD steel specimens, c) ductile cup and cone fracture in the S235JRG2 steel specimen, d) ductile cup and cone fracture in the S235J2 steel specimen

Additional tensile tests of the AW-6060 T6 aluminium alloy were conducted by (Chybiński et al. 2019). It was found that the strain rate sensitivity of the alloy was low at room temperature. The size of the sample did not impact the tensile strength when the flat samples were proportional and prepared in accordance with the EN ISO 6892-1 standard (European Committee for Standardization 2016).

The mechanical properties of the concrete were determined in compressive and splitting tests. The results of said tests are shown in Table 5.2. The types of failure of the concrete specimens are presented in Fig. 5.2. The failure of concrete cubes may be explosive or non-explosive (Neville and Brooks 2010) (Subramanian 2013). Some authors also distinguish a third type – semi-explosive failure of concrete cubes (Hamad 2017). In the compressive tests, the non-explosive failure of concrete cubes was observed. In the splitting tests, the concrete cylinders were split into two parts. During the compressive tests the cone failure of the concrete cylinders was observed.

Chapter 5. RESULTS AND DISCUSSIONS

Table 5.2. Set of concrete specimens, measured mean values (Polus and Szumigała 2019a)

No.	Specimens	Quantity/ age	$f_{c,cube}$ [MPa]	f_c [MPa]	v [-]	$E_{c,0}$ [GPa]	$E_{c,s}$ [GPa]	f_{ct} [MPa]
Concrete from the shear connection tests							
1		4 28 days	34.33 ± 2.65 7.71% [c] 1.66 [a]	–	–	–	–	–
2		12 70 days	43.46 ± 2.09 4.81% [f] 2.69 [a]	–	–	–	–	–
Concrete from the bending tests							
3		4 28 days	56.63 ± 2.12 3.74% [c] 1.33 [a]	–	–	–	–	–
4		8 196 days	65.71 ± 1.67 2.54% [e] 2.00 [a]	–	–	–	–	–
5		3 269 days	–	–	–	–	–	4.61 ± 0.75 16.19% [b] 0.30 [a]
6		5 274 days	–	61.82 ± 3.85 6.22% [d] 3.10 [a]	–	–	–	–
7		4 314 days	–	–	0.19 ±0.03 15.24% [c] 0.02 [a]	33.51 ± 1.53 4.58% [c] 0.96 [a]	37.33 ± 1.44 3.86% [c] 0.91 [a]	–

[a] Sample standard deviation
[b] Measurement errors were calculated according to Student's t-distribution using 2 degrees of freedom and a confidence level of 0.95.
[c] Measurement errors were calculated according to Student's t-distribution using 3 degrees of freedom and a confidence level of 0.95.
[d] Measurement errors were calculated according to Student's t-distribution using 4 degrees of freedom and a confidence level of 0.95.
[e] Measurement errors were calculated according to Student's t-distribution using 7 degrees of freedom and a confidence level of 0.95.
[f] Measurement errors were calculated according to Student's t-distribution using 11 degrees of freedom and a confidence level of 0.95.

a)

b)

c)

d)
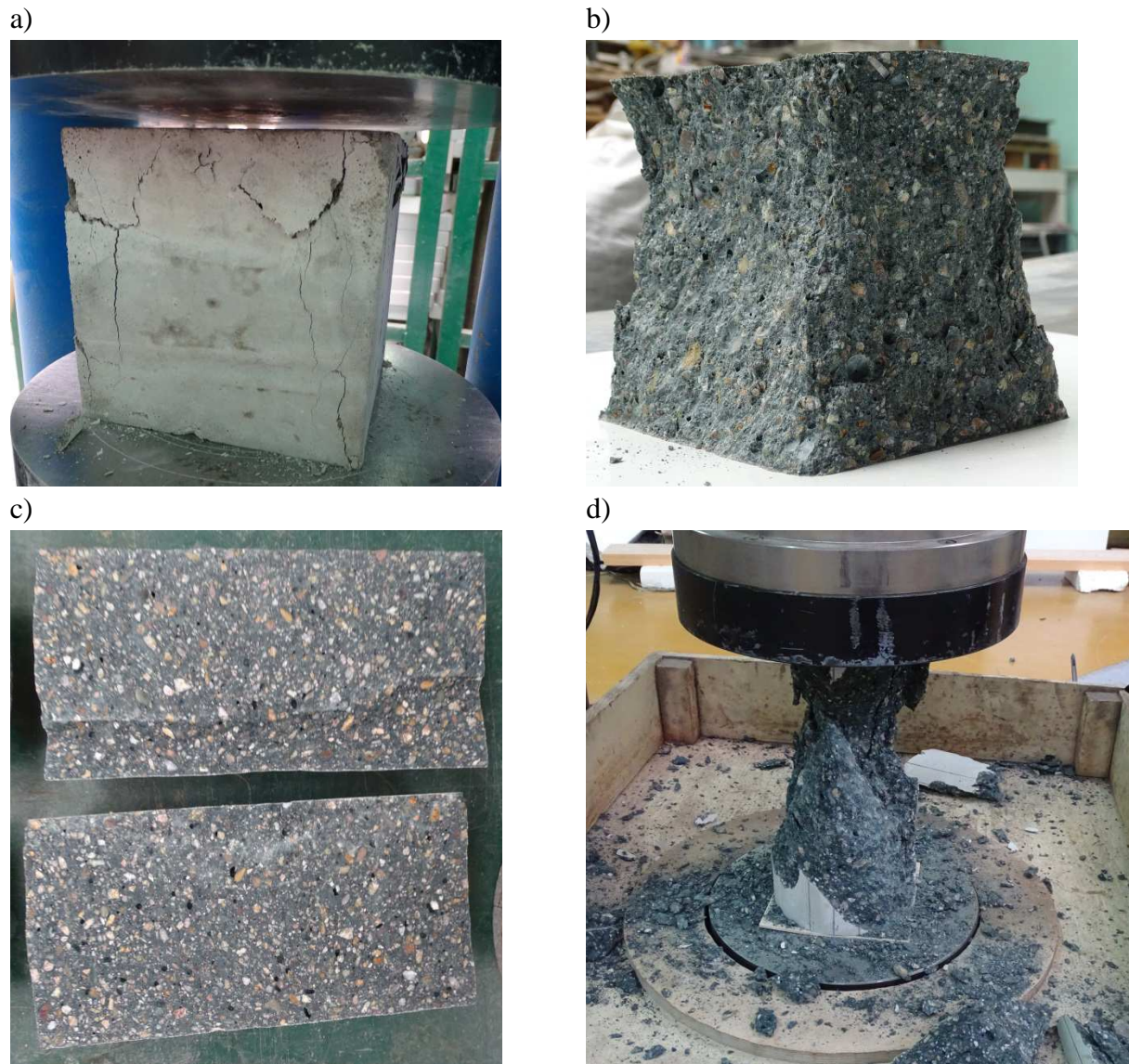
Figure 5.2. Types of failure of the concrete specimens: a) non-explosive failure of the cube made of concrete from the shear connection tests b) non-explosive failure of the cube made of concrete from the bending tests c) concrete cylinder split into two parts d) cone failure of the concrete cylinder

5.2. The results of the shear connection test

The shear force–slip curves for all the specimens are presented in Figs. 5.3–5.6. Each curve represents the mean value of the slip measured by two LVDTs. The curves reflect the behaviour of the specimens when the cyclical load and the failure load were applied. The dotted lines illustrate performance of the connections for the slip moduli $k_{0.4}$ and $k_{0.6}$. The slip modulus $k_{0.4}$ is calculated as the secant value at 40% of the load-carrying capacity of the connection and is suggested for serviceability limit state calculations (Łukaszewska, Johnsson and Fragiacomo 2008). The slip modulus $k_{0.6}$ is calculated as the secant value at 60% of the load-carrying capacity of the connection and is suggested for the ultimate limit state calculations (Ceccotti, Fragiacomo and Giordano 2007) (Szumigała M., Szumigała E. and Polus 2018).
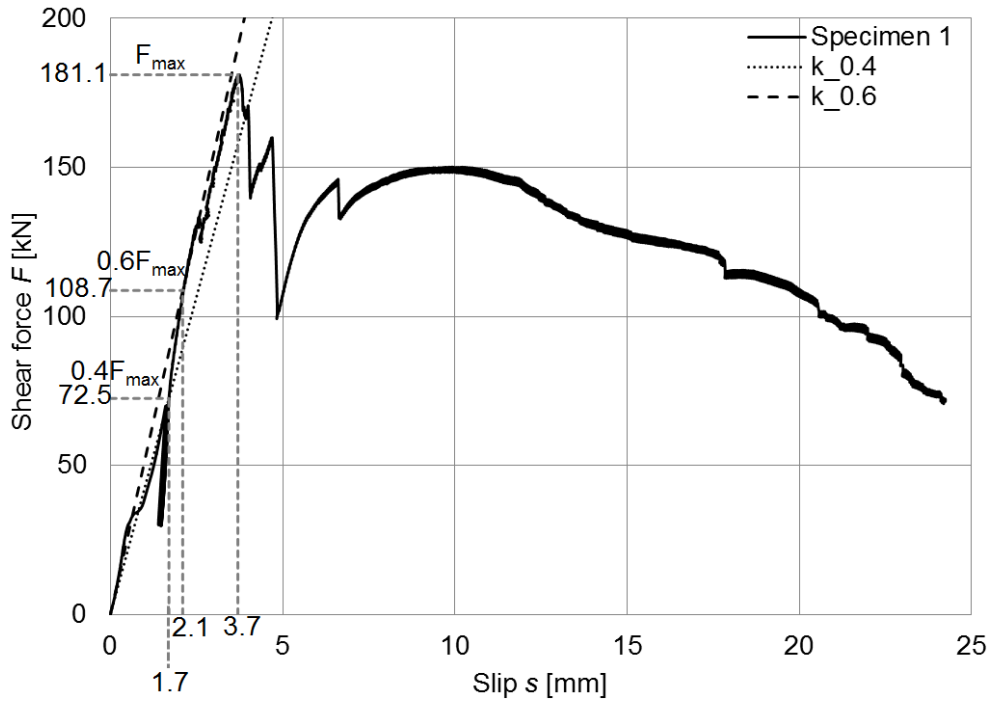
Figure 5.3. The shear force–slip curve for specimen 1
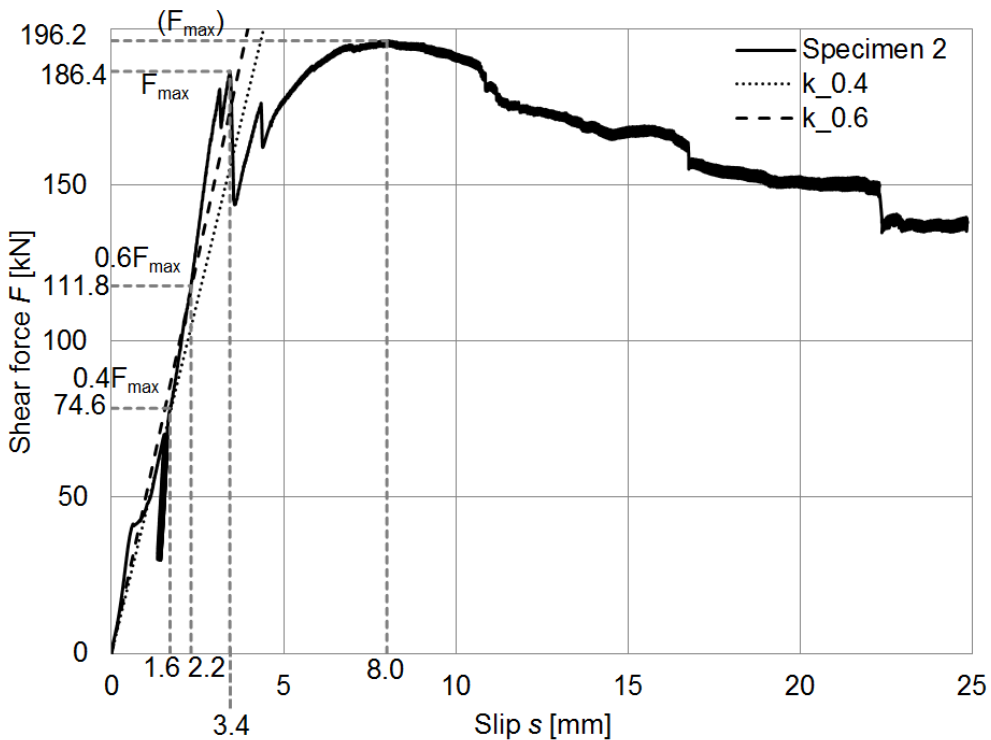
Figure 5.4. The shear force–slip curve for specimen 2

The shape of the shear force–slip curves obtained from the tests is not as regular as the one shown in Fig. B.2 of the EN 1994-1-1 standard (European Committee for Standardization 2004). For each specimen the shear force–slip relationship was linear elastic up to the first crack. Beyond this point, the curves were bumpy. During the tests, premature concrete-related failure modes occurred and they had a negative impact on the margin of scatter of test results and on the maximum shear force.
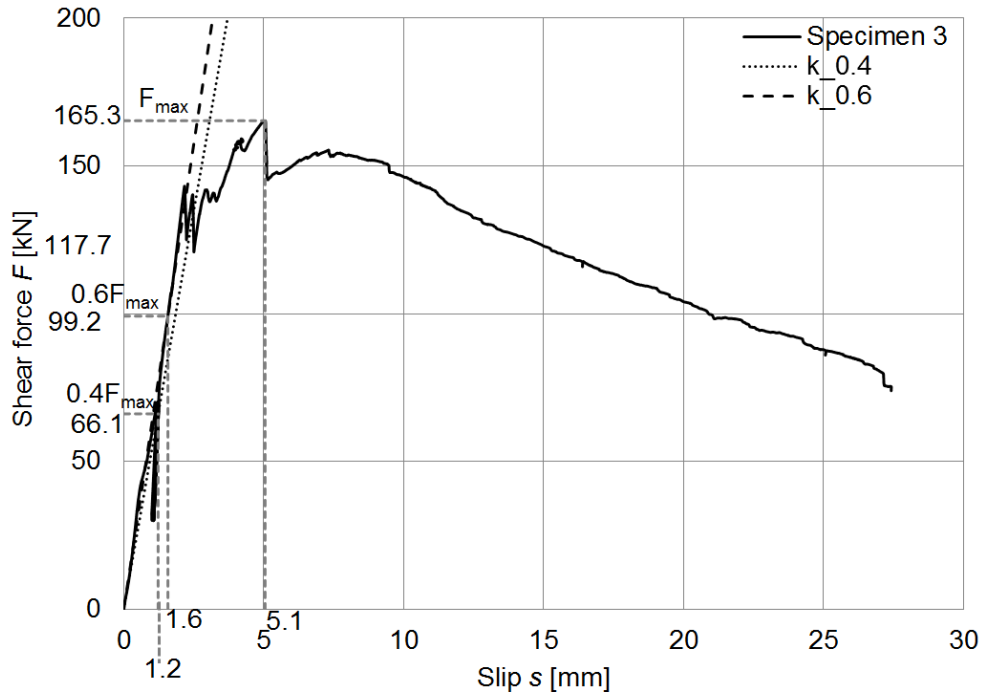
Figure 5.5. The shear force–slip curve for specimen 3
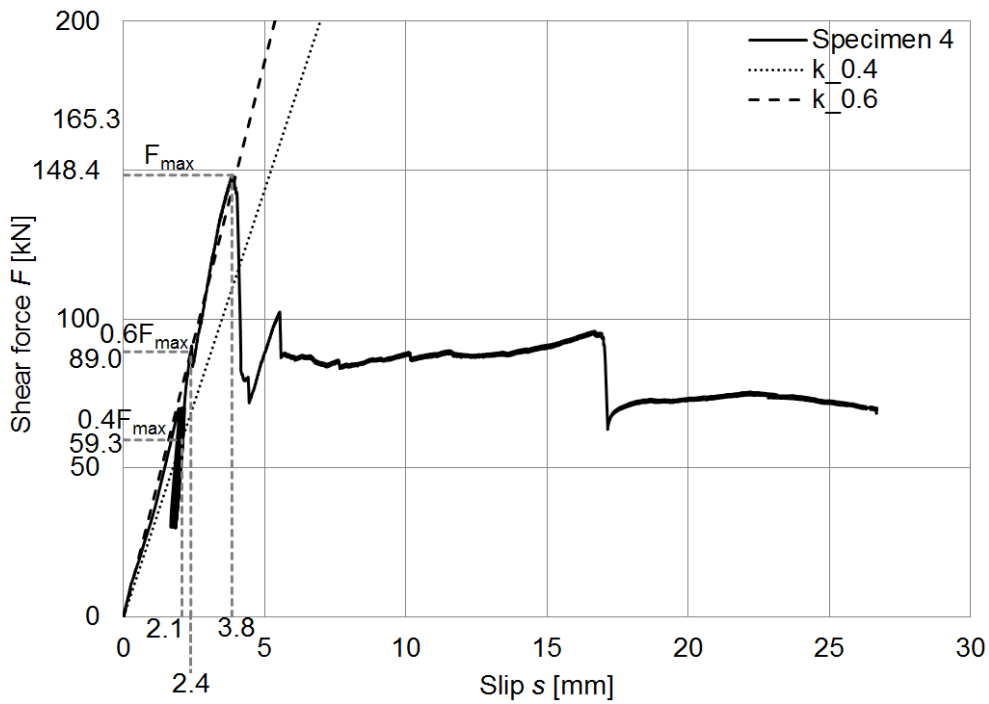
Figure 5.6. The shear force–slip curve for specimen 4

Figure 5.7. presents the shear force–slip curves for the specimens 1–3 and the mean shear force–slip curve for the analysed connection.
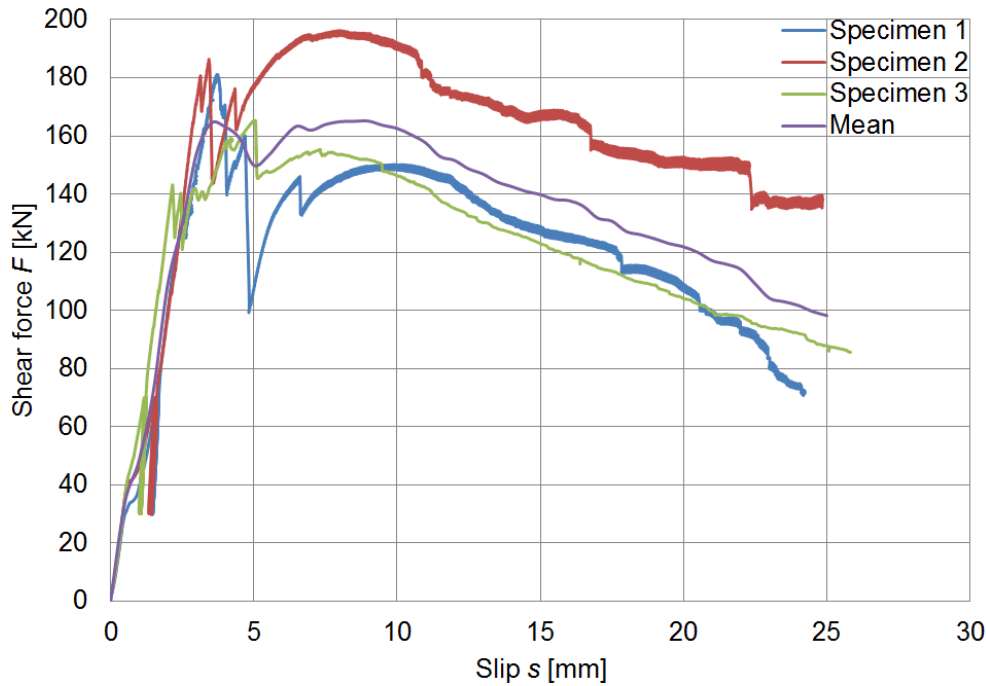
Figure 5.7. The shear force–slip curves for specimens 1–3 and the mean shear force–slip curve for the analysed connection (Polus and Szumigała 2016)

For each specimen, a sharp fall of the load-slip curve at the peak load was recorded (see Figs. 5.3–5.7). The sudden drop from the peak load was also observed by Etim et al. (2020) in the push-out tests with 19 mm bolts used as shear connectors. However, the cause of the sharp fall observed by Etim et al. (2020) was different than in the tests presented in this dissertation. In the test conducted by Etim et al. (2020), the sudden fall from the peak load resulted from the bearing failure. In the push-out tests presented in this dissertation, cracks in the concrete slabs were observed (see Figs. 5.8 and 5.9). The first premature cracks were the result of tension in the concrete slab. They appeared in the ribless section of the slab, where the stiffness of the slab was the lowest. This type of failure is known as the back-breaking failure (Hicks 2008). The aforesaid tension occurred in the concrete slab because the slab was not thick enough and it bent towards the aluminium beam. Each crack caused the decrease of the load. Afterward, rib-shearing caused by a longitudinal force appeared in the concrete ribs. The rib-shear failures also caused the decrease of the load. The connectors were bent, but they were not cut off. The failure mode of the connections was associated with the concrete cracking and the formation of a plastic hinge within the connector. Mirza, Uy and Krezo (2008, 2009 & 2011) also observed concrete damage in the thin layer of the concrete slab (the ribless section of the concrete slab). They conducted push-out tests of 19 mm headed stud shear connectors used in solid slabs or slabs with profiled steel sheeting. For the slab with profiled steel sheeting, the failure mode was concrete failure, and for the solid slab, the failure mode was stud fracture (the shear connectors were sheared off). According to Mirza and Uy (2009), the back-breaking failure was not the primary cause of the sample damage. The authors suggested that this type of failure had been exacerbated by the concrete tensile and compression failure in the specimen, which had then given rise to large deformations and the bending failure of the slab.

a)

b)

c)

d)
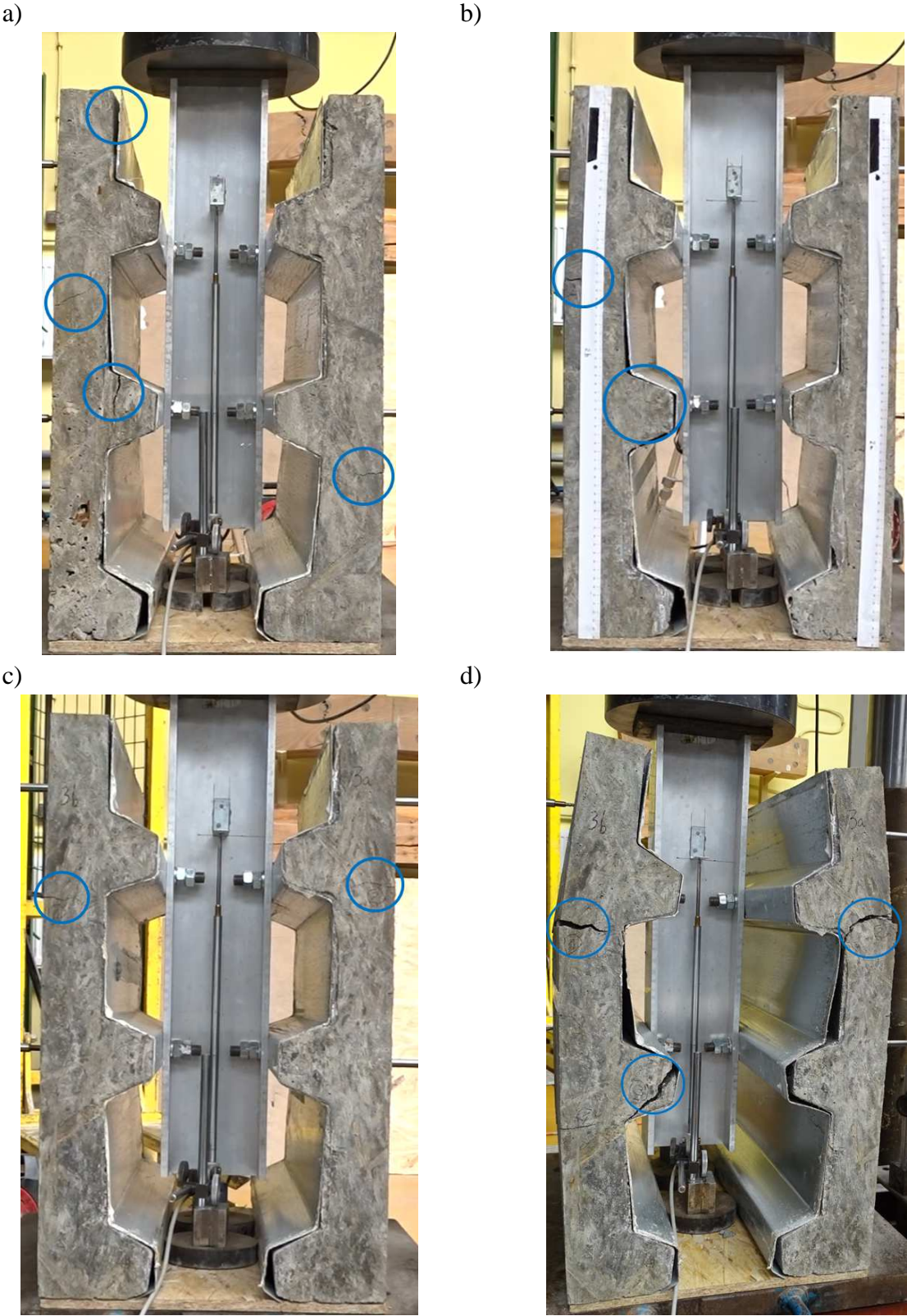
Figure 5.8. Failure modes of specimens 1–3: a) the profiled sheeting separated from the concrete slab, cracks in the concrete slabs caused by tension, rib-shear failure in specimen 1; b) the profiled sheeting separated from the concrete slab, a crack in the concrete slab caused by tension in specimen 2; c) cracks in the concrete slabs caused by tension in specimen 3; d) the profiled sheeting separated from the concrete slab, cracks in the concrete slabs caused by tension, rib-shear failure in specimen 3 at the end of the test

a)   b)
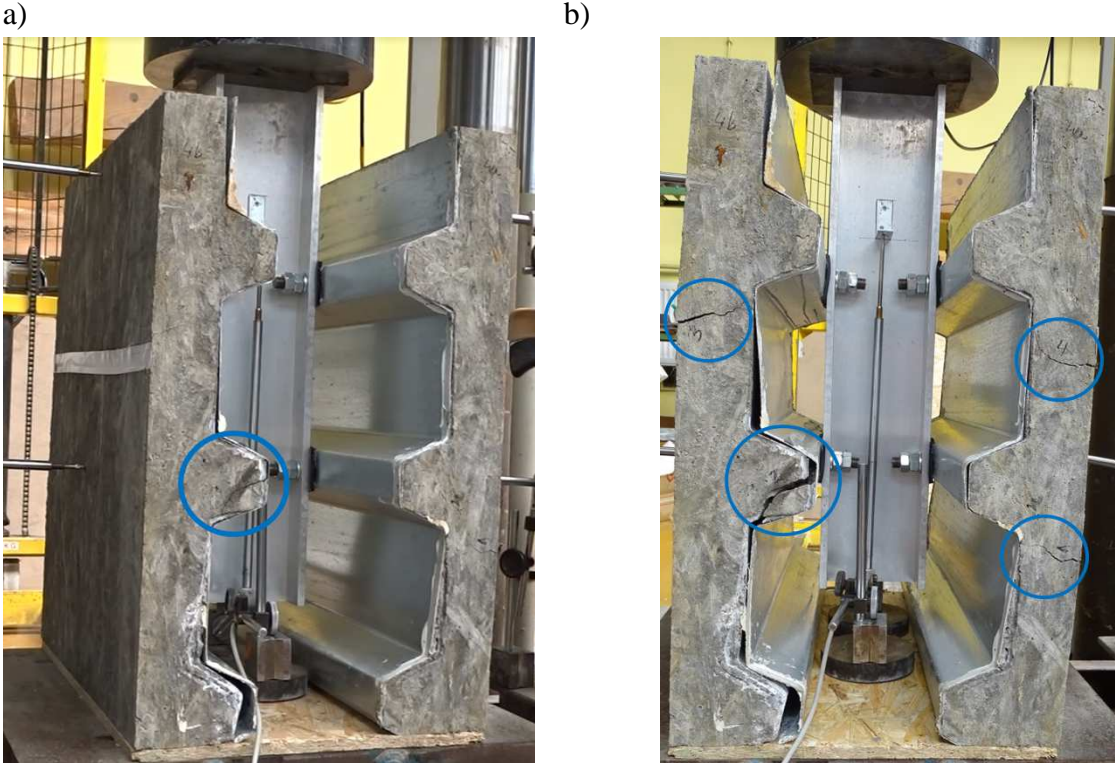
Figure 5.9. Failure modes of specimen 4: a) rib-shear failure; b) the profiled sheeting separated from the concrete slab, cracks in the concrete slabs caused by tension, rib-shear failure at the end of the test

The cracks caused by tension might have been prevented by using thicker slabs and two reinforcing meshes in both concrete slabs. If the tension-induced cracks had not occurred, the maximum shear force of the tested specimens could have been higher. The reason why thicker slabs with two reinforcing meshes were not used in the shear connection tests was that the author of this dissertation was trying to reflect the behaviour of the connections in the aluminium-concrete composite beams with profiled steel sheeting. The author used the same thickness of concrete slabs in the shear connection tests as in the bending tests. What is more, only one reinforcing mesh was used in each concrete slab, which is usually the case in steel-concrete composite beams. Kim, Wrigth and Cairns (2001) also used one reinforced mesh placed on top of the profiled sheeting in the push-out tests. However, the push out test is mainly suitable for solid slabs and connectors small enough for shank failure to occur. The test is not comprehensive, especially when profiled sheeting is used (Johnson 2012). It is difficult to prepare a correct model in which the strength is the result of the shearing of the steel connector. What is more, the stress state in the connector is impossible to determine in the traditional push-out test. For this reason, new tests of shear connectors or improved standard push tests are proposed. A new shear test was presented by Lorenc et al. (2010). It can be used to determine stresses in a steel connector under conditions similar to those occurring in a composite beam subjected to the positive bending moment, where the metal beam is under tension and the concrete slab is under compression. A tension tie may be used between concrete slabs as a modification of the standard test (Roik and Hanswille 1987) (Smith and Couchman 2010). An improved standard push test was presented by Smith and

Couchman (2010), and Hicks and Smith (2014). Horizontal jacks which applied lateral load to the push-out specimen were added to more accurately reflect the conditions that exist in a composite beam subjected to bending. Thanks to the horizontal jacks, compression force occurs at the interface between the flange of the steel beam and the concrete slab, which represents the floor loading in real composite beams.

Table 5.3 presents the calculation of the load-carrying capacity of the shear connector used in aluminium-concrete composite joints.

Table 5.3. The load-carrying capacity of the shear connector used in aluminium-concrete composite joints

Parameters	Value
Shank diameter d [mm]	16.0
Partial factor γ_v [–]	1.0
Reduction factor k_t [–]	0.52
Coefficient α [–]	1.0
Cylindrical compressive strength f_c [MPa]	30.0
Mean secant modulus of concrete E_{cm} [GPa]	32.0
Coefficient β [–]	0.74
Ultimate strength of the steel used in the shear connector f_u [MPa]	557.2
Cross-sectional area of the shear connector A_{sc} [cm^2]	2.0
Coefficient α_v [–]	0.6
Gross cross-section area of the connector A [cm^2]	2.0
Partial factor γ_{M2} [–]	1.0
Coefficient α_b [–]	1.0
Coefficient k_1 [–]	1.4
Ultimate strength of the steel used in the shear connector f_{uf} [MPa]	207.7
Load-carrying capacity from Eq. (3.6) P_{ult} [kN]	min(46.4, 28.0, 66.9, 46.5) = 28.0

The maximum shear force (per one connector) with the corresponding slip, and the secant slip moduli $k_{0.4}$, $k_{0.6}$ and $k_{0.8}$ obtained in the laboratory tests and calculated in the theoretical analysis are reported in Table 5.4. It is worth nothing that the maximum shear force, the slip capacity and the stiffness of the specimens from the tests might be undervalued, because of the problem of concrete slab bending and premature cracks. The stiffness per one 16 mm shear connector ($k_{0.4}$ = 5.9 ± 1.8 kN/mm) from the presented tests was 2.3 times lower than the stiffness per one 16 mm bolt (13.8 kN/mm) from the test conducted by Etim et al. (2020). The stiffness of the connection ($k_{0.4}$ = 5.9 ± 1.8 kN/mm) obtained in the tests presented in this dissertation was similar to the stiffness of the connection ($k_{0.4}$ = 5.8 kN/mm) for the timber-concrete composite beams tested by Szumigała M., Szumigała E. and Polus (2018), and Polus and Szumigała (2014d). The stiffness of one 16 mm shear connector ($k_{0.4}$ = 5.9 ± 1.8 kN/mm) was low when compared with the stiffness of one 19 mm shear connector (100.0 kN/mm) recommended by the European Convention for Constructional Steelwork (1999).

The stiffness of specimen 4 ($k_{0.4}$ = 3.6 kN/mm) was 1.64 times lower than the mean stiffness of specimens 1–3 ($k_{0.4}$ = 5.9 kN/mm). A rubber element between the aluminium beam and the profiled sheeting had a negative impact on the connection stiffness.

Table 5.4. The maximum shear force with the corresponding slip, and the secant slip moduli (per one connector), the characteristic resistance, the slip capacity of the connector and the ductility of the connection

	Specimen				Mean (M) 1–3	T [e]	T/M
	4	1	2	3			
Secant slip modulus $k_{0.4}$ [kN/mm]	3.6	5.3	5.7	6.7	5.9 ± 1.8 (31.1%) [b] 0.74 [a]		0.93 [c] 2.12 [d]
Secant slip modulus $k_{0.6}$ [kN/mm]	4.7	6.4	6.3	7.9	6.9 ± 2.2 (31.5%) [b] 0.91 [a]	5.5 [c] 12.5 [d]	0.80 [c] 1.81 [d]
Secant slip modulus $k_{0.8}$ [kN/mm]	4.8	6.1	6.9	8.2	7.1 ± 2.6 (37.3%) [b] 1.06 [a]		0.77 [c] 1.76 [d]
Maximum shear force F_{max} [kN]	18.5	22.6	23.3	20.7	22.2 ± 3.3 (20.9%) [b] 1.35 [a]	28.0 $(\gamma_v = 1.0)$ 22.4 $(\gamma_v = 1.25)$	1.26 $(\gamma_v = 1.0)$ 1.01 $(\gamma_v = 1.25)$
Corresponding slip s_{Fmax} [mm]	3.8	3.7	3.4	5.1	4.1 ± 2.3 (55.4%) [b] 0.91 [a]	5.1 $(\gamma_v = 1.0)$ 4.1 $(\gamma_v = 1.25)$	1.24 $(\gamma_v = 1.0)$ 1.00 $(\gamma_v = 1.25)$
Characteristic resistance P_{Rk} [kN]	0.9×18.5 $= 16.7$	$0.9 \times 20.7 = 18.6$ from Eq. (4.1)			–	28.0 from Eq. (3.6)	0.66
Slip capacity δ_u [mm]	3.8	4.0	3.5	5.1	4.2 ± 2.0 (48.4%) [b] 0.82 [a]	–	–
Ductility according to (Deam et al. 2008)	Brittle	Brittle	Brittle	Brittle	–	–	–
Ductility according to (Johnson 2012)	Brittle	Brittle	Brittle	Brittle	–	–	–

[a] Sample standard deviation

[b] Measurement errors were calculated according to Student's t-distribution using 2 degrees of freedom and a confidence level of 0.95.

[c] For a shank diameter of the connector equal to 16 mm

[d] For a mean diameter of the connector taking into account its head, shank, flange (nut) and weld

[e] Theoretical

The failure mode of the specimens was brittle because the slip capacity was below 6 mm and the premature cracks and longitudinal cracks caused the decrease of the load in the shear force–slip curves. Brittle failure was also observed by Pavlović et al. (2013a) in their push-out tests. They used M16 bolts with embedded nuts as shear connectors in concrete slabs.

The bolted connections tested by Pavlović et al. (2013a) could not be classified as ductile because the characteristic ultimate slip was lower than 6 mm, just like in the tests presented in this dissertation. Hicks and Smith (2014) compared the slip in the composite beam with the slip of the companion push-out tests. The slip capacity investigated in the push-out tests was lower than 6 mm and it suggested that the connectors were not ductile. However, the slips measured in the beam were well over the levels achieved in the push-out tests. Hicks and Smith (2014) demonstrated that the brittle behaviour of the push-out specimen was a result of a deficiency in the standard specimen rather than the shear connection. The improved standard push test presented by Hicks and Smith (2014) may eliminate the problem of the concrete slab bending thanks to the compression force at the interface between the flange of the metal beam and the concrete slab, which presses both elements together.

The mean shear force–slip curve for specimens 1–3 was compared with the shear force–slip curve from the theoretical model of the connection (see Fig. 5.10).
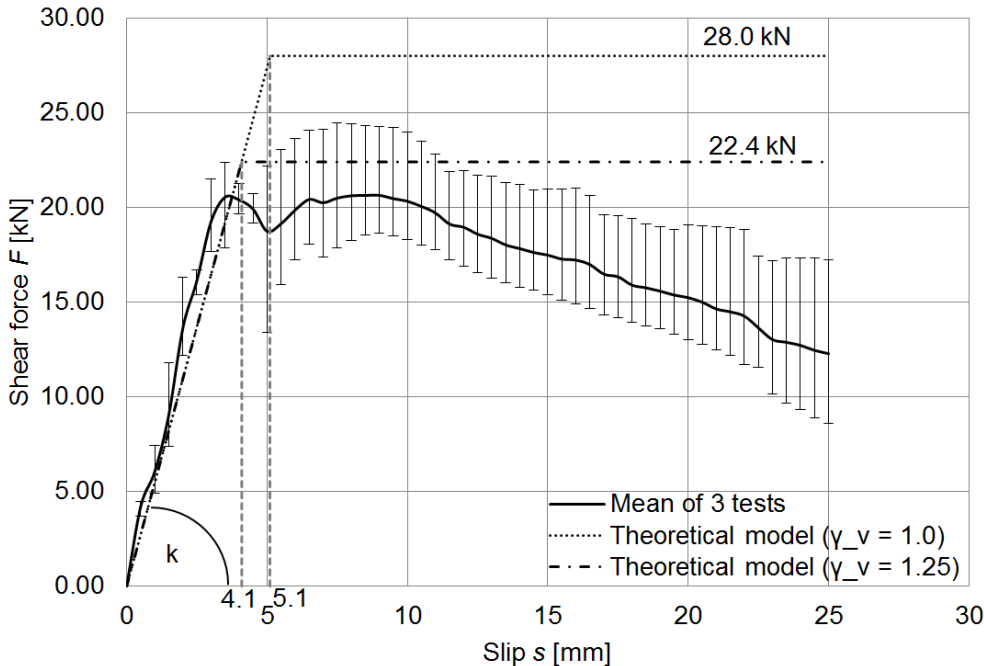
Figure 5.10. The shear force–slip curve for one connector from the laboratory tests and the theoretical analysis

The theoretical stiffness of the connector (5.5 kN/mm) was 1.07 times lower than the mean stiffness of the specimens 1–3 ($k_{0.4} = 5.9 \pm 1.8$ kN/mm), and it was calculated for the 16 mm connector. However, the connector consisted of a head, a shank, a flange (nut) and a weld, which all had different diameters. To take this fact into account, a mean diameter (19.7 mm) of the connector was determined using the Autodesk Robot Structural Analysis program and the beam model presented in Fig. 3.2. Two cantilever beams subjected to a uniform load were modelled in the program. The first beam had a constant cross-section with the mean diameter.

Chapter 5. RESULTS AND DISCUSSIONS

The second beam had a variable cross-section, to take into account the specific parts of the connector. The deflections at beam ends were equal. The theoretical stiffness of the connector with the mean diameter (12.5 kN/mm) was 2.11 times higher than the mean stiffness of the specimens 1–3 (5.9 kN/mm). The slip modulus $k = 12.5$ kN/mm was 1.76 times higher than the slip modulus $k_{0.8}$ from the laboratory tests ($k_{0.8} = 7.1 \pm 2.6$ kN/mm).

The model presented in Fig 3.2. takes into account the diameter of the connector. However, the stiffness of a connection in a composite beam also depends on the moment of tightening torque, the concrete in the slab, and the clearance hole. The clearance between the bolt and the hole made it easier to install demountable shear connectors through the holes in the aluminium beam flange. However, it had a negative impact on the stiffness of the connection. Clearances often appear at structure joints as a result of cyclic loading or manufacturing tolerances and they influence the structural response (Rzeszut and Garstecki 2011).

The pre-tensioning of shear connectors may increase the initial stiffness of a connections. Kozma et al. (2019) recorded that pre-tensioned demountable shear connectors, which were the object of their studies, had the initial stiffness equal to 250 kN/mm. When the friction resistance was overcome, the stiffness decreased to 15 kN/mm.

The maximum shear force from the theoretical analysis was 1.26 times (28.0 kN, $\gamma_v = 1.0$) and 1.01 times (22.4 kN, $\gamma_v = 1.25$) higher than the mean maximum shear force for specimens 1–3 (22.2 $\pm$ 3.3 kN). The maximum shear force obtained in the theoretical analysis was higher than the mean maximum shear force obtained from the tests. The author of this dissertation emphasises the fact that the premature cracks appeared during the tests and decreased the maximum load. Ernst et al. (2007) suggested that the reduction factor k_t does not provide reliable connector resistance for open trough profiled steel sheeting and by using it one may overestimate the connector resistance.

After the tests, the two specimens were disassembled (see Fig. 5.11). The author of this dissertation observed:

- ❖ a plastic hinge formed within each connector (see Figs. 5.11a and 5.11e),
- ❖ the local yielding of the aluminium flange near the holes where the connectors had been placed (see Fig. 5.11b),
- ❖ cracks in the concrete rib near the shear connectors (see Fig. 5.11c),
- ❖ the local yielding of the profiled steel sheeting near the holes where the connectors had been placed, caused by the contact between the aluminium beam and the profiled steel sheeting (see Fig. 5.11d).

The rubber elements used in specimen 4 were sheared (see Fig. 5.11f).

a)

b)

c)

d)

e)

f)
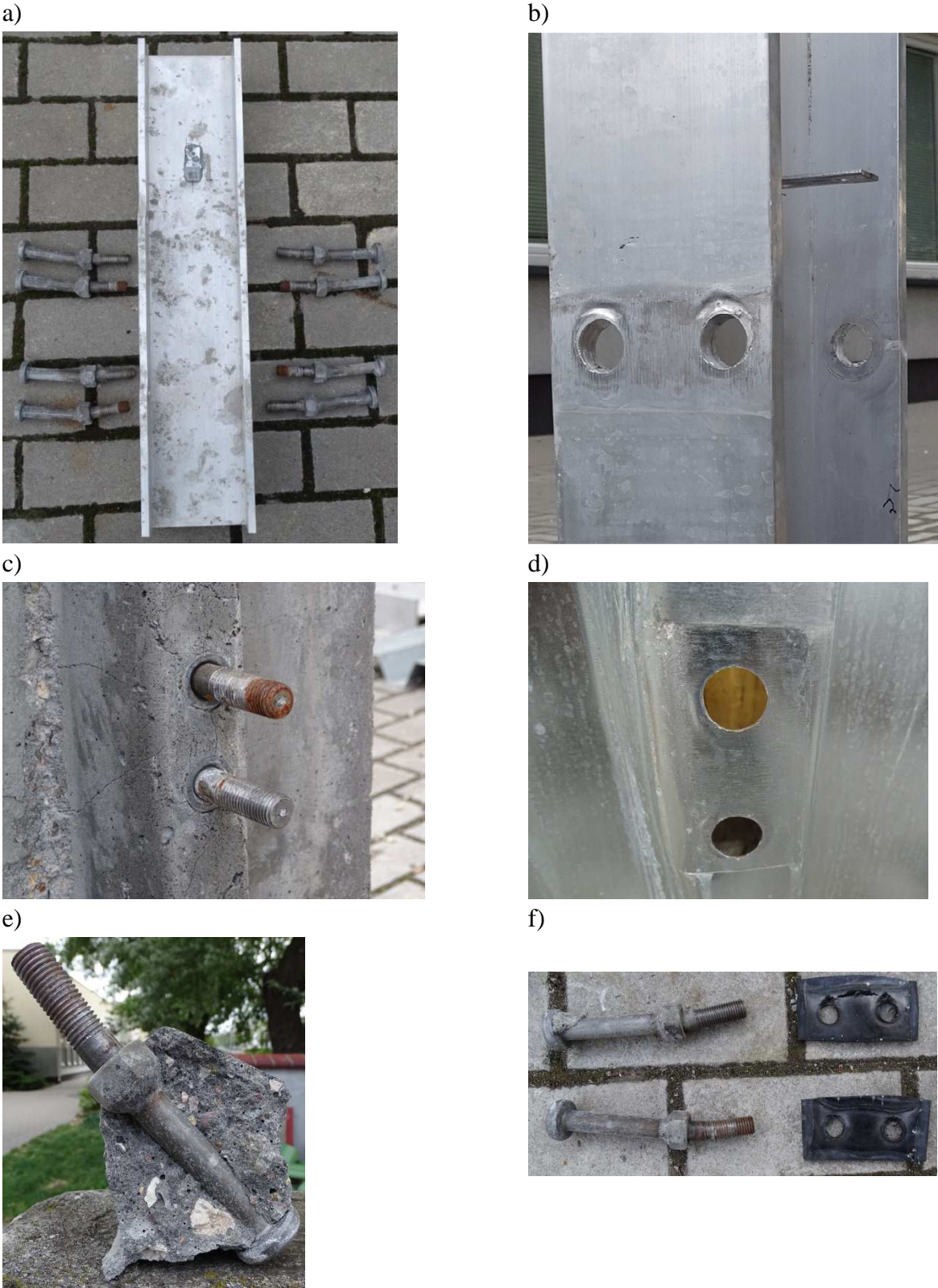
Figure 5.11. Specimens after the disassembly: a) bent connectors from one of the specimens 1–3; b) local yielding of the aluminium flat near the holes, c) cracks in the concrete rib near the shear connectors, d) local yielding of the profiled steel sheeting near the holes, caused by the contact between the aluminium beam and the profiled steel sheeting, e) connector embedded in concrete, f) bent connectors from specimen 4 and shear failure in rubber elements used in specimen 4

5.3. Bending test results

The behaviour of the aluminium-concrete composite beams during the tests is described below. Small gaps (< 1 mm) were observed between the profiled sheeting and the concrete slab for the load equal to 30% of the ultimate test load (see Figs. 5.12a and 5.12b).

a)

b)

c)

d)

e)

f)
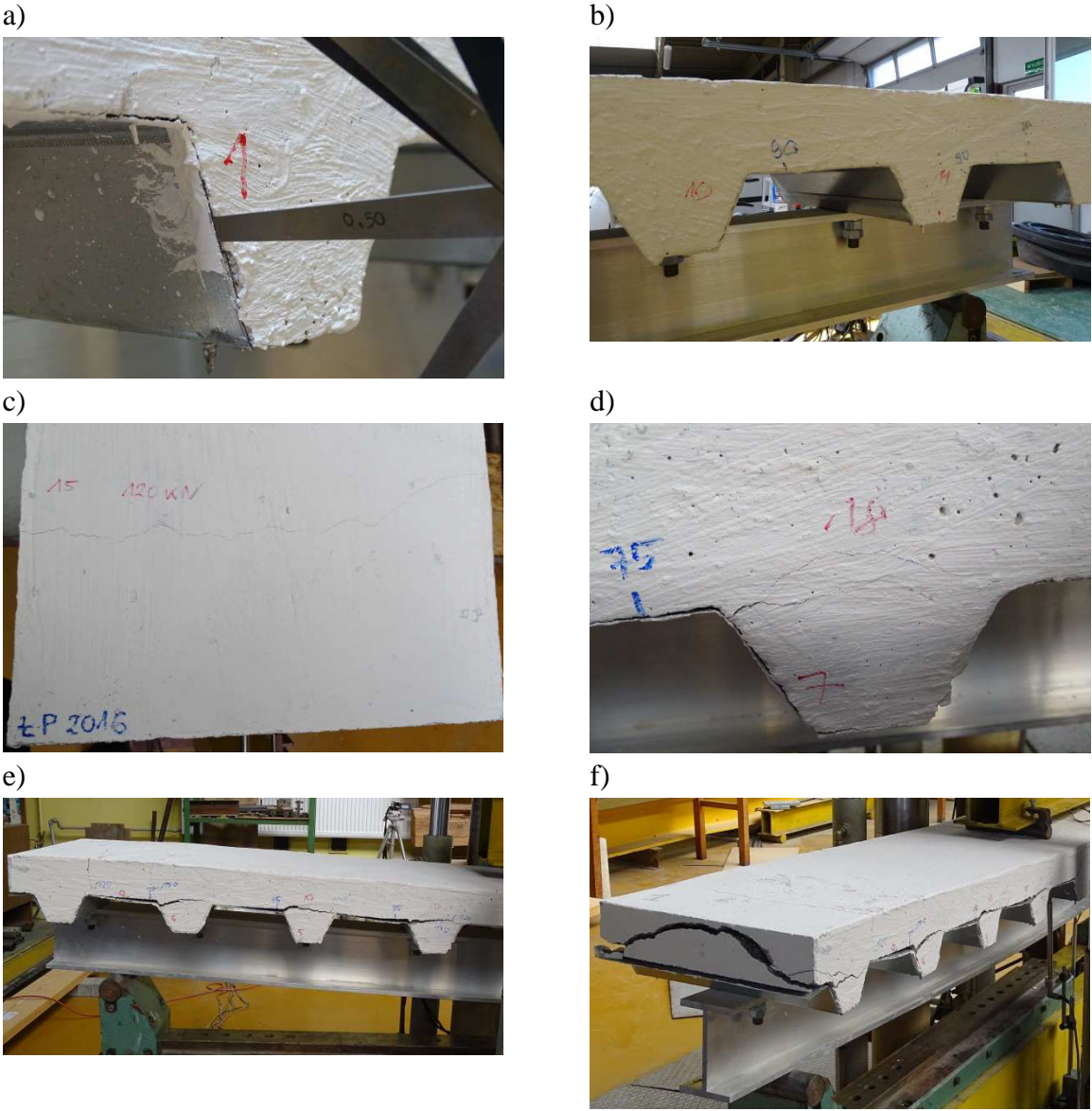
Figure 5.12. Beam 1: a) gap 1 between the profiled sheeting and the concrete slab at a load equal to 75.0 kN; b) gaps 10 and 11 between the profiled sheeting and the concrete slab at a load equal to 100.0 kN; c) horizontal crack 15 near the support at a load equal to 120.0 kN; d) crack 18 at a load equal to 135.0 kN; e) cracks 16 and 17 at a load equal to 145.0 kN; f) cracks at failure load (156.0 kN)

It was because there were too few self-tapping screws, and they did not prevent the separation of the sheeting from the concrete slab. What is more, the adhesion between the profiled steel sheeting and the concrete was insufficient to transfer forces, which is often the case in smooth profile steel sheeting (Niedośpiał, Grzeszykowski and Szmigiera 2018).

If profiled sheeting with embossments had been used the separation could have been reduced (Kim, Wrigth and Cairns 2001) (Rackham, Couchman and Hicks 2009). When the load reached 47–69% (depending on the beam), a horizontal crack appeared in the concrete slab near the support of the beam (see Fig. 5.12c). It was a back-breaking failure (Hicks 2008). The width and the length of the crack continuously increased during the test. The first longitudinal crack appeared for the load equal to 81–94% of the ultimate test load. It formed between the profiled sheeting and the concrete ribs near one of the two supports. When the crack appeared, the load decreased rapidly by 5.2–18.7 kN (depending on the beam). Shortly afterwards, the load started to rise and the width and length of the longitudinal crack were continuously increasing. The longitudinal crack was caused by the longitudinal shear force. At the ultimate load, the profiled sheeting was detached from the concrete and the ribs were sheared in the shear span (see Figs. 5.12e and 5.12f).

Figure 5.13 presents beams 1–4 at failure load.

a)

b)

c)

d)

Figure 5.13. Beams at failure load: a) beam 1, b) beam 2, c) beam 3, d) beam 4

Chapter 5. RESULTS AND DISCUSSIONS

The values of the crack width did not exceed the limiting value (0.3 mm) given in EN 1992-1-1 (European Committee for Standardization 2004) until the ultimate load was applied (see Appendix 2). The cracking pattern in beam 1 is presented in Figure 5.14 (in beams 2–4 in Appendix 3).

a)

b)

c)
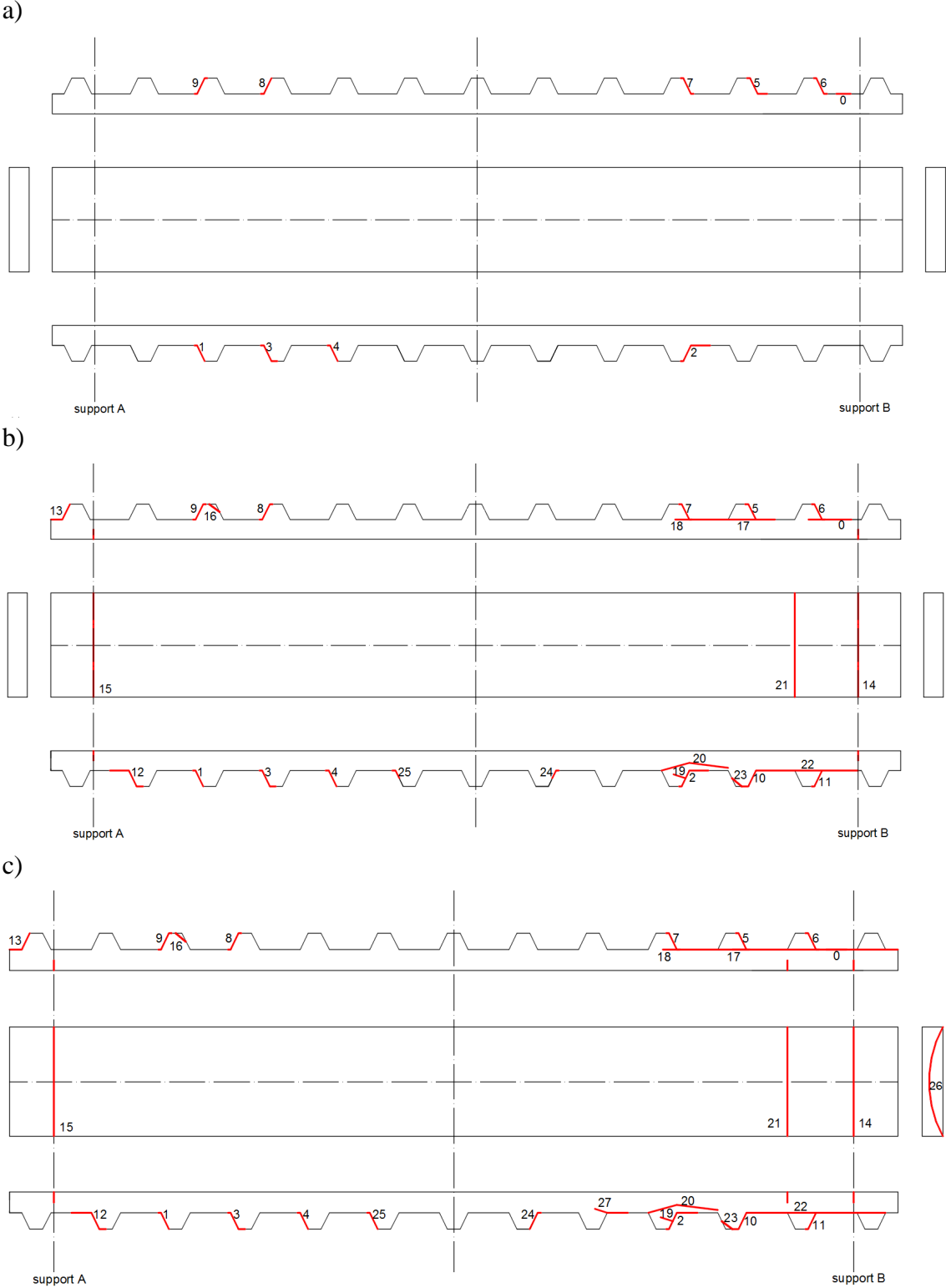
Figure 5.14. The cracking pattern in beam 1: a) at a load equal to 75.0 kN, b) at a load equal to 135.0 kN, c) at failure load

The moment–deflection and moment–end slip curves for beams 1–4 are presented in Figs. 5.15 and 5.16.
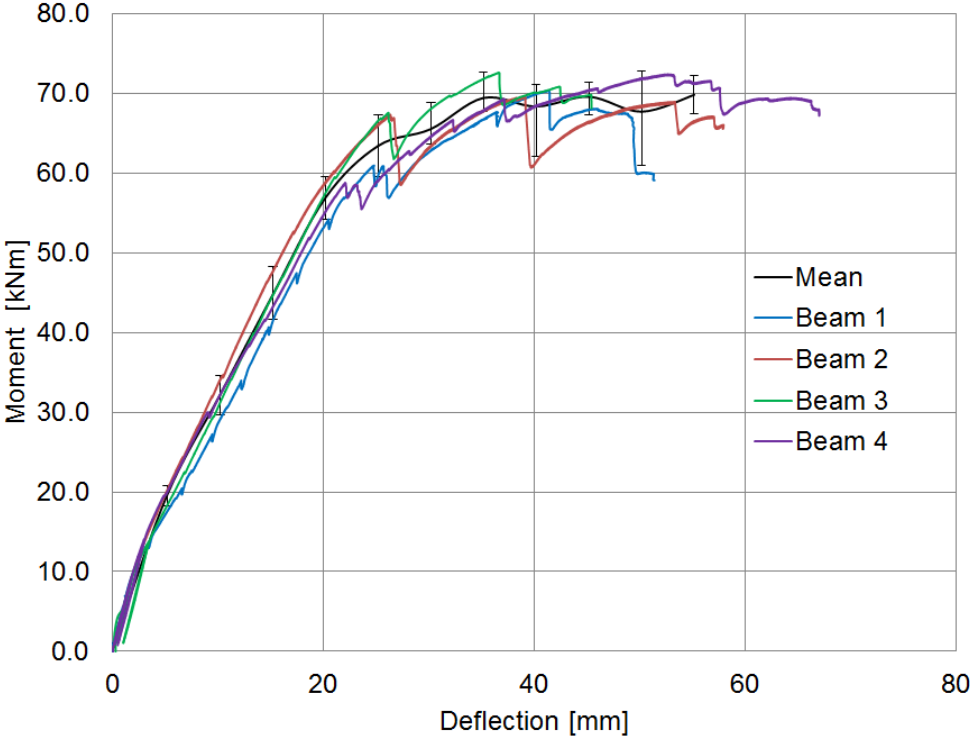
Figure 5.15. The moment–deflection curves for beams 1–4
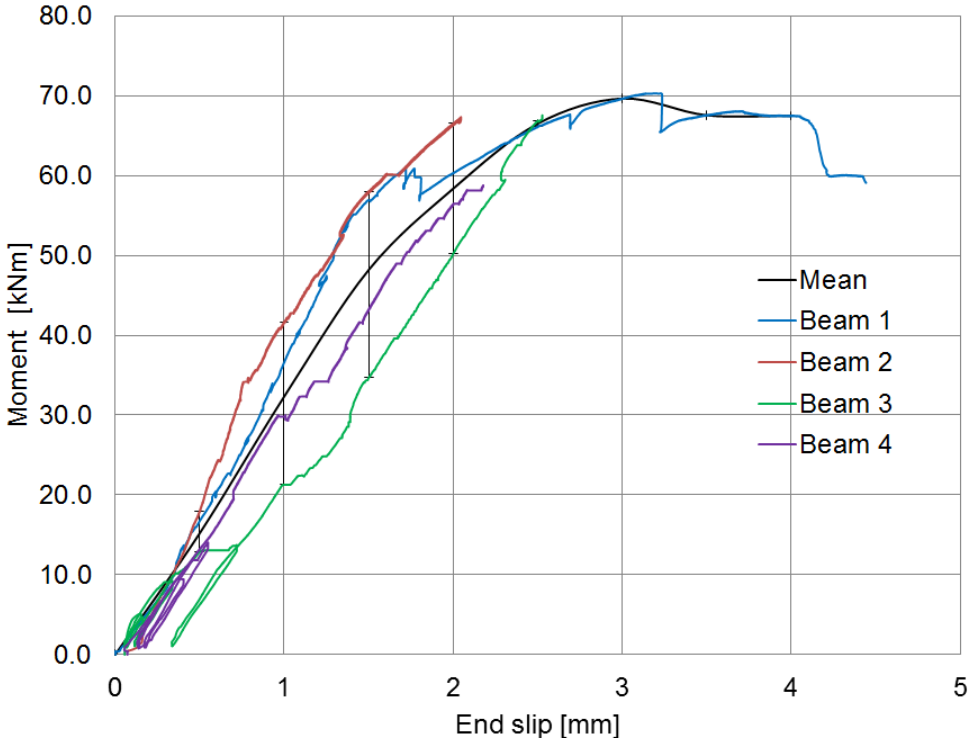
Figure 5.16. The moment–end slip curves for beams 1–4

The test results were summarised in Table 5.5.

Table 5.5. Measured results from the laboratory tests

Result	Beam 1	Beam 2	Beam 3	Beam 4	Mean
M_o [kN·m]	52.6	54.7	53.8	53.9	53.8 ± 1.38 2.56% [b] 0.87 [a]
M_{crack} [kN·m]	62.0	67.9	68.6	59.6	64.5 ± 7.03 10.90% [b] 4.42 [a]
M_{ult} [kN·m]	71.3	70.6	73.6	73.4	72.2 ± 2.39 3.31% [b] 1.50 [a]
δ_o [mm]	19.4	17.9	18.5	19.3	18.8 ± 1.13 6.01% [b] 0.71 [a]
δ_{crack} [mm]	25.0	26.8	26.3	23.2	25.3 ± 2.56 10.10% [b] 1.61 [a]
δ_{ult} [mm]	41.4	39.2	36.8	52.9	42.6 ± 11.35 26.66% [b] 7.14 [a]
M_{ult}/M_o	1.36	1.29	1.37	1.36	1.35 ± 0.06 4.37% [b] 0.04 [a]
M_{ult}/M_{crack}	1.15	1.04	1.07	1.23	1.12 ± 0.14 12.10% [b] 0.09 [a]
δ_{ult}/δ_0	2.13	2.19	1.99	2.74	2.26 ± 0.52 23.15% [b] 0.33 [a]

[a] Sample standard deviation,

[b] Measurement errors were calculated according to Student's t-distribution using 3 degrees of freedom and a confidence level of 0.95,

M_o – measured mid-span moment corresponding to the first yielding of the aluminium beam, M_{crack} – measured mid-span moment corresponding to the first cracking between the concrete slab and the profiled sheeting, M_{ult} – measured mid-span ultimate strength of the composite section, δ_0 – measured mid-span deflection corresponding to M_0, δ_{crack} – measured mid-span deflection corresponding to M_{crack}, δ_{ult} – measured mid-span deflection corresponding to M_{ult}

The end slip for beams 2–4 was measured only up to the moment when the first longitudinal crack appeared at one of the beam ends. The concrete damage occurred where the LVDTs used for end slip measurement in beams 2–4 were located. It distorted the values of the measured end slip for beams 2–4. Therefore, a full moment–end slip curve is presented for beam 1 only. A slip not exceeding 6 mm was recorded at the end of beam 1, which did not

meet the Eurocode 4 (European Committee for Standardization 2004) requirement of ductility for shear connectors. This requirement was not met in the shear connection tests either. The connections presented in this dissertation showed brittle behaviour, which was caused by the small width of the profiled steel sheeting rib. The rib-shear failure is a brittle mode of longitudinal shear failure. Longitudinal cracking may appear in composite beams with open trough profiled steel sheeting as well as in composite beams with re-entrant profiled steel sheeting (Nie, Cai and Wang 2005) (Kania 2008). Open trough profiled steel sheeting can significantly reduce the strength and ductility of the shear connection in composite beams (Ernst et al. 2007).

Johnson and Shepherd (2013) demonstrated that reinforcing bars placed within the troughs of concrete slabs could not only improve their resistance to fire but also to longitudinal shear.

Patrick (2000) reported that the brittle rib-shearing failure might also occur in composite beams similar to the ones tested in this dissertation, with a narrow concrete slab (< 450 mm) and shear connectors grouped together in narrow ribs. He also noted that waveform reinforcement made of welded-wire and laid directly on the profiled steel sheeting could prevent the rib-shear failure and improve the ductility of shear connections.

Ernst, Bridge and Wheeler (2009) also demonstrated that not every shear connection incorporating profiled steel sheeting could be classified as ductile. They observed rib-shear failures both in narrow concrete slabs and in specimens with up to 1200 mm wide slabs. Ernst, Bridge and Wheeler (2009) proposed to use a stud performance-enhancing device consisting of a round steel wire spiralled around the stud and waveform reinforcement, to prevent brittle behaviours.

Rehman et al. (2016) reported that connections with demountable shear connectors may show very ductile behaviour. They used demountable shear connectors in 5.6 m steel-concrete composite beams with profiled steel sheeting (Cofraplus 60). In their tests, the width of the rib was 62 mm at the narrowest point. In the tests presented in this dissertation, the width of the rib was 40 mm at the narrowest point and for this reason the shear connectors were located in relatively narrow concrete ribs.

Taken the above into consideration, the ductility of the connection analysed in this dissertation should be improved. The use of the profiled sheeting with wider ribs and of the waveform reinforcement suggested by Patrick (2004) to prevent the rib-shearing failure is recommended in the future.

Figure 5.17 presents strain distribution measured along cross-section 3–3. Strain gauges were glued onto the upper surface of the concrete slab and onto the aluminium beam. Strain in the bottom part of the concrete slab was calculated with the assumption that the curvatures of the aluminium beam and the curvature of the concrete slab were the same. In Fig. 5.17 one can observe the slip between the concrete slab and the aluminium beam. Due to the slip, two neutral axes appeared. At the ultimate load, the beams reached a deflection level of about $L/60$ (beams 1, 2 and 3) and about $L/45$ (beam 4). Once the load had been removed, the residual deflections exceeded 40 mm (beam 4). At the deflection level of $L/250$, the load reached about 45% of the ultimate load. The aluminium-concrete composite beams showed big deflections due to the low value of the Young's modulus of the aluminium.
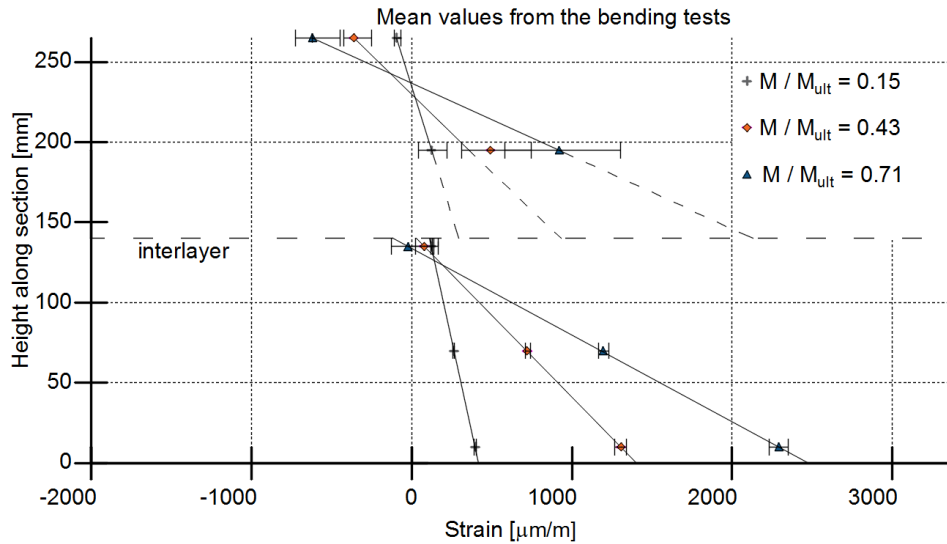
Figure 5.17. Strain distribution (mean values) measured along cross-section 3–3 (Polus and Szumigała 2019a)

Table 5.6. presents the calculation of the load-carrying capacity of the shear connector used in the aluminium-concrete composite beams.

Table 5.6. The load-carrying capacity of the shear connector used in the aluminium-concrete composite beams

Parameters	Value
Shank diameter d [mm]	16.0
Partial factor γ_v [–]	1.0
Reduction factor k_t [–]	0.52
Coefficient α [–]	1.0
Cylindrical compressive strength f_c [MPa]	61.8
Mean secant modulus of concrete E_{cm} [GPa]	37.3
Coefficient β [–]	0.74
Ultimate strength of the steel used in the shear connector f_u [MPa]	557.2
Cross-sectional area of the shear connector A_{sc} [cm^2]	2.0
Coefficient α_v [–]	0.6
Gross cross-section area of the connector A [cm^2]	2.0
Partial factor γ_{M2} [–]	1.0
Coefficient α_b [–]	1.0
Coefficient k_1 [–]	1.4
Ultimate strength of the steel used in the shear connector f_{uf} [MPa]	207.7
Load-carrying capacity from Eq. (3.6) P_{ult} [kN]	min(46.4, 43.4, 66.9, 46.5) = 43.4

The calculations of the elastic flexural capacity and the plastic flexural capacity of the aluminium-concrete composite beam with partial shear interaction are presented in Tables 5.7 and 5.8.

Table 5.7. The calculation of the elastic flexural capacity of the aluminium-concrete composite beam with partial shear interaction

Parameter	Value
Young's modulus of aluminium E_a [kN/cm^2]	6290
Young's modulus of concrete E_c [kN/cm^2]	3730
Modular ratio n [-]	1.69
Cross section area of the aluminium beam A_a [cm^2]	28.8
Ideal cross section area of the concrete slab $(h_c b_{eff}/n)\, A_{c,i}$ [cm^2]	153.3
Ideal cross-section area of the composite beam A_i [cm^2]	182.1
First moment of area of the aluminium beam (for the top fibre of the slab) S_a [cm^3]	214.1
First moment of area of the slab (for the top fibre of the slab) [cm^3] S_c	536.6
Position of the centroid axis x [cm]	4.1
Second moment of area of the ideal cross-section I_y [cm^4]	8388.6
Section modulus of the ideal cross-section W_y [cm^3]	374.5
Elastic resistance to bending of the cross-section of the aluminium-concrete composite beam with full shear connection M_{el} [kN·m]	57.4
Span length L [cm]	270
Depth of the entire section h [cm]	26.5
Thickness of the concrete slab h_c [cm]	5.0
Height of the profiled sheeting e_p [cm]	5.5
Moment of inertia of aluminium I_a [cm^4]	877.2
Moment of inertia of the concrete slab section with the rib I_1 [cm^4]	6022.1
Moment of inertia of the concrete slab section with the rib I_2 [cm^4]	1057.6
Moment of inertia of concrete I_c [cm^4]	1408.4
Moment of inertia I_0 [cm^4]	1712.4
Area of the concrete section at the rib A_{c1} [cm^2]	462.5
Area of the concrete section at the rib A_{c2} [cm^2]	259.0
Equivalent concrete area A_c [cm^2]	298.71
Distance between the top of the aluminium girder and its neutral axis y_1 [cm]	7.0
Dimension d_c [cm]	13.3
Shear stiffness of the connector K [kN/cm]	55.0
Parameter A_0 [cm^2]	24.8
Parameter A_1 [1/cm^2]	0.00359
Longitudinal spacing of shear connectors p [cm]	23.5
Coefficient α_1 [-]	0.00778
Coefficient β_1 [-]	0.02032
Coefficient η_c [-]	7.9
Parameter for the slip effect ξ_s [-]	0.66
Stiffness of the transformed section of the composite beam $(EI)_e$ [kNcm^2]	31 289 478.0
Effective stiffness $(EI)_{eff}$ [kNcm^2]	18 841 536.6
Area of the top flange of the aluminium beam A_{ft} [cm^2]	9.0
Area of the web of the aluminium beam A_w [cm^2]	9.6
Coefficient ζ [-]	0.68
Elastic flexural capacity of the aluminium-concrete composite beam with partial shear interaction $M_{y,Rk}$ [kN·m]	39.0
Deflection at a moment equal to $M_{y,Rk}$ $f(M_{y,Rk})$ [cm]	19.4

Table 5.8. The plastic flexural capacity of the aluminium-concrete composite beam
with partial shear interaction

Parameters	Value
Load-carrying capacity of the shear connector P_{ult} [kN]	43.4
Number of connectors in the shear span n_d [–]	8
Cross section area of the aluminium beam A_a [cm^2]	28.8
Yield strength of aluminium f_y [MPa]	153.3
Width of the top flange b_f [cm]	9.0
Effective width of the composite slab b_{eff} [cm]	37.0
Distance between the neutral axis of the aluminium beam and its top d_1 [cm]	7.0
Compression force of concrete equal to the shear force supplied by all the connectors F_c [kN]	347.0
Cylinder compressive strength of concrete f_c [MPa]	61.8
Thickness of the concrete slab in a section with no rib h_c [cm]	7.0
Overall depth of the profiled steel sheeting h_p [cm]	5.5
Ultimate strength of the composite section M_{ult} [kN·m]	75.5

Table 5.9. compares the mid-span ultimate strength of the composite section obtained experimentally and theoretically.

Table 5.9. Comparison

	M_o [kN·m]	M_{ult} [kN·m]	δ_o [mm]	δ_{ult} [mm]
Laboratory tests (LT)	53.8 [c] ± 1.38	72.2 [c] ± 2.39	18.8 [c] ± 1.13	42.6 [c] ± 11.35
	2.56% [b]	3.31% [b]	6.01% [b]	26.66% [b]
	0.87 [a]	1.50 [a]	0.71 [a]	7.14 [a]
Theoretical analysis (T)	39.0	75.5	19.4	–
T/LT	0.72	1.05	1.03	–

[a] Sample standard deviation,

[b] Measurement errors were calculated according to Student's t-distribution using 3 degrees of freedom and a confidence level of 0.95,

[c] Mean values from tests 1–4,

M_o – mid-span moment corresponding to the first yielding of the aluminium beam,

M_{ult} – mid-span ultimate strength of the composite section, δ_0 – mid-span deflection corresponding to M_0, δ_{ult} – mid-span deflection corresponding to M_{ult}

The theoretical elastic flexural capacity of the aluminium-concrete composite beam with partial shear interaction (39.0 kN·m) was 1.38 times lower than the mean elastic flexural capacity of beams 1–4 (53.8 ± 1.38 kN·m) when the theoretical shear stiffness of the connector (5.5 kN/mm) was taken into account. The theoretical ultimate strength of the composite section (75.5 kN·m) was 1.05 times higher than the mean ultimate strength of the composite section from the laboratory tests (72.2 ± 2.39 kN·m). The theoretical mid-span deflection corresponding to M_o (19.4 mm) was 1.03 times higher than the mean mid-span deflection corresponding to M_o from the laboratory tests (18.8 ± 1.13 mm).

5.4. The results of the finite element modelling of the concrete cylinder subjected to compression

Figure 5.18 presents the non-linear stress–strain relationships obtained from the FE analyses for different mesh sizes. The numerical analyses were terminated by the author after the load peak.
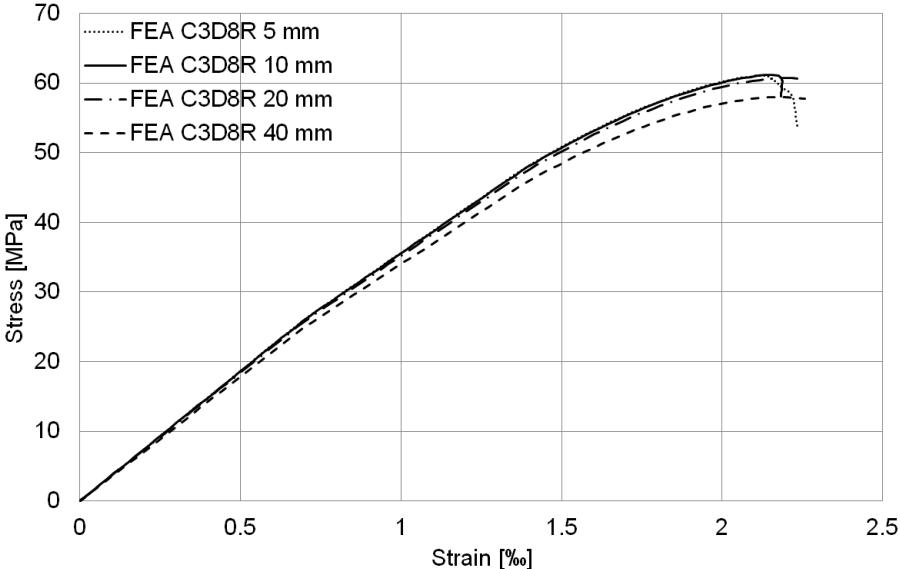
Figure 5.18. The non-linear stress–strain relationships for different mesh sizes (Polus and Szumigała 2019c)
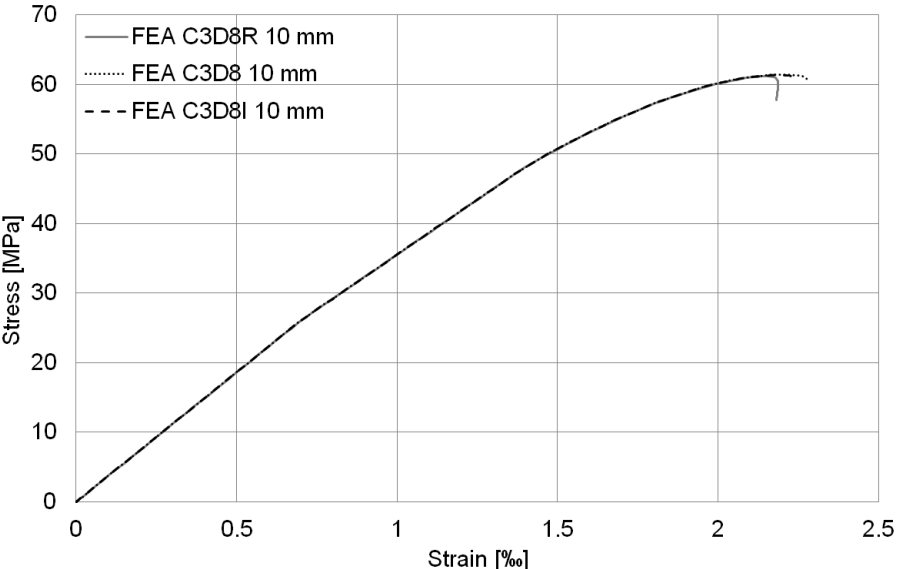
Figure 5.19. The non-linear stress–strain relationships for different finite elements (Polus and Szumigała 2019c)

As evident from the figure above, the 40 mm mesh was too big for the analysed concrete cylinder and the stress–strain relationship from the FE analysis for this mesh size is different from the stress–strain relationships from other FE analyses. Up to the load peak, the stress–

105

strain relationships from the FE analyses for the 5, 10 and 20 mm mesh sizes have the same shape.

The non-linear stress–strain relationships from the FE analyses for different finite elements are presented in Figure 5.19. The stress–strain relationships from the FE analyses for the C3D8R, C3D8 and C3D8I elements have the same shapes up to the load peak.

Figure 5.20 presents a comparison between the results of the laboratory tests and the numerical analysis (C3D8R, 10 mm).
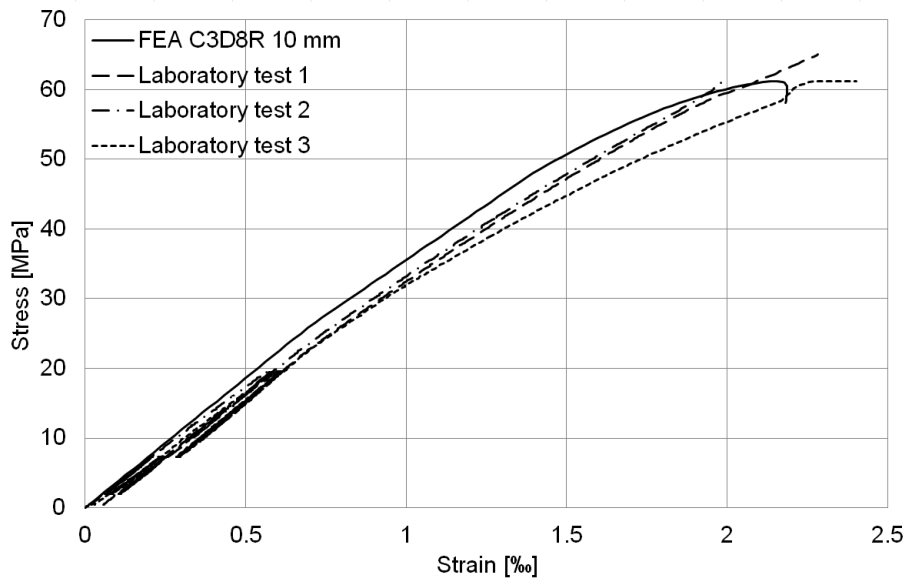
Figure 5.20. A comparison between the results of the non-linear stress–strain relationships obtained from the laboratory tests and the FE analysis (Polus and Szumigała 2019c)

The stiffness of the numerical model of the cylinder was higher than the stiffness of the tested cylinders. The curves from the laboratory tests reflect the behaviour of the specimens when the cyclical load and then the failure load were applied. When the cyclical load was applied, the strain increased and the stiffness decreased. The failure mode from the FE analysis is presented in Fig. 5.21. The maximum principal plastic strains show the direction of the cracking (Genikomsou and Polak 2015).

The cylinder exhibited a single diagonal band of damage. The impact of the boundary conditions on the damage modes of concrete cylinders subjected to compression was presented by (Bazant and Planas 1998). The ends of the concrete cylinder were not fixed. Friction and surface-to-surface "hard" contact were defined between the steel plates and the upper and lower surfaces of the concrete cylinder. In cylinders with fixed ends, two diagonal bands of damage appear (Bazant and Planas 1998) (Murray et al. 2007).

The actual behaviour of the concrete cylinder was compared with the behaviour of its numerical model. The adopted 3D model captured the response of the concrete cylinder subjected to compression relatively well. The model turned out to be insensitive to the type of finite element and the mesh size (5, 10, 20 mm) before failure.
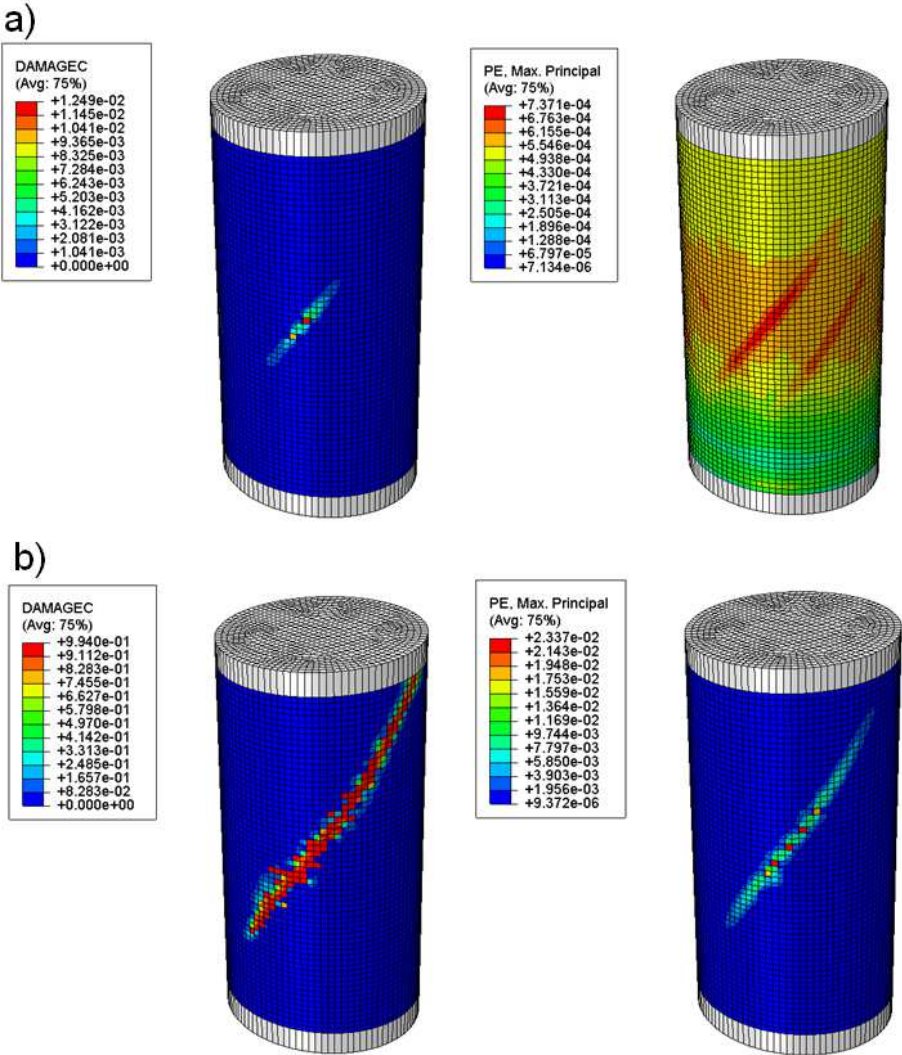
Figure 5.21. The cracking pattern on the concrete cylinder: a) at the ultimate load, b) at the end of the FE analysis

5.5. The results of the finite element modelling of the shear connection test

The shear connection test was simulated in FE models using the Abaqus software. The influence of the connection model, the concrete model, the mesh size and the finite element type was investigated.

At the outset, it is essential to discuss the chosen connection models. Four models of the shear connector were used. In FEA 1 and FEA 2 the first model of connection (F–s 1) was used, and the response of the connector was non-linear to reflect the average shear force-slip curve for the three specimens from the push-out tests.

The results of FEA 1 and FEA 2 are consistent with the results of the push-out tests (see Fig. 5.22).
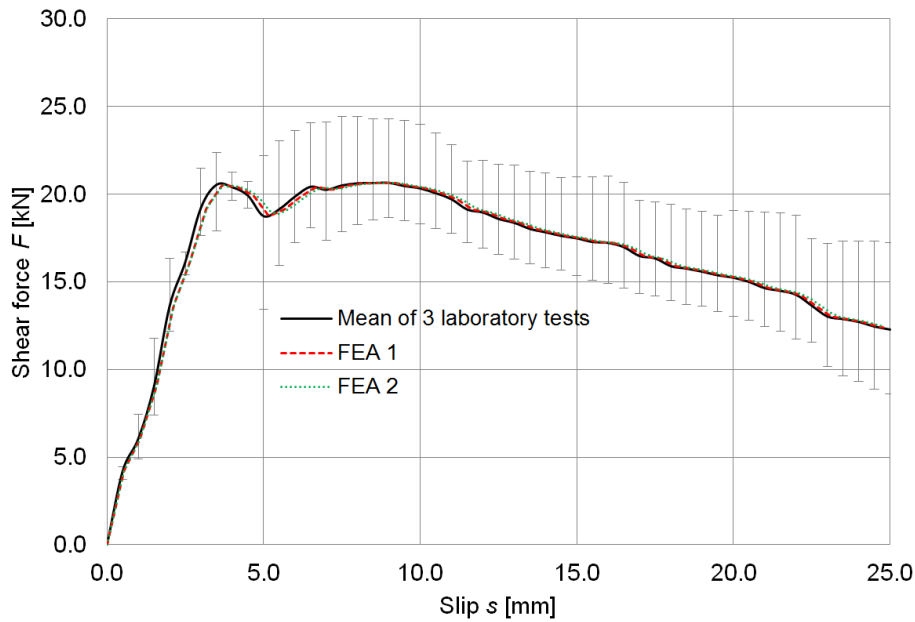
Figure 5.22. The shear force–slip curve for one connector based on the laboratory tests, the theoretical analyses and the FE analyses (FEA 1, FEA 2)

The first model of the shear connector (F–s 1) was used in FEA 1 and FEA 2 and it accurately reflected the mean shear force–slip curve for one connector from the push-out tests. The elastic model of concrete was used in FEA 1 and the CDP model was used in FEA 2. There was no difference between these two analyses, because the model of the connection accurately reflected the average shear force-slip curve for the three specimens from the push-out tests. As a consequence, the model took into account the decrease in the stiffness and the load, which occurred when the concrete was cracking. The load peak occurred on the numerical shear force–slip curves because it was modelled using the connection model. For this reason, the simple elastic model of concrete was adequate for the finite element modelling of the shear connection test. However, the elastic model of concrete is too simple to reflect the behaviour of the aluminium-concrete composite beam (see Section 5.6).

In FEA 3 and FEA 5 the second (F–s 2, $\gamma_v = 1.25$) and third models (F–s 3, $\gamma_v = 1.0$) were used, respectively. The response of the connector was elasto-plastic to reflect the theoretical model for the dowel-bolt connector presented in Section 3.1. The results of FEA 3 are consistent with the theoretical shear force–slip curve ($\gamma_v = 1.25$) and the results of FEA 5 are consistent with the theoretical shear force–slip curve ($\gamma_v = 1.0$) (see Fig. 5.23). The CDP model of concrete was used in both analyses. However, it did not have any impact on the load-slip curve, because the rate of weakening value was low ($n_w = 0.7$) and because the load peak appeared on the numerical shear force–slip curves. The peak was modelled using the connection model.
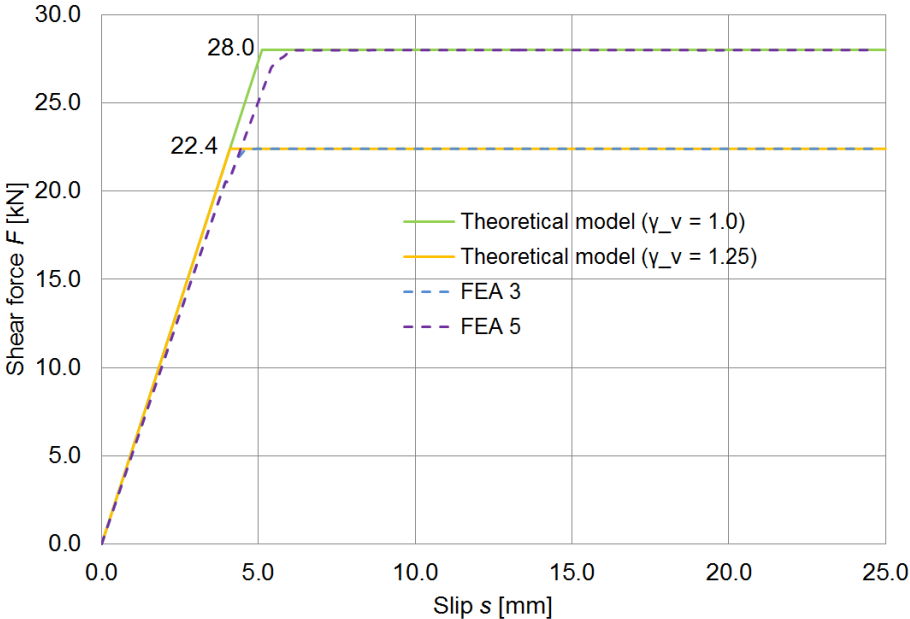
Figure 5.23. The shear force–slip curve for one connector based on the laboratory tests, the theoretical analyses and the FE analyses (FEA 3, FEA 5)

In FEA 7 the fourth model (F–s 4) of connection was used. The response of the connector was linear to only reflect the first branch of the shear force-slip curve for the dowel-bolt connector presented in Section 3.1. The results of FEA 7 are consistent with respect to the stiffness of the connector (see Fig. 5.24). The fourth model of the shear connector (F–s 4) did not accurately predict the maximum shear force for one connector. It was an elastic model and it only reflected the first (elastic) branch of the shear force–slip curve. The peak on the shear force–slip curve from FEA 7 occurred when the concrete was damaged.
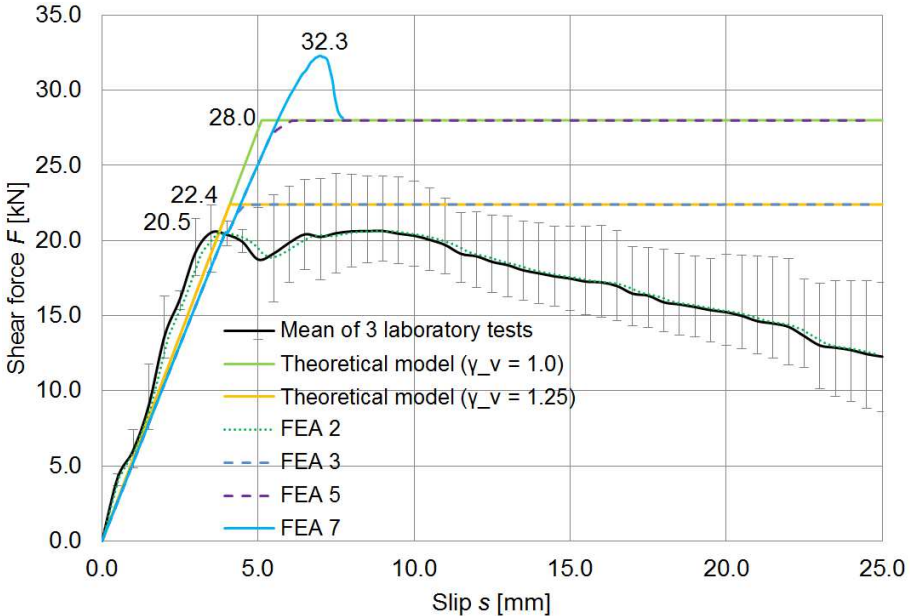
Figure 5.24. The shear force–slip curve for one connector based on the laboratory tests, the theoretical analyses and the FE analyses (FEA 2, FEA 3, FEA 5, FEA 7)

109

The implicit modelling of connectors works well. The FE models of the shear connection test strongly depended on the connection model.

The numerically predicted failure mode was compared with the one observed in the laboratory tests. The failure mode was a combination of the rib-shear failure and the horizontal crack on the tensioned edges of the concrete slabs as observed experimentally and confirmed in the finite element analyses (see Figs. 5.25 and 5.26).
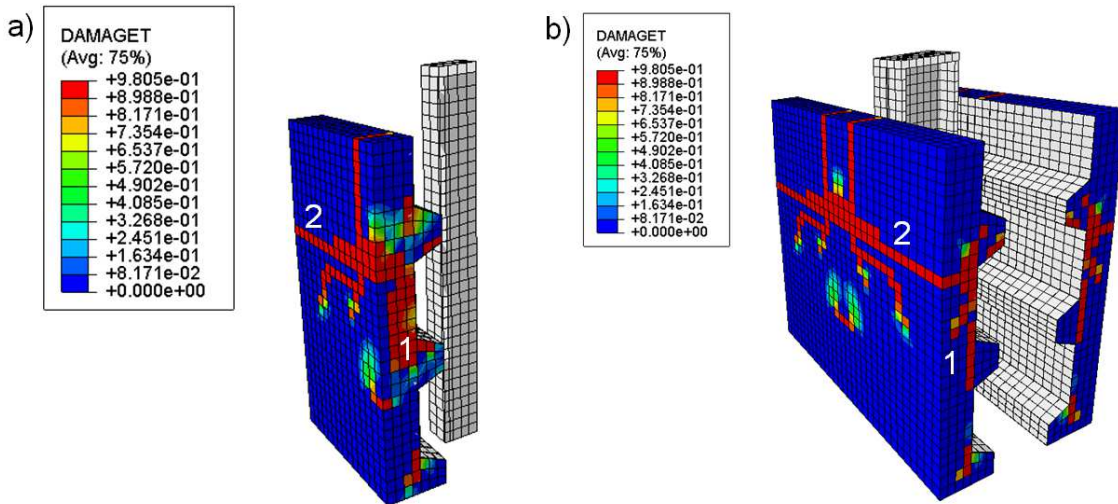
Figure 5.25. The cracking pattern of the concrete slabs in the shear connection test at failure load (FEA 11) (F_{max} = 23.1 kN/connector, s_{Fmax} = 4.9 mm): a) ¼ of the model, b) complete model, 1 – rib-shear failure 2 – crack on the tensioned surface
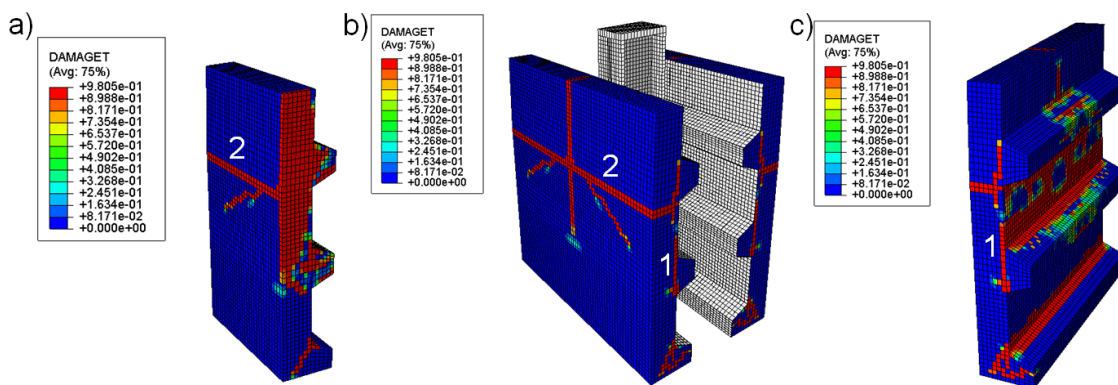
Figure 5.26. The cracking pattern of the concrete slabs in the shear connection test at failure load (FEA 14) (F_{max} = 19.3 kN/connector, s_{Fmax} = 4.3 mm): a) ¼ of the model, b) complete model, c) concrete slab, 1 – rib-shear failure 2 – crack on the tensioned surface

The impact of the rate of weakening (n_w) used in the concrete model on the shear force–slip curve is presented in Fig. 5.27.
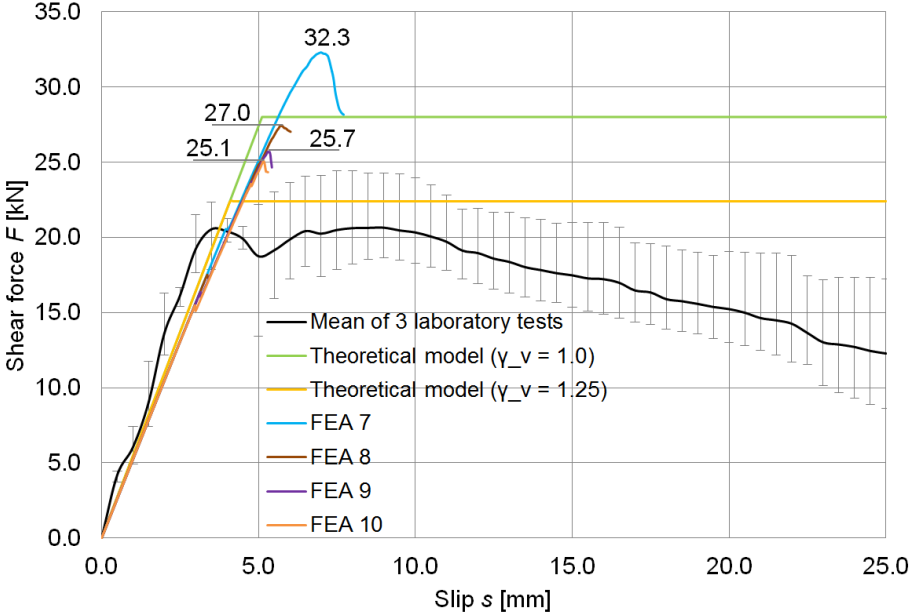
Figure 5.27. The shear force–slip curve for one connector based on the laboratory tests, the theoretical analyses and the FE analyses (FEA 7–10)

The maximum shear force was obtained for $n_w = 0.7$ in FEA 7 and it was decreasing with the increase of parameter n_w.

The impact of the mesh size (10, 20, 30 mm) on the shear force–slip curve is shown in Fig. 5.28.
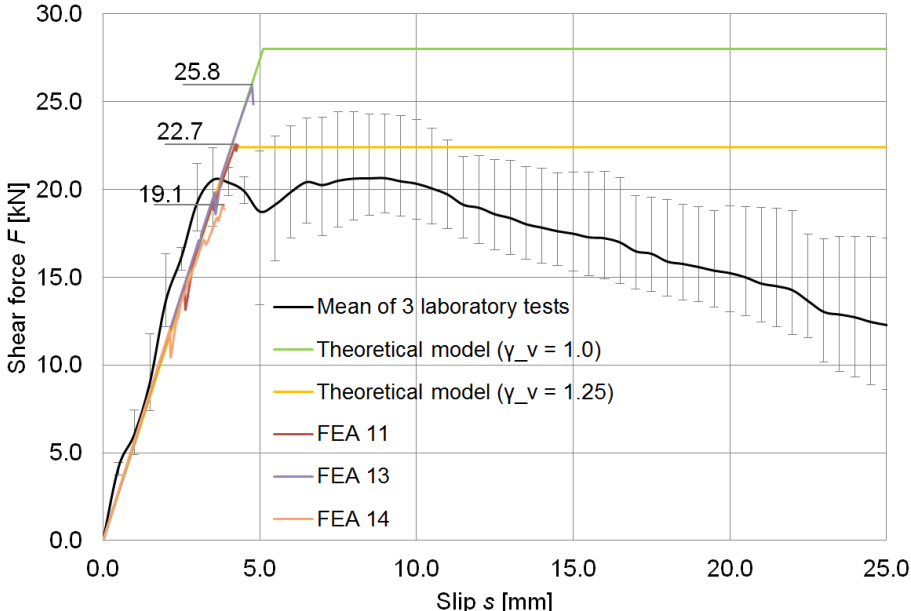
Figure 5.28. The shear force–slip curve for one connector based on the laboratory tests, the theoretical analyses and the FE analyses (FEA 11, FEA 13, FEA 14)

The maximum shear force was obtained for the mesh size 30 mm in FEA 13 and it was decreasing with the decrease of the mesh size.

The impact of the finite element on the shear force–slip curve is presented in Fig. 5.29.
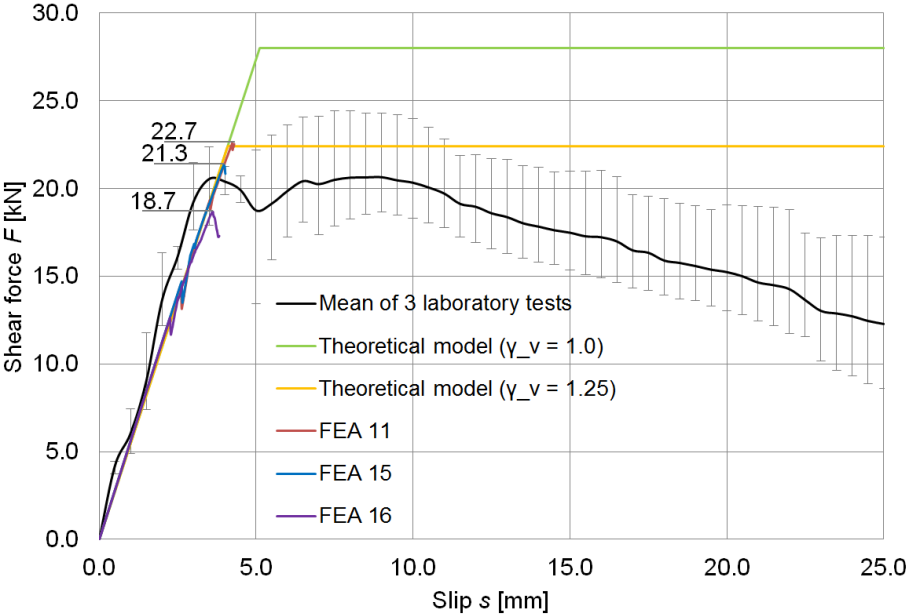
Figure 5.29. The shear force–slip curve for one connector based on the laboratory tests, the theoretical analyses and the FE analyses (FEA 11, FEA 15, FEA 16)

The finite element used for concrete slab modelling had an impact on the maximum shear force (compare the results of FEA 11, FEA 15 and FEA 16). In FEA 5 the connector was modelled using different elements (C3D10) than in FEA 6 (C3D8R). However, it did not have any influence on the results. The results of FEA 5 and FEA 6 were the same.

The impact of the friction on the shear force–slip curve is shown in Fig. 5.30.
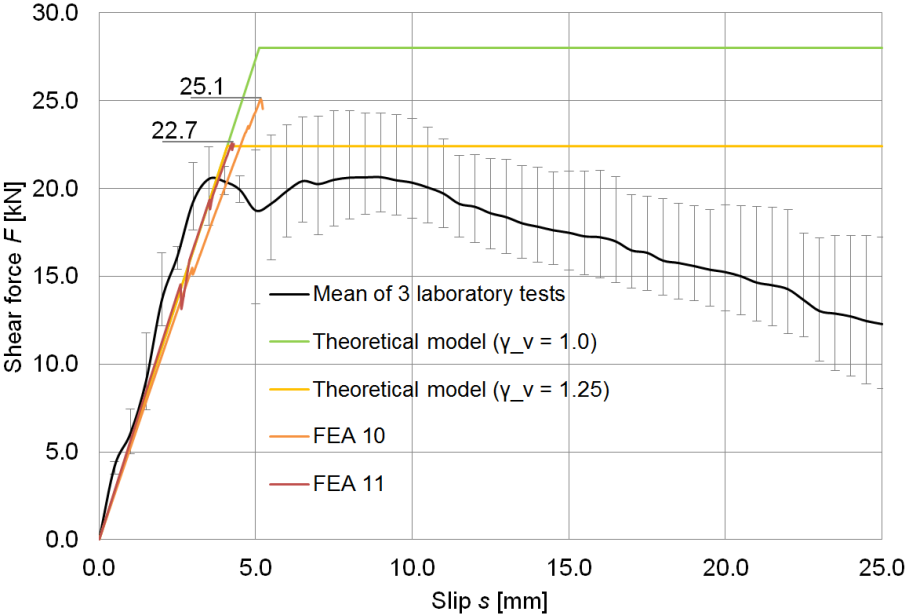
Figure 5.30. The shear force–slip curve for one connector based on the laboratory tests, the theoretical analyses and the FE analyses (FEA 10, FEA 11)

The friction between the concrete slab and the aluminium beam had an impact on the maximum shear force and the stiffness of the model.

112

Chapter 5. RESULTS AND DISCUSSIONS

Table 5.10. summarises the results of the FEAs. It also compares the results obtained in the laboratory tests, the theoretical analysis and the numerical simulations.

Table 5.10. The maximum shear force with the corresponding slip, and the secant slip moduli $k_{0.4}$ and $k_{0.6}$ (per one connector)

	Secant slip modulus $k_{0.4}$ [kN/mm]	Secant slip modulus $k_{0.6}$ [kN/mm]	Maximum shear force F_{max} [kN]	Corresponding slip s_{Fmax} [mm]
Laboratory tests (LT)	5.9 [c] ± 1.8 [b] (31.1%) [b] 0.74 [a]	6.9 [c] ± 2.2 [b] (31.5%) [b] 0.91 [a]	22.2 [c] ± 3.3 [b] (20.9%) [b] 1.35 [a]	4.1 [c] ± 2.3 [b] (55.4%) [b] 0.91 [a]
Theoretical analysis (T)	5.5	5.5	28.0 ($\gamma_v = 1.0$) 22.4 ($\gamma_v = 1.25$)	5.1 ($\gamma_v = 1.0$) 4.1 ($\gamma_v = 1.25$)
FEA 1	5.7 0.97 [d]	6.3 0.91 [d]	20.5 0.92 [d]	3.7 0.90 [d]
FEA 2	5.7 0.97 [d]	6.3 0.91 [d]	20.5 0.92 [d]	3.7 0.90 [d]
FEA 3	5.2 0.88 [d]	5.2 0.75 [d]	22.4 1.01 [d]	4.6 1.12 [d]
FEA 4	5.3 0.90 [d]	5.3 0.77 [d]	22.4 1.01 [d]	4.6 1.12 [d]
FEA 5	5.2 0.88 [d]	5.2 0.75 [d]	28.0 1.26 [d]	6.1 1.49 [d]
FEA 6	5.2 0.88 [d]	5.2 0.75 [d]	28.0 1.26 [d]	6.4 1.56 [d]
FEA 7	5.2 0.88 [d]	5.2 0.75 [d]	32.3 1.45 [d]	7.0 1.71 [d]
FEA 8	5.2 0.88 [d]	5.2 0.75 [d]	27.0 1.26 [d]	5.8 1.41 [d]
FEA 9	5.2 0.88 [d]	5.2 0.75 [d]	25.7 1.16 [d]	5.3 1.29 [d]
FEA 10	5.2 0.88 [d]	5.2 0.75 [d]	25.1 1.13 [d]	5.2 1.27 [d]
FEA 11	5.6 0.95 [d]	5.6 0.81 [d]	22.7 1.03 [d]	4.3 1.05 [d]
FEA 12	5.5 0.93 [d]	5.6 0.81 [d]	25.1 1.13 [d]	4.9 1.20 [d]
FEA 13	5.6 0.95 [d]	5.6 0.81 [d]	25.8 1.16 [d]	4.8 1.17 [d]
FEA 14	5.7 0.97 [d]	5.6 0.81 [d]	19.1 0.86 [d]	3.8 0.93 [d]
FEA 15	5.6 0.95 [d]	5.6 0.81 [d]	21.3 0.96 [d]	4.0 0.98 [d]
FEA 16	5.6 0.95 [d]	5.6 0.81 [d]	18.7 0.84 [d]	3.6 0.88 [d]

[a] Sample standard deviation
[b] Measurement errors were calculated according to Student's t-distribution using 2 degrees of freedom and a confidence level of 0.95.
[c] Mean values from tests 1–3
[d] FEA\LT

5.6. The results of the finite element modelling of the bending test

The bending tests conducted in the laboratory were used to validate the developed finite element model of the aluminium-concrete composite beam subjected to bending. The numerical results were compared to the bending test results in terms of strength, deflections, end slips and crack patterns. Furthermore, the numerical ultimate load was compared with the theoretical ultimate load of the aluminium-concrete composite beam with partial shear connection. What is more, the sensitivity of the numerical model to various parameters, such as the connection model, the concrete model, the mesh size and the finite element type, was discussed.

The numerical model used in the FEA 5 was the most accurate and reliable. The numerical curves obtained in the FEA 5 were compared with the experimental load–slip curves (see Figs. 5.31 and 5.32). It can be seen that the numerical results are in good agreement with the results from the laboratory tests.

In the laboratory tests, the post-peak load behaviour of the composite beams was also tracked, whereas the numerical analyses were terminated when the ultimate moment appeared, because of the problem with the cracking of concrete and with high non-linearity.
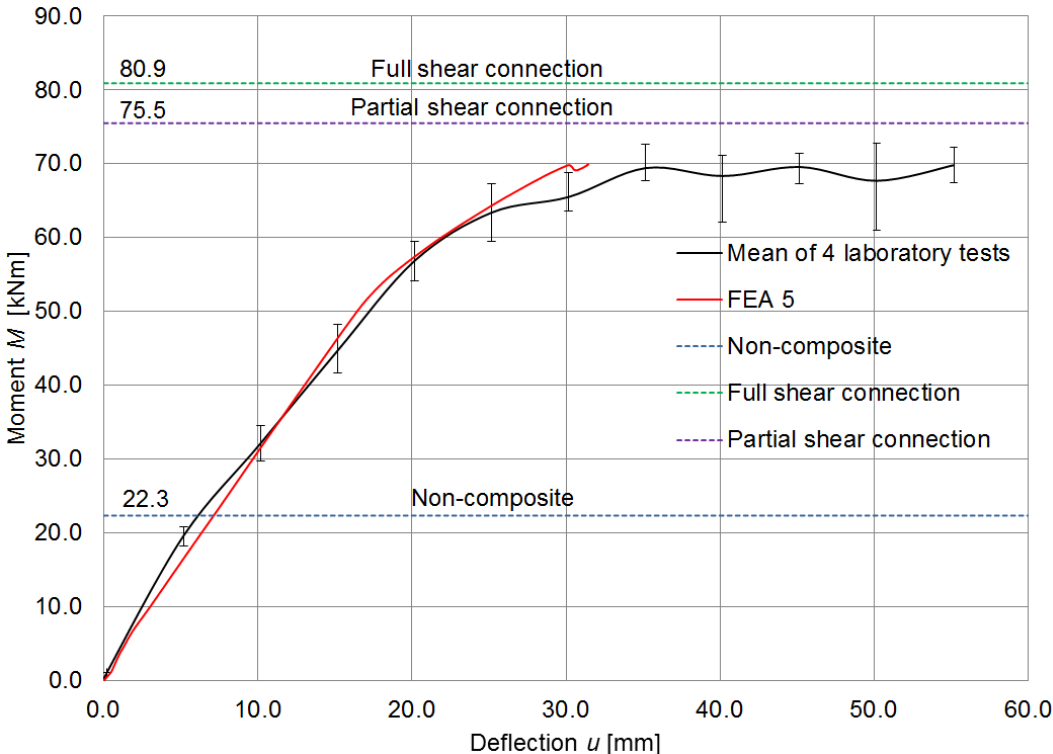
Figure 5.31. The mid-span moment–deflection curve based on the laboratory tests and the FE analysis (FEA 5)
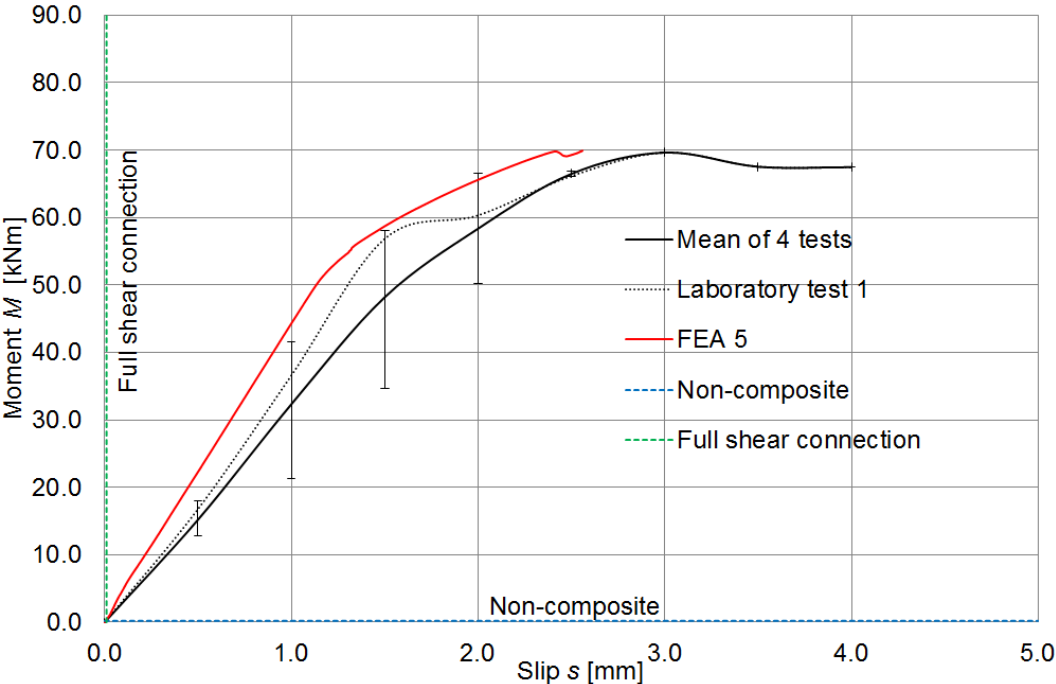
Figure 5.32. The mid-span moment–end slip curve based on the laboratory tests and the FE analysis (FEA 5)

In Figs. 5.31 and 5.32, the dashed lines represented the theoretical ultimate load of the aluminium-concrete composite beam with full shear connection calculated by the sectional rigid plastic analysis, the theoretical ultimate load of the aluminium-concrete composite beam with partial shear connection, and the theoretical ultimate load of the non-composite beam based on the plastic moment capacity of the aluminium beam only, respectively. It can be observed that the ultimate load obtained in the laboratory test and the ultimate load obtained from the FE analysis are located between these lines. This indicates that the tested aluminium-concrete composite beams had partial shear connections. It can also be seen that the theoretical model of the aluminium-concrete composite beam with partial shear connection overestimates the ultimate load of the aluminium-concrete composite beam with partial shear connection, but the difference is less than 5%.

The slight discrepancy of the load–slip behaviour could be attributed to the asymmetric behaviour of the beam, such as the rib-shear failure suddenly appearing at one end of the beam. The distance between the mean value and the max/min test values is greater in the moment–slip curve than in the moment–deflection curve (compare error bars in Fig. 5.31 and Fig. 5.32). The big margin of scatter of test results for the slip may be connected with the form of failure – the longitudinal crack formed between the profiled sheeting and the concrete ribs close to one of the supports (depending on the beam it was close to the left or the right support). The slip was measured close to one of the supports only. The moment–slip curve from the FE analysis had a better correlation to the moment–slip curve from test 1 than to the moment–slip curve for the mean value from all the laboratory test.

Table 5.11. summarises the results of the FEAs. It also shows a comparison between the mid-span ultimate strength of the composite section obtained experimentally, numerically and in the theoretical analysis.

Table 5.11. The results from the finite element analyses, the laboratory tests and the theoretical analysis

	M_o [kN·m]	M_{crack} [kN·m]	M_{ult} [kN·m]	δ_o [mm]	δ_{crack} [mm]	δ_{ult} [mm]
Laboratory tests (LT)	53.8 [c] ± 1.38 2.56% [b] 0.87 [a]	64.5 [c] ± 7.03 10.90% [b] 4.42 [a]	72.2 [c] ± 2.39 3.31% [b] 1.50 [a]	18.8 [c] ± 1.13 6.01% [b] 0.71 [a]	25.3 [c] ± 2.56 10.10% [b] 1.61 [a]	42.6 [c] ± 11.35 26.66% [b] 7.14 [a]
Theoretical analysis	39.0	–	75.5	19.4	–	–
FEA 1	69.7 1.30 [d]	–	238.2 3.30 [d]	17.9 0.95 [d]	–	111.6 2.62 [d]
FEA 2	59.0 1.10 [d]	59.8 0.93 [d]	84.7 1.17 [d]	10.8 0.57 [d]	10.9 0.43 [d]	23.9 0.56 [d]
FEA 3	45.2 0.84 [d]	56.8 0.88 [d]	56.8 0.79 [d]	18.5 0.98 [d]	27.4 1.08 [d]	27.4 0.64 [d]
FEA 4	42.9 0.80 [d]	58.2 0.90 [d]	58.2 0.81 [d]	18.9 1.00 [d]	31.1 1.23 [d]	31.1 0.73 [d]
FEA 5	48.9 0.91 [d]	63.8 0.99 [d]	69.8 0.97 [d]	16.0 0.85 [d]	25.6 1.01 [d]	31.1 0.73 [d]
FEA 6	48.9 0.91 [d]	65.4 1.01 [d]	85.2 1.18 [d]	16.0 0.85 [d]	25.9 1.02 [d]	61.5 1.44 [d]
FEA 7	47.1 0.88 [d]	66.0 1.02 [d]	66.0 0.91 [d]	15.7 0.84 [d]	27.4 1.08 [d]	27.4 0.64 [d]
FEA 8	47.3 0.88 [d]	64.3 1.00 [d]	64.3 0.89 [d]	15.8 0.84 [d]	26.3 1.04 [d]	26.3 0.62 [d]
FEA 9	52.2 0.97 [d]	91.0 1.41 [d]	91.0 1.26 [d]	16.5 0.88 [d]	75.8 3.00 [d]	75.8 1.78 [d]
FEA 10	48.1 0.89 [d]	52.2 0.81 [d]	52.2 0.72 [d]	15.9 0.85 [d]	17.5 0.69 [d]	17.5 0.41 [d]

M_o – mid-span moment corresponding to the first yielding of the aluminium beam

M_{crack} – measured mid-span moment corresponding to the first cracking between the concrete slab and the profiled sheeting

M_{ult} – mid-span ultimate strength of the composite section

δ_0 – mid-span deflection corresponding to M_0

δ_{crack} – mid-span deflection corresponding to M_{crack}

δ_{ult} – mid-span deflection corresponding to M_{ut}

[a] Sample standard deviation

[b] Measurement errors were calculated according to Student's t-distribution using 3 degrees of freedom and a confidence level of 0.95.

[c] Mean values from 1–4 tests

[d] FEA\LT

In FEA 5, the predicted mid-span moment corresponding to the first yielding of the aluminium beam for the aluminium-concrete composite beam was 48.9 kN·m, which is only 9% lower than the mean value from the laboratory tests (53.8 ± 1.38 kN·m) (see Table 5.11). The predicted mid-span deflection at the mid-span moment corresponding to the first yielding of the aluminium beam for the aluminium-concrete composite beam was 16 mm, which is 15% lower than the mean value from the laboratory tests (18.8 ± 1.13 mm). It can be seen that good agreement was achieved between the ultimate moment for the aluminium-concrete composite beam obtained in the laboratory tests and in the FEA 5. The predicted ultimate

moment for the aluminium-concrete composite beam was 69.8 kN·m, which is only 1% lower than the mean value from the laboratory tests (72.2 kN·m). The predicted mid-span deflection at the maximum moment for the aluminium-concrete composite beam was 31.1 mm, which is 27% lower than the mean value from the laboratory tests (42.6 ± 11.35 mm).

The failure mode predicted numerically was compared with that observed in the laboratory tests. It was a combination of the rib shear failure and the horizontal crack near the support as observed experimentally and confirmed in the finite element analyses (see Figs. 5.33 and 5.34). The results of the numerical analyses are presented as coloured maps of the concrete tension damage parameter (D_t) in Figs. 5.33 and 5.34. The value of the tension damage parameter equal to 1 signifies the damage of the finite element, while 0 means that the finite element is in virgin state (Szczecina and Winnincki 2015).
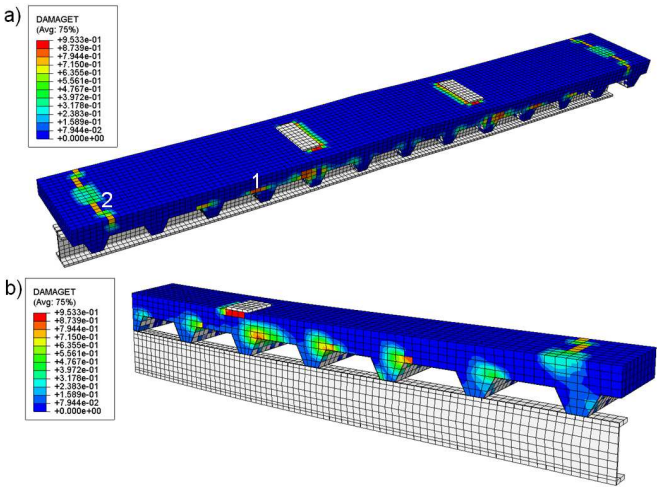
Figure 5.33. The cracking pattern for the aluminium-concrete beam (FEA 5, M_{ult} = 69.8 kN·m): a) complete model (1 – rib-shear failure, 2 – horizontal crack near the support); b) ¼ of the model
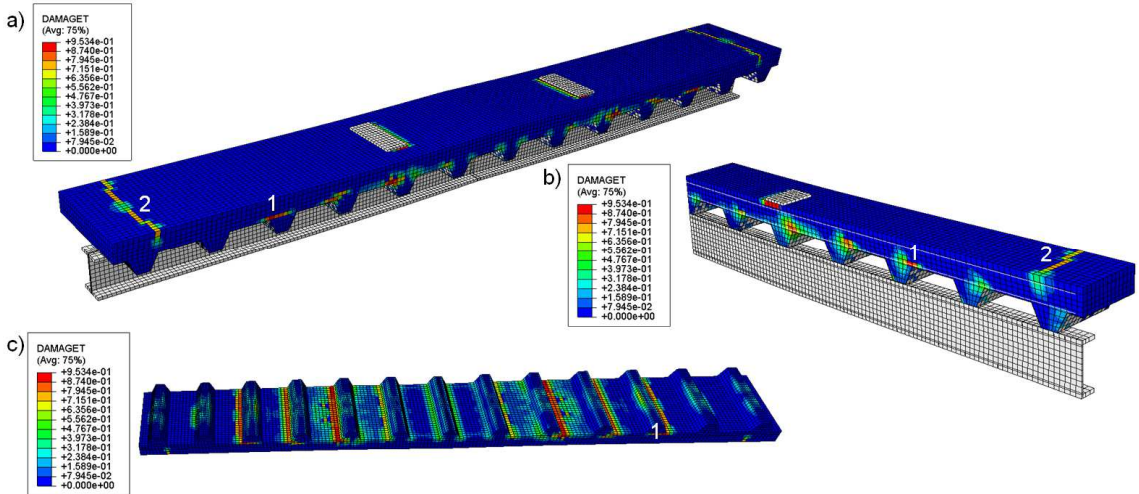
Figure 5.34. The cracking pattern for the aluminium-concrete beam (FEA 8, M_{ult} = 64.3 kN·m): a) complete model (1 – rib-shear failure, 2 – horizontal crack near the support); b) ¼ of the model; c) concrete slab

It is shown that the finite element model successfully predicted the ultimate moment, the stiffness and the failure mode of the aluminium-concrete composite beam. The finite element model is reliable and can accurately capture the behaviour of the aluminium-concrete composite beam. The sensitivity of the FE model to various parameters is discussed below.

The impact of the connection model on the mid-span moment–deflection curve and the mid-span moment–end slip curve is shown in Figs. 5.35 and 5.36.

The connection models considered in this study were: the tie function (FEA 2), the shear force–slip curve for one connector from the laboratory tests (FEA 3), the shear force–slip curve for one connector from the theoretical analysis ($k = 5.5$ kN/mm and $P_{ult} = 43.4$ kN) (FEA 4), and the shear force–slip curve for one connector from the theoretical analysis ($k = 12.5$ kN/mm and $P_{ult} = 43.4$ kN, FEA 5).

The model of connection was crucial for the finite element modelling. The ultimate moment and the stiffness of the aluminium-concrete composite beam were significantly influenced by the stiffness of the connectors. It shows that the connection model proposed in this paper can predict the slip between the aluminium beam and the concrete slab with good accuracy.
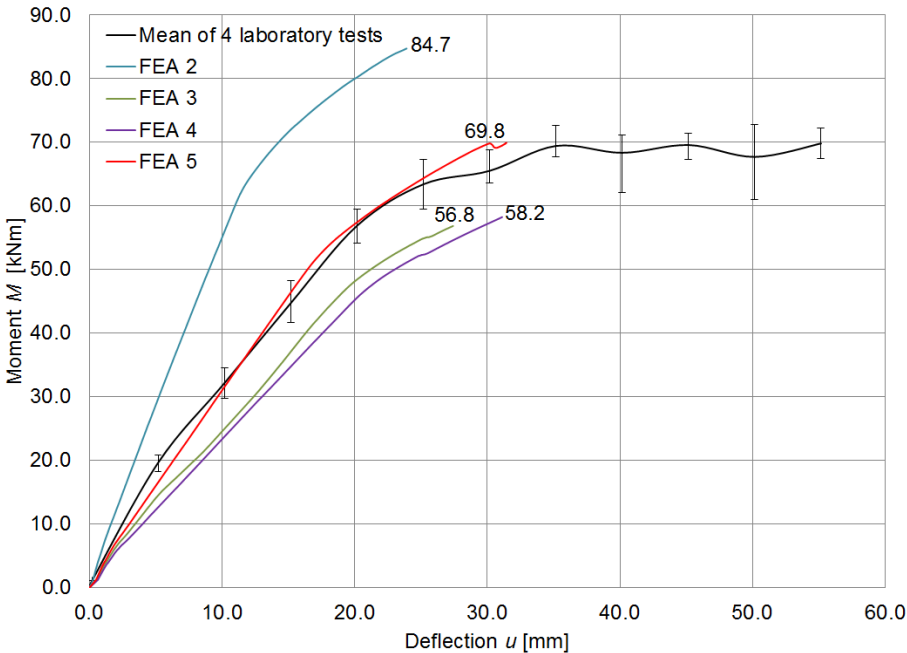
Figure 5.35. The mid-span moment–deflection curve based on the laboratory tests and the FE analyses (FEA 2–5)
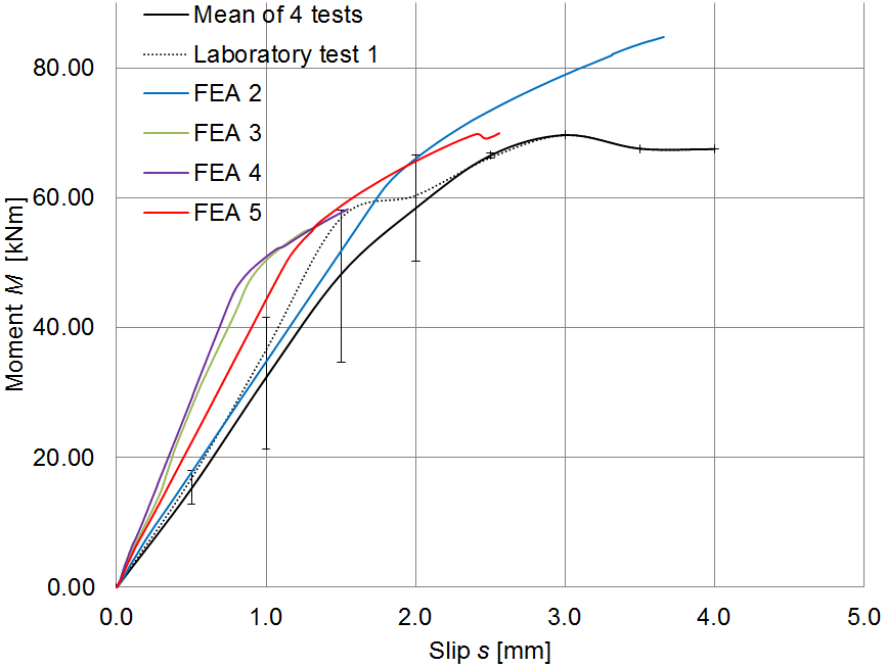
Figure 5.36. The mid-span moment–end slip curve based on the laboratory tests and the FE analyses (FEA 2–5)

The impact of the concrete model (elastic, CDP) on the mid-span moment–deflection curve and mid-span moment–end slip curve is shown in Figs. 5.37 and 5.38. The elastic model of concrete used in FEA 1 did not take into account the fracturing of the concrete. FEA 1 was terminated when a large deflection occurred. In FEA 1, the failure mode of the composite beam was associated with the yielding of the aluminium beam. The elastic model was too simple for the analysis of the aluminium-concrete composite beam. The CDP model of concrete used in FEA 4 took into account the cracking of the concrete.
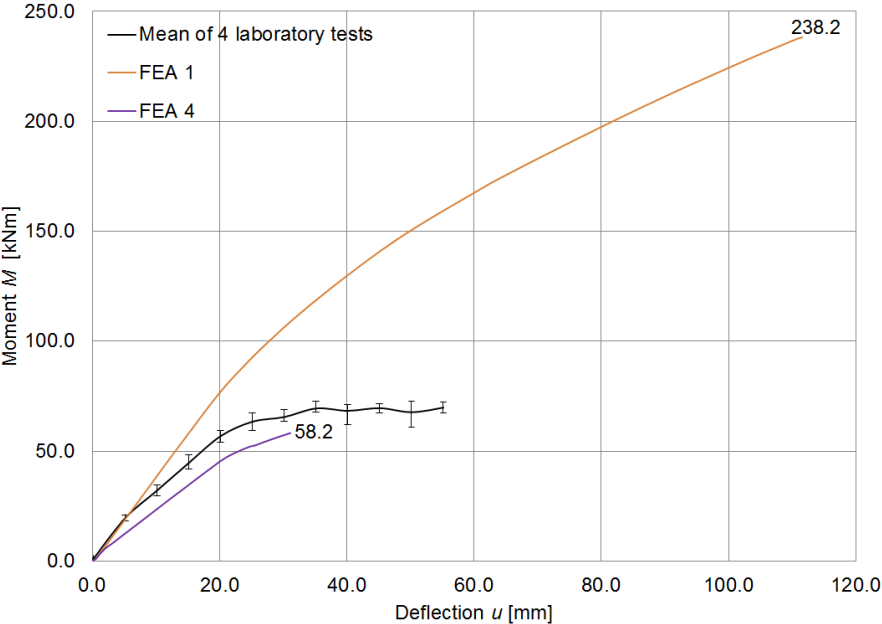
Figure 5.37. The mid-span moment–deflection curve based on the laboratory tests and the FE analyses (FEA 1, FEA 4)

119
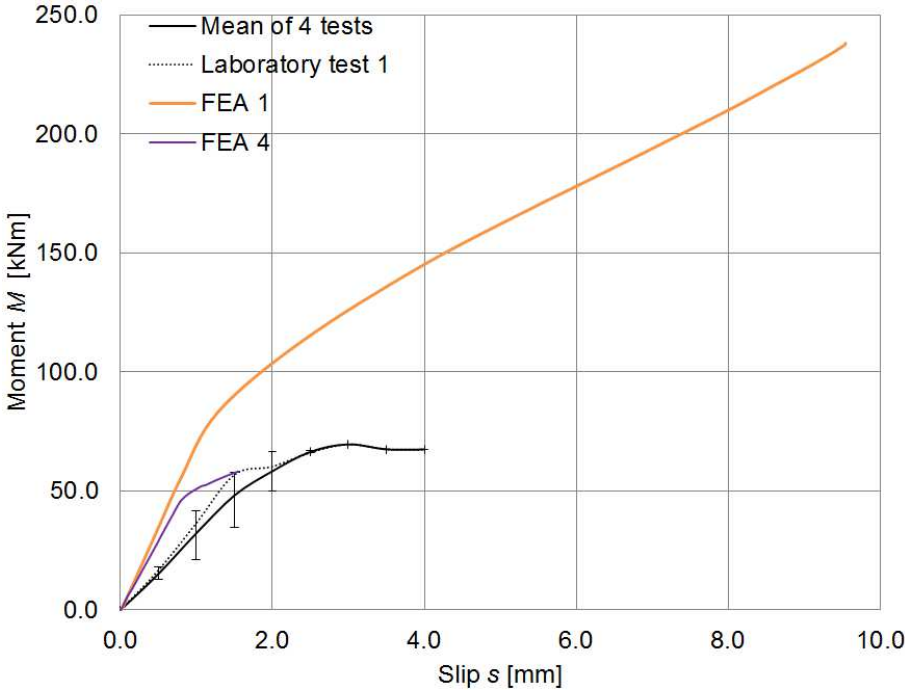
Figure 5.38. The mid-span moment–end slip curve based on the laboratory tests and the FE analyses (FEA 1, FEA 4)

Figures 5.39 and 5.40 show a comparison between the mid-span moment–deflection curves and the mid-span moment–end slip curves with variation in the viscosity parameter (w_p) used in the concrete model It can be seen that the viscosity parameter can change the results of the numerical analysis. The ultimate moment increases along with the viscosity parameter. It is worth noting that for the higher value of the viscosity parameter, the numerical calculation were terminated when larger deflections occurred. Kmiecik and Kamiński (2011) noted that problems with solution convergence may occur in the numerical analysis when full non-linearity of the concrete with its gradual degradation under increasing (mainly tensile) stress is assumed. The viscosity parameter allows one to regularise the constitutive equations. However, it may have a significant influence on the results of the analysis conducted in the Abaqus/Standard finite element code and a correct minimum value of this parameter should be used, i.e., the viscosity parameter should amount to ca. 15% of the time increment step (Genikomsou and Polak 2015) or the ratio of the time increment step to the viscosity parameter should tend to infinity (Śledziewski 2016a and 2016b) (Faściszewski 2011).
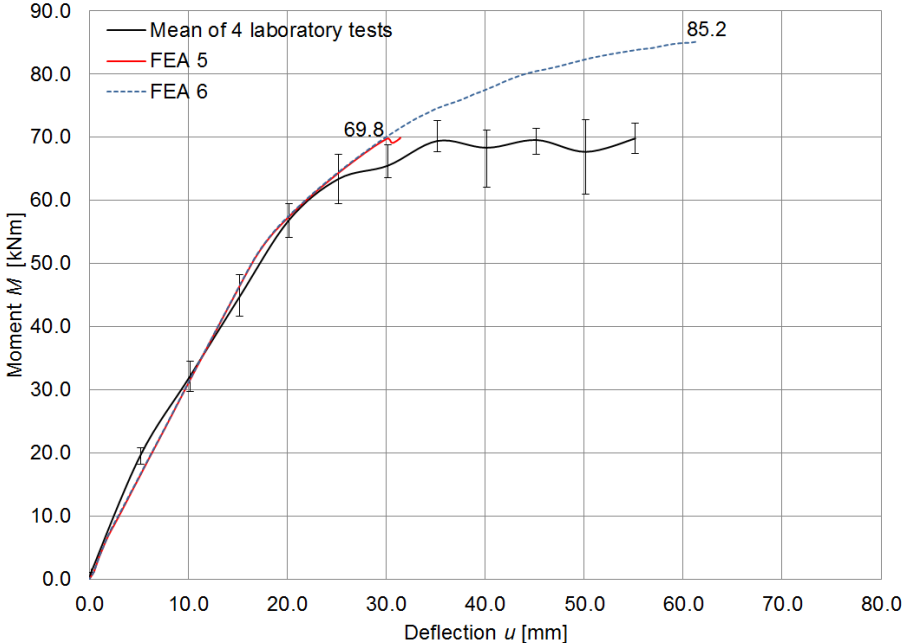
Figure 5.39. The mid-span moment–deflection curve based on the laboratory tests and the FE analyses (FEA 5, FEA 6)
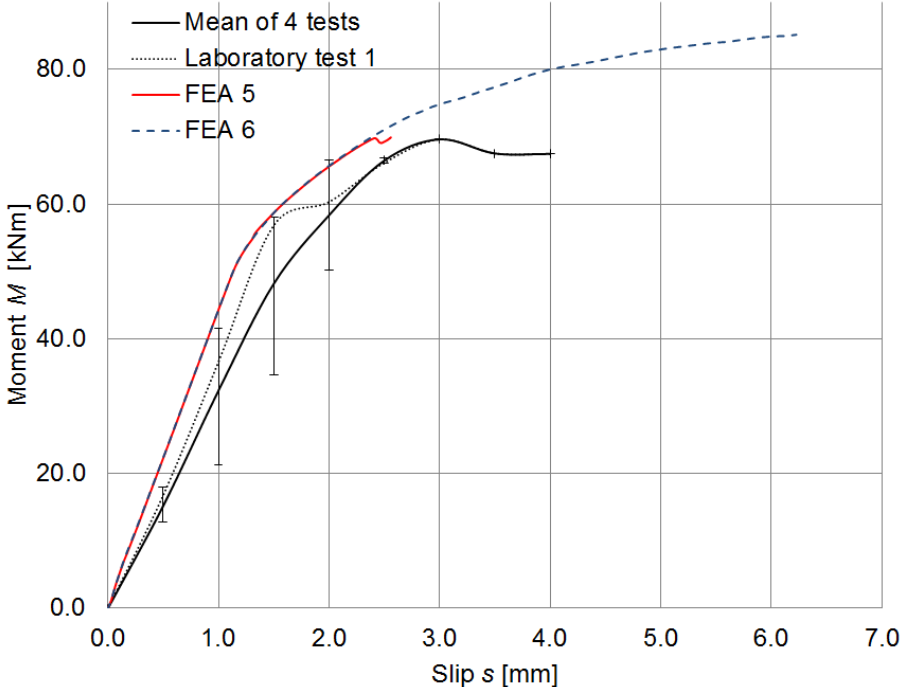
Figure 5.40. The mid-span moment–end slip curve based on the laboratory tests and the FE analyses (FEA 5, FEA 6)

Figures 5.41 and 5.42 show the variation of the mid-span moment–deflection curves and the mid-span moment–end slip curves with respect to the mesh size. The mesh sizes chosen in these analyses were: 15 mm, 20 mm and 30 mm. It can be seen that the numerical results of FEA 5 are in good agreement with the results from FEA 7 and 8. However, the ultimate moments are different in each analysis.

121
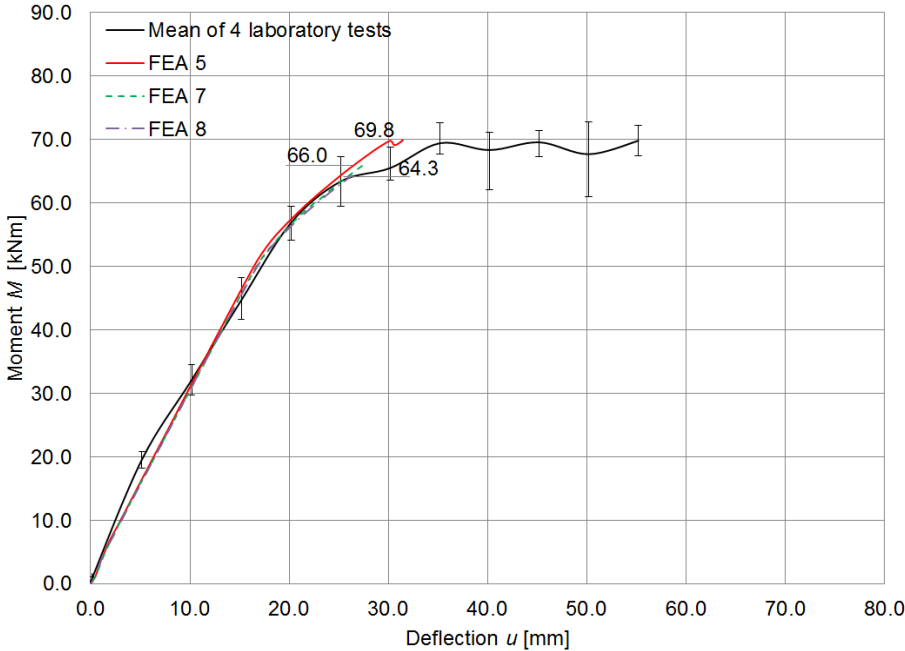
Figure 5.41. The mid-span moment–end slip curve based on the laboratory tests and the FE analyses (FEA 5, FEA 7, FEA 8)
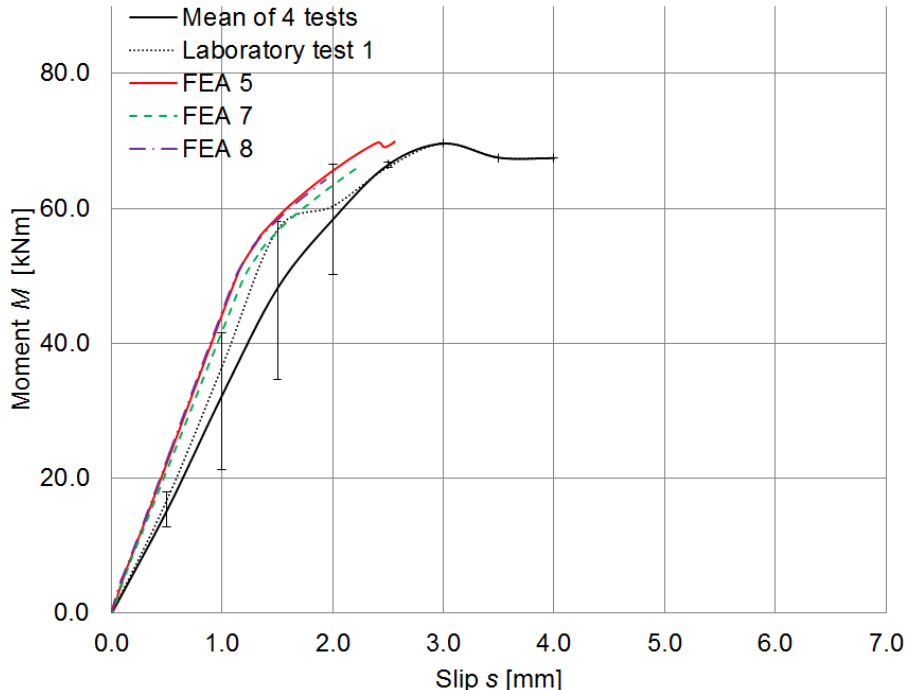
Figure 5.42. The mid-span moment–deflection curve based on the laboratory tests and the FE analyses (FEA 5, FEA 7, FEA 8)

The impact of the finite element type used to model the concrete slab on the mid-span moment–deflection curve and the mid-span moment–end slip curve is shown in Figs. 5.43 and 5.44. It can be seen that the finite element type may change the results of the numerical analysis. The ultimate moments are different in each analysis. In FEA 5 the concrete slab was meshed using C3D8R solid elements. These elements are often used for a non-linear analysis,

including of large deformation, contact, plasticity and failure (Nguyen and Kim 2009). Previous numerical analyses of composite elements described in the literature have employed this type of element, yielding accurate results when compared against laboratory tests (Jankowiak 2011) (Kyvelou, Gardner and Nethercot 2018) (Jabłoński and Halicka 2019).
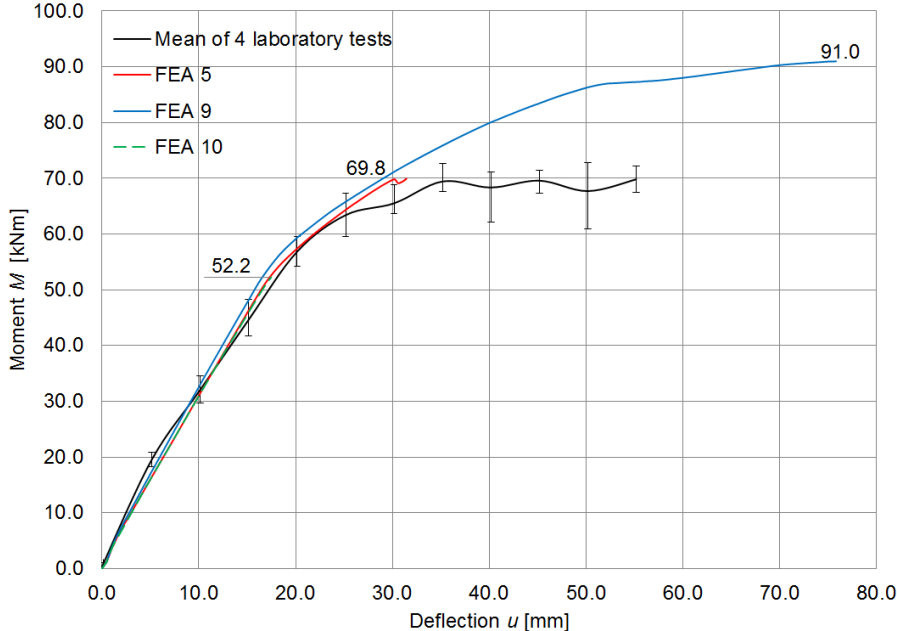
Figure 5.43. The mid-span moment–deflection curve based on the laboratory tests and the FE analyses (FEA 5, FEA 9, FEA 10)
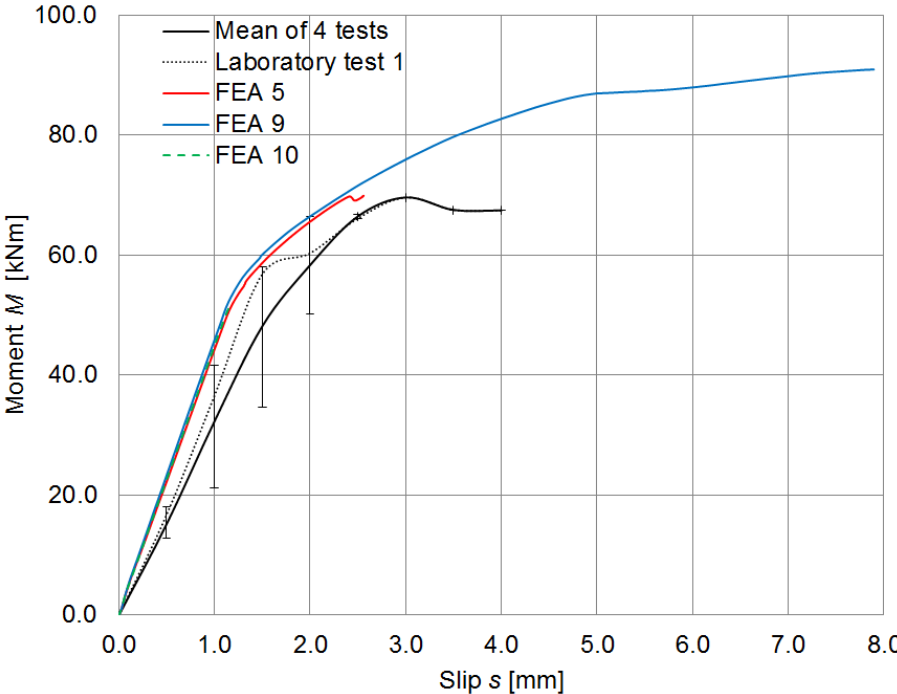
Figure 5.44. The mid-span moment–end slip curve based on the laboratory tests and the FE analyses (FEA 5, FEA 9, FEA 10)

Chapter 5. RESULTS AND DISCUSSIONS

Conclusions

This chapter presents the main conclusions of this thesis and provides answers to the research questions presented in Chapter 1.

The relatively unknown aluminium-concrete composite beams may provide an alternative to steel-concrete composite structures. They meet the requirements of sustainable construction due to their high durability. Furthermore, they fulfil the concept of circular economy because they are easily deconstructed at the end of the service life of a structure, if demountable shear connectors were used. A new type of demountable shear connector was described in the patent specification and used by the author of this dissertation in aluminium-concrete composite beams.

The answers to the research questions presented in Chapter 1 are provided below.

❖ How can demountable shear connectors reduce the drawbacks of non-demountable shear connectors?

Dowel-bolt connectors offer several advantages, including:

- Demountable shear connectors allow for the dismantling of a composite beam at the end of its structural life.
- The connector may be used in aluminium-concrete composite beams with profiled sheeting.
- Composite action is achieved without welding, which causes the formation of heat-affected zones and the reduction of strength parameters of aluminium alloys.
- Parts of different materials (aluminium, steel, concrete) are connected in an easy way.
- Demountable shear connectors can be easily installed on the construction site in a predrilled flange of an aluminium beam and profiled steel sheeting, while concrete can be poured into the steel sheeting.
- A concrete slab can be prefabricated off-site, with dowel-bolt connectors cast in required locations, and then transported to the site and connected to an aluminium beam with predrilled holes.
- Demountable dowel-bolt connectors may be used in aluminium-concrete composite beams as an environmentally-friendly alternative to channel shear connectors and bolts.

❖ How does the stiffness of new connectors affect the short-term performance of aluminium-concrete composite beams?

Shear connectors ensure composite action between an aluminium beam and a concrete slab. The analysed aluminium-concrete beams were with partial interaction. This was mainly due to the low slip moduli of the connections ($k_{0.4}$ = 5.9 ± 1.8 kN/mm). The clearance between the bolt and the hole had a negative impact on the stiffness of the connection. However, it made it easier to install demountable shear connectors through the holes in the aluminium beam flange. The slipping in the connection had an impact on the stiffness and the load bearing capacity of the aluminium-concrete beam. Furthermore, the analysed shear connectors showed a lower level of ductility, as the slip capacity was only 4.2 ± 2.0 mm. Due to this fact, the shear connectors did not have enough slip capacity to redistribute the shear force to adjacent shear connectors after yielding. The failure mode of the shear connection was brittle. For this reasons, the load capacities of the connectors were achieved before the load-carrying capacity of the full composite beam was attained in the bending tests.

❖ Can the guidelines for the design of steel-concrete composite structures be applied for the ultimate limit state verification of aluminium-concrete composite structures?

The bending plastic resistance of the aluminium-concrete composite beam with partial shear connection calculated from Eq. (3.27), which took slip into account, was 1.05 times higher than the bending resistance from the test. The proposed method of calculating the bending plastic resistance of the aluminium-concrete composite beam with partial shear connection produced similar results to the bending test. However, only four beams of the same geometry were tested. Therefore, it is advisable to perform complementary tests on composite beams of different geometries and to verify the method against a greater number of test results.

Furthermore, the problem of the rib-shearing failure which occurred in the analysed beams should be addressed in the future. The use of profiled sheeting with wider ribs, and of the waveform reinforcement presented by Patrick (2004) to prevent the rib-shearing failure is recommended.

Due to the significant deflections of the ACC beams, the serviceability limit state requirements may be more difficult to meet than the ultimate limit state requirements. However, deflections can be reduced by using an ACC beam with a higher cross-section of the aluminium girder and a wider concrete slab.

❖ Can zero-length springs be used in the numerical model of an aluminium-concrete composite beam to model the connection between the aluminium beam and the concrete slab?

The shear connectors were modelled using zero-length springs. The model had an impact on the ultimate moment and the stiffness of the aluminium-concrete composite beam. The connection model proposed in this PhD dissertation allows for predicting the slip between the aluminium beam and the concrete slab with good accuracy.

Future research

There have been extensive studies on composite structures in recent decades. However, the investigation presented in this thesis is the only one where a concrete slab is poured into steel sheeting and connected with an aluminium beam using demountable shear connectors. The presented studies have answered many questions. However, new problems and questions have been raised and they should be addressed in future analyses of aluminium-concrete composite beams.

7.1 Experimental investigations

The experimental programme presented in the dissertation had certain limitations, and further experimental shear connection tests and bending tests should be performed. In the case of shear connectors, the effects of the hole size, shear connector diameter, torque moment, and concrete rib width were not examined. For this reason, further investigation of the effects of varying geometry of the connection is recommended. The stiffness of the connection should be improved. It could be increased by bolt tightening, hole clearance reduction and concrete rib width extension. All the proposed improvements of the shear connections should be verified in shear connection tests to evaluate their impact on stiffness and resistance. In the case of aluminium-concrete composite beams, only four beams of the same geometry were tested, so it would be reasonable to perform complementary tests to identify the optimal geometry of an aluminium-concrete composite beam. The impact of the profiled sheeting type, shear connector spacing and diameter, concrete class, slab thickness, aluminium alloy and aluminium beam height on the resistance and stiffness of the aluminium-concrete composite beam should also be investigated. Furthermore, only one type of connection was tested, so it would be advisable to perform complementary tests on beams with a different type of connection (e.g. adhesive connection, continuous shear connection). What is more, long-term behaviour of aluminium-concrete composite beams should be analysed in the future, along with the influence of the shrinkage and creep of concrete on the long-term behaviour of aluminium-concrete composite beams. Furthermore, guidelines for structural health monitoring and damage detection in aluminium-concrete composite structures should be developed. Periodic visual inspections may not suffice to find all the problems (Abramowicz, Berczyński and Wróblewski 2020). Strategic structures should be controlled using structural health monitoring systems. Such systems may control, measure and analyse the response of the structure. An irregular signal may mean there is damage in the structure, which can be quickly repaired once detected (Szumigała et al. 2018). Wavelet transforms or energy transfer ratios were suggested for damage diagnosis, e.g., in steel-concrete composite structures, sandwich panels or plates (Wróblewski et al. 2017) (Pozorska J. and Pozorski Z. 2018) (Knitter-Piątkowska and Guminiak 2016 & 2020). Studies on damage detection in

aluminium-concrete composite structures are recommended. Finally, the fire resistance of aluminium-concrete composite beams should be analysed in fire tests.

7.2 Numerical analyses

The comparison between the experimental and numerical results indicates that the adopted 3D model can capture the response of the aluminium-concrete composite beam, because the results obtained in the numerical analyses of the composite beam were very similar to the experimental values. For this reason, the numerical model can be used to simulate the behaviour of composite beams with different configurations, and geometrical and mechanical properties. As a result, the numerical analyses can help generate savings, since no additional laboratory tests are required to investigate the behaviour of said beams.

 Further numerical analyses may help to improve aluminium-concrete composite beams. Such analyses should include parametric studies to identify the optimal cross-section of a composite beam. What is more, only a static analysis in the Abaqus/Standard module was used. For this reason, it is advisable to perform a complementary analysis in the Abaqus/Explicit module. This would allow for a more detailed analysis of non-linear problems (relatively high deformations accompanying the cracking of concrete) and for studying the post-ultimate behaviour of composite beams. The Abaqus/Explicit module can be used to perform analyses of composite beams subjected to dynamic loads and quasi-static loads (Jankowiak 2011).

7.3 Theoretical analyses

In order to provide design guidance for aluminium-concrete composite beams with profiled sheeting and demountable shear connectors, the proposed theoretical models should be verified by further experimental shear connection and bending tests.

7.4 Industrial implementation

Aluminium-concrete composite beams may be used in the building frame system. However, some aspects of aluminium-concrete structures were not discussed in the dissertation. The making of the shear connectors was time-consuming. For this reason, an automated and less time-consuming process of shear connector production should be developed. Furthermore, the cost of the aluminium-concrete composite floor system should be estimated and the connection details between the aluminium-concrete beams and the vertical structural elements should be considered to ensure that the beams are compatible with the remaining structural elements of the building frame system. Last but not least, the aluminium-concrete beams should be used in a full-scale floor in a real building in order to monitor any problems which may occur during the construction and use of the building.

Bibliography

Abendroth, R. E., Sanders, W. W. and Mahadevan, V. (1996). *A continuous span aluminium girder concrete deck bridge, Final Report, Part I: Field test performance and evaluation.* Bridge Engineering Center, Iowa State University. [cited at p. 6-7, 15, 19]

Abendroth, R. E., Sanders, W. W. and Hansz, S. (1997). *A continuous span aluminium girder concrete deck bridge, Final Report, Part II: Fatigue tests of aluminum girders.* Bridge Engineering Center, Iowa State University. [cited at p. 6-7, 15, 19]

Abramowicz, M., Berczyński S. and Wróblewski, T. (2020). Modelling and parameter identification of steel-concrete composite beams in 3D rigid finite element method. *Archives of Civil and Mechanical Engineering*, 20, article 103, doi: 10.1007/s43452-020-00100-7. [cited at p. 127]

Abu-Obeidah, A. S., Abdalla, J. A. and Hawileh, R. A. (2019). Shear strengthening of deficient concrete beams with marine grade aluminium alloy plates. *Advances in Concrete Construction*, 7(4), pp. 249-262, doi.10.12989/acc.2019.7.4.249. [cited at p. 14]

Ahn, J.-K. and Lee, C.-H. (2017). Fire behavior and resistance of partially encased and slim-floor composite beams. *Journal of Constructional Steel Research*, 129, pp. 276-285, doi: 10.1016/j.jcsr.2016.11.018. [cited at p. 11]

Aliawdin, P. and Urbańska, K. (2011). Limit analysis of steel-concrete composite structures with slip. *Civil and Environmental Engineering Reports*, 7, pp. 19-34. [cited at p. 76]

Alison, G. A. (1984). Evaluation of seven aluminum highway bridges after two to three decades of service. *Transportation Research Record*, 950, pp. 123-129. [cited at p. 3-4, 6-7, 10-11]

Aluminum Association (1994). *Specifications for Aluminum Structures*. Sixth Ed., New York. [cited at p. 19-20]

Aluminium Federation of South Africa (2011). *Corrosion resistance of aluminium and protective measures where appropriate*. Pocket Guide 3. [cited at p. 12]

American Association of State Highway and Transportation Officials (1994), *AASHTO LRFD Bridge Design Specifications*. Washington. [cited at p. 20]

American Institute of Steel Construction (2016). *ANSI/AISC 360-16. Specification for Structural Steel Buildings*. Chicago. [cited at p. 34]

BIBLIOGRAPHY

Ashby, M. F., Balas, D. F. and Coral, J. S. (2016). *Materials and Sustainable Development*. Oxford: Butterworth-Heinemann, 328. [cited at p. 1]

Ataei, A., Chiniforush, A. A., Bradford, M. and Valipour, H. (2019). Cyclic behaviour of bolt and screw shear connectors in steel-timber composite (STC) beams. *Journal of Constructional Steel Research*, 161, pp. 328-340, doi: 10.1016/j.jcsr.2019.05.048. [cited at p. 3, 24]

Barbosa, W. C. S., Bezerra, L. M., Chater, L. and Cavalcante, O. R. O. (2019). Experimental evaluation on the structural behavior of truss shear connectors in composite steel-concrete beams. *Ibracon Structures and Materials Journal*, 12(5), pp. 1157-1182, doi: 10.1590/S1983-41952019000500010. [in Portuguese] [cited at p. 23]

Bazant, Z. P. and Becq-Giraudon, E. (2002). Statistical prediction of fracture parameters of concrete and implications for choice of testing standard. *Cement and Concrete Research*, 32, pp. 529-556. [cited at p. 62]

Bazant, Z. P. and Planas, J. (1998). *Fracture and size effect in concrete and other quasibrittle materials*. New York: Routledge, 640. [cited at p. 106]

Bedon, C. and Fragiacomo, M. (2019). Numerical analysis of timber-to-timber joints and composite beams with inclined self-tapping screws. *Composite Structures*, 207, pp. 13-28, doi: 10.1016/j.compstruct.2018.09.008. [cited at p. 1]

Biegus, A. and Lorenc, W. (2014). Development of shear connections in steel-concrete composite structures. *Civil and Environmental Engineering Reports*, 15(4), pp. 23-32, doi: 10.1515/ceer-2014-0032. [cited at p. 23-24]

Błaszczyński, T., Ksit, B. and Dyzman, B. (2012). *Sustainable construction with elements of energy certification*. Wrocław: Dolnośląskie Educational Publisher. [in Polish] [cited at p. 1]

Bonenberg, W. and Kapliński, O. (2017). The architect and the paradigms of sustainable development: A review of dilemmas. *Sustainability*, 10(1), article 100, doi: 10.3390/su10010100. [cited at p. 1]

Brandt, A. (2008). Durability of building and civil engineering structures and sustainable development. In: A. Łapko, M. Broniewicz, J. A. Prusiel, eds., *The scientific research problems of building, Volume IV: Sustainable development in building industry*, Białystok: Technical University of Bialystok Publisher, pp. 169-183. [in Polish] [cited at p. 1].

British Standards Institution (2010). *BS 5950-3.1:1990+A1:2010: Design in composite construction. Part 3: structural use of steelwork in building*. London. [cited at p. 25]

BIBLIOGRAPHY

Bromberek, Z. (2014). Energy efficiency and urban development. *Izolacje*, 1, pp. 14-18. [in Polish] [cited at p. 1]

Broniewicz, M. (2008). Design based on sustainable development. In: A. Łapko, M. Broniewicz and J. A. Prusiel, eds., *The scientific research problems of building, Volume IV: Sustainable development in building industry*, Białystok: Technical University of Bialystok Publisher, pp. 185-206. [in Polish] [cited at p. 2]

Bruzzese, E., Cappelli, M. and Mazzolani, F. M. (1989). Experimental investigation on aluminium-concrete beams. *Construzioni Metalliche* 5, pp. 265-282. [cited at p. 11, 15, 18-19, 29]

Bruzzese, E., De Martino, A., Mandara, A. and Mazzolani, F. M. (1991). Aluminium-concrete systems: behavioural parameters. In: *International Conference on Steel and Aluminium Structures ICSAS 91, Singapore, 22-24 May 1991*, pp. 113-122. [cited at p. 19]

Ceccotti, A., Fragiacomo, M. and Giordano, S. (2007). Long-term and collapse tests on timber-concrete composite beam with glued-in connection. *Materials and Structures*, 40(1), pp. 15-25, doi: 10.1617/s11527-006-9094-z. [cited at p. 85]

Chen, J., Wang, W., Ding, F.-X., Xiang, P., Yu, Y.-J., Liu, X.-M., Xu, F., Yang, C.-Q. and Long, S.-G. (2019). Behavior of an advanced bolted shear connector in prefabricated steel-concrete composite beams. *Materials*, 12, article 2958, doi:10.3390/ma12182958. [cited at p. 26]

Chen, Y., Feng, R. and Xu, J. (2017). Flexural behaviour of CFRP strengthened concrete-filled aluminium alloy CHS tubes. *Construction and Building Materials*, 142, pp. 295-319. [cited at p. 13-14]

Chen, Z., Lei, Q., He, R., Zhang, Z. and Chowdhury, A. (2016). Review on antibacterial biocomposites of structural laminated veneer lumber. *Saudi Journal of Biological Sciences*, 23(1), pp. 142-147. [cited at p. 14]

Chybiński, M. and Polus, Ł. (2018). Bending resistance of metal-concrete composite beams in a natural fire. *Civil and Environmental Engineering Reports*, 4(28), pp. 149-162, doi: 10.2478/ceer-2018-0058. [cited at p. 11-12, 15]

Chybiński, M. and Polus, Ł. (2019). Theoretical, experimental and numerical study of aluminium-timber composite beams with screwed connections. *Construction and Building Materials*, 226, pp. 317-330, doi: 10.1016/j.conbuildmat.2019.07.101. [cited at p. 1, 14-15, 27]

Chybiński, M., Polus, Ł., Ratajczak, M. and Sielicki, P. W. (2019). The evaluation of the fracture surface in the AW-6060 T6 aluminium alloy under a wide range of loads. *Metals*, 9(3), article 9030324, doi: 10.3390/met9030324. [cited at p. 83]

BIBLIOGRAPHY

Chybiński, M. and Garstecki, A. (2017). Diagonal versus orthogonal ribs in stability of steel I beams, *Procedia Engineering*, 172, pp. 172-177. [cited at p. 14]

Cicero, M. T. (55 BC). *On the Orator*. [in Latin] [cited at p. 9]

Ciesielczyk, K. and Studziński, R. (2017). Experimental and numerical investigation of stabilization of thin-walled Z-beams by sandwich panels. *Journal of Constructional Steel Research*, 133, pp. 77-83, doi: 10.1016/j.jcsr.2017.02.016. [cited at p. 79]

Ciesielczyk, K., Szumigała, M. and Ścigałło, J. (2017). The numerical analysis of the effective flange width in T-section reinforced concrete beams. *Procedia Engineering*, 172, pp. 178-185. [cited at p. 78]

Claisse, P. (2016). *Civil Engineering Materials*. Butterworth-Heinemann, 528. [cited at p. 1]

Comite Euro-International du Beton (1991). *CEB-FIP Model Code 1990*. London: Thomas Telford. [cited at p. 62]

Czarnecki, L., Deja, J., Furtak, K., Halicka, A., Kapliński, O., Kaszyńska, M., Kruk, M., Kuczyński, K., Szczechowiak, E. and Śliwiński, J. (2017). Ideas shaping innovation challenges of construction technology in searching of construction development paradigm. *Materiały Budowlane*, 7, pp. 28-33. [in Polish] [cited at p. 1]

Dai, X. H., Lam, D. and Saveri, E. (2015). Effect of concrete strength and stud collar size to shear capacity of demountable shear connectors. *Journal of Structural Engineering*, 141(11), doi: 10.1061/(ASCE)ST.1943-541X.0001267. [cited at p. 24]

Das, S. K. and Kaufman, J. G. (2007). Aluminium alloys for bridges and bridge decks. In: S. K. Das and W. Yin, eds., *Aluminium alloys for transport, packing, aerospace and other applications*, Warrendale (USA): The Minerals, Metals & Materials Society. [cited at p. 6-7, 10-11]

Dassault Systèmes (2013). *Abaqus 6.13 Online Documentation*. [cited at p. 62-64, 67, 71, 73, 75]

David, R. and Meyerhof, G. G. (1958). Composite construction of bridges using steel and concrete. *The Engineering Journal*, 41(51), pp. 41-47. [cited at p. 40]

Deam, B. L., Fragiacomo, M. and Buchanan, A. H. (2008). Connections for composite concrete slab and LVL flooring systems. *Materials and Structures*, 41, pp. 495-507. [cited at p. 49, 92]

Ding, F.-X., Liu, J., Liu, X.-M., Guo, F.-Q. and Jiang, L.-Z. (2016). Flexural stiffness of steel-concrete composite beam under positive moment. *Steel and Composite Structures*, 20(6), pp. 1369-1389, doi: 10.12989/scs.2016.20.6.1369. [cited at p. 68]

132

BIBLIOGRAPHY

Dokšanović, T., Džeba, I. and Markulak, D. (2017). Applications of aluminium alloys in civil engineering. *Technical Gazette*, 24(5), pp. 1609-1618, doi: 10.17559/TV-20151213105944. [cited at p. 10-11]

Dudziński, W., Pękalski, G., Harnatkiewicz, P., Kopczyński, A., Lorenc, W., Kożuch, M. and Rowiński, S. (2011). Study on fatigue cracks in steel-concrete shear connection with composite dowels. *Archives of Civil and Mechanical Engineering*, 11(4), pp. 839-858. [cited at p. 24]

Ellobody, E. and Young, B. (2006). Performance of shear connection in composite beams with profiled steel sheeting. *Journal of Constructional Steel Research*, 62, pp. 682-694. doi: 10.1016/j.jcsr.2005.11.004. [cited at p. 34]

Ernst, S., Bridge, R. Q. and Wheeler, A. (2007). Strength of headed stud shear connection in composite beams. *Australian Journal of Structural Engineering*, 7(2), pp. 111-121, doi: 10.1080/13287982.2007.11464969. [cited at p. 94, 101]

Ernst, S., Bridge, R. Q. and Wheeler, A. (2009). Push-out tests and a new approach for the design of secondary composite beam shear connections. *Journal of Constructional Steel Research*, 65, pp. 44-53, doi: 10.1016/j.jcsr.2008.04.010. [cited at p. 101]

Errera, S. J. and Mindlin, H. L. (1959). *Test of a composite aluminium and concrete highway bridge (For Oral Presentation at ASCE Annual Convention in Washington). Report 275.2.* Fritz Engineering Laboratory, Lehigh University. [cited at p. 4]

Etim, O., Gand, A. K., Saidani, M., Fom, P., Ganjian, E. and Okon, E. (2020). Shear characterisation of pultruded superstructural FRP-concrete push-outs. *Structures*, 23, pp. 254-266, doi: 10.1016/j.istruc.2019.10.004. [cited at p. 27, 88, 91]

European Committee for Standardization (2004). *EN 1992-1-1. Eurocode 2. Design of concrete structures - Part 1-1: General rules and rules for buildings.* Brussels. [cited at p. 59, 61, 72, 80, 98]

European Committee for Standardization (2005), *EN 1993-1-8, Eurocode 3: Design of steel structures - Part 1-8: Design of joints* Brussels. [cited at p. 25, 33]

European Committee for Standardization (2004), *EN 1994-1-1, Eurocode 4: Design of composite steel and concrete structures - Part 1-1: General rules and rules for buildings*, Brussels. [cited at p. 25, 33, 40, 49, 51, 54, 73, 86, 101]

European Committee for Standardization (2007), *EN 1999-1-1, Eurocode 9: Design of aluminium structures - Part 1-1: General structural rules*, Brussels. [cited at p. 10, 15, 33]

BIBLIOGRAPHY

European Committee for Standardization (2009 and 2016), *EN ISO 6892-1, Metallic materials-tensile testing – Part 1: Method of test at room temperature*, Brussels. [cited at p. 43, 83]

European Committee for Standardization (2003), *EN 206-1, Concrete - Part 1: Specification, performance, production and conformity*, Brussels. [cited at p. 54]

European Committee for Standardization (2011), *EN 12390-3, Testing hardened concrete – Part 3: Compressive strength of test specimens,* Brussels. [cited at p. 45-46]

European Committee for Standardization (2011), *EN 12390-6, Testing hardened concrete – Part 6: Tensile splitting strength of test specimens*, Brussels. [cited at p. 45-46]

European Committee for Standardization (2013), *EN 12390-13, Testing hardened concrete – Part 13: Determination of secant modulus of elasticity in compression*, Brussels. [cited at p. 45-46, 48]

European Convention for Constructional Steelwork (1988). *Calculation of the fire resistance of centrally loaded composite steel-concrete columns exposed to the standard fire*. Brussels: European Convention for Constructional Steelwork, Technical Committee 3, Fire Safety of Steel Structures, No 55. [cited at p. 11]

European Convention for Constructional Steelwork (1999). *Design of composite joints for buildings*. Brussels: European Convention for Constructional Steelwork, Technical Committee 11, Composite Structures, No 109. [cited at p. 91]

European Council, European Parliament (2011). *Regulation (EU) No 305/2011 of the European Parliament and of the Council of 9 March 2011 laying down harmonised conditions for the marketing of construction products and repealing Council Directive 89/106/EEC*. Official Journal of the European Union, L 88/5, 4/4/2011. [cited at p. 1]

Faggiano, B., De Matteis, G., Landolfo, R. and Mazzolani, F. M. (2004). Behaviour of aluminium alloy structures under fire. *Journal of Civil Engineering and Management*, 10(3), pp. 183-190. [cited at p. 11]

Faściszewski, Ł. (2011). *Analiza numeryczna ściany żelbetowej obciążonej wybuchem*. Master Thesis. Poznan University of Technology, Poznań. [cited at p. 120]

Feng, R., Chen, Y. and Gong, W. (2017). Flexural behaviour of concrete-filled aluminium alloy thin-walled SHS and RHS tubes. *Engineering Structures*, 137, pp. 33-49, doi: 10.1016/j.engstruct.2017.01.036. [cited at p. 14]

BIBLIOGRAPHY

Flaga, K. (2015). The influence of concrete shrinkage on durability of reinforced structural members. *Bulletin of the Polish Academy of Sciences: Technical Sciences*, 63(1), pp. 15-22, doi: 10.1515/bpasts-2015-0002. [cited at p. 79]

Formisano, A., De Matteis, G. and Mazzolani, F. M. (2016). Experimental and numerical researches on aluminium alloy systems for structural applications in civil engineering fields. *Key Engineering Materials*, 710, pp. 256-261, doi: 10.4028/www.scientific.net/KEM.710.256. [cited at p. 10]

Furtak, K. (2015). Evaluation of the influence of shrinkage strain on the fatigue strength of the connection in steel-concrete composite beams. *Archives of Civil and Mechanical Engineering*, 15(3), pp. 767-774. [cited at p. 79]

Furtak, K. (2017). Ocena ugięć belki zespolonej typu aluminium-beton od skurczu betonu. In: T. Biliński and J. Korentz, eds., *XI Konferencja Naukowa Konstrukcje zespolone, Zielona Góra, 29-30 czerwca 2017*, Zielona Góra: Oficyna Wydawnicza Uniwersytetu Zielonogórskiego, pp. 65-66. [in Polish] [cited at p. 40]

Gajewski, T. and Garbowski, T. (2014). Mixed experimental/numerical methods applied for concrete parameters estimation. In: T. Łodygowski, J. Rakowski and P. Litewka, eds., *Recent advances in computational mechanics: Proceedings of the 20th International Conference on Computer Methods in Mechanics (CMM 2013), Poznań, 27-31 August, 2013*, CRC Press: Leiden, pp. 293-302. [cited at p. 59]

Genikomsou, A. S. and Polak, M. A. (2015). Finite element analysis of punching shear of concrete slabs using damaged plasticity model in Abaqus. *Engineering Structures*, 98, pp. 38-48, doi: 10.1016/j.engstruct.2015.04.016. [cited at p. 67, 73, 106, 120]

Gitter, R. (2008). *Design of aluminium structures: Selection of structural alloys. Structural design according to Eurocode 9: Essential properties of materials and background information*. Workshop, Brussels. [cited at p. 11]

Gluhović, N., Marković, Z., Spremić, M. and Pavlović, M. (2017). Experimental investigation and specific behaviour of X-HVB shear connectors in prefabricated composite decks. *CE/Papers*, 1(2 & 3), pp. 2080-2089, doi: 10.1002/cepa.253. [cited at p. 23]

Golewski, G. L. (2007). Analiza wpływu D_{max} na parametry mechaniki pękania betonów wapiennych określane przy trójpunktowym zginaniu. *Budownictwo i Architektura*, 1, pp. 5-16. [cited at p. 62]

Göner, H. and Marx, S. (1969). *Aluminium-handbuch*. Berlin: VEB Verlag Technik, 775. [in German] [cited at p. 4]

BIBLIOGRAPHY

Guezouli, S. and Lachal, A. (2012). Numerical analysis of frictional contact effects in push-out tests. *Engineering Structures*, 40, pp. 39-50. [cited at p. 66, 70, 79]

Gwóźdź, M. (2007). Project problems of contemporary aluminium structures. *Technical Transactions*, Z4-A, pp. 281-286. [in Polish] [cited at p. 9-10]

Gwóźdź, M. (2014). *Konstrukcje aluminiowe. Projektowanie według Eurokodu 9*. Kraków: Wydawnictwo Politechniki Krakowskiej, 318. [in Polish] [cited at p. 3]

Habashi, F. (1988). A hundred years of the Bayer Process for alumina production. *CIM Bulletin*, 81(909), pp. 70-74. [cited at p. 3]

Hag-Elsafi, O. and Alampalli, S. (2002). Cost-effective rehabilitation of two aluminum bridges on Long Island, New York. *Practice Periodical on Structural Design and Construction* 7, pp. 111-117. [cited at p. 4]

Hamad, A. J. (2017). Size and shape effect of specimen on the compressive strength of HPLWFC reinforced with glass fibres. *Journal of King Saud University – Engineering Sciences*, 29, pp. 373-380. [cited at p. 83]

Hanus, J. P., Ray, J. C., Bank, L. C. and Velazquez, G. I. (2006). Optimized design and testing of a prototype military bridge system for rapid in-theater construction. In: *Proceedings of the 25th Army Science Conference – Transformational Army Science and Technology, 27-30 November, Orlando*, pp. 1-8. [cited at p. 14]

Hassanieh, A., Valipour, H. R. and Bradford, M. A. (2016a). Experimental and analytical behaviour of steel-timber composite connections. *Construction and Building Materials*, 118, pp. 63-75, doi: 10.1016/j.conbuildmat.2016.05.052. [cited at p. 1, 27]

Hassanieh, A., Valipour, H. R. and Bradford, M. A. (2016b). Experimental and numerical study of steel-timber composite (STC) beams. *Journal of Constructional Steel Research*, 122, pp. 367-378, doi: 10.1016/j.jcsr.2016.04.005. [cited at p. 1, 31]

Hawkins, N. M. (1987). Strength in shear and tension of cast-in-place anchor bolts. In: *Anchorage to Concrete*, Special Publication 103, Detroit: American Concrete Institute, pp. 233-256. [cited at p. 26]

Hechler, O., Berthellemy, J., Lorenc, W., Seidl, G. and Viefhues, E. (2011). Continuous shear connectors in bridge construction, In: R. T. Leon; T. Perea; G. A. Rassati and J. Lange, eds., *Composite Construction in Steel and Concrete VI, Proceedings of the sixth International Conference on Composite Construction in Steel and Concrete, July 20-24, 2008*, Devil's Thumb Ranch: ASCE, pp. 78-91, doi: 10.1061/41142(396). [cited at p. 24]

BIBLIOGRAPHY

Hicks, S. (2008). *EN 1994 - Eurocode 4: Design of composite steel and concrete structures*. Dissemination of information workshop, Brussels, 18-20 February 2008. [cited at p. 13, 88, 97]

Hicks, S. J. and Smith, A. L. (2014). Stud shear connectors in composite beams that support slab with profiled steel sheeting. *Structural Engineering International*, 2, pp. 246-253. [cited at p. 91, 93]

Hillerborg, A., Modéer, M. and Petersson, P.-E. (1976). Analysis of crack formation and crack growth in concrete by means of fracture mechanics and finite elements. *Cement and Concrete Research*, 6, pp. 773-782. [cited at p. 62]

Holomek, J., Bajera, M. and Vilda, M. (2016). Test arrangement of smallscale shear tests of composite slabs. *Procedia Engineering*, 161, pp. 716-721. [cited at p. 13]

Hordijk, D. A. (1991). *Local approach to fatigue of concrete*. PhD Thesis, Delft University of Technology, Delft. [cited at p. 62]

Hu, H. T., Huang, C. S., Wu, M. H. and Wu, Y. M. (2003). Nonlinear analysis of axially loaded concrete-filled tube columns with confinement effect. *Journal of Structural Engineering*, 129(10), pp. 1322-1329. [cited at p. 13]

Ismail, R. E. S., El-Katt, M. T. H., Zien Eldin, H. A. and Kasem, Y. M. Y. (2012). Analytical modeling of nonlinear behavior of composite stub-girders. *International Journal of Steel Structures*, 12(4), pp. 599-613, doi: 10.1007/s13296-012-4007-1. [cited at p. 31]

Jabłoński, Ł. and Halicka, A. (2019). Influence of surface based cohesive parameters on static performance of concrete composite T-shaped beams. *Matec Web of Conferences*, 262, article 08003, doi: 10.1051/matecconf/201926208003. [cited at p. 123]

Jankowiak, I., Kąkol, W. and Madaj, A. (2005). Identyfikacja modelu numerycznego ciągłej belki zespolonej na podstawie badań laboratoryjnych. In: T. Biliński, ed., *VII Konferencja Naukowa Konstrukcje Zespolone, Zielona Góra 15-16 czerwca 2005*, Oficyna Wydawnicza Uniwersytetu Zielonogórskiego: Zielona Góra, pp. 163-178. [in Polish] [cited at p. 1]

Jankowiak, I. (2012). Analysis of RC beams strengthened by CFRP strips – Experimental and FEA study. *Archives of Civil and Mechanical Engineering*, 12, pp. 376-388, doi: 10.1016/j.acme.2012.06.010. [cited at p. 62]

Jankowiak, I. and Madaj, A. (2014). Load carrying capacity of RC beams strengthened by pre-tensioned CFRP strips. In: T. Łodygowski, J. Rakowski and P. Litewka, eds., *Recent advances in computational mechanics: Proceedings of the 20th International Conference on Computer Methods in Mechanics (CMM 2013), Poznań, 27-31 August, 2013*, CRC Press: Leiden, pp. 95-101. [cited at p. 62]

BIBLIOGRAPHY

Jankowiak, I. and Madaj, A. (2015). Analiza numeryczna wzmocnienia taśmami CFRP betonu w strefie rozciąganej stalowo-betonowej belki zespolonej. *Inżynieria i Budownictwo*, 4, pp. 208-212. [in Polish] [cited at p. 62]

Jankowiak, I. and Madaj, A. (2017). Numerical analysis of effectiveness of strengthening concrete slab in tension of the steel-concrete composite beam using pretensioned CFRP strips. *Civil and Environmental Engineering Reports*, 27(4), pp. 5-15, doi: 10.1515/ceer-2017-0046. [cited at p. 78]

Jankowiak, I. (2018). Case study of flexure and shear strengthening of RC beams by CFRP using FEA. *AIP Conference Proceedings*, 1922, article 130004, doi: 10.1063/1.5019134. [cited at p. 62]

Jankowiak, T. (2011). *Kryteria zniszczenia betonu poddanego obciążeniom quasi-statycznym i dynamicznym* [Failure criteria for concrete under quasi-static and dynamic loadings]. Poznań: Wydawnictwo Politechniki Poznańskiej, 137. [in Polish] [cited at p. 123, 128]

Jankowiak, T. and Łodygowski, T. (2005). Identification of parameters of concrete damage plasticity constitutive model. *Foundations of Civil and Environmental Engineering*, 6, pp. 53-69. [cited at p. 59]

Jankowiak, T. and Łodygowski, T. (2010). Quasi-static failure criteria for concrete. *Archives of Civil Engineering*, 56(2), pp. 53-69, doi: 10.2478/v.10169-010-0007-8. [cited at p. 59]

Jarek, B. and Radoń, M. (2009). The slip in bending composite steel-concrete beams on the base of experimental researches. In: L. Szopa, M. Pantak and B. Jarek, eds., *Composite Bridge Structures*, Kraków: Cracow University of Technology, pp. 199-208. [in Polish] [cited at p. 35]

Jasiczak, J. and Hajkowski, M. (2008). Corrosion susceptible elevations made with aluminium plates working in treatment's plant environment. *Ochrona Przed Korozją*, 5s/A, pp. 79-85. [in Polish] [cited at p. 9]

Jianxia, S. (2012). Durability design of concrete hydropower structures. *Comprehensive Renewable Energy*, 6, pp. 377-403, doi: 10.1016/B978-0-08-087872-0.00619-3. [cited at p. 79]

Johnson, R. P. and Yuan, H. (1998). Models and design rules for stud shear connectors in troughs of profiled sheeting. *Proceedings of the Institution of Civil Engineers - Structures and Buildings*, 128, pp. 252-263, doi: 10.1680/istbu.1998.30459. [cited at p. 13]

Johnson, R. P. (2012). *Designers' guide to Eurocode 4: Design of composite steel and concrete structures, EN 1994-1-1*. London: ICE Publishing. [cited at p. 49, 90, 92]

BIBLIOGRAPHY

Johnson, R. P. and Shepherd, A. J. (2013). Resistance to longitudinal shear of composite slabs with longitudinal reinforcement. *Journal of Constructional Steel Research*, 82, pp. 190-194, doi: 10.1016/j.jcsr.2012.12.005. [cited at p. 101]

Jurczak, W. (2010). Problemy i perspektywy stopów aluminium w zastosowaniu na konstrukcje morskie [Problems and perspectives for aluminum alloys in marine structures]. *Zeszyty Naukowe Akademii Marynarki Wojennej*, 4(183), pp. 89-106. [in Polish] [cited at p. 10]

Kania, P. (2008). Connection of steel-concrete composite beam made by shot fired studs. In: T. Biliński, ed., *Composite structures*, Zielona Góra: University of Zielona Góra Publisher, pp. 159-171. [in Polish] [cited at p. 101]

Kamyk, Z. and Szelka, J. (2014). Military composite bridges. In: T. Biliński, J. Korentz, eds., *X Conference Composite Structures*, Zielona Góra: University of Zielona Góra Publisher, pp. 245-254. [in Polish] [cited at p. 14]

Keipour, N. (2018). *Assessment of beam-to-column joint behaviour in steel-timber composite systems*. PhD. University of New South Wales. [cited at p. 27]

Khorsandnia, N., Valipour, H., Foster, S. and Crews, K. (2014). A force-based frame finite element formulation for an analysis of two-and three-layered composite beams with material non-linearity. *International Journal of Non-Linear Mechanics*, 62, pp. 12-22, doi: 10.1016/j.ijnonlinmec.2014.02.001. [cited at p. 31]

Kim, B., Wrigth, H. D. and Cairns, R. (2001). The behaviour of through-deck welded shear connectors: an experimental and numerical study. *Journal of Constructional Steel Research*, 57, pp. 1359-1380. [cited at p. 90, 97]

Kisała, D. and Furtak, K. (2016). The assessment of the slip influence on the deflection of the steel plate-concrete composite beams. *Archives of Civil Engineering*, 62(2), pp. 59-76, 10.1515/ace-2015-0065. [cited at p. 35]

Kmiecik, P. and Kamiński, M. (2011). Modelling of reinforced concrete structures and composite structures with concrete strength degradation taken into consideration. *Archives of Civil and Mechanical Engineering*, 11(3), pp. 623-636. [cited at p. 59-63, 72-73, 120]

Knitter-Piątkowska, A. and Guminiak, M. (2016). Defect detection in plate structures using wavelet transformation. *Engineering Transactions*, 64(2), pp. 139-156. [cited at p. 127]

Knitter-Piątkowska, A. and Guminiak, M. (2020). Application of 1-D and 2-D discrete wavelet transform to crack identification in statically and dynamically loaded plates. *Engineering Transactions*, 68(2), pp. 137-157, doi: 10.24423/EngTrans.1115.20200304. [cited at p. 127]

BIBLIOGRAPHY

Komorowski, M. (2017). *Manual of design and build in the STEICO system, Basic information, Building physics, Guidelines*. Warsaw: Forester Communication. [in Polish] [cited at p. 14]

Kossakowski, P. (2016). Stopy aluminium jako materiał konstrukcyjny ustrojów nośnych mostów [Aluminium alloys as structural material in bridges]. *Zeszyty Naukowe Politechniki Częstochowskiej. Budownictwo*, Z. 22 (172), pp. 159-170, doi: 10.17512/znb.2016.1.15. [cited at p. 3]

Kossakowski, P., Wciślik, W. and Bakalarz, M. (2017). Selected aspects of application of aluminium alloys in building structures. *Structure and Environment*, 9(4), pp. 256-263. [cited at p. 11]

Kozma, A., Odenbreit, C., Braun, M. V., Veljkovic, M. and Nijgh, M. P. (2019). Push-out tests on demountable shear connectors of steel-concrete composite structures. *Structures*, 21, pp. 45-54, doi: 10.1016/j.istruc.2019.05.011. [cited at p. 3, 24, 27-28, 33, 94]

Kożuch, M. and Lorenc, W. (2019). Stress concentration factors of shear connection by composite dowels with MCL shape. *Archives of Civil and Mechanical Engineering*, 19(1), pp. 32-46, doi: 10.1016/j.acme.2018.08.006. [cited at p. 24]

Köster & Co. (2005). KÖCO SD, Shear connector, Data sheet. [cited at p. 30, 45, 49]

Kwaśniewski, L., Szmigiera, E. and Siennicki, M. (2011) Finite element modeling of composite concrete-steel columns. *Archives of Civil Engineering*, 57(4), pp. 373-388. [cited at p. 67]

Kwiatkowski, T. (2012). Aluminium w nowoczesnych konstrukcjach budowlanych [Aluminum in the modern building constructions]. *Zeszyty Naukowe Politechniki Częstochowskiej. Budownictwo*, Z. 18 (168), pp. 108-115. [cited at p. 3]

Kwon, G., Engelhardt, M. D. and Klinger, R. E. (2010). Behavior of post-installed shear connectors under static and fatigue loading. *Journal of Constructional Steel Research*, 66, pp. 532-541. [cited at p. 27, 49]

Kucharczuk, W. and Labocha, S. (2013). Analysis of the resistance and the stiffness of the composite beams, depending on the degree of shear connection. *Journal of Civil Engineering, Environment and Architecture*, 60(2), pp. 175-188, doi: 10.7862/rb.2013.24. [cited at p. 23]

Kuczma, M. and Kuczma, B. (2006). Partially connected composite beams. In: *Proceedings in Applied Mathematics and Mechanics*, 6, pp. 233-234, doi: 10.1002/pamm.200610097. [cited at p. 23]

BIBLIOGRAPHY

Kuczma, M. and Kuczma, B. (2011). Steel-concrete composite beams with elasto-plastic connection. In: K. Wilmański, B. Michalak and J. Jędrysiak, eds., *Mathematical methods in continuum mechanics*, Lodz: Technical University of Lodz Press, pp. 451-464. [cited at p. 23]

Kuczma, M. and Kuczma, B. (2016). Composite steel-concrete beams with partial interaction: experimental, theory, simulation. In: J. T. Katsikadelis, G. E. Stavroulakis, eds., *Recent advances in Mechanics. Book of abstracts, 9th German-Greek-Polish Symposium, Orthodox Academy of Crete, Kolympari, Greece, September 4-9*, Chania: Technical University of Crete, pp. 57-58. [e-book] [cited at p. 23]

Kyvelou, P., Gardner, L. and Nethercot, D. A. (2018). Finite element modelling of composite cold-formed steel flooring systems. *Engineering Structures*, 158, pp. 28-42. [cited at p. 31, 123]

Lacki, P. and Derlatka, A. (2017). Strength evaluation of beam made of the aluminum 6061-T6 and titanium grade 5 alloys sheets joined by RFSSW and RSW. *Composite Structures*, 159, pp. 491-497, doi: 10.1016/j.compstruct.2016.10.003. [cited at p. 10]

Lacki, P., Kasza, P. and Derlatka, A. (2017). Numerical analysis of prefabricated steel-concrete composite floor in typical Lipsk building. *Civil and Environmental Engineering Reports*, 27(4), pp. 43-53, doi: 10.1515/ceer-2017-0049. [cited at p. 10]

Lam, D. and Dai, X. (2013). Demountable shear connectors for sustainable composite construction. *The World Congress on Advances in structural engineering and mechanics (ASEM13), Jeju, Korea, 8-12 September 2013*, pp. 93-100. [cited at p. 24]

Lam, D., Dai, X., Ashour, A. and Rehman, N. (2017). Recent research on composite beams with demountable shear connectors. *Steel Construction*, 10(2), pp. 125-134, doi: 10.1002/stco.201710016. [cited at p. 24-25, 28]

Lawson, R. M., Popo-Ola, S. O. and Bode, H. (2001). *Design tables and graphs for composite beams to Eurocode 4*. Brussels: European Convention for Constructional Steelwork, Technical Committee 11, Composite Structures, No 113. [cited at p. 13]

Lee, J. and Fenves, G. L. (1998). Plastic-damage model for cyclic loading of concrete structures. *Journal of Engineering Mechanics*, 124, pp. 892-900. [cited at p. 59]

Lee, P.-G., Shim, C.-S. and Chang, S.-P. (2005). Static and fatigue behavior of large stud shear connectors for steel-concrete composite bridges. *Journal Construction Steel Research*, 61, pp. 1270-1285, doi: 10.1016/j.jcsr.2005.01.007. [cited at p. 13]

Lee, S.-S. M. and Bradford, M. A. (2013). Sustainable composite beam behaviour with deconstructable bolted shear connectors. *The World Congress on Advances in structural engineering and mechanics (ASEM13), Jeju, Korea, 8-12 September 2013*, pp. 3188-3199. [cited at p. 23, 25, 27]

BIBLIOGRAPHY

Leskelä, M. V. (2017). *Shear connections in composite flexural members of steel and concrete*. Mem Martins: European Convention for Constructional Steelwork, Technical Committee 11, Composite Structures, No 138. [cited at p. 23, 33]

Li, A. and Cederwall, K. (1996). Push-out tests on studs in high strength and normal strength concrete. *Journal Construction Steel Research*, 36(1), pp. 15-29. [cited at p. 33]

Liu, X., Bradford, M., Chen, Q.-J. and Ban, H. (2016). Finite element modelling of steel-concrete composite beams with high-strength friction-grip bolt shear connectors. *Finite Elements in Analysis and Design*, 108, pp. 54-65, doi: 10.1016/j.finel.2015.09.004. [cited at p. 25]

Liu, X., Bradford, M. A. and Ataei, A. (2017). Flexural performance of innovative sustainable composite steel-concrete beams. *Engineering Structures*, 130, pp. 282-296, doi: 10.1016/j.engstruct.2016.10.009. [cited at p. 25, 28]

Lorenc, W., Kubica, E. and Kożuch, M. (2010). Testing procedures in evaluation of resistance of innovative shear connection with composite dowels. *Archives of Civil and Mechanical Engineering*, 10(3), pp. 51-63. [cited at p. 90]

Lorenc, W., Kożuch, M. and Rowiński, S. (2014a). The behaviour of puzzle-shaped composite dowels – Part I: Experimental study. *Journal of Constructional Steel Research*, 101, pp. 482-499, doi: 10.1016/j.jcsr.2014.05.013. [cited at p. 24]

Lorenc, W., Kożuch, M. and Rowiński, S. (2014b). The behaviour of puzzle-shaped composite dowels – Part II: Theoretical investigation. *Journal of Constructional Steel Research*, 101, pp. 500-518, doi: 10.1016/j.jcsr.2014.05.012. [cited at p. 24]

Lubliner, J., Oliver, J., Oller, S., and Oñate, E. (1989). A plastic-damage model for concrete. *International Journal of Solids Structures*, 25, pp. 229-326. [cited at p. 59]

Łukaszewska E., Johnsson H. and Fragiacomo M. (2008). Performance of connections for prefabricated timber-concrete composite floors. *Materials and Structures*, 41, pp. 1533-1550, doi: 10.1617/s11527-007-9346-6. [cited at p. 85]

Łukaszewska, E. (2009). *Development of prefabricated timber-concrete composite floors*. PhD. Luleå University of Technology. [cited at p. 1, 31]

Major, M. and Major, I. (2015). Konstrukcje zespolone w budownictwie zrównoważonym. *Budownictwo o Zoptymalizowanym Potencjale Energetycznym*, 2(16), pp. 51-56. [in Polish] [cited at p. 30]

BIBLIOGRAPHY

Mandara, A. and Mazzolani, F. M. (1997). Plastic design of aluminium-concrete composite sections: a simplified method. In: M. W. Braestrup, ed., *Proceedings of the International Conference on Composite Construction – Conventional and Innovativ*e, *Innsbruck, Austria, 16-18 September 1997*, Zurich: International Association for Bridge and Structural Engineering, pp. 349-354. [cited at p. 13, 40]

Marcinowski, J. (1997). Large deflections of shells subjected to an external load and temperature changes. *International Journal of Solids and Structures*, 34(6), pp. 755-768. [cited at p. 14]

Marcinowski, J. (2018). Stresses in a layered, composite structure fabricated from materials of different thermal expansions [in Polish]. *Materiały Budowlane*, 4, pp. 107-109. [cited at p. 14]

Martin, O. (2010). *Comparison of different constitutive models for concrete in ABAQUS/Explicit for missile impact analyses*. European Commission, Joint Research Centre, Institute for Energy. [cited at p. 60]

Maryland Department of Transportation (2012). *Management plan for historical highway bridges*. Prepared by: KCI Technologies, Inc. & TranSystems. [cited at p. 6-7]

Marzec, I. (2008). *Zastosowanie modelu sprężysto-plastycznego betonu z degradacją sztywności i nielokalnym osłabieniem do modelowania elementów betonowych cyklicznie obciążonych*. PhD. Gdańsk University of Technology. [in Polish] [cited at p. 58]

Marzec, I. and Tejchman, J. (2013). Computational modelling of concrete behaviour under static and dynamic conditions. *Bulletin of the Polish Academy of Sciences. Technical Sciences*, 61(1), pp. 85-96. [cited at p. 58]

Mazzolani, F. M. and Mandara, A. (2002). Modern trends in the use of special metals for the improvement of historical and monumental structures. *Engineering Structures*, 24, pp. 843-856. [cited at p. 14]

Mazzolani, F. M. (2003). *Aluminium Structural Design*. Wien: Springer-Verlag GmbH. [cited at p. 10, 13]

Mazzolani, F. M. (2006). Structural applications of aluminium in civil engineering. *Structural Engineering International*, 16(4), pp. 280-285, doi: 10.2749/101686606778995128. [cited at p. 9]

Mazzolani, F. M. (2012). 3D aluminium structures. *Thin-Walled Structures*, 61, pp. 258-266. [cited at p. 3]

Mindlin, H. L. and Errera, S. J. (1959). *Test of a composite aluminium and concrete highway bridge*. Report 275.1, Fritz Engineering Laboratory, Lehigh University. [cited at p. 4, 9, 15]

BIBLIOGRAPHY

Mirza, O. (2008). *Behaviour and design of headed stud shear connectors in composite steel-concrete beams*. PhD. University of Western Sydney. [cited at p. 88]

Mirza, O. and Uy, B. (2009). Effects of steel fibre reinforcement on the behaviour of headed stud shear connectors for composite steel-concrete beams. *Advanced Steel Construction*, 5(1), pp. 72-95. [cited at p. 88]

Mirza, O., Uy, B. and Krezo, S. (2011). Experimental studies on the behaviour of headed stud shear connectors for composite steel-concrete beams under elevated temperatures. In: *7th International Conference on Steel & Aluminium Structures 13-15 July 2011, Kuching, Sarawak, Malaysia*. [cited at p. 88]

Moynihan, M. C. and Allwood, J. M. (2014). Viability and performance of demountable composite connectors. *Journal of Constructional Steel Research*, 99, pp. 47-56, doi: 10.1016/j.jcsr.2014.03.008. [cited at p. 25]

Mromliński, R. (1975). *Aluminium structures*. 3rd ed. Warszawa: Arkady, 392. [cited at p. 13]

Murray, Y. D., Abu-Odeh, A. and Bligh, R. (2007). *Evaluation of LS-DYNA concrete material model 159*. Report No. FHWA-HRT-05-063, APTEK and Texas Transportation Institute, 190. [cited at p. 106]

Nawrot, J. (2012). Analiza porównawcza nośności połączenia ścinanego zespolonej belki stalowo-betonowej dla dwóch wybranych typów łączników [Comparative analysis of the shear connection capacity of steel-concrete composite beam for two types of connectors]. *Zeszyty Naukowe Politechniki Częstochowskiej. Budownictwo*, Z. 18(168), pp. 182-187. [in Polish] [cited at p. 23]

Neville, A. M. and Brooks, J. J. (2010). *Concrete Technology*. Harlow: Pearson Education, Prentice Hall, 464. [cited at p. 83]

Nguyen, H. T. and Kim, S. E. (2009). Finite element modeling of push-out tests for large stud shear connectors. *Journal of Constructional Steel Research*, 65, pp. 1909-1920, doi: 10.1016/j.jcsr.2009.06.010. [cited at p. 123]

Nie, J. and Cai, C. S. (2003). Steel-concrete composite beams considering shear slip effects. *Journal of Structural Engineering*, 129, 4, pp. 495-505, doi: 10.1061/(ASCE)0733-9445(2003)129:4(495). [cited at p. 23, 35-38]

Nie, J., Cai, C. S. and Wang, T. (2005). Stiffness and capacity of steel-concrete composite beams with profiled sheeting. *Engineering Structures*, 27, pp. 1074-1085, doi.: 10.1016/j.engstruct.2005.02.016. [cited at p. 23, 34-35, 38, 101]

BIBLIOGRAPHY

Niedośpiał, M., Grzeszykowski, B. and Szmigiera, E. (2018). *Przewodnik projektanta. Prawa autorskie projektanta. Projektowanie akustyki sal sportowych. Projektowanie stropów zespolonych na blachach fałdowych według Eurokodu 4*. Warszawa: Wydawnictwo Polskiej Izby Inżynierów Budownictwa, 64. [in Polish] [cited at p. 96]

Nijgh, M., Gîrbacea, A. and Veljković, M. (2018). Optimization of a composite (steel-concrete) floor system for fast execution and easy demolition. In: *14th International Scientific Conference on Planning, Design, Construction and Building Renewal Conference, iNDiS, Novi Sad, 21-23 November 2018*, pp. 45-52. [cited at p. 23]

Okura, I. (2003). Application of aluminium alloys to bridges and joining technologies. *Welding International*, 17(10), pp. 781-785. [cited at p. 11-12]

Oliveira, W. L. A., De Nardin, S., El Debs, A. L. H. C. and El Debs, M. K. (2010). Evaluation of passive confinement in CFT columns. *Journal of Constructional Steel Research*, 66, pp. 487-495. [cited at p. 13]

Pashan, A. (2006). *Behaviour of channel shear connectors: push-out tests*. Master's Thesis. University of Saskatchewan. [cited at p. 23].

Pathirana, S. W., Uy, B., Mirza, O. and Zhu, X. (2016). Bolted and welded connectors for rehabilitation of composite beams. *Journal of Constructional Steel Research*, 125, pp. 61-73. [cited at p. 23]

Patrick, M. (2000). Experimental investigation and design of longitudinal shear reinforcement in composite edge beams. *Progress in Structural Engineering and Materials* 2, pp. 196-217. [cited at p. 101]

Patrick, M. (2004). *Composite beam shear connection, Design and detailing practices for Australian steel decks*. University of Western Sydney, Report No. CCTR-CBSC-001-04. [cited at p. 101, 126]

Pavlović, M., Marković, Z., Veljković, M. and Budevac, D. (2013a). Bolted shear connectors vs. headed studs behaviour in push-out tests. *Journal of Constructional Steel Research*, 88, pp. 134-149, doi: 10.1016/j.jcsr.2013.05.003. [cited at p. 26, 28, 33, 93]

Pavlović, M., Spremić, M., Marković, Z. and Veljković, M. (2013b). Headed shear studs versus high-strength bolts in prefabricated composite decks. In: M. Bradford and B. Uy, eds., *Composite Construction in Steel and Concrete VII, Proceedings of 2013 International Conference on Composite Construction in Steel and Concrete 2013, July 28-31, 2013, North Queensland, Australia*, Reston: American Society of Civil Engineers, pp. 687-702, doi: 10.1061/9780784479735.052. [cited at p. 26]

BIBLIOGRAPHY

Pavlović, M., Spremić, M., Marković, Z., Buđevac, D. and Veljković, M. (2014). Bolted shear connectors vs. headed studs behaviour in push-out tests. *Journal of Applied Engineering Science*, 12(279), pp. 75-80. doi: 10.5937/jaes12-5676. [cited at p. 30]

Pavlović, M. and Veljković, M. (2017). FE validation of push-out tests using bolts as shear connectors. *Steel Construction*, 10(2), doi: 10.1002/stco.201710017. [cited at p. 30]

Pełka-Sawenko, A., Wróblewski, T. and Szumigała, M. (2016). Validation of computational models of steel-concrete composite beams. *Engineering Transactions*, 64(1), pp. 53-67. [cited at p. 67]

Pengzhen, L. (2014). Analysis model of slip for composite box girders. *Structural Engineering International*, 24(4), pp. 474-481. [cited at p. 35]

Pitts, J. W. (1967). *Final report on corrosion of aluminum embedded in concrete*. U.S. Department of Commerce, National Bureau of Standards. [cited at p. 12]

Pliny the Elder (77–79), *Natural History*. [in Latin] [cited at p. 3]

Płoszewski, K. (1998). Fluorine compounds in the atmospheric air. *Aura* 5, pp. 12-15. [in Polish] [cited at p. 2]

Polus, Ł., Chybiński, M. and Szumigała, M. (2018). Bending resistance of metal-concrete composite beams under standard fire conditions. *Przegląd Budowlany*, 7-8, pp. 128-132. [in Polish] [cited at p. 11]

Polus, Ł. and Szumigała, M. (2014a). *Connector for composite structures*, Patent, Exclusive right no. 232822, Application no. 406833, Application Date 13 January 2014, Patent published 31 July 2019, Warsaw: Polish Patent Office. [cited at p. 29]

Polus, Ł. and Szumigała, M. (2014b). A numerical analysis of the resistance and stiffness of the aluminium and concrete composite beam. *Civil and Environmental Engineering Reports*, 15(4), pp. 99-112. [cited at p. 13]

Polus, Ł. and Szumigała, M. (2014c). Analiza numeryczna nośności i sztywności belki zespolonej aluminiowo-betonowej. In: T. Biliński and J. Korentz, eds., *Jubileuszowa X Konferencja Naukowa Konstrukcje zespolone, Zielona Góra, 26-27 czerwca 2014*, Zielona Góra: Oficyna Wydawnicza Uniwersytetu Zielonogórskiego, pp. 393-405. [in Polish] [cited at p. 13]

Polus, Ł. and Szumigała, M. (2014d). *Connector for timber-concrete composite structures*, Patent, Exclusive right no. 233174, Application no. 406834, Application Date 13 January 2014, Patent published 30 September 2019, Warsaw: Polish Patent Office. [cited at p. 91]

BIBLIOGRAPHY

Polus, Ł. and Szumigała, M. (2016). Tests of shear connectors used in aluminium-concrete composite structures. In: M. A. Giżejowski, A. Kozłowski, J. Marcinowski and J. Ziółko, eds., *Recent Progress in Steel and Composite Structures: Proceedings of the XIII International Conference on Metal Structures (ICMS2016), Zielona Góra, Poland, 15-17 June 2016*, Boca Raton:CRC Press, pp. 113-136. [cited at p. 29]

Polus, Ł. and Szumigała, M. (2017a). Badania belek zespolonych aluminiowo-betonowych. In: T. Biliński and J. Korentz, eds., *XI Konferencja Naukowa Konstrukcje zespolone, Zielona Góra, 29-30 czerwca 2017*, Zielona Góra: Oficyna Wydawnicza Uniwersytetu Zielonogórskiego, pp. 99-100. [in Polish] [cited at p. 57, 81]

Polus, Ł. and Szumigała, M. (2017b). Wpływ zespolenia na nośność i sztywność belki metalowej współpracującej z płytą betonową. *Inżynieria i Budownictwo*, 6, pp. 320-324. [in Polish] [cited at p. 10]

Polus, Ł. and Szumigała, M. (2019a). An experimental and numerical study of aluminium-concrete joints and composite beams. *Archives of Civil and Mechanical Engineering*, 19(2), pp. 375-390, doi: 10.1016/j.acme.2018.11.007. [cited at p. 1, 31, 57, 63, 70, 72-77, 79, 81-82, 84, 102]

Polus, Ł. and Szumigała, M. (2019b). Theoretical and numerical analyses of an aluminium-concrete composite beam with channel shear connectors. *Engineering Transactions*, 67(4), pp. 535-556, doi: 10.24423/EngTrans.984.20190802. [cited at p. 58, 60, 63-66, 81, 105-106]

Polus, Ł. and Szumigała, M. (2019c). Laboratory tests vs. FE analysis of concrete cylinders subjected to compression. *AIP Conference Proceedings*, 2078, article number 020089, doi: 10.1063/1.5092092. [cited at p. 31]

Polus, Ł. and Szumigała, M. (2019d). Finite element modelling of the connection for timber-concrete composite beams. *IOP Conference Series: Materials Science and Engineering*, 471, article 052081, doi: 10.1088/1757-899X/471/5/052081. [cited at p. 31]

Pozorska J. and Pozorski Z. (2018). Application of the wavelet transform and Lipschitz exponent for the evaluation of sandwich panel deformations at the support. In: *23rd International Conference on Methods and Models in Automation and Robotics, MMAR 2018, Miedzyzdroje, Poland, August 27-30, 2018*, Institute of Electrical and Electronics Engineers, pp. 177-181, doi: 10.1109/MMAR.2018.8485985. [cited at p. 128]

Puchalska, D. and Kuczma, M. (2017). Shrinkage and creep of concrete according to standards, a comparative analysis, part 1. *Builder*, 1, pp. 69-71. [in Polish] [cited at p. 80]

Pyrak, S. (2012). *Konstrukcje budowlane 5. Konstrukcje z betonu*. Warszawa: WSiP, 296. [in Polish] [cited at p. 73]

BIBLIOGRAPHY

Queiroza, F. D., Vellascob, P. C. G. S. and Nethercot, D. A. (2007). Finite element modelling of composite beams with full and partial shear connection. *Journal of Constructional Steel Research*, 63, pp. 505-521, doi: 10.1016/j.jcsr.2006.06.003. [cited at p. 31]

Rackham, J. W., Couchman, G. H. and Hicks, S. J. (2009). *Composite slabs and beams using steel decking: Best practice for design and construction*. The Steel Construction Institute and The Metal Cladding & Roofing Manufacturers Association. [cited at p. 97]

Raczkiewicz, W. (2012). Skurcz betonu – cechy istotne ze względu na projektowanie konstrukcji z betonu. *Przegląd Budowlany*, 2, pp. 43-46. [in Polish] [cited at p. 79]

Rajpolt, B. and Tomaszewska, B. (2011). *Fluorine contamination in soil and aquatic environment on the example of Aluminium Smelter in Skawina*. Kraków: The Mineral and Energy Economy Research Institute of the Polish Academy of Sciences Publisher. [in Polish] [cited at p. 2]

Ramachandran, K. M. and Tsokos, C. P. (2015). *Mathematical statistics with applications in R*. Academic Press, Elsevier, doi: 10.1016/C2012-0-07341-3. [cited at p. 81]

Ranzi, G., Bradford, M. A., Ansourian, P., Filinov, A., Rasmmussen, K. J. R., Hogan, T. J. and Uy, B. (2009). Full-scale tests on composite steel-concrete beams with steel trapezoidal decking. *Journal of Constructional Steel Research*, 65, pp. 1490-1506, doi: 10.1016/j.jcsr.2009.03.006. [cited at p. 13]

Rasheed, H. A., Abdalla, J., Hawileh, R. and Al-Tamimi, A. K. (2017). Flexural behavior of reinforced concrete beams strengthened with externally bonded aluminum alloy plates. *Engineering Structures*, 147, pp. 473-485, doi: 10.1016/j.engstruct.2017.05.067. [cited at p. 14]

Rehman, N., Lam, D., Dai, X. and Ashour, A. F. (2016). Experimental study on demountable shear connectors in composite slabs with profiled decking. *Journal of Constructional Steel Research*, 122, pp. 178-89. doi: 10.1016/j.jcsr.2016.03.021. [cited at p. 34, 101]

Rehman, N., Lam, D., Dai, X. and Ashour, A. F. (2018). Testing of composite beam with demountable shear connectors. *Proceedings of the Institution of Civil Engineers, Structures and Buildings*, 171(SB1), pp. 3-16. doi: 10.1680/jstbu.16.00172. [cited at p. 24-25]

Rodacki, K. (2017). The load-bearing capacity of timber-glass composite I-beams made with polyurethane adhesives. *Civil and Environmental Engineering Reports*, 27(4), pp. 105-120, doi: 10.1515/ceer-2017-0054. [cited at p. 1]

Roik, K. and Hanswille, G. (1987). Zur Dauerfestigkeit von Kopfbolzendübeln bei Verbundträgern. *Bauingenieur*, 62, pp. 273-285. [in German] [cited at p. 90]

BIBLIOGRAPHY

Rom, S. and Agerskov, H. (2014). Fatigue in aluminum highway bridges under random loading. *International Journal of Applied Science and Technology*, 4(6), pp. 95-107. [cited at p. 11]

Roylance, D. (2001). *Stress-strain curves*. Cambridge: Massachusetts Institute of Technology, 14. [cited at p. 81]

Rzeszut, K. and Garstecki, A. (2011). Thin-walled structures with slotted connections stability problems. *Thin-Walled Structures*, 49, pp. 674-681, doi: 10.1016/j.tws.2010.09.015. [cited at p. 94]

Rzeszut, K., Szumigała, M. and Polus, Ł. (2015). Selected aspects of the proper application of structural materials in terms of corrosion. *Technical Transactions*, 1-B(11), pp. 97-105. [cited at p. 15]

Saleh, S. M. (2014). *Behavior of timber-aluminum composite beams under static and impact loads*. PhD. University of Basrah. [cited at p. 14]

Saleh, S. M. and Jasim, N. A. (2014a). Structural behavior of timber aluminum composite beams under impact loads. *International Journal of Scientific and Engineering Research*, 5(10), pp. 865-873. [cited at p. 14]

Saleh, S. M. and Jasim, N. A. (2014b). Structural behavior of timber aluminum composite beams under static loads. *International Journal of Engineering Research and Technology*, 3(10), pp. 1166-1173. [cited at p. 14]

Sarri, A. (2019). *Assessment of steel-concrete composite shear connector system with resin injected bolts*. Master's Thesis. Delft University of Technology. [cited at p. 27]

Scotta, R., Marchi, L., Trutalli, D. and Pozza, L. (2017). Engineered aluminium beams for anchoring timber buildings to foundation. *Structural Engineering International*, 2, pp. 158-164. [cited at p. 14]

Scotta, R., Trutalli, D., Marchi, L. and Pozza, L. (2018). On the anchoring of timber walls to foundations: available strategies to prevent wood deterioration and on-site installation problems, *Procedia Structural Integrity*, 11, pp. 282-289. [cited at p. 14]

Seidl, G. (2009). *Behaviour and load bearing capacity of composite dowels in steel-concrete composite girders*. PhD. Wrocław University of Science and Technology. [cited at p. 24]

Seidl, G., Viefhues, E., Berthellemy, J., Mangerig, I., Wagner, R., Lorenc, W., Kozuch, M., Franssen, J.-M., Janssen, D., Ikäheimonen, J., Lundmark, R., Hechler, O. and Popa, N. (2013). *Prefabricated enduring composite beams based on innovative shear transmission (Preco-Beam)*. Brussels: European Commission, 212. [cited at p. 24]

BIBLIOGRAPHY

Siekierski, W. (2014). Structural aspects of railway truss bridges affecting transverse shear forces in steel-concrete composite decks. *Civil and Environmental Engineering Reports*, 15(4), pp. 113-126, doi: 10.1515/ceer-2014-0038. [cited at p. 23]

Siess, C. P., Viest, I. M. and Newmark, N. M. (1952). Studies of slab and beam highway bridges, Part III: Small scale tests of shear connectors and composite T-beams. *University of Illinois Bulletin*, 396. [cited at p. 17]

Siwowski, T. (2005). Aluminium road bridges – past, present and future. *Drogi i mosty*, 1, pp. 39-74. [in Polish] [cited at p. 1, 6-7, 9, 29]

Siwowski, T. (2006). Aluminium bridges – past, present and future. *Structural Engineering International*, 16(4), pp. 286-293. [cited at p. 4, 6-7]

Siwowski, T. (2009a). Structural behaviour of aluminium bridge deck panels. *Engineering Structures*, 31, pp. 1349-1353. [cited at p. 9]

Siwowski, T. (2009b). FEM modelling and analysis of a certain aluminium bridge deck panel. *Archives of Civil Engineering*, 55(3), pp. 347-365. [cited at p. 9]

Skejić, D., Boko, I. and Torić, N. (2015). Aluminium as a material for modern structures. *Građevinar*, 11, pp. 1075-1085, doi: 10.14256/JCE.1395.2015. [cited at p. 10]

Skejić, D., Ćurković, I. and Rukavina, M. J. (2015). Behaviour of aluminium structures in fire. A review. In: F. Wald et al., eds., *Applications of Structural Fire Engineering, 15-16 October 2015, Dubrovnik, Croatia*, doi: 10.14311/asfe.2015.047. [cited at p. 10]

Słowik, M. and Bartkowiak, M. (2015). Calculation of measurement uncertainty for stiffness modulus of asphalt mixture. *Journal of Civil Engineering and Architecture*, 9, pp. 1325-1333, doi: 10.17265/1934-7359/2015.11.007. [cited at p. 81]

Słowik, M. and Bartkowiak, M. (2016). Elementy statystycznej analizy wyników pomiarów na przykładzie badań wybranych cech mieszanek mineralno-asfaltowych. *Drogownictwo*, 7-8, pp. 247-253. [in Polish] [cited at p. 81]

Smith, A. L. and Couchman, G. H. (2010). Strength and ductility of headed stud shear connectors in profiled steel sheeting. *Journal of Constructional Steel Research*, 6, pp. 748-754. [cited at p. 13, 90]

Snilsberg, K. E., Westermann, I., Holmedal, B., Hopperstad, O. S., Langsrud, Y. and Marthinsen, K. (2010). Anisotropy of bending properties in industrial heat-treatable extruded aluminium alloys. *Materials Science Forum*, volumes 638-642, pp. 487-492. [cited at p. 43]

BIBLIOGRAPHY

Song, Y., Uy, B. and Wang, J. (2019). Numerical analysis of stainless steel-concrete composite beam-to-column joints with bolted flush endplates. *Steel and Composite Structures*, 33(1), pp. 143-162, doi: 10.12989/scs.2019.33.1.143. [cited at p. 27]

Stacey, M. (2014). *Aluminium and Durability. Towards Sustainable Cities*. Nottingham: Cwningen Press, 361. [cited at p. 3]

Stark, J. W. B. (1989). Composite steel and concrete beams with partial shear connection. *Heron*, 34(4), pp. 1-64. [cited at p. 35]

Stonehewer, J. (1962). *A study of composite concrete-aluminum beams*. Master of Engineering. McGill University, Montreal. [cited at p. 4, 6-7, 11-12, 15-17, 29, 41]

Studziński, R. and Ciesielczyk, K. (2019). Connection stiffness between thin-walled beam and sandwich panel. *Journal of Sandwich Structures & Materials*, 21(6), pp. 2042-2056, doi: 10.1177/1099636217750539. [cited at p. 31]

Stüssi, F. (1947). Zusammengesetzte vollwandtrager. *International Association for Bridge and Structural Engineers* 8, pp. 249-269. [in German] [cited at p. 17]

Subramanian, N. (2013). *Design of reinforced concrete structures*. Oxford University Press, 928. [cited at p. 83]

Suwaed, A. S. H. (2017). *Development of novel demountable shear connectors for precast steel-concrete composite bridges*. PhD. University of Warwick. [cited at p. 26-27]

Szczechowiak, E. (2007). The role of industrialization in energy saving building. *Materiały Budowlane* 9, pp. 115-119. [in Polish] [cited at p. 1]

Szczecina, M. and Winnicki, A. (2015). Calibration of the CDP model parameters in Abaqus. In: *The 2015 World Congress on Advances in Structural Engineering and Mechanics (ASEM15), Incheon, Korea, 25-29 August*. [cited at p. 118]

Szczecina, M. and Winnicki, A. (2017). Relaxation time in CDP model used for analyses of RC structures. *Procedia Engineering* 193, pp. 369-376, doi: 10.1016/j.proeng.2017.06.226. [cited at p. 59]

Szelka, J. and Kamyk, Z. (2013). Kompozytowe mosty wojskowe. *Budownictwo i Architektura*, 12(2), pp. 63-70. [in Polish] [cited at p. 14]

Szewczyk, P. and Szumigała, M. (2015). Numerical modelling of the strengthening process of steel-concrete composite beams. *Civil and Environmental Engineering Reports*, 19(4), pp. 99-110, doi: 10.1515/ceer-2015-0056. [cited at p. 72]

BIBLIOGRAPHY

Szewczyk, P. (2016). *Wzmacnianie pod obciążeniem belek zespolonych stalowo-betonowych w eksperymencie numerycznym i fizycznym*. PhD. West Pomeranian University of Technology in Szczecin. [in Polish] [cited at p. 64]

Szewczyk, P. and Szumigała, M. (2018). Static equilibrium paths of steel-concrete composite beam strengthened under load. *Civil and Environmental Engineering Reports*, 28(2), pp. 101-111, doi: 10.2478/ceer-2018-0022. [cited at p. 72]

Szewczyk, P. (2019). *Wzmacnianie pod obciążeniem stalowo-betonowych belek zespolonych w analizie numerycznej i badaniach doświadczalnych*. Szczecin: West Pomeranian University of Technology in Szczecin. [in Polish] [cited at p. 64]

Szmigiera, E. (2007). Influence of concrete and fibre concrete on the load-carrying capacity and deformability of composite steel-concrete columns. *Journal of Civil Engineering and Management*, 13(1), pp. 55-61. [cited at p. 11]

Szumigała, M., Chybiński, M. and Polus, Ł. (2017a). Preliminary analysis of the aluminium-timber composite beams. *Civil and Environmental Engineering Reports*, 27(4), pp. 131-141. [cited at p. 14]

Szumigała, M., Chybiński, M. and Polus, Ł. (2017b). Innovative composite structures. *Przegląd Budowlany*, 9, pp. 108-110. [in Polish] [cited at p. 14]

Szumigała, M., Pełka-Sawenko, A., Wróblewski, T. and Abramowicz, M. (2018). Damage detection of steel-concrete composite beam. *Civil and Environmental Engineering Reports*, 28(3), pp. 30-49. doi: 10.2478/ceer-2018-0033. [cited at p. 127]

Szumigała, M. and Polus, Ł. (2014a). Wpływ zespolenia na nagrzewanie się aluminiowej belki wg standardowej krzywej pożarowej ISO 834. In: L. Runkiewicz and T. Błaszczyński, eds., *Ekologia w budownictwie*, Wrocław: Dolnośląskie Wydawnictwo Edukacyjne, pp. 137-150. [in Polish] [cited at p. 11]

Szumigała, M. and Polus, Ł. (2014b). A numerical modelling of the load capacity of the shear connector of aluminium and concrete structures. In: T. Heizing and E. Urbańska-Galewska, eds., *II International Polish-Ukrainian Scientific-Technical Conference "Current Problems of Metal Structures"*, *Gdańsk, 27-28 November 2014*, Gdansk: Foundation for the Development of Civil Engineering, pp. 221-224. [cited at p. 67]

Szumigała, M. and Polus, Ł. (2015). Applications of aluminium and concrete composite structures. *Procedia Engineering*, 108, pp. 544-549. [cited at p. 1, 13]

Szumigała, M. and Polus, Ł. (2017). A numerical simulation of an aluminium-concrete beam. *Procedia Engineering*, 172, pp. 1086-1092. [cited at p. 19]

BIBLIOGRAPHY

Szumigała, M., Rzeszut, K. and Polus, Ł. (2017). Wybrane rodzaje konstrukcji stosowanych w budownictwie zrównoważonym. In: J. Gęsikowska and A. Mreła, eds., *Cywilizacja techniczna: nauka i technika w pierwszej dekadzie XXI wieku*, Bydgoszcz: Wydawnictwo Kujawsko-Pomorskiej Szkoły Wyższej, pp. 153-174. [in Polish] [cited at p. 1]

Szumigała, M., Szumigała, E. and Polus, Ł. (2018). Laboratory tests of new connectors for timber-concrete composite structures. *Engineering Transactions*, 66(2), pp. 161-173. [cited at p. 85, 91]

Śledziewski, K. (2016a). *Studium zachowania zespolonej belki ciągłej z uwzględnieniem zarysowania płyty*. Lublin: Lublin University of Technology, 119. [cited at p. 120]

Śledziewski, K. (2016b). Experimental and numerical studies of continuous composite beams taking into consideration slab cracking. *Maintenance and Reliability*, 18(4), pp. 578-589, doi: 10.17531/ein.2016.4.13. [cited at p. 120]

Štrkalj, A., Radenović, A. and Malina, J. (2010). The use of metallurgical waste material from aluminium production for the removal of chromium (VI) ions from aqueous solution. *Archives of Metallurgy and Materials*, 55(2), pp. 449-454. [cited at p. 2]

Tan, E. L. (2010). *The effects of partial shear connection on composite steel-concrete beams subjected to combined flexure and torsion*. PhD. University of Western Sydney. [cited at p. 64]

Thompson, K. (2012). Aluminum bridge decks mounted to galvanized steel: Potentially a superstructure with an indefinite life. In: *Heavy Movable Structures, Inc. 14th Biennial Symposium, Orlando*. [cited at p. 8-9, 12]

Titoum, M., Mazoz, A., Benanane, A. and Ouinas, D. (2016). Experimental study and finite element modelling of push-out tests on a new shear connector of I-shape. *Advanced Steel Construction*, 12(4), pp. 487-506. [cited at p. 23]

Van der Linden, M. (1999). Timber-concrete composite beams. *Heron*, 44(3), pp. 215-239. [cited at p. 31]

Viami International Inc. and The Technology Strategies Group (2013). *Market Study for Aluminium Use in Roadway Bridges*. Report prepared for the Aluminium Association of Canada. [cited at p. 2]

Viest, I. M., Siess, C. P., Appleton, J. H. and Newmark, N. M. (1952). Studies of slab and beam highway bridges, Part IV: Full-scale tests of channel shear connectors and composite T-beams. *University of Illinois Bulletin*, 405. [cited at p. 16, 17]

BIBLIOGRAPHY

Walbridge, S. and de la Chevrotière, A. (2012). Opportunities for the use of aluminum in vehicular bridge construction. MAADI group. [online], p. 7. Available at: http://www.maadigroup.com/wp-content/uploads/2013/02/Aluminum-Bridge-Report.pdf. [Accessed 1 Mar. 2018]. [cited at p. 11, 19]

Wang, A. J. (2009). Numerical studies on structural behaviour of shear connectors in push-out tests. *Australian Journal of Structural Engineering*, 9(2), pp. 79-96. [cited at p. 68]

Wang, D., Wu, M., Ming, J. and Shi, J. (2020). Inhibitive effect of sodium molybdate on corrosion behaviour of AA6061 aluminium alloy in simulated concrete pore solutions. *Construction and Building Materials*, article 121463, doi: 10.1016/j.conbuildmat.2020.121463. [cited at p. 12]

Wang, T. and Hsu, T. T. C. (2001). Nonlinear finite element analysis of concrete structures using new constitutive models. *Computers and Structures*, 79(32), pp. 2781-2791. [cited at p. 60, 72]

Web site, UC RUSAL, The History of Aluminium Industry (www.aluminiumleader.com/history/industry_history/) (05.11.2019) [cited at p. 3]

Web site, Library of Congress, 86th Street Overpass, Spanning Interstate 35 & 80 at Northwest Eighty-sixth Street, Urbandale, Polk County, IA, Historic American Engineering Record (http://loc.gov/pictures/item/ia0410/) (29.08.2018) [cited at p. 5]

Web site, Bridgehunter.com, Historic and notable bridges of the USA (http://bridgehunter.com/va/chesterfield/appomattox-river/) (30.08.2018) [cited at p. 8]

Web site, Preservation Maryland, (http://www.preservationmaryland.org/online-exploration-of-marylands-historic-bridges/) (30.08.2018) [cited at p. 9]

Web site, F. Robby, The Sykesville Bypass Bridge (https://www.hmdb.org/m.asp?m=115066) (31.08.2018) [cited at p. 7]

Web site, Wikipedia, Ajka alumina plant accident (http://en.wikipedia.org/wiki/Ajka_alumina_plant_accident) (30.01.2015) [cited at p. 2]

Web site, Bridgehunter.com (https://bridgehunter.com/ny/st-lawrence/mstr---grasse-river/) (30.08.2018) [cited at p. 4]

Web site, Wikipedia, Arvida, Quebec (https://en.wikipedia.org/wiki/Arvida,_Quebec) (30.08.2018) [cited at p. 4]

BIBLIOGRAPHY

Wittmann, F. H., Rokugo, K., Bruhwiler, E., Mihashi, H. and Simonin, P. (1988). Fracture energy and strain softening of concrete as determined by means of compact tension specimens. *Materials and Structures*, 21, pp. 21-32. [cited at p. 62]

Włodarczyk, W. (1987). Electrolytic cathode carbon waste of the aluminium smelter in Skawina. *Zeszyty Naukowe AGH, Sozologia i Sozotechnika*, 23. [in Polish] [cited at p. 2]

Wosatko, A., Pamin, J. and Polak, M. A. (2015). Application of damage-plasticity models in finite element analysis of punching shear. *Computers and Structures*, 151, pp. 73-85, doi: 10.1016/j.compstruc.2015.01.008. [cited at p. 58]

Wosatko, A., Genikomsou, A., Pamin, J., Polak, M. A. and Winnicki, A. (2018). Examination of two regularized damage-plasticity models for concrete with regard to crack closing. *Engineering Fracture Mechanics*, 194, pp. 190-211, doi: 10.1016/j.engfracmech.2018.03.002. [cited at p. 59]

Wróblewski, T., Berczyński S. and Abramowicz M. (2013). Estimation of the parameters of the discrete model of a steel-concrete composite beam. *Archives of Civil and Mechanical Engineering*, 13, pp. 209-219, doi: 10.1016/j.acme.2013.01.009. [cited at p. 1]

Wróblewski, T., Pełka-Sawenko, A., Abramowicz M. and Berczyński S. (2013). Parameter identification of steel-concrete composite beams by finite element method. *Diagnostyka*, 14(1), pp. 43-46. [cited at p. 67]

Wróblewski, T., Jarosińska, M., Abramowicz M. and Berczyński S. (2017). Experimental validation of the use of energy transfer ratio (ETR) for damage diagnosis of steel-concrete composite beams. *Journal of Theoretical and Applied Mechanics*, 55(1), pp. 241-252, doi: 10.15632/jtam-pl.55.1.241. [cited at p. 127]

Xu, Y., Wang, Q., Xie, M. and Wei, Q. (2020). Shear behavior of reinforced concrete beams strengthened with aluminum alloy sheets. *Huazhong Keji Daxue Xuebao (Ziran Kexue Ban)/Journal of Huazhong University of Science and Technology (Natural Science Edition)*, 48(2), pp. 47-53. [cited at p. 14]

Yu, X, Xing, G. and Chang, Z. (2020). Flexural behavior of reinforced concrete beams strengthened with near-surface mounted 7075 aluminum alloy bars. *Journal of Building Engineering*, 31, article 101393. [cited at p. 14]

Zhou, F. and Young, B. (2008). Tests of concrete-filled aluminum stub columns. *Thin-Walled Structures*, 46, pp. 573-583. [cited at p. 10, 13]

Zhou, F. and Young, B. (2009). Concrete-filled aluminium circular hollow section column tests. *Thin-Walled Structures*, 47, pp. 1272-1280. [cited at p. 13]

BIBLIOGRAPHY

Zhou, F. and Young, B. (2012). Numerical analysis and design of concrete-filled aluminum circular hollow section columns. *Thin-Walled Structures*, 50, pp. 45-55. [cited at p. 13]

Zieliński, K. (2010). *Podstawy technologii betonu*. 2nd ed. Poznań: Wydawnictwo Politechniki Poznańskiej, 194. [cited at p. 45]

Zieliński, T. (1972). Tablice statystyczne [Statistical tables]. Warszawa: Państwowe Wydawnictwo Naukowe. [in Polish] [cited at p. 81]

Zienkiewicz, O. C., Taylor, R. L. and Zhu, J. Z. (2005). *The Finite Element Method: Its Basis and Fundamentals*. Sixth Ed., Elsevier Butterworth-Heinemann, 752. [cited at p. 65]

Appendices

APPENDICES

Appendix 1. Composition of the concrete mixture

Table A.1. Composition of the concrete mixture
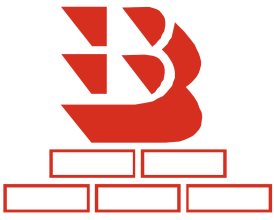
	"Stanbud" Concrete laboratory	STANBUD Sp. z o.o. 3 Łozinowa Street 62-020 Garby, Poland VAT number: PL 777-27-46-909	
Ready-mixed concrete			
Exposure class:		X0		
Strength class:		C35/45		
Consistency class:		S3	Slump range:	100–150
Maximum aggregate size:		8 mm		
Specification, performance, production and conformity in accordance with the standard:		PN-EN 206-1		
Composition of the concrete mixture: no. 245316 as of 1 June 2014				
No.	Material	Amount of material in 1 m^3 of the concrete mixture	Unit	Comments
1	Sand (0–2 mm)	650	kg	ŻwirPol-Garby
2	Gravel (2–8 mm)	1086	kg	G. Kruszywa
3	CEM III/A 42.5N-HSR	410	kg	Górażdże Cement
4	Water	170	kg	Water supply
5	Air	2	%	
6	Sikament 400/30 superplasticizer	4.51	kg	
Parameters of the concrete mixture				
1	Amount of aggregate in 1 m^3 of the concrete mixture	1736.6	kg	
2	Volume of aggregate in 1 m^3 of the concrete mixture	663.2	dcm^3	
3	Amount of binder (cement)	410.0	kg/m^3	
4	Amount of paste + air	336.8	dm^3/m^3	
5	Amount of mortar + air	622.7	dm^3/m^3	
6	Theoretical density of the concrete mixture	2321.2	kg/m^3	
7	Water-cement ratio	0.41	–	
8	Volume of cement, fly ash and aggregate < 0.125 mm	340.3	l/m^3	
9	Amount of cement, fly ash and aggregate < 0.125 mm	419.3	kg	
10	Amount of cement, fly ash and aggregate < 0.25 mm	493.2	kg	
11	Sand content	43.1	%	

APPENDICES

Appendix 2. Crack width

Table B.1. Crack width (beam 1)

No.	Load [kN]	Width [mm]	Comments	No.	Load [kN]	Width [mm]	Comments
0	45.0	1.0 ± 1.0	gap*	15	120	< 0.02	crack
	75.0	2.0 ± 1.0			135	0.05 ± 0.02	
	156.0	14.0 ± 1.0			150	0.3 ± 0.02	
1	60.0	0.4 ± 0.02	gap*		156	0.5 ± 0.02	
	75.0	0.5 ± 0.02		16	135	0.15 ± 0.02	crack
	156.0	0.9 ± 0.02			156	25.0 ± 1.0	
2	60.0	0.4 ± 0.02	gap*	17	135	0.1 ± 0.02	crack
	75.0	0.5 ± 0.02			156	10.0 ± 1.0	
	105.0	1.0 ± 0.02		18	135	0.10 ± 0.02	crack
	156.0	> 1.0			156	15.0 ± 1.0	
3	75.0	0.05 ± 0.02	gap*	19	135	0.15 ± 0.02	crack
	90.0	0.15 ± 0.02			156	10.0 ± 1.0	
	105.0	0.25 ± 0.02		20	135	–	crack
	156.0	0.7 ± 0.02			156	2.0 ± 1.0	
4	75.0	0.05 ± 0.02	gap*	21	135	0.05 ± 0.02	crack
	156.0	0.7 ± 0.02			156	0.05 ± 0.02	
5	75.0	0.05 ± 0.02	gap*	22	135	–	crack
	156.0	> 1.0			156	12.0 ± 1.0	
6	75.0	0.05 ± 0.02	gap*	23	135	0.1 ± 0.02	crack
	105.0	0.7 ± 0.02			156	10.0 ± 1.0	
	156.0	> 1.0		24	135	–	crack
7	75.0	0.05 ± 0.02	gap*		156	0.7 ± 0.02	
	105.0	1.0 ± 0.02		25	135	–	crack
	156.0	1.0 ± 0.02			156	0.4 ± 0.02	
8	75.0	0.05 ± 0.02	gap*	26	156	27.0 ± 1.0	crack
	156.0	1.0 ± 0.02		27	156	10.0 ± 1.0	crack
9	75.0	0.05 ± 0.02	gap*	28	156	–	concrete crushing
	105.0	0.7 ± 0.02		29	156	–	concrete crushing
	156.0	4.0 ± 1.0		30	156	3.0 ± 1.0	crack
10	90.0	0.15 ± 0.02	gap*	31	156	0.05 ± 0.02	crack
	156.0	12.0 ± 1.0		32	156	0.05 ± 0.02	crack
11	90.0	0.05 ± 0.02	gap*				
	156.0	0.5 ± 0.02					
12	105.0	0.05 ± 0.02	gap*				
	156.0	3.0 ± 1.0					
13	105.0	0.25 ± 0.02	gap*				
	156.0	3.0 ± 1.0					
14	120.0	< 0.02	crack				
	135.0	0.05 ± 0.02					
	150.0	0.7 ± 0.02					
	156.0	0.7 ± 0.02					

*between the profiled sheeting and the concrete slab

Table B.2. Crack width (beam 2)

No.	Load [kN]	Width [mm]	Comments
0	30.0	> 1	gap*
1	40.0	0.3 ± 0.05	gap*
	130.0	0.8 ± 0.05	
2	45.0	< 0.05	gap*
	55.0	0.1 ± 0.05	
	110.0	0.25 ± 0.05	
	130.0	0.7 ± 0.05	
3	60.0	< 0.05	gap*
	130.0	> 1 ± 0.05	
4	70.0	< 0.05	crack
	75.0	0.4 ± 0.05	
	130.0	> 1	
5	70.0	0.1 ± 0.05	gap*
	130.0	0.9 ± 0.05	
6	75.0	0.1 ± 0.05	gap*
	130.0	0.9 ± 0.05	
7	75.0	0.1 ± 0.05	gap*
	130.0	0.9 ± 0.05	
8	75.0	0.05 ± 0.05	gap*
	140.0	0.9 ± 0.05	
9	80.0	0.05 ± 0.05	gap*
10	85.0	0.05 ± 0.05	gap*
	140.0	> 1	
11	90.0	0.05 ± 0.05	gap*
	130.0	0.8 ± 0.05	
12	90.0	0.05 ± 0.05	gap*
	140.0	0.6 ± 0.05	
13	90.0	0.05 ± 0.05	gap*
	140.0	0.6 ± 0.05	
14	100.0	0.05 ± 0.05	gap*
	140.0	0.4 ± 0.05	
15	100.0	0.05 ± 0.05	gap*
	140.0	0.1 ± 0.05	
16	110.0	0.25 ± 0.05	gap*
	140.0	0.7 ± 0.05	
17	110.0	0.05 ± 0.05	crack
	120.0	0.1 ± 0.05	
	150.0	0.2 ± 0.05	
18	115.0	0.05 ± 0.05	crack
	120.0	0.05 ± 0.05	
	150.0	0.1 ± 0.05	
19	140.0	0.05 ± 0.05	gap*
20	150.0	> 1	gap*
21	150.0	0.05 ± 0.05	crack
22	150.0	0.05 ± 0.05	crack
23	150.0	0.05 ± 0.05	crack
24	150.0	0.05 ± 0.05	crack
25	150.0		concrete crushing

*between the profiled sheeting and the concrete slab

Table B.3. Crack width (beam 3)

No.	Load [kN]	Width [mm]	Comments
0	45.0	–	gap*
1	45.0	–	gap*
	60.0	0.6 ± 0.05	
2	45.0	–	gap*
	70.0	0.2 ± 0.05	
3	45.0	–	gap*
4	50.0	–	gap*
5	55.0	–	gap*
6	65.0	–	gap*
7	65.0	–	gap*
8	75.0	–	gap*
9	80.0	–	gap*
10	70.0	–	gap*
11	80.0	–	gap*
12	85.0	> 1	gap*
13	85.0	–	gap*
14	90.0	–	crack
	105.0	0.1 ± 0.05	
	120.0	0.2 ± 0.05	
	130.0	0.25 ± 0.05	
	150.0	0.3 ± 0.05	
15	100.0	–	gap*
16	100.0	–	gap*
17	105.0	–	gap*
18	130.0	–	gap*
19	150.0	0.3 ± 0.05	crack
20	150.0	–	crack
21	150.0	–	crack

*between the profiled sheeting and the concrete slab

APPENDICES

Table B.4. Crack width (beam 4)

No.	Load [kN]	Width [mm]	Comments
1	50		gap*
2	60		gap*
3	65		gap*
4	65		gap*
5	65		gap*
6	75		gap*
7	75	0.05 ± 0.05	crack
	100	0.1 ± 0.05	
	115	0.2 ± 0.05	
	130	0.3 ± 0.05	
8	75		gap*
9	80		gap*
10	80		gap*
11	90		gap*
12	90		gap*
13	90		gap*
14	100		gap*
15	100		gap*
16	120		gap*
17	126	1.1 ± 1.0	crack
18	126		crack
19	126	$< 0.05 \pm 0.05$	crack
	130	0.3 ± 0.05	
20	126		crack
21	130	1.1 ± 1.0	crack
22	130	1.1 ± 1.0	crack
23	130		crack
24	138		crack
25	138		crack
26	140		gap*
27	160		crack
28	150		crack

*between the profiled sheeting and the concrete slab

APPENDICES

Appendix 3. Cracking pattern at failure

a)

b)

c)

d)
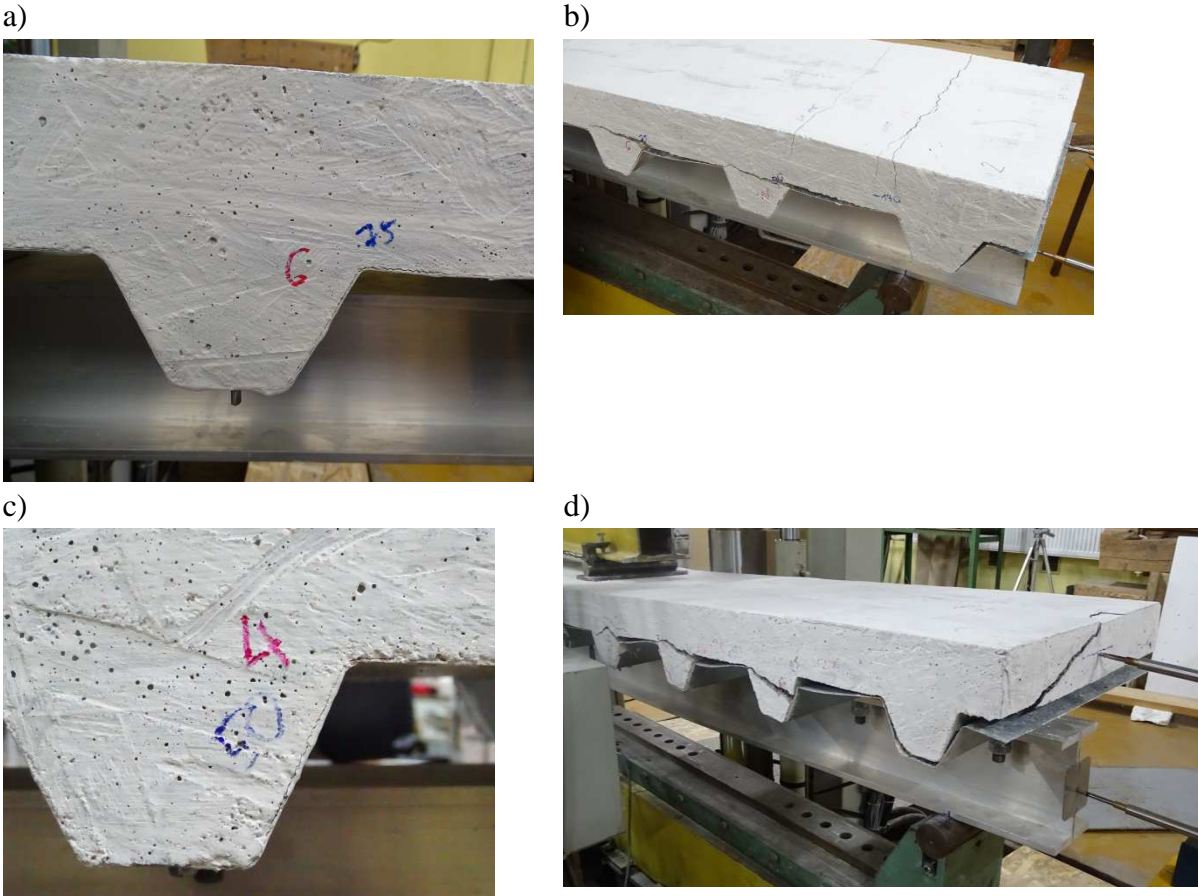
Figure C.1. a) gap 6 between the profiled sheeting and the concrete slab at a load equal to 75.0 kN (beam 2); b) cracks at failure load (beam 2); c) gap 4 between the profiled sheeting and the concrete slab at a load equal to 50.0 kN (beam 3); d) cracks at failure load (beam 3)

a)

b)

c)
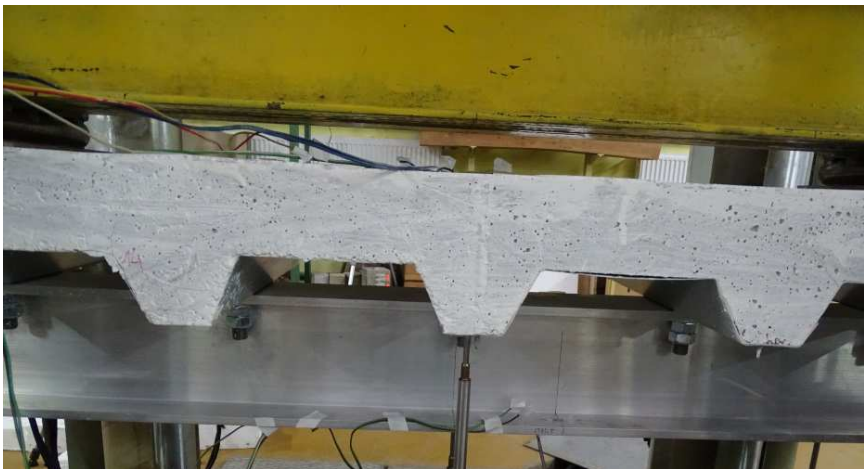
Figure C.2. Beam 4: a) failure at support A; b) failure at support B; c) undamaged middle part of the beam

a)

b)

c)
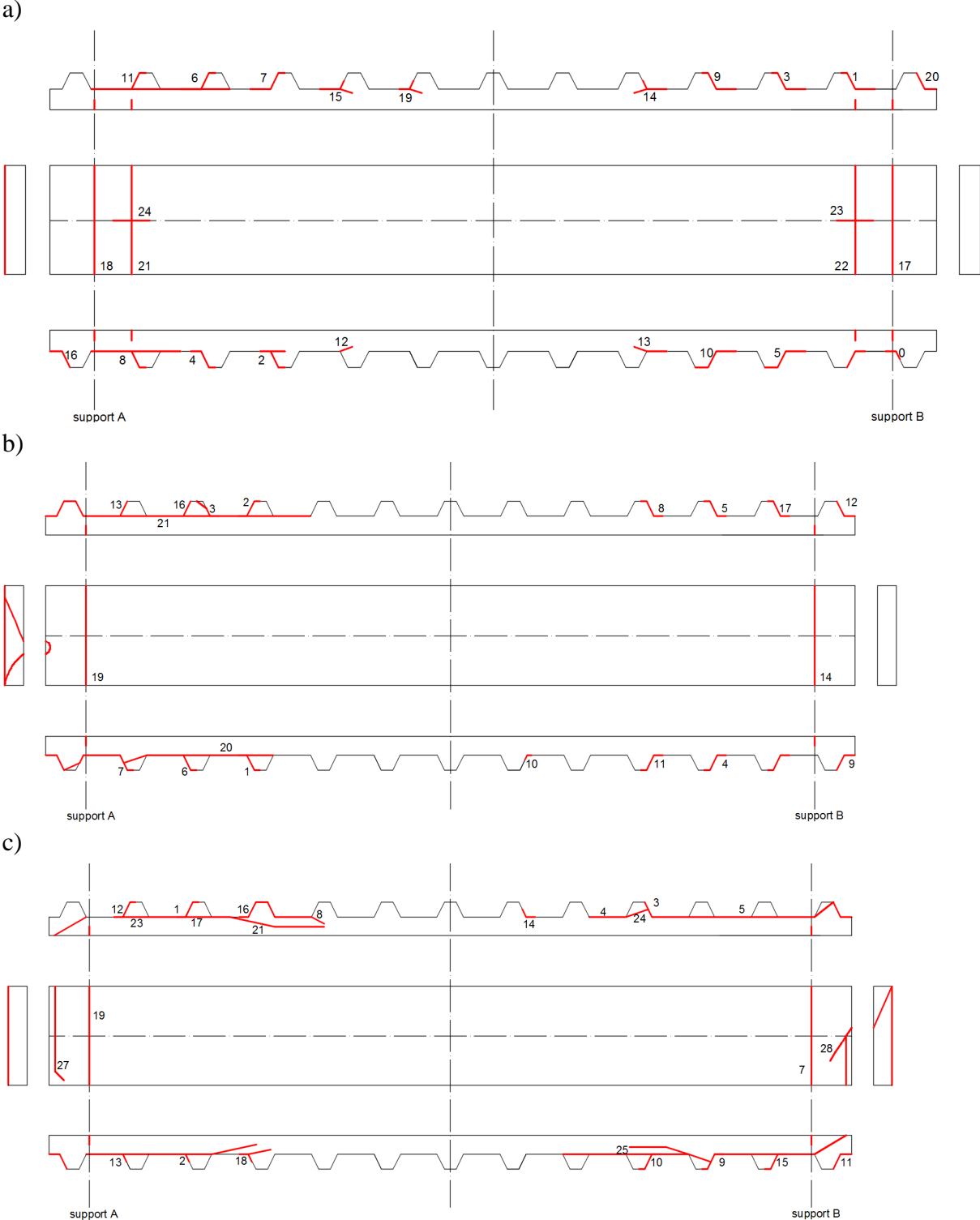
Figure C.3. Cracking pattern at failure: a) beam 2, b) beam 3, c) beam 4